Anion binding studies with responsive lanthanide complexes

Ben Murray

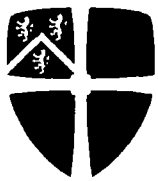

Durham
University

Department of Chemistry

Anion Binding Studies With Responsive Lanthanide Complexes

Ben Murray

A thesis submitted for the degree of Doctor of Philosophy

2008

Abstract

The binding of a range of biologically prevalent anions to several novel lanthanide(III) complexes has been studied by emission spectroscopy, ^{1}H-NMR and mass spectrometry. In each case, the resultant solution adduct and the mode of anion binding was characterised through analysis of spectral response. Following the first chapter, in which relevant background work and literature reports are discussed, the novel lanthanide(III) complexes described herein are separated into three chapters.

Chapter 2 describes a range of complexes bearing a pendant azaxanthone or azathioxanthone derived chromophore. Binding of anions was examined largely through sensitised emission, additionally the cellular localisation and toxicity profiles of each complex was studied. Of particular interest was the discovery of a family of complexes that localised within the mitochondria of the cell lines examined, and exhibited pCO_2 dependent luminescence, notwithstanding protein quenching.

Chapter 3 describes the synthesis and evaluation of two stereoisomeric dimeric complexes, in which the conformation of each was controlled by the differing relative stereochemistry of their linking unit. A range of luminescence and NMR studies was performed to establish the relative affinities of these complexes for selected anionic species, and to compare their binding properties to that of the related monomeric complex.

Chapter 4 describes the immobilization of two related complexes onto various solid-phase supports. The ability of the immobilized complexes to selectively bind to, retain then release phospho-anions on addition of a competitive aqueous anionic buffer is examined. The utility and advantages of using such materials as tools for the enrichment of phospho-peptides is discussed in relation to previously published procedures and materials.

Declaration

The work described herein was carried out in the Department of Chemistry, University of Durham between October 2005 and December 2008. All of the work is my own, except where specifically stated otherwise. No part has previously been submitted for a degree at this or any other university.

Statement of Copyright

Acknowledgements

I would like to say thanks to all of the following people, without their contributions the work presented in this thesis would not have been possible:-

My supervisor, Prof. David Parker, whose help, support and creativity has been greatly appreciated.

Dr. Alan Kenwright, Catherine Hefferman and Ian McKeag for their assistance with NMR spectroscopy. Dr. Mike Jones and Lara Turner for their help and advice with mass spectrometry measurements. Dr. Jackie Mosely for help and advice also with mass spectrometry measurements, ECD sequencing, and for the considerable amount of time she gave to setting up LCMS calibration methods and the analysis of results. Dr. Andrei Batsanov, Dr. Ehmke Pohl and Dr. Mike Probert for analysis of crystals. Judith Magee and Jarka Dostal for elemental analysis.

Dr. Chris Ottley in the Department of Earth Sciences for ICP-MS measurements.

Dr. Bob Peacock, at the University of Glasgow, for assistance with CPL measurements, and for useful directions to the chippy.

Dr. Cidália dos Santos, at Trinity College Dublin, for her analysis of binding titrations.

All the past and present members of CY27 for their friendship and making the lab such a great place to work. Furthermore, I would like to thank Filip for his advice and generous gift of 7-methoxycarbonyl-2-methyl-1-azathioxanthone, Robek for help with binding titrations, Lars for measuring triplet energies, analysis of immobilised complexes and useful discussions, Ga-lai and Gary for arranging and carrying out variable CO_2 microscopy experiments at the City University of Hong Kong, Craig for footy facts, Liz for carrying out cell microscopy and cytotoxicity experiments

and David for help with analysis of the LCMS calibrations.

My friends in Durham and farther afield, for many a footy match, gig or night out.

Elena for her love, support, and for improving her cooking skills.

A special thanks to Mum and Dad for their love and support, and for giving me the opportunity to achieve so much, and to Dan and Carina and my grandparents Jean, Colin and Margaret for their love and support.

For Mum and Dad

Contents

List of Abbreviations

AIBN - *N*,*N*′-azoisobutyronitrile

cAMP - adenosine 3′,5′-cyclic monophosphate

AMP - adenosine 5′-monophosphate

ADP - adenosine 5′-diphosphate

ATP - adenosine 5′-triphosphate

bicine - *N*,*N*-bis(2-hydroxyethyl)glycine

BOC_2O - di-*tert*-butyl dicarbonate

BP - band pass

CCD - charge coupled device

CD - circular dichroism

CHO cells - chinese hamster ovarian cells

CPL - circularly polarised luminescence

cyclen - 1,4,7,10-tetraazacyclododecane

d - doublet

dd - doublet of doublets

DCM - dichloromethane

DMEM - Dulbeccos modified eagle media

DMF - *N*,*N*-dimethylformamide

DO3A - 1,4,7,10-tetraazacyclododecane-1,4,7-triacetic acid

DOTA - 1,4,7,10-tetraazacyclododecane-1,4,7,10-tetraacetic acid

(*SSSS*)-DOTMPhA - *N*-((S)-1-phenyl-ethyl)-2-(4,7,10-tris-[((S)-1-phenyl-ethylcarbamoyl)-methyl]-1,4,7,10-tetraaza-cyclododec-1-yl)-acetamide

dpa - dipicolylamine

ECD - electron-capture dissociation

EDC.HCl - *N*-(3-dimethylaminopropyl)-*N*′-ethylcarbodiimide hydrochloride

emf - electromotive force

EPA glass - Et_2O-isopentane-ethanol frozen glass

ES^+ - electrospray ionization with positive ion detection

ES^- - electrospray ionization with negative ion detection

ESI - electrospray ionization

ESMS - electrospray mass spectrometry

Glc-1,6-P - α-D-glucose 1,6-bisphosphate potassium salt

Glc-6-P - D-glucose-6-(dihydrogen phosphate)

HEPES - 4-(2-hydroxyethyl)-1-piperazineethanesulfonic acid

HOBt.xH_2O - 1-hydroxybenzotriazole hydrate

HPLC - high performance liquid chromatography

HRMS - high-resolution mass spectrometry

HSA - human serum albumin

ICP-MS - inductively coupled plasma mass spectrometry

IRK - insulin receptor kinase

IMAC - immobilized metal ion affinity chromatography

LCMS - liquid chromatography mass spectrometry

LIS - lanthanide induced shift

LP - long pass

MALDI-TOF - matrix-assisted laser desorption/ionization-time of flight

MAS - magic angle spinning

MOPS - 3-(*N*-morpholino)propanesulfonic acid

MS - mass spectrometry

MTT - 3-(4,5-dimethylthiazol-2-yl)-2,5-diphenyltetrazolium bromide

NBS - *N*-bromosuccinimide

NCS - newborn calf serum

NHS - *N*-hydroxysuccinimide

NMR - nuclear magnetic resonance

PEG - polyethylene glycol

Ph - phenyl

PPA - polyphosphoric acid

q - quartet

RNA - ribonucleic acid

RNP - ribonucleopeptide

s - singlet

SAP - square anti-prism

SDS-PAGE - sodium dodecyl sulfate polyacrylamide gel electrophoresis

Ser - L-serine

O-P-Ser - *O*-phospho-L-serine

t - triplet

TBTU - *O*-(benzotriazol-1-yl)-*N*,*N*,*N*′,*N*′-tetramethyluronium tetrafluoroborate

TFA- trifluoroacetic acid

TLC - thin layer chromatography

TOCSY - total correlation spectroscopy

Thr - L-threonine

O-P-Thr - *O*-phospho-L-threonine

TRIS - tris(hydroxymethyl)aminomethane

TSAP - twisted square anti-prism

Tyr - L-tyrosine

O-P-Tyr - *O*-phospho-L-tyrosine

Chapter 1

Introduction and literature review

1.1 Introduction

The role of anions in Nature is wide ranging and significant, exemplified by the regulation of many biological processes at the intracellular level. These often involve anionic species that play roles as signaling molecules and distributors of chemical energy. To fully understand the role of anions in events at the intracellular level, the development of selective synthetic probes is required. These probes may act as receptors for the specific anion of interest and then subsequently report upon the binding event. To this end, recent research has focused on the development of receptors that can reversibly bind to anions in aqueous media.

During the design of aqueous phase anion receptors there are several major points to consider. The first of these is the free energy of hydration of the anion (Table 1.1). Due to the high free energy of hydration, in particular for oxyanions, a large electrostatic contribution to binding is required so that the receptor can compensate for the unfavourable desolvation term. Indeed, it is often anion desolvation that is the key factor in determining the free energy of binding to the receptor.[1,2] In addition, the local hydrophobicity of the receptor binding site must be considered. The energetic cost of desolvation of the receptor binding site upon anion binding will also be a key factor in determining the overall free energy change accompanying the anion binding process. The overall free energy of binding will usually be greater when there is less local hydration around the receptor binding site.

Anion	Radius (Å)	$\Delta G^0_{hyd}(kJmol^{-1})$
I^-	2.20	-275
CN^-	1.91	-295
Br^-	1.96	-315
HCO_3^-	1.56	-335
Cl^-	1.81	-340
F^-	1.33	-465
$H_2PO_4^-$	2.00	-465
SO_4^{2-}	2.30	-1080
CO_3^{2-}	1.78	-1315
PO_4^{3-}	2.38	-2765

Table 1.1 – Thermochemical radii and experimental standard molar Gibbs free energy of hydration for various anions,[3] highlighting the high free energies of hydration observed for oxyanions.

Certain anions exist within defined pH limits, whilst others vary in charge within a narrow pH window, thereby changing their electrostatic interactions. The pH of an analyte needs to be monitored and controlled to establish the relative proportions of anionic species in solution. Therefore, a suitable receptor needs to be effective within a defined pH region. Finally, anions occur in a range of shapes and geometries. For example, halides are spherical, CN^- linear, HCO_3^- trigonal planar and PO_4^{3-} tetrahedral, meaning careful receptor design is required to provide shape complementarity with respect to the target anion.

1.2 The development of synthetic anion receptors

Many functionalities forming the basis of early synthetic anion receptors can be seen in analogous systems present in nature. For example, the protonated forms of spermidine and spermine, naturally occurring polyamines, are reported to bind to phosphates in aqueous solution.[4,5] The active centres of phosphatases make use of the guanidinium functionality,[6] reflected in the widespread use of the guanidinium functionality in synthetic phosphate receptors. Receptors based upon metal cations find analogous examples in many enzyme active sites. For example, phospholipase C and alkaline phosphatase contain Zn(II) ions that provide the electrostatic basis for phosphate binding in these systems. This section will briefly highlight the use of various functionalities commonly employed in synthetic anion receptors.

The earliest synthetic anion receptors incorporated highly charged binding sites to provide a basis for strong electrostatic interactions, in order to compensate for unfavourable solvation in aqueous media. Early work described 'molecular inclusion' complexes with anions bound inside a molecular cavity by a tetrahedral array of $^{+}$N-H$\cdots$X^{-} hydrogen bonds and electrostatic interactions.[1] Incorporated into a receptor, the ammonium functionality offers high charge density, hence efficient ion pairing. Also, ammonium groups can impart structural rigidity into a macrocyclic structure that can help complement the shape of a target anion. Halide anions were amongst the first anionic species to be recognised in aqueous media. For example, chloride ions were shown to be bound by the tetra-protonated form of the spheroidal cryptand, **1**. This cryptand was more than a thousand-fold more selective for chloride than bromide.[7]

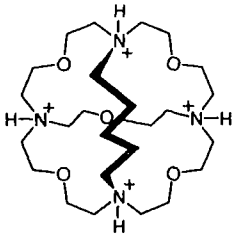

1

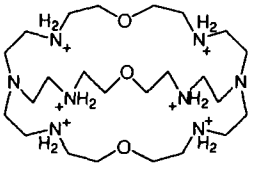

2

Later work extended the scope of recognition. For example, **2** bound to linear triatomic anions selectively over non-linear anions.[8] In both cases anion selectivity was controlled by cavity shape and size. The major limitation of such polyammonium receptors is the limited pH range in which they are operational. Despite this, there are many examples of such polyammonium receptors being developed for use in the field of aqueous phase anion recognition.[9]

Early anion binding studies with macrocyclic guanidinium salts utilised the guanidinium pKa of 13.5 to ensure that anion binding properties of such systems were relatively pH independent.[10] In addition, the positive charge of the functionality, combined with its hydrogen bonding capabilities, make it an effective receptor

for carboxylate and phosphate recognition.[11,12] One of the main disadvantages of the guanidinium functionality in aqueous media is that it suffers from high levels of competitive solvation. Because of this, anion binding studies are often carried out in less polar aqueous alcohol solutions to increase binding specificity. Additionally, the guanidinium functionality may be incorporated next to a hydrophobic structure in an effort to reduce guanidinium solvation, although this reduces receptor solubility in aqueous conditions. In either case, the resulting receptors will perform optimally in non-aqueous conditions, rendering them less suitable for use in a biological environment. One such example is the ditopic guanidinium receptor, **3**, which was shown to bind to dicarboxylates in methanol.[13] This receptor exhibited a preference for malonate (log K = 4.2) over longer and shorter dicarboxylates. However, significant guest binding (log K = 2.4-3.4) was observed for all other dicarboxylates indicating the flexibility of the receptor with respect to guest anion structure.

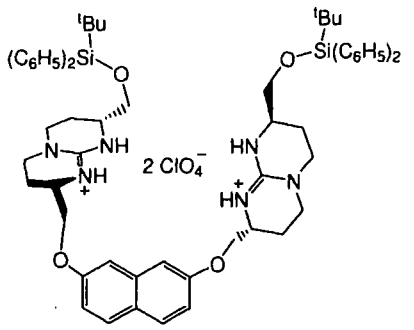

3

In addition to the polyamine and guanidinium functionalities present in early synthetic anion receptors, many other functionalities have since been utilised. Most commonly these functional groups are ureas, thioureas, amides, thioamides, pyrroles, indoles and hydroxyl groups, often present as part of a macrocycle.[12] Not all of these functionalities have been utilised in aqueous media.

One other class of synthetic anion receptors are those based upon a central metal cation. An appropriately positioned metal cation in a synthetic anion receptor can provide a strong basis for electrostatic attraction; often the metal cation is encapsulated inside a macrocyclic ligand. A strong contribution from electrostatic attraction

is beneficial for aqueous phase anion receptors and metals of different charge density can be used to modulate the electrostatic affinity. Examples commonly include those containing Zn(II) or Ln(III) cations; several examples are covered in detail later.

1.3 Methods of signal transduction

There are several methods by which a binding event at a synthetic receptor may be reported. However, it is important to realise at the outset that some signal transduction methods are intrinsically restrictive and will impact upon the final utility of the probe. With regards to the design of synthetic receptors that can report upon anion binding events at a cellular level, it is clear that very few signal transduction methods fulfil the requirements needed to report on events with high spatial resolution. For such biological systems the use of luminescent probes is dominant. Luminescent probes offer the advantages of high sensitivity, with detection limits down to a single molecule,[14] and spatial resolution down to the submicron level.[15] Optical probes are able to relay information about anion binding events through changes to the local environment of the reporting unit. In general, anion binding is followed using UV/visible absorption and emission spectroscopy, by the monitoring of an intensity change or wavelength shift. Monitoring of emission lifetime and polarisation is also possible. There are many examples of fluorescent organic molecules that may be utilised to create luminescent organic probes. However, the excited state chemistry of Ln(III) ions is well suited to such applications and research into Ln(III) probes is now widespread.

Other methods of signal transduction methods have been utilised. Of these, magnetic resonance is one of the most informative. Monitoring of the chemical shift or relaxation rate properties of a system can result in a large amount of structural information. In particular, the introduction of a paramagnetic metal ion into a probe can yield detailed results. Paramagnetic Ln(III) probes will be discussed later in this chapter. Magnetic resonance is restricted by the fact that its spatial resolution is insufficient to monitor events at a cellular level. Also, it is relatively insensitive

and requires expensive instrumentation.

Electrochemical methods have also been reported where changes in current or emf, proportional to the anion concentration, are detected. Examples include the development of potentiometric ion-selective electrodes, created by the incorporation of neutral, anion selective ionophore molecules into a polymer membrane.[16,17] Binding of target anions is monitored by changes in the measured potential across the membrane. In general anion recognition by an ionophore is based upon hydrogen bonding or Lewis acidic interactions. The use of electrochemical methods is restricted by the invasiveness of the techniques, the need for careful calibration, slow response times and often short working lifetimes of the polymer membranes.

1.4 Approaches to selective anion recognition

Much of the published research on anion recognition has been based on receptors operating in non-aqueous environments. This is of little surprise when considering the energetic cost of anion desolvation in aqueous media. However, research into systems operating in an aqueous environment is becoming more common. Much of this report will discuss our approach to anion recognition utilising Ln(III) complexes in an aqueous environment. This section will review recent reports of synthetic anion receptors that function in aqueous media and have been or possess the potential to be utilised as analytical probes. Each is based on strategies that do not involve Ln(III) complexation to achieve selective anion binding. Receptors of anions most relevant to the results published in this report will be emphasised, these include phosphorus(V) oxyanions, bicarbonate and citrate.

1.4.1 Receptors and probes for phosphorylated anions

Phosphates are ubiquitous in biological systems. For example, it is well understood that *O*-phosphorylated proteins play an important role in intracellular communication and also in the functioning of the nervous and immune systems. Phosphorylation of these proteins is carried out by protein kinases - these enzymes are phosphotransferases and rely upon the nucleoside triphosphate, ATP^{4-}, as the source

of the phosphoryl group.[18–22] ATP^{4-} itself is established as an intracellular energy source and is now understood to be involved in extracellular signalling, as are other nucleoside pyrophosphates.[23,24] Because of the importance of this family of oxy anions much effort has been devoted to the development of selective phospho-anion probes.[25]

Anthracene bis(zinc(II)-dipicolylamine) complexes were reported to be the first selective artificial receptors of a phosphorylated peptide in aqueous solution.[26–28] These bis-Zn(II) receptors, loosely mimicking the alkaline phosphatase active site, were found to selectively recognize a singly-phosphorylated peptide, phosphorylated on tyrosine. Binding was monitored by a fluorescence enhancement of $[Zn_2\mathbf{L}^4]^{4+}$ or $[Zn_2\mathbf{L}^5]^{4+}$ at 420 nm. This recognition, at pH 7.2, contrasted with the absence of fluorescence enhancement observed in binding studies with the non-phosphorylated analogue. Fluorescence enhancement upon anion binding was ascribed to suppression of photoinduced electron transfer quenching by a benzylic amine of the ligand.

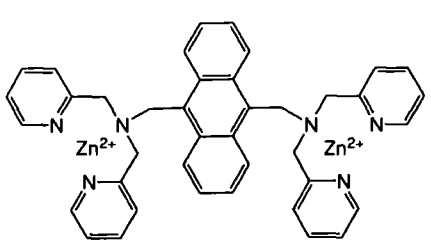

$[Zn_2\mathbf{L}^4]^{4+}$

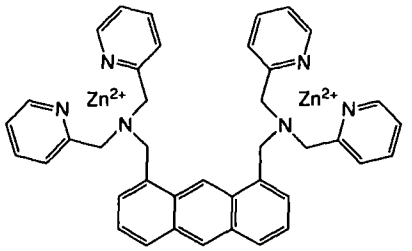

$[Zn_2\mathbf{L}^5]^{4+}$

Binding studies with other singly-phosphorylated peptides revealed that the overall peptide charge was crucial to recognition, with negatively charged peptides being recognised whilst neutral and positively charged phospho-peptides resulted in either very weak or no receptor fluorescence enhancement. Accordingly, the apparent binding constant increased as the charge on the peptide increased. In addition, $[Zn_2\mathbf{L}^4]^{4+}$ was shown to discriminate between $(O\text{-P-Tyr})^{2-}$ and $HPO_4{}^{2-}$; only $(O\text{-P-Tyr})^{2-}$ gave rise to receptor fluorescence enhancement. In contrast, both anions caused a fluorescent enhancement with $[Zn_2\mathbf{L}^5]^{4+}$. Subsequently $[Zn_2\mathbf{L}^4]^{4+}$ and $[Zn_2\mathbf{L}^5]^{4+}$ were used to monitor the phosphatase-catalyzed dephosphorylation of a peptide,

utilising the change in receptor fluorescence intensity during the dephosphorylation process to follow the reaction. $[Zn_2\mathbf{L}^4]^{4+}$ was also used as a selective staining reagent in SDS-PAGE, preferentially staining phosphoproteins in a mixture of other proteins on the gel.[29] A major limitation of these receptors as potential intracellular probes is their reported lack of discrimination between different nucleoside pyrophosphates and phosphorylated proteins and peptides. In each case binding was signalled by a fluorescence change.

In related work, complexes of two Zn(II)-(Dpa) units connected by various 2,2′-bipyridine linkers were prepared, as receptors targeting di-phosphorylated peptides via intrapeptide cross-linking.[30]

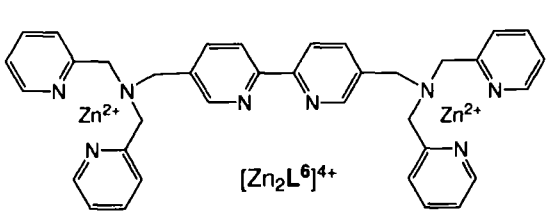

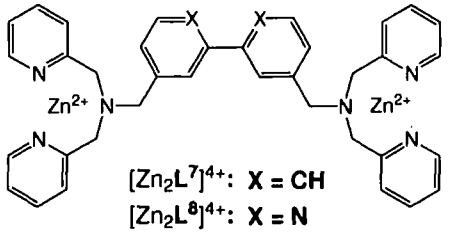

$[Zn_2\mathbf{L}^6]^{4+}$ was tested with model α-helical di-phosphorylated peptides and a singly phosphorylated analogue (phosphorylated at serine), and also with residues 1154-1165 of the activation loop of insulin receptor kinase (IRK) in non-, mono- and di-phosphorylated forms (phosphorylated at tyrosine). Aqueous conditions at pH 8 were used. Results showed that binding affinity was highly dependent on the number of phosphorylated residues. The di-phosphorylated peptides were bound over ten times more strongly than their mono-phosphorylated analogue in the case of the model system. A modest 3-fold selectivity within the series of model di-phosphorylated peptides was observed despite phosphorylation being at positions 5 and 16, 9 and 16 or 12 and 16 respectively, suggesting a high degree of peptide and receptor flexibility. These studies utilised circular dichroism (CD) to show an increase of the diphosphorylated peptides α-helix conformation upon binding with $[Zn_2\mathbf{L}^6]^{4+}$, attributed to intrapeptide cross-linking stabilization. Fluorescence emission decreases at 389 nm were also used to monitor peptide binding to $[Zn_2\mathbf{L}^6]^{4+}$.

Studies with the IRK peptide yielded similar results. A 20-fold binding selectivity between di-phosphorylated and mono-phosphorylated fragments was recorded; binding to the non-phosphorylated fragment was not observed. The authors later utilised this intrapeptide cross-linking strategy with receptors $[Zn_2\mathbf{L}^7]^{4+}$ and $[Zn_2\mathbf{L}^8]^{4+}$ to disrupt the interaction between a di-phosphorylated peptide and a phosphoprotein binding domain via competitive receptor-peptide binding.[31] Studies were performed under aqueous conditions at neutral pH. In each of these reports, no competitive binding studies between the receptors and other common endogenous anionic species (e.g. HCO_3^-, citrate, lactate) was reported.

Zn(II)-(dpa) complexation chemistry has been exploited more recently as part of a hybrid receptor where one Zn(II)-(dpa) unit was conjugated to a phosphoprotein binding domain.[32]

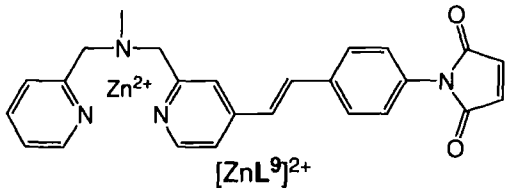

$[Zn\mathbf{L}^9]^{2+}$

Protein Pin1 binds selectively to the multiphosphorylated C-terminal domain repeat sequence of RNA polymerase II through the phosphoprotein binding (group IV WW) domain. Crystallographic analysis of a di-phosphorylated peptide (pS2,5-CTD, phosphorylated at $(O\text{-P-Ser})^{2-}$ residues 2 and 5) bound to the phosphoprotein binding domain had shown only the pS5 residue interacted strongly with the binding domain. $[Zn\mathbf{L}^9]^{2+}$ was incorporated into three mutant WW domains at side-chains which, from crystallographic evidence, were in close proximity to the weakly bound $(O\text{-P-Ser})^{2-}$. Only one hybrid receptor, retaining the native-like conformation of the binding domain, was examined further. Following addition of a bis-phosphorylated pS6,9-CTD peptide to a solution of the chosen hybrid receptor, the stilbazole fluorescence emission at 440 nm increased by up to 60 %, following excitation at 340 nm. This increase in emission is reported to be due to binding causing the stilbazole to rigidify, minimising relaxation associated with the torsional rotational freedom of the

two aromatic groups. The binding constant of the hybrid receptor with the peptide was found to be ~10-fold larger than that with the native WW domain and ~1000-fold larger than that with $[ZnL^9]^{2+}$ alone, suggesting a large degree of cooperativity in the binding process. A much lower binding constant was observed in binding studies with a bis-phosphorylated segment of IRK (1156-1164) compared to pS6,9-CTD. In addition, the affinity of the hybrid receptor for nucleoside pyrophosphates was comparatively low. This marked selectivity was utilised in a real-time assay monitoring kinase-catalyzed phosphorylation by fluorescence enhancement. Phosphorylation of a substrate peptide, pS9-CTD, at Ser-6 was monitored by the hybrid receptor. No fluorescence intensity increase was observed in the absence of either ATP^{4-}, pS9-CTD or the kinase enzyme, but a gradual increase occurred when all three were present.

A strategy has been reported affording ribonucleopeptides (RNPs) as receptors that selectively bind to $(O\text{-P-Tyr})^{2-}$ or short peptide sequences containing $(O\text{-P-Tyr})^{2-}$. Initially, the authors reported the isolation of RNP receptors specific for $(O\text{-P-Tyr})^{2-}$ that discriminated $(O\text{-P-Tyr})^{2-}$ from Tyr, $(O\text{-P-Ser})^{2-}$ and $(O\text{-P-Thr})^{2-}$.[33] *In vitro* selection was used to select RNPs that bound $(O\text{-P-Tyr})^{2-}$ from a pool of $(4)^{30}$ RNA sequences. Later work extended the RNP concept by isolating RNPs capable of distinguishing between two $(O\text{-P-Tyr})^{2-}$ containing tetra-amino-acid motifs within the same protein (Figure 1.1).[34]

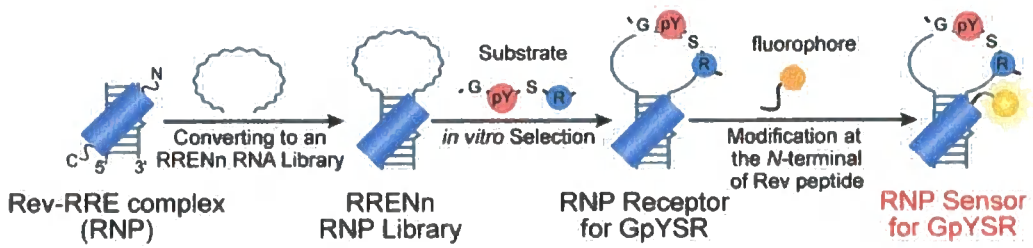

Figure 1.1 – Graphical illustration of the methodology used to isolate fluorescent RNP probes selective for a single $(O\text{-P-Tyr})^{2-}$ site in a tetra-amino-acid motif.[34]

Receptors that bound to the desired $(O\text{-P-Tyr})^{2-}$ containing peptide sequence were converted into fluorescent probes via replacement of the peptides used with fluorescently labelled peptides. This yielded a fluorescent RNP that selectively responded,

via a fluorescence intensity increase, to the binding of the desired substrate phospho-peptide and not to structurally related phospho-peptides. A 95-fold difference between the binding affinities of the two (O-P-Tyr)$^{2-}$ containing tetra-amino-acid motifs was observed. Despite the promising selectivities observed in these two reports the dissociation constants are not low enough for practical use. Dissociation constants, at best, were in the low μM range. However by using larger phospho-peptide or phospho-protein targets affinities may be increased.

Selective probes for nucleoside polyphosphates have been developed based upon the high affinity observed for them by probes such as $[Zn_2\mathbf{L}^5]^{4+}$ and related complexes.[35] One particular approach was based upon the switching on of the fluorescence of $[Zn_2\mathbf{L}^{10}]^{4+}$ upon nucleoside polyphosphate binding. The complex was reported to detect ATP^{4-} at concentrations of less than 10^{-6} M.[36]

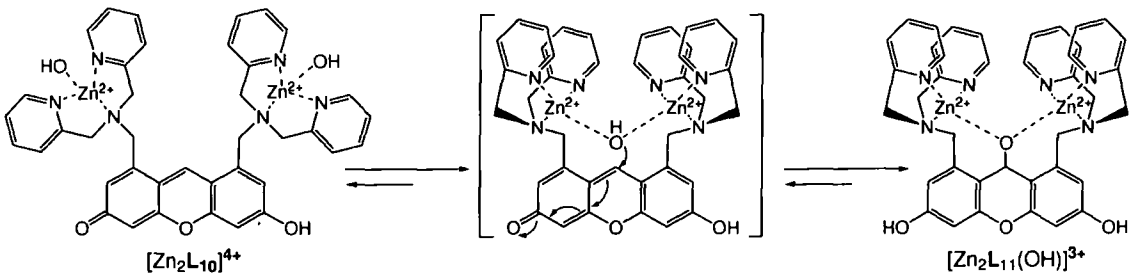

In a neutral aqueous solution $[Zn_2\mathbf{L}^{10}]^{4+}$ exists in a deconjugated form, due to nucleophilic attack of a water molecule coordinated to the two Zn(II) ions, resulting in the formation of $[Zn_2\mathbf{L}^{11}(OH)]^{3+}$. Upon addition of ATP^{4-} to the solution, a 30-fold fluorescence increase at 523 nm (λ_{ex}=488 nm) was observed as binding saturation was reached. This behaviour was attributed to recovery of the conjugated form of the xanthene ring. Binding studies of $[Zn_2\mathbf{L}^{11}(OH)]^{3+}$ with nucleoside monophosphates, phosphodiesters and oxyanions such as bicarbonate resulted in no recovery of fluorescence. The response of the complex to ATP^{4-} was stable between pH 6 and 8. As a result of the observed selectivity, an acetylated analogue of $[Zn_2\mathbf{L}^{11}(OH)]^{3+}$ was used to visualise local particulate stores of ATP^{4-} in Jurkat cells following intracellular complex hydrolysis by local esterases.

1.4.2 Receptors and probes for citrate and bicarbonate

Outside the family of phosphate anions, there is a variety of other oxyanions that play key roles in intracellular events. For example, bicarbonate plays important roles in intracellular signal transduction (e.g. via bicarbonate regulation of cAMP synthesis),[37] in the regulation of intracellular pH and volume, in photosynthesis and the Krebs cycle.[38] The citrate anion is of interest as an *in vivo* marker for several diseases. For example, the marked difference in citrate accumulation and secretion by healthy and cancerous human prostate secretory epithelial cells is well established.[39] Citrate is also a key component in the Krebs cycle and has roles in fatty acid synthesis, photorespiration, the glyoxylate cycle and nitrogen metabolism. Despite the importance of these two anions, and in contrast to the field of selective phosphate recognition, there are very few reports detailing the development of selective receptors for bicarbonate and citrate. This section outlines the limited number of selective receptors and probes that have been studied in competitive aqueous media.

One recent communication reported a fluorescent HCO_3^- probe constructed from a pyrene residue linked, via a triamine linker, to γ-cyclodextrin (**12**).[40]

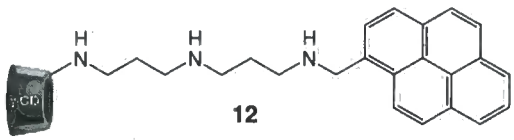

12

Between pH 7 and 9, an association dimer of **12** is formed that can act as a receptor for HCO_3^-. Upon addition of HCO_3^-, a distinctive change in the form and intensity of the fluorescence spectrum of pyrene is induced that is not observed with other common anions. This selective response suggests that only HCO_3^- binds to the probe. This behaviour was tentatively attributed to the formation of a pseudo azacrown ring by the triamine linker, under the experimental conditions, that can selectively bind to HCO_3^-. The change of the fluorescence spectra upon HCO_3^- addition was assigned to a change in conformation, from parallel to twisted, of the two pyrene rings in the cavity of the association dimer. This twist reduces the overlap of the aromatic functionalities and therefore reduces overlap of π orbitals,

causing the excimer fluorescence to shift to shorter wavelength. The probe could reportedly signal changes in the concentration of aqueous solutions of HCO_3^- at a concentration of 1 mM and above.

Another approach to HCO_3^- recognition was reported by Fabbrizzi, based on a displacement assay.[41]

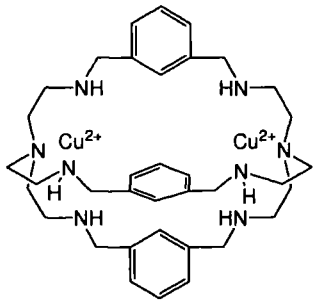

$[Cu_2L^{13}]^{4+}$

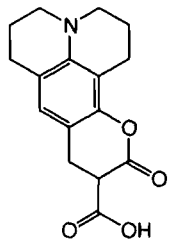

14

The dicopper(II) complex, $[Cu_2L^{13}]^{4+}$, was earlier shown to possess some selectivity for HCO_3^-, N_3^- and NCO^- in aqueous solution at pH 8. However, $[Cu_2L^{13}]^{4+}$ was limited by its low response to anion binding with indistinct changes to the absorption spectra. Research into the use of $[Cu_2L^{13}]^{4+}$ was subsequently extended by the use of coumarin 343 (**14**) to signal anion binding. At pH 7, coumarin 343 and $[Cu_2L^{13}]^{4+}$ formed a 1:1 complex in which strong coumarin fluorescence at 487 nm was completely quenched (λ_{exc}=424 nm). Upon competitive titration of the complex with HCO_3^-, N_3^- or NCO^-, the titrated anion displaced coumarin 343 and its fluorescence was completely restored. Titrations with other anions (e.g. SO_4^{2-}, HPO_4^{2-}) yielded only minor fluorescence enhancements. The coumarin 343-$[Cu_2L^{13}]^{4+}$ complex was subsequently used in the determination of HCO_3^- concentration in mineral water samples. The main disadvantage of such multi-component probes is that, for them to work, each component has to be spatially localised. This means that applications of these multi-component systems are limited to controlled assay environments.

In addition, a recent report was published of a 'sensor' that chromogenically signalled the presence of HCO_3^- in neutral aqueous solution, Figure 1.2.[42]

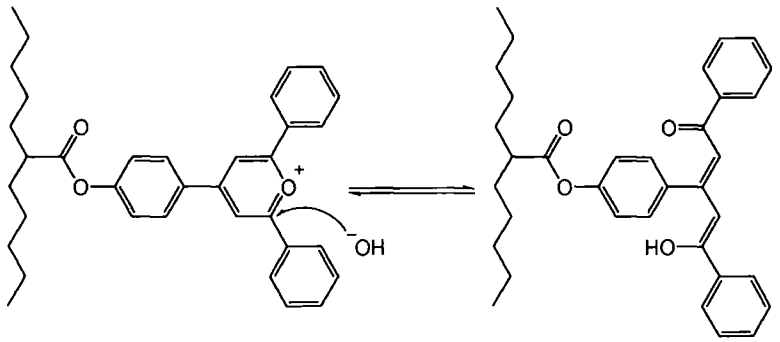

Figure 1.2 – Proposed mechanism of operation of the pyrylium-containing polymer film

The sensor was based on a pyrylium-containing polymer film that exhibited a colorimetric response to the presence of HCO_3^- in aqueous solution. Sensitivity was determined to be as low as 1 ppm from the published titration curves. The postulated mechanism of the sensor suggested that it is not based upon direct anion recognition, but is related to an acid-base reaction between HCO_3^- and H_2O. This releases OH^- that attacks, in turn, the pyrylium sensor resulting in a colour change. This suggests a huge pH dependence of the response of the sensor that may lower its range of applicability.

Zn(II) complexes that can act as HCO_3^- receptors have been used as models for the active site of carbonic anhydrase enzymes,[43–45] the aim being to more fully understand the role of the Zn(II) ion present in these proteins. Carbonic anhydrase enzymes catalyse the reversible hydration of CO_2 and dehydration of HCO_3^-, Figure 1.3.

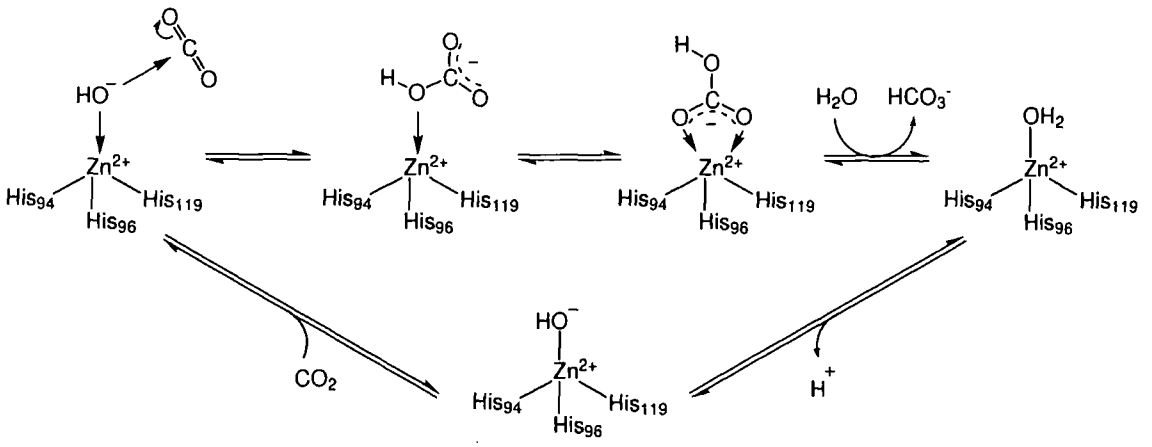

Figure 1.3 – Carbonic anhydrase catalysis of CO_2 hydration.[43]

One complex in particular, $[ZnL^{15}]^{2+}$, has proved extremely useful as the ligand provides the Zn(II) ion with a similar ligand field to that surrounding the Zn(II) ion in carbonic anhydrase.

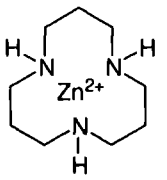

$[ZnL^{15}]^{2+}$

Studies have been carried out comparing anion recognition of Zn(II) active site model complexes and the carbonic anhydrase active site. Differences in ligand affinity and pK_a values have been used to elucidate information about the enzyme mode of action. For example, it is important to understand the role of amino acid residues surrounding the carbonic anhydrase active site in the catalytic cycle. For $[ZnL^{15}]^{2+}$ catalysed hydration of CO_2 to occur the complex has to be able to activate H_2O at physiological pH. It was found that one water molecule bound to $[ZnL^{15}]^{2+}$.[44] The pK_a value of the bound H_2O was determined to be 7.3 (25°C) and the stability constant of the hydroxide complex was log K = 6.4. Zn^{2+}-OH was a good nucleophile in the catalysis of ester hydrolysis and acetaldehyde hydration. For the enzyme, the pK_a value of Zn^{2+} bound H_2O is reported as 6.8.[43] This suggests that the carbonic anhydrase Zn^{2+}-OH complex is more stabilised than the model complex, possibly by hydrogen bonding to surrounding amino acid side chains. HCO_3^-

recognition by $[ZnL^{15}]^{2+}$ was demonstrated during its catalysis of CO_2 hydration and HCO_3^- dehydration reactions.[45] The affinity constant of Zn-HCO_3^- in carbonic anhydrase and $[ZnL^{15}]^{2+}$ was reported to be log K = 1.6 (pH 8.5) and log K = 2.8 (pH 8.4, 25°C) respectively.[43] These catalytic studies showed that the complex could mimic the action of carbonic anhydrase, and that it exhibited moderate catalytic activity. Large differences between the reactivity observed for the complex and for carbonic anhydrase unsurprisingly suggest that further factors play a role in favouring the carbonic anhydrase system. These may include effective preassociation of substrates CO_2 and HCO_3^- with the hydrophobic and hydrophilic pockets of the enzyme respectively. Binding studies of $[ZnL^{15}]^{2+}$ with various anionic species known to inhibit carbonic anhydrase catalysed HCO_3^- were carried out. Anions examined included N_3^-, NCS^- and deprotonated sulfonamides. It was concluded that inhibition was due to competitive coordination to Zn(II), however it gave experimental confirmation that other functionalities within the carbonic anhydrase active site were not involved in inhibition.[43] In conclusion, this work highlighted that even simple synthetic anion receptors can play an important role in deducing mechanistic the behaviour of complex natural analogues such as enzymes.

Amongst the earliest synthetic citrate receptors were those reported by Anslyn, who described a guanidinium based receptor that exhibited selectivity for citrate over other di-carboxylates such as succinate and glutarate.[46] Citrate was found to bind with the greatest affinity to **16** followed by **18** then **17**. Binding was monitored by ^{1}H-NMR. This suggests that preorganisation (contrast **16** and **17**) and hydrogen bonding (contrast **16** and **18**) are important in terms of complementary receptor design. **16**, in general, exhibited a binding affinity for citrate one order of magnitude greater than that of other carboxylates (10^3 M^{-1} compared to 10^2 M^{-1} in D_2O at pD 7.8). ATP^{4-} was also demonstrated to bind to **16** with a lower affinity than citrate, a result that further emphasises the need for receptor-substrate complementarity.

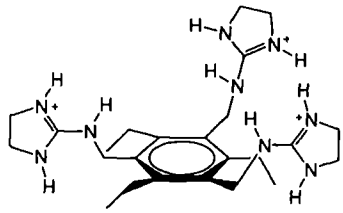

16

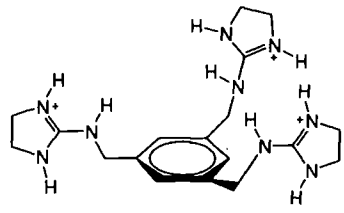

17

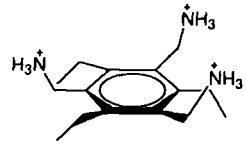

18

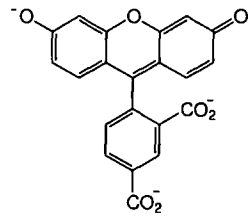

19

Despite the degree of citrate selectivity exhibited by **16**, it was also observed that high phosphate and sulfonate buffer concentrations impaired binding to the receptor. This may limit future applications of such receptors in biological media. This was exemplified in following work which combined **16** with a pH sensitive fluorophore such as carboxyfluorescein (**19**). In this case, changes in the absorption and fluorescence spectra of a complex of **16** and carboxyfluorescein were used to monitor citrate binding optically through fluorophore displacement.[47,48] Due to fluorophore pH sensitivity a buffer was needed to maintain a constant pH. This required the use of methanol:H_2O mixtures to minimize competitive buffer-receptor interactions, highlighting a disadvantage of using such pH sensitive fluorophores.

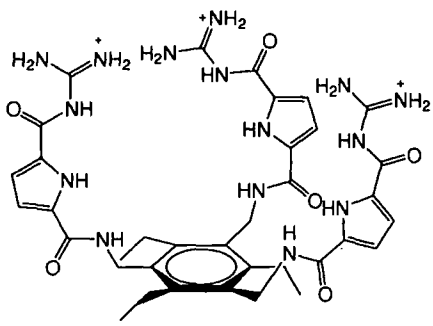

20

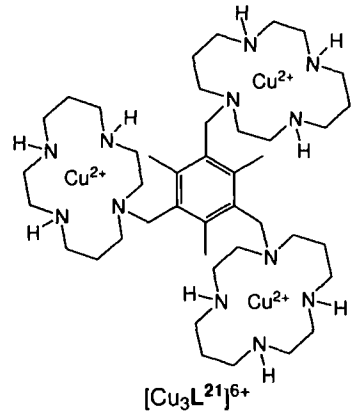

$[Cu_3L^{21}]^{6+}$

Recent work has described the further use of indicator displacement assays to monitor citrate binding to related receptors. Reports described a receptor, **20**,

similar to **16**, incorporating a guanidinium functionality.[49,50] Citrate detection is based on displacement of the receptor bound indicator carboxyfluorescein. As carboxyfluorescein is liberated from **20** fluorescence at 518 nm and 335 nm is restored. Titrations determined the binding affinity of **20** with citrate to be 1.6 x 10^5 M^{-1} (pH 6.3, H_2O). A greater than ten-fold selectivity over the closely related structures of malate and tartrate was observed. The high binding constant and selectivity of this receptor for citrate derives primarily from the greater electrostatic binding with the citrate tri-anion. Additionally, the short wavelength fluorescence of the pyrrole unit limits its use in the presence of strongly absorbing biological molecules.

Separate work based on carboxyfluorescein displacement from the copper(II) cyclam complex, $[Cu_3\mathbf{L}^{21}]^{6+}$, was also recently reported.[51] The binding affinity of this complex for citrate was determined to be log K = 5.59 (pH 7, H_2O, HEPES), compared to log K values of 4.5, 4.1 and 3.8 for malate, tartrate and succinate respectively. This is one of the highest citrate-receptor binding affinity values reported. However, despite the affinities realised and the selectivities observed, the use of dye displacement as an indicator of citrate binding is restrictive, and may be impractical in biological media due to competitive electron transfer quenching of the dyes used by protein or other reductants. In addition, no binding studies of these complexes with other common anions such as phosphates have been carried out to establish a full range of binding selectivities amongst biological anions.

1.5 Anion binding utilising Ln(III) complexes

The choice of kinetically stable chiral Ln(III) complexes based upon substituted cyclen ligands has proved to be a promising line of research in the development of synthetic anion receptors.[2,52] These Ln(III) complexes offer several features that are desirable. Ln(III) ions exhibit a high coordination number, usually 8 or 9. This allows the Ln(III) to be encapsulated by a macrocycle, such as a cyclen derivative, whilst retaining vacant coordination sites (occupied by labile solvent molecules) required for anion ligation. Anion affinity may be tuned through variation of the

Ln(III) ion and/or the macrocycle. For example, anion affinity follows the charge-density trend Yb≈Tm>Tb>Gd>Eu>>Ce. The macrocyclic ligand may be varied in numerous ways. For example, anion affinity may also be tuned by changing the electrostatic gradient around the Ln(III) ion centre, through variation of the charge carried by the ligand substituents. The steric bulk of the ligand may also be adjusted via variation of the ligand substituents.

The excited state chemistry of Ln(III) ions may be utilised to develop emissive complexes that can be used to monitor anion binding. For example, the incorporation of a suitable sensitiser into the ligand structure offers the possibility to develop highly sensitive probes (e.g. selected emission bands in the luminescence spectra of Eu(III) complexes can be used to analyse the coordination environment around the Eu(III) ion). The use of paramagnetic Ln(III) complexes facilitates structural analysis of bound anionic species by NMR, with the relationship between NMR properties of Eu(III)/Yb(III) complexes and the axial ligand proving to be a reliable means of determining the solution structure of complexes. This section will outline key points of these properties, and review recent examples of Ln(III) based synthetic anion receptors.

1.5.1 Ln(III) luminescence

The excited state chemistry of Ln(III) ions is well understood. Emission spectra contain characteristically sharp bands, Figure 1.4, due to their shielded valence $4f$ orbitals, and excited state lifetimes are long lived as ff transitions are Laporte forbidden. Owing to the forbidden nature of the ff transitions, the Ln(III) ions have low extinction coefficients. Unless the Ln(III) excited state is populated directly by an intense laser light source, unsuitable for many biological samples, sensitised emission is required, Figure 1.5.

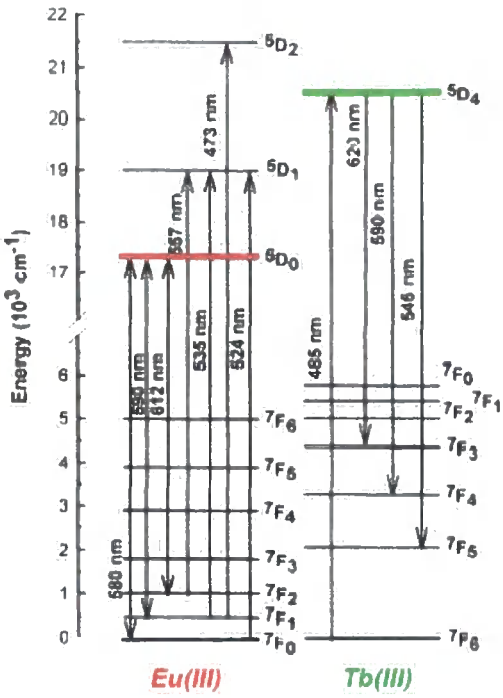

Figure 1.4 – Partial energy level diagrams for Eu(III) (left) and Tb(III) (right).

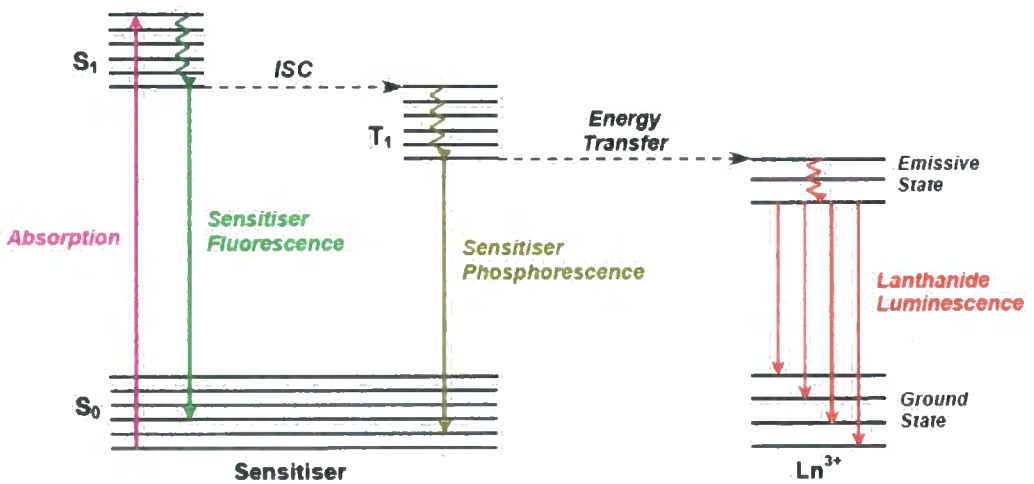

Figure 1.5 – Photochemical pathway of sensitized Ln(III) luminescence.

The properties required of a sensitiser, in order to maximise the efficiency of the sensitiser → Ln(III) energy transfer process, are well known.[53] The choice of sensitiser is greatly dependent upon the energy of the emissive state of the Ln(III) ion. A range of sensitisers that efficiently populate the excited state of Eu(III) and Tb(III) ions, encapsulated within functionalized cyclen ligands, has recently been

devised and examined in detail.[54]

Each of the excited states present in Figure 1.5 are susceptible to quenching, Figure 1.6. This results in a reduction of the quantum yield and/or radiative lifetime of the complex.

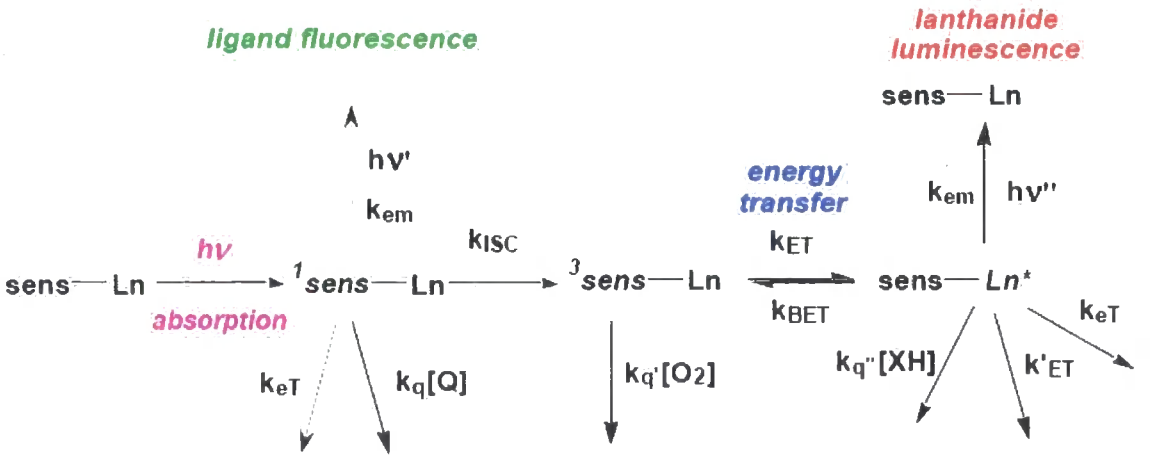

Figure 1.6 – Illustration of the sensitiser and Ln(III) excited states, showing how each may be peturbed through various deactivation processes.

Of particular importance in the aqueous phase is non-radiative deactivation of the Ln(III) excited state by energy matched XH oscillators, such as water molecule stretches and vibrations. Early work, comparing fluorescent yields and lifetimes of various Ln(III) salts, reported enhancements in their respective values when measurements were carried out in D_2O compared to H_2O.[55,56] Later work assessed the relative contributions to the deactivation of the Ln(III) excited state, by ligand NH and CH oscillators and closely diffusing solvent molecules, of a wide range of Eu(III), Tb(III) and Yb(III) complexes.[57] This allowed relationships to be established between excited state radiative decay constants, k, in H_2O and D_2O, and the degree of inner sphere hydration of the complexes. The formulation of these relationships has since been used to determine the binding mode of various anions with such complexes (e.g. monodentate or bidentate ligation), through analysis of complex hydration levels before and after anion addition.[58]

Finally, the emission spectra of Eu(III) complexes are perhaps the most informative of all the Ln(III) ions, due to the sensitivity of various transitions to the local Eu(III) coordination environment.[59,60] For example, the number of distinct Eu(III) environments ($^5D_0 \rightarrow {}^7F_0$), ligand field strength and symmetry ($^5D_1 \rightarrow {}^7F_0$) and coordination environment around the metal ($^5D_2 \rightarrow {}^7F_0$) can be deduced from analysis of the stated transitions. For this reason the Eu(III) ion is the most widely utilised Ln(III) ion in synthetic anion receptors reported so far. Correlations between structural and electronic spectral information for Ln(III) complexes of derivatised cyclen ligands are discussed below.

1.5.2 Ln(III) NMR properties

All the Ln(III) ions, apart from La^{3+} (f^0) and Lu^{3+} (f^{14}), possess unpaired electrons. Any NMR active nuclei within close proximity to the Ln(III) ion will experience the fluctuating magnetic field induced by its unpaired electrons. This leads to the broadening of the nuclei resonant signal due to the enhancement of the longitudinal and transverse relaxation rates (T_1 and T_2 respectively). Due to the asymmetric distribution of electrons of the Ln(III) ions, a shift of the nucleus resonant frequency may occur, the exception being Gd(III). The paramagnetic properties of these ions have found valuable uses either as NMR shift reagents or as probes for protein calcium binding sites.[61,62]

For the nuclei of a ligand coordinated to a Ln(III) ion, there are three contributions to the lanthanide induced shift (LIS, Δ), the diamagnetic (Δ_d), contact (Δ_c) and pseudocontact (Δ_p) shifts.[63]

$$\Delta = \Delta_d + \Delta_c + \Delta_p \qquad \text{(eqn. 1)}$$

The contribution of the diamagnetic shift, originating from conformational and inductive effects, is usually small enough to be neglected except for nuclei directly coordinated to the Ln(III) ion. Contact shifts arise from a 'through-bond' transmission of Ln(III) ion unpaired electron density to the bound nucleus. The contact shift contribution is normally huge for a bound nucleus but decreases rapidly as the

number of bonds between the Ln(III) ion and the nucleus increases, hence facilitating the identification of any Ln(III) bound nuclei. The pseudocontact (dipolar) shift results from a through space interaction between the magnetic moments of the unpaired electrons of the Ln(III) and the nucleus in question. The pseudo-contact contribution usually dominates as unpaired electron spin density resides mainly on the Ln(III) ion. The magnitude of the dipolar shift is dependent on the geometric position of the resonating nucleus with respect to the Ln(III) ion, allowing useful structural information to be obtained from analysis of the LIS.

Each of the Ln(III) ions possess differing electronic configurations, electronic magnetic moments and electronic relaxation times, so therefore behave differently under NMR conditions. The choice of which Ln(III) ion to use as a shift reagent is a balance between the shifting ability of the ion and the extent of associated line broadening. In the development of synthetic anion receptors, Eu(III) and Yb(III) ions have proved particularly useful as they offer informative spectra due to a good balance between these two factors. In fact, it has been shown that with well defined Ln(III) complexes, the magnitude of selected paramagnetically shifted ligand proton resonances provides a clear indication of the local coordination environment of the Ln(III) ion (i.e. allowing correlations between the shift of the selected ligand resonance and the nature of ligating anion to be made).[64-66] The following section will discuss such correlations in relation to coordinatively unsaturated Eu(III) and Yb(III) complexes of substituted cyclen ligands.

1.5.3 Ligand structure

In order for the solution state characterisation of any synthetic receptor and resultant adduct to be relatively simple it is desirable that the receptor and adduct exist as one major isomer in solution. The solution isomerism of Ln(III) complexes based upon the DOTA ($\mathbf{L}^{22}$) ligand and further chiral derivatives is well understood and has been recently reviewed.[63]

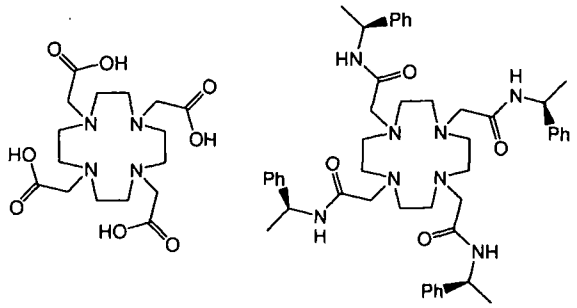

22 23

Conformational isomerism exhibited by Ln(III) complexes of substituted cyclen ligands may be related to two independent exchange processes. These are rotation of the pendant arms clockwise (Δ) or anticlockwise (Λ), and the two conformations that may be adopted by the ring where the NCCN torsion angle is either positive ($\delta\delta\delta\delta$) or negative ($\lambda\lambda\lambda\lambda$). In theory, this results in 4 possible isomers (Figure 1.7).

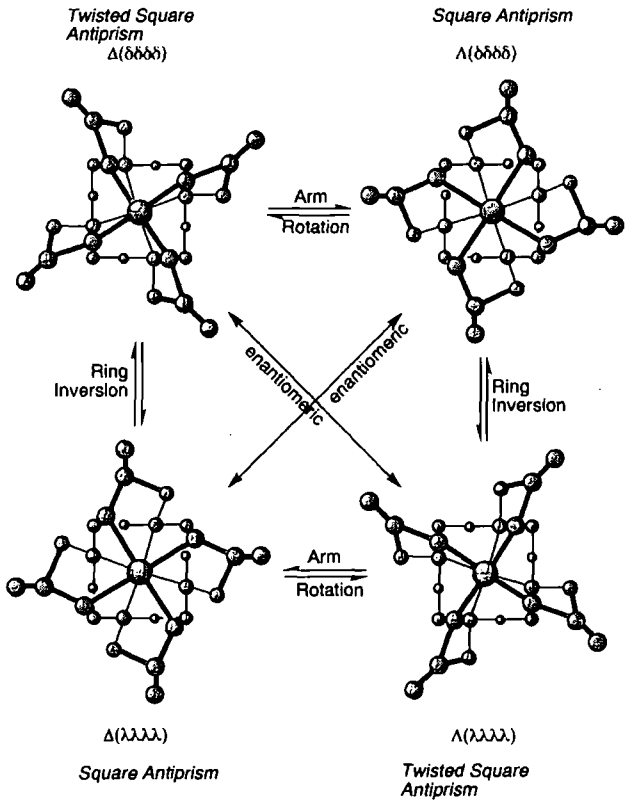

Figure 1.7 – Schematic of the four possible stereoisomers of $[LnL^{22}]^-$ (and related tetraamide complexes) and route of interconversion.[67]

With ligands such as DOTMPhA ($\mathbf{L}^{23}$), each isomer is rendered diastereomeric due to the chiral centre δ to the ring nitrogen. The considerable conformational rigidity

imparted by this remote chiral centre inhibits arm rotation and results in the exclusive formation of only one of the diastereomers in solution. The helicity of the amide arms and the macrocyclic ring conformation is determined by the configuration at the chiral centre, resulting in square anti-prismatic geometries ($\Delta(\lambda\lambda\lambda\lambda)$ and $\Lambda(\delta\delta\delta\delta)$ for S and R configurations respectively).[68,69]

The relative simplification of spectral analysis of Ln(III) complexes, such as those of DOTMPhA, due to the presence of a single isomer, facilitated work into the effect of the axial ligand of such complexes on their magnetic and electronic properties.[65,70] This work has shown that for Eu(III) and Yb(III) complexes, the second order crystal field coefficient, B_o^2, sensitive to the polarisability of the axial ligand, determines the dipolar NMR shift; a conclusion also verified for complexes lacking a C_n axis.[64] For these complexes, selected ligand resonances for which the shift is purely dipolar, e.g. the most shifted axial macrocyclic proton H-4 (Figure 1.8), can be used as a reliable probe for local magnetic anisotropy and hence complex solution structure.

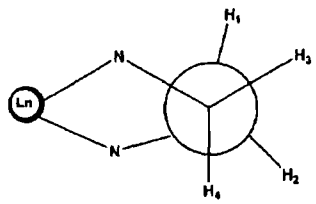

Figure 1.8 – A view along the cyclen ethylene C-C bond showing the relative orientations of the protons including orientation of the paramagnetically shifted axial H_4 proton[65]

In accordance with theoretical ideas,[71] this work also concluded that for Eu(III) complexes the ratio of the integrated emission intensities for the ΔJ=2/ΔJ=1 spectral bands correlates with axial ligand polarisability. The relative intensity of the magnetic-dipole allowed ΔJ=1 transition is insensitive to changes in coordination environment whilst the intensity of the electric-dipole allowed ΔJ=2 transition considerably changes with axial ligand variation.

The role of the axial ligand field has recently been defined: 'the more polarisable

the axial donor the smaller the dipolar NMR shift - and the greater the affinity of that axial donor for the lanthanide ion'.[65]

1.6 Ln(III) based anion probes

1.6.1 Ln(III) probes for phosphorylated anions

Early work with Eu(III) complexes of $\mathbf{L}^{24}$, and related ligands, established that inorganic phosphate bound to these systems with an affinity constant of log K = 4.15 (295 K, pH 7.4, collidine buffer).[58]

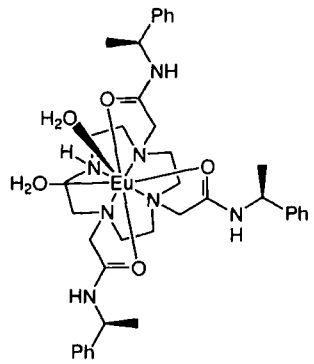

$[EuL^{24}]^{3+}$

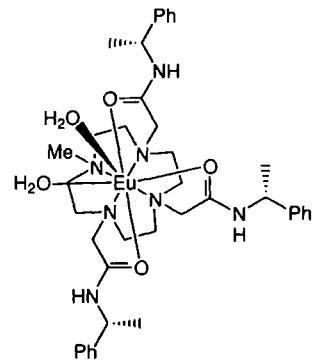

$[EuL^{25}]^{3+}$

These encouraging early results led to binding studies of a variety of phospho-anions with similar Ln(III) complexes.[66,72,73] The binding of *O*-phosphorylated amino acids to the complexes $[LnL^{24}]^{3+}$ (Ln = Tm(III), Yb(III) and Eu(III)) were monitored by NMR, and to complexes $[EuL^{26}]^{3+}$, $[EuL^{27}]$ and $[EuL^{28}]^{3-}$ by luminescence measurements, at physiological pH. The NMR measurements revealed that amino acid chelation competed with phosphate ligation for complexes of the more charge dense metals, e.g. Tm(III) and Yb(III). However, for the corresponding Eu(III) complex only phosphate ligation was observed (Figure 1.9). Binding was monitored by the mean shift of the 'pseudo-axial' proton of the macrocyclic ligand, as detailed in section 1.5.3. In addition, the chelated binding modes of amino acids and dipeptides, with the Yb(III) complex, had been previously observed.[74] This work correlated axial proton NMR shifts with X-ray structures of amino acid adducts to identify solution state isomers.

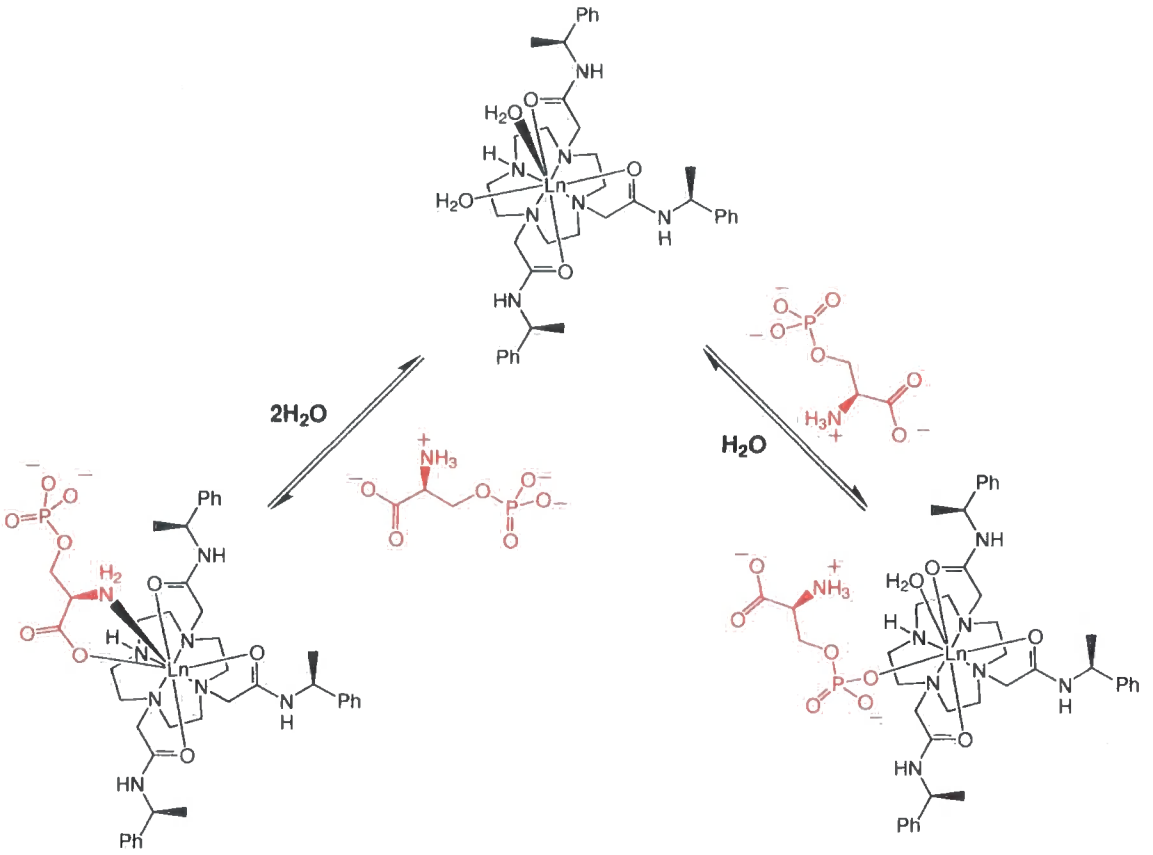

Figure 1.9 – When Ln = Yb(III) or Tm(III), amino acid chelation competes with phosphate ligation (typically in a 1:3 ratio); when Ln = Eu(III), only phosphate ligation is observed. pH 7.4, 295 K.[66]

Identical *O*-phosphorylated amino acid binding studies with Tm(III) and Yb(III) complexes of the *N*-methylated ligand, $\mathbf{L}^{25}$, revealed that amino acid chelation became the dominant binding mode in a 4:1 ratio. The conclusion reached was that the free energy of hydration of these complexes is reduced, hence favouring the closed nature of the chelated binding mode. The most interesting observation of these NMR studies was an unprecedented selectivity for $(O\text{-P-Tyr})^{2-}$ over $(O\text{-P-Ser})^{2-}$ of approximately 30:1, observed in competitive binding studies with complexes of $\mathbf{L}^{24}$. This selectivity was probed further in luminescence studies with Eu(III) complexes of $\mathbf{L}^{26}$, $\mathbf{L}^{27}$ and $\mathbf{L}^{28}$.

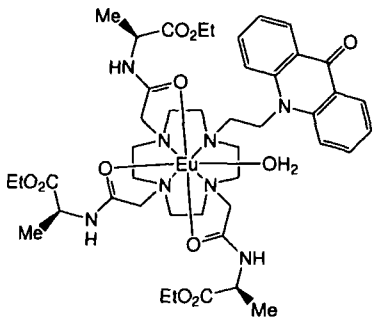

$[EuL^{26}]^{3+}$

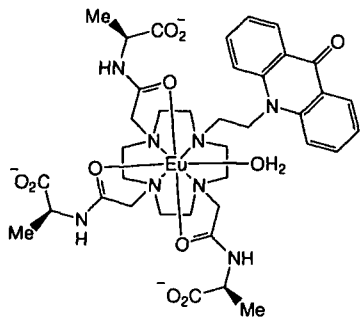

$[EuL^{27}]$

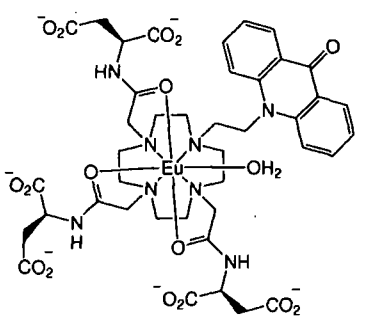

$[EuL^{28}]^{3-}$

It was observed that the luminescence spectra for $(O\text{-P-Tyr})^{2-}$ adducts differed to that of $(O\text{-P-Ser})^{2-}$ adducts; notably in the relative intensities of the ΔJ=1 and ΔJ=2 bands. Values of log K for the binding of $(O\text{-P-Ser})^{2-}$ and $(O\text{-P-Tyr})^{2-}$ to [Eu**L**^{27}] were reported as 2.7 and 4.2 respectively (295 K, pH 7.4, 0.1 M MOPS, 5 mM $NaHCO_3$). This chemoselectivity was also conserved with phosphorylated $(O\text{-P-Ser})^{2-}$ and $(O\text{-P-Tyr})^{2-}$ residues of various hexapeptides, and was retained in the presence of protein (HSA, 0.35 mM) and background bicarbonate (5 mM). The greater chemoselectivity for $(O\text{-P-Tyr})^{2-}$ was attributed to its lesser degree of hydration in aqueous media.

A 1:1 complex of Tb(III) with esculetin (**29**) was recently demonstrated to report on the presence of O-phosphorylated amino acids and the phosphorylated residue of a peptide, but not on the presence of non-phosphorylated analogues.[25]

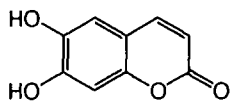

29

The complex had a λ_{max} of 465 nm (λ_{exc} = 405 nm), attributed to ligand fluorescence, whilst no Tb(III) emission was observed. It was reported that, at pH 7.0, ligand fluorescence increased by up to 50% in the presence of O-phosphorylated amino acids and phospho-peptide, whilst fluorescence remained unperturbed in the presence of non-phosphorylated analogues. Whilst respectable limits of detection of between 5.1-21.8 μM for the O-phosphorylated amino acids and phospho-peptide

were reported, there was no discussion regarding the utility of the probe in the presence of competing anions.

Recent work has probed the interactions of several Eu(III) and Tb(III) complexes with various phosphates, with the aim of achieving selective binding of specific nucleoside polyphosphates in the presence of competing phosphorylated species and nucleotides.[75–77]

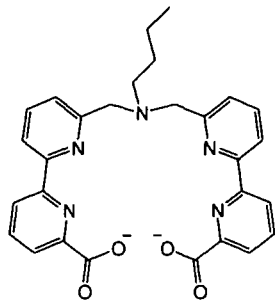

30

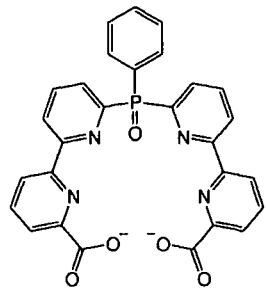

31

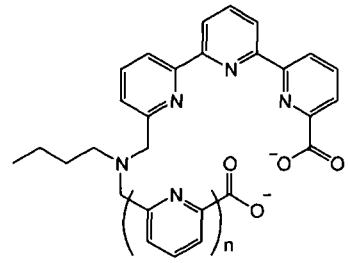

32; n = 1
33; n = 2
34; n = 3

The complex $[EuL^{30}]^{+}$ was reported to possess selectivity for ATP^{4-} (log K = 4.3, H_2O, pH 7.0, TRIS/$HClO_4$ 0.01 M buffer) compared to ADP^{3-} and AMP^{2-}, however a sensitivity towards inorganic phosphate (log K = 4.2, H_2O, pH 7.0, TRIS/ $HClO_4$ 0.01 M buffer) was also observed, as was the weak stability of the complex at submicromolar concentrations. The adduct formed on binding to anions was postulated to possess a ligand bipyridyl arm that was more weakly complexed to the metal as a result of direct phosphate-Ln(III) coordination. This resulted in a hypsochromic shift in the absorption spectra and a concomitant decrease in luminescence intensity.[75,76] Ligand L^{31} was synthesised in order to form more stable Ln(III) complexes.[76] The authors anticipated that the increased stability of resultant complexes would result in their exclusive binding to only the most negatively charged anion of the phospho-nucleotides studied, ATP^{4-}. However, luminescence titrations of $[EuL^{31}]^{+}$ with various anions revealed a loss in selectivity for ATP^{4-} as observed for $[EuL^{30}]^{+}$. Instead, strong binding to ADP^{3-}, ATP^{4-} and $HPO_4{}^{2-}$ was observed (log K = 5.5, 5.5 and 5.2 respectively, H_2O, pH 7.0, TRIS/HCl 0.01 M buffer), but not to AMP^{2-}.

Similar binding studies with a further series of ligands was reported recently ($\mathbf{L}^{32}$-$\mathbf{L}^{34}$).[77] $[Eu\mathbf{L}^{33}]^{+}$ selectively reported the presence of ATP^{4-} in aqueous solution, but not AMP^{2-}, ADP^{3-} and $HPO_4{}^{2-}$. Binding was monitored through emission and absorption spectra, results were consistent with displacement of the terpyridyl arm upon ATP^{4-} binding. No quantitative analysis of binding was possible due to the weakness of the spectroscopic changes observed. Binding studies with $[Eu\mathbf{L}^{32}]^{+}$ suggested that there was no interaction with any anion, whilst $[Eu\mathbf{L}^{34}]^{+}$ showed interactions with ADP^{3-}, ATP^{4-} and $HPO_4{}^{2-}$. For this complex, quantitative analysis of binding was again not possible, apart from with ATP^{4-}, where an upper limit of the association was estimated to be $1.5 \times 10^3\ M^{-1}$. In conclusion, early work with $[Eu\mathbf{L}^{30}]^{+}$ revealed promising selectivity for an important class of phospho-anions. However, it appears this selectivity did not carry through in the synthesis of the more stable complex, $[Eu\mathbf{L}^{31}]^{+}$. Later work with $[Eu\mathbf{L}^{33}]^{+}$ again identified possible selectivities, though reported interactions and responses were weak. Such interactions need strengthening then evaluating in a competitive environment before such complexes can be used as probes in biological media.

A different approach to achieve selective reporting on pyrophosphate in the presence of competitive anions such as ATP^{4-} and ADP^{3-} was recently demonstrated.[78] The series of Eu(III) probes reported in this work based their reporting of anion binding on competitive displacement of their β-diketone ligands acting as Eu(III) sensitisers. Anion selectivity was tuned by the relative affinities of the ligands and anions for the metal ion.

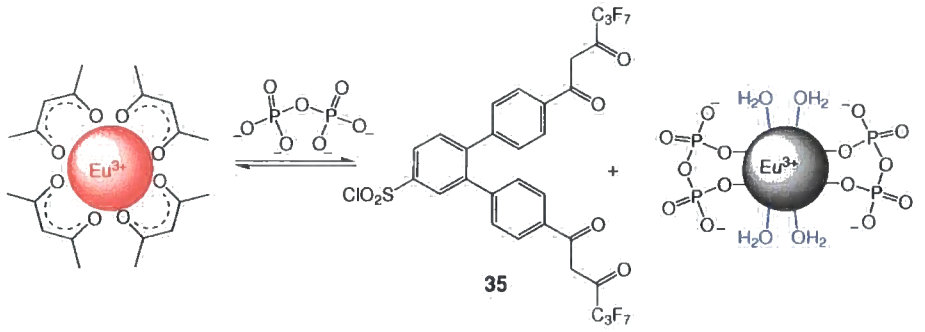

Figure 1.10 – $\mathbf{L}^{35}$ and a schematic representation highlighting the pathway of reduction in Eu(III) emission intensity through displacement of the β-diketone ligands.[78]

$[Eu(\mathbf{L}^{35})_2]^{3+}$ was used to monitor the hydrolysis of pyrophosphate by pyrophosphatase. The quenched luminescence of $[Eu(\mathbf{L}^{35})_2]^{3+}$ was restored as pyrophosphate was hydrolyzed. This highlighted a practical use of such a probe, but also demonstrated that such displacement systems will only work with anions of higher affinity than the ligand. This typically restricts these probes to detection of anions of highest negative charge and therefore highest affinity.

1.6.2 Ln(III) probes for citrate and bicarbonate

To date, only one Ln(III) probe which is chemoselective for citrate has been reported. $[Eu\mathbf{L}^{36}]^{3+}$, reported by Parker in 2005. It is based on a heptadentate cyclen ligand, with a coordinated azathioxanthone sensitising moiety[79] increasing the steric demand at the metal centre.

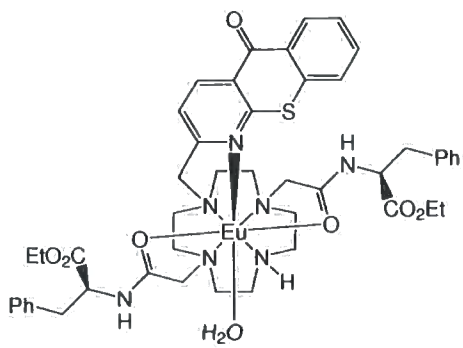

$[Eu\mathbf{L}^{36}]^{3+}$

Ratiometric analysis of citrate concentrations in the presence of a mixed background of endogenous anions was achieved through analysis of the changes to the ratio of

the $\Delta J=2/\Delta J=0$ bands of the Eu(III) emission. The affinity of $[EuL^{36}]^{3+}$ for citrate at pH 7.4 was determined to be 3.7 x 10^3 M^{-1} in the presence of competing anions. The emission intensity of $[EuL^{36}]^{3+}$ also remained constant between the pH range of 7 and 8.2, and the $\Delta J=2/\Delta J=0$ ratio remained constant over a wider range. The affinity and chemoselectivity of $[EuL^{36}]^{3+}$ for citrate is probably related to both a strong Coulombic interaction between the two species and the postulated chelated binding mode of citrate involving the α-hydroxy group and adjacent carboxylate. The binding of malate and tartrate were reported to yield similar limiting emission spectra to that of citrate, but only at much higher concentrations. Therefore, such affinity and chemoselectivity as offered by $[EuL^{36}]^{3+}$ demonstrates that selective anion recognition in biological media can be achieved, and makes the possibility of anion sensing *in cellulo* much more feasible.

HCO_3^- concentrations have been selectively monitored using ratiometric methods, in work similar to that described above.[80]

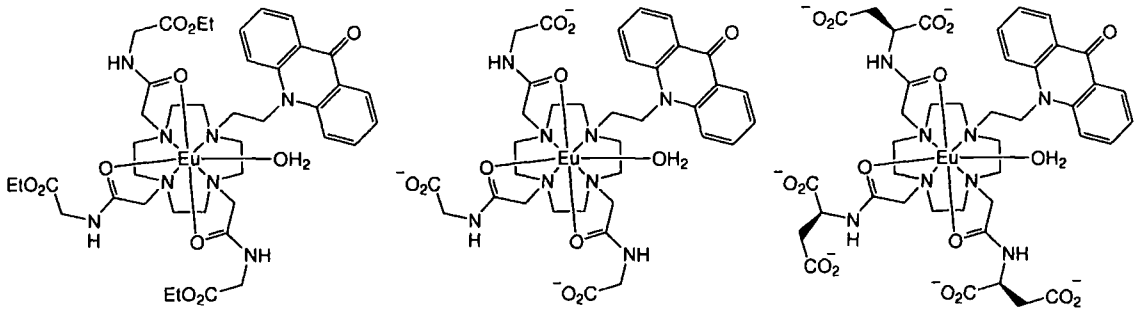

A series of cationic, neutral and anionic Eu(III) complexes was analysed, $[EuL^{37}]^{3+}$, $[EuL^{38}]$ and $[EuL^{28}]^{3-}$ are representative examples of the series studied. Overall complex charge was modulated through permutation of the cyclen pendant arms. Binding of the bicarbonate anion to the complexes could be monitored through changes to the ratios of the $\Delta J=2/\Delta J=1$ or $\Delta J=2/\Delta J=4$ Eu(III) emission bands. The work demonstrated that HCO_3^- concentrations could be selectively monitored in aqueous solutions (pH 7.4), in the presence of a background of competing anions. The greatest affinity for HCO_3^- was observed, unsurprisingly, with cationic

complexes followed by neutral then anionic complexes. Affinity constants of complexes in competitive media were measured and the highest observed value was with $[EuL^{37}]^{3+}$, whilst other affinity constants decreased as complex negative charge increased, Table 1.2.

Complex	Log *K*
$[EuL^{37}]^{3+}$	2.27
$[EuL^{38}]$	1.28
$[EuL^{28}]^{3-}$	0.99

Table 1.2 - Apparent affinity constants for complexation of HCO_3^- (295 K, 0.1 M MOPS, pH 7.4; 100 mM NaCl, 2.3 mM sodium lactate, 0.9 mM Na_2HPO_4, 0.13 mM potassium citrate).[80]

Additionally, several of the complexes studied were also examined in cellular media and in cellular uptake experiments. A clear response of the complexes in cellular lysate to added HCO_3^- (3 - 20 mM) was observed. The complexes were taken up into the cellular environment of NIH 3T3 cells and exhibited defined localisation. The complexes were reportedly non-toxic to the cells over a 3 h incubation period. It can be envisaged that such complexes could be used to report upon HCO_3^- concentrations in targeted organelles by read-out of the relative intensities of Eu(III) emission bands. In addition, binding was selective at HCO_3^- concentrations found in the cellular environment, placing the response of the complexes at an optimal level.

1.6.3 Other Ln(III) anion probes

Other recent examples of Ln(III) based anion probes include those reported by Gunnlaugsson. One approach is based on competitive ligation to $[EuL^{39}]^{3+}$.[81]

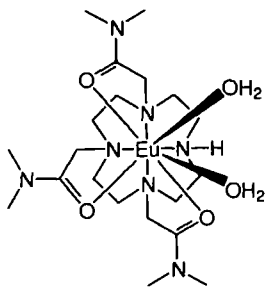

$[EuL^{39}]^{3+}$

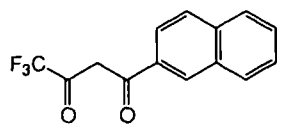

40

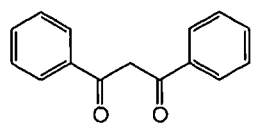

41

In this case, at pH 7.5, the aromatic β-diketonate (**40**) ligates to $[EuL^{39}]^{3+}$ and can act as a sensitiser for Eu(III) emission. Other β-diketonate ligands, such as **41**, were found not to act as a sensitiser of $[EuL^{39}]^{3+}$ emission. It was shown that upon addition of certain anions (e.g. lactate, HCO_3^-, acetate, fluoride) to a solution of the initial adduct displacement of the β-diketonate sensitiser occurred and Eu(III) emission was 'switched off'. This early communication did not report any observed anion selectivities or affinity constants. Like the displacement systems described earlier, the decreasing luminescence of the complex upon increasing anion concentrations is not ideal for a probe. Issues such as signal to noise ratio at higher anion concentrations will reduce its sensitivity. In addition, in a biological environment such probes could relay no information on the time dependence of local anion concentrations due to emission being switched off upon anion binding.

Other work by Gunnlaugsson developed trimetallic lanthanide luminescent complexes as anion probes bearing an internal reference channel.[82] The complex possessed one cyclen unit and two 1-aza-18-crown-6-ether units, allowing up to three metal ions to be complexed. One system was synthesised containing two Tb(III) cations and one Eu(III) cation, $[EuTb_2L^{42}]^{9+}$.

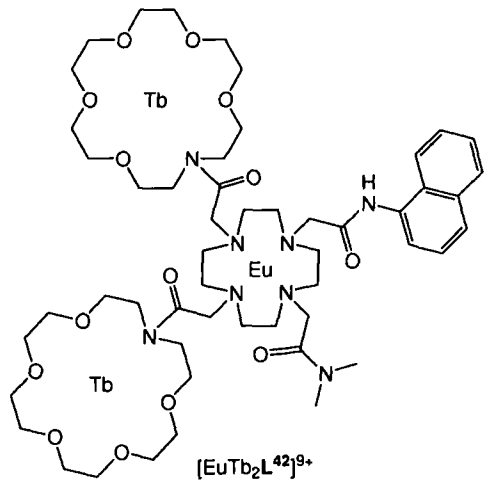

Binding of malonate to the complex was studied through changes to metal based emission. Upon anion binding, the observed enhancement of Eu(III) emission was much greater than the concomitant decrease in Tb(III) emission, allowing Tb(III)

emission to be used as an internal reference channel. It was postulated that the anion bound at the cyclen encapsulated Eu(III) centre, with formation of a 1:1 complex:anion adduct formed at low anion concentrations, whilst a 1:2 adduct was observed at high anion concentrations. Such multi-metallic luminescent systems may seem uneccesarily complicated in the quest for ratiometric analysis, when it could be achieved through analysis of Eu(III) emission alone, as observed with previously mentioned complexes.

1.7 Summary

It is interesting to note the opinion of other scientists working in the field of aqueous phase Ln(III) based anion probes. Most strikingly, a recent article stated '....it is doubtful that europium probes can be used to quantify the concentration of ATP (or any of the other analytes listed above) in complex biological samples. Rather, their applications are limited to situations in which the specificity of the probe is not crucial and the amount of interferences can be minimized.'.[83] The 'other analytes' referred to includes citrate, amino acids and HCO_3^-, amongst others. This statement was made in a report detailing the use of a Eu(III) tetracycline complex, as a non-selective fluorescent probe in controlled assay environments, in determining the activity of kinase enzymes.

Whilst achieving selective anion binding in aqueous media is difficult, and the intricacies of this task should not be understated, the pessimism of Schäferling and Wolfbeis is probably undue at this early stage in the development of Ln(III) based anion recognition. There are important examples of selectivity having been achieved, or at least steady progress towards this goal. Because of these early foundations, the selective recognition and monitoring of certain essential anionic species, in the cellular environment and in real time, is very close to being achieved.

The work presented in the following chapters explores the utility of several Ln(III) complexes as selective probes for anionic species. This work has focussed on the de-

velopment of novel sensitised Ln(III) complexes, the development of dimeric Ln(III) complexes and the immobilisation of Ln(III) complexes on solid supports. Examinations of the probes *in vitro* and *in cellulo* have been carried out. These results will be reported and discussed.

Chapter 2

Anion binding studies with luminescent Ln(III) complexes

2.1 An initial luminescence binding study

As outlined in section 1.6.1, early anion binding studies with complexes of $[LnL^{24}]^{3+}$ and related ligands observed a binding selectivity for the inorganic phosphate anion, even when in the presence of a background of competing anions and protein. Further studies, examining the relative affinities of $[LnL^{24}]^{3+}$ complexes for a series of phospo-anions, reported an unprecedented selectivity for $(O\text{-P-Tyr})^{2-}$ over $(O\text{-P-Thr})^{2-}$ and $(O\text{-P-Ser})^{2-}$. This was conserved when the residues were present in small peptides. In addition, a competitive chelated binding mode (Figure 1.9) observed during binding studies with the more charge dense lanthanides (Yb(III), Tm(III)) was not observed when $[EuL^{24}]^{3+}$ was examined.

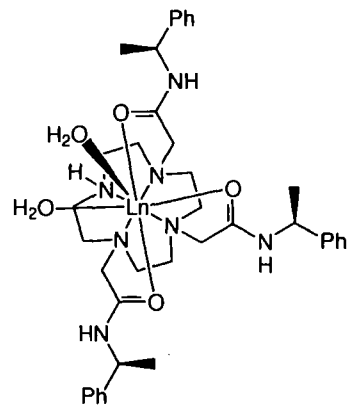

$[LnL^{24}]^{3+}$

The behaviour of $[EuL^{24}]^{3+}$ encouraged further selectivity experiments with this

complex. Recent work examined the binding of $[EuL^{24}]^{3+}$ to a peptide, the insulin receptor fragment 1154-1165, containing three tyrosine residues.[73] Binding analysis of $[EuL^{24}]^{3+}$ was carried out with three peptides of differing states of phosphorylation (**43b-d**) and the 'parent' non-phosphorylated peptide (**43a**). It was hypothesised that due to the chemoselectivity of $[EuL^{24}]^{3+}$ for $(O\text{-P-Tyr})^{2-}$ residues, the regioselectivity of complex binding on **43d** would be determined by local electrostatic contributions from the peptide.

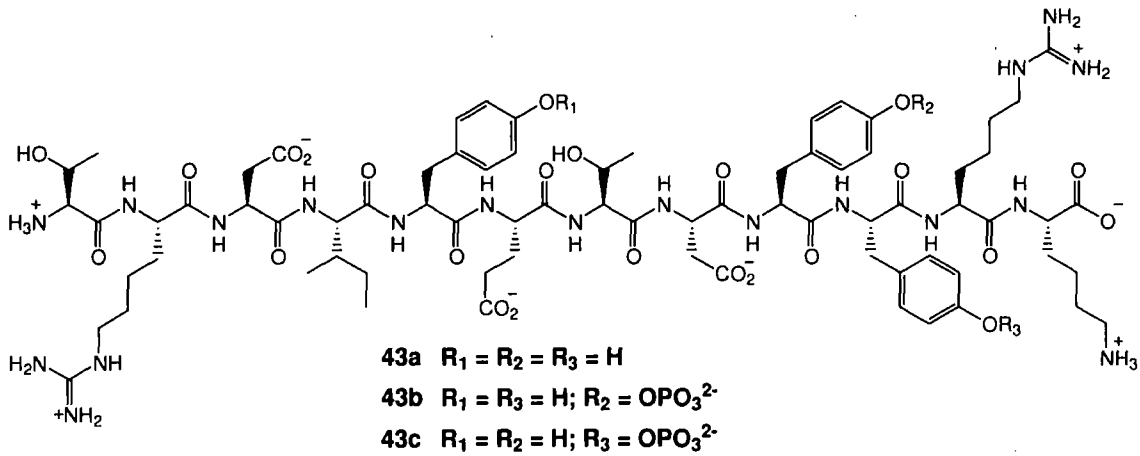

This work established that following addition of $[EuL^{24}]^{3+}$ to each phosphopeptide a phosphate-bound ternary adduct was formed. Upon complex-peptide binding, amino acid nuclei in close proximity to the phosphate binding site undergo dipolar coupling to the unpaired electrons of the Eu(III) ion resulting in a paramagnetic shift. Due to the modest magnetic anisotropy of Eu(III) the distance over which paramagnetic shifts are observed is small (<10Å). Comparison of the ^{1}H-NMR TOCSY spectra of the various peptides before and after addition of $[EuL^{24}]^{3+}$ enabled the assignment of amino acid resonances that were previously undetermined based upon the analysis of the peptide NMR alone. A modest binding preference of $[EuL^{24}]^{3+}$ for $(O\text{-P-Tyr})^{2-}$ at residue 9 of the triphosphorylated peptide (**43d**) was observed. The binding preference can be explained by local coulombic attraction and repulsion within the peptide, with respect to the phosphorylated residues.

To complement the NMR studies described above, emission spectra of $[EuL^{27}]$

were recorded in the presence of peptides **43a** and **43c**, Figure 2.1. The Eu(III) emission spectrum of [Eu$\mathbf{L}^{27}$] with the non-phosphorylated peptide **43a** was identical to that of the complex on its own, but very different to that observed in the presence of $(O$-P-Tyr$)^{2-}$.

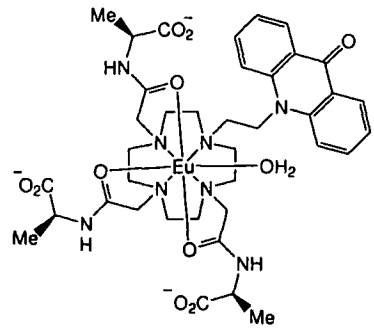

[EuL^{27}]

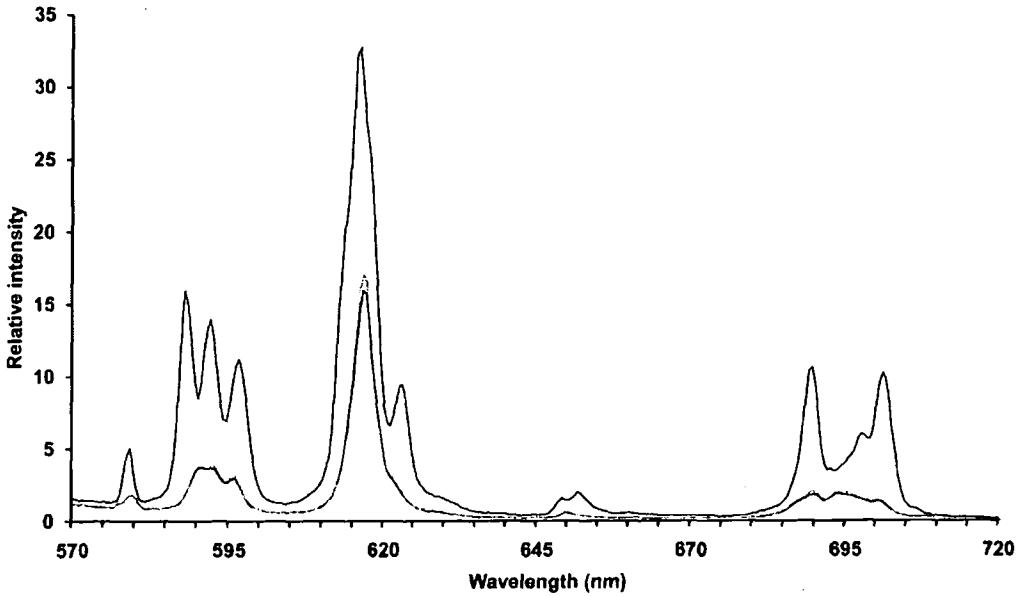

Figure 2.1 – Europium emission spectra for [Eu$\mathbf{L}^{27}$] (50μM) (lower, black), [Eu$\mathbf{L}^{27}$] & **43a** (50μM/100μM) (lower, grey) and [Eu$\mathbf{L}^{27}$] & $(O$-P-Tyr$)^{2-}$ (50μM/100μM) (top). pH = 7.4, 0.1 M MOPS buffer, λ_{exc} = 408 nm.

The emission spectrum of [Eu$\mathbf{L}^{27}$] in the presence of phosphopeptide **43c** was similar to that of [Eu$\mathbf{L}^{27}$] in the presence of $(O$-P-Tyr$)^{2-}$, Figure 2.2. The similarity of the splitting pattern of the three bands of the magnetic-dipole allowed ΔJ=1 manifold at ~590 nm, as well as the analogous form and relative intensity of the hypersensitive

ΔJ=2 and ΔJ=4 transitions at ~616 and ~695 nm respectively provide a clear indication of the similarity of the environment around the Eu(III) ions in each adduct. This is consistent with selective binding of the complex to the phospho-anion site of **43c** and consequently confirms the weak binding of [Eu$\mathbf{L}^{27}$] to **43a**.

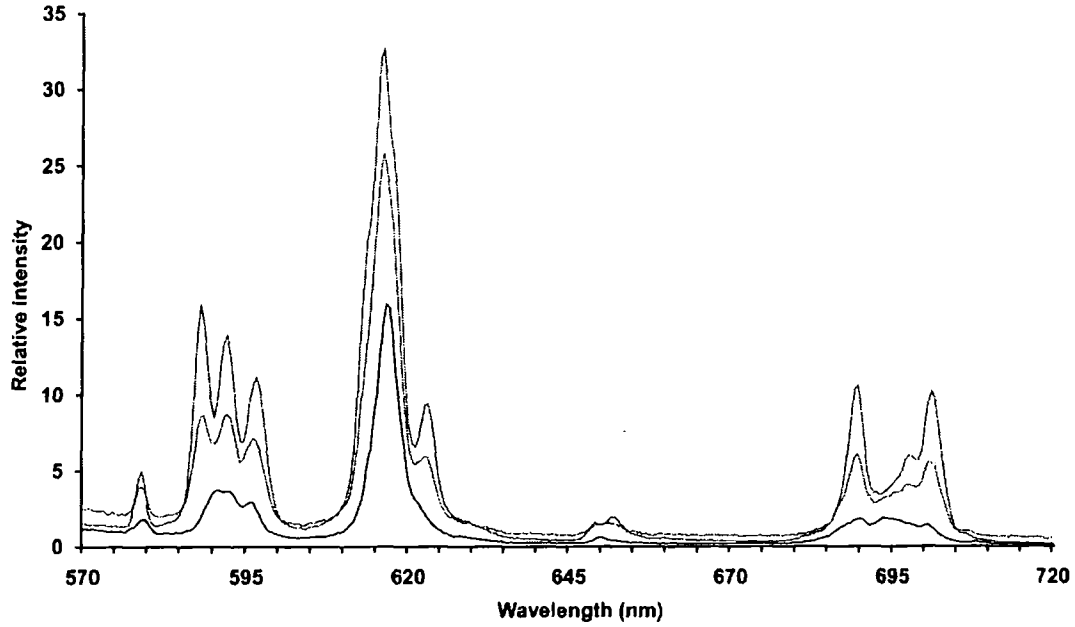

Figure 2.2 – Europium emission spectra for [Eu$\mathbf{L}^{27}$] (50μM) (lower), [Eu$\mathbf{L}^{27}$] & **43c** (50μM/100μM) (centre) and [Eu$\mathbf{L}^{27}$] & (*O*-P-Tyr)$^{2-}$ (50μM/100μM) (top). pH = 7.4, 0.1 M MOPS buffer, λ_{exc} = 408 nm.

This work provides further confirmation that [Eu$\mathbf{L}^{24}$]$^{3+}$ binds to the phosphorylated peptides (**43b-43d**) via the phosphate functionality only. It can therefore be established that the paramagnetically shifted resonances observed in the peptide ^{1}H-NMR TOCSY originate only from nuclei in close proximity to phosphate binding sites. As described above, the comparison of the peptide ^{1}H-NMR TOCSY spectra before and after addition of the complex enabled the correlation of shifted resonances with specific amino acid residues of the peptide that were undetermined, based upon the analysis of the peptide spectra alone. The complex [Eu$\mathbf{L}^{24}$]$^{3+}$, has therefore been shown to serve as a chemoselective paramagnetic probe that targets phospho-tyrosine sites in phosphorylated peptides, allowing such complexes to be considered as prototypical chemoselective paramagnetic derivatising agents.[84]

2.2 Novel sensitised Ln(III) complexes

The design and synthesis of novel Ln(III) complexes originated from the above mentioned work and phosphate[66,72,73] and citrate[79] binding studies, as outlined in sections 1.6.1 and 1.6.2 respectively. The structures of the new ligands were designed with previous ligands in mind. A key feature was the retention of certain structural features essential in defining anion binding preferences of complexes. The rationale behind the design and synthesis of these ligands will be discussed in this section.*

2.2.1 Design and synthesis of analogues of $[EuL^{24}]^{3+}$

Following the successful use of $[EuL^{24}]^{3+}$ as a phospho-anion probe in NMR studies, it was decided to synthesise a structurally related complex incorporating a sensitising moiety into the ligand structure (L^{44a}). This allows sensitised emission of the Eu(III) ion to be used to monitor anion binding events. It was essential that the synthesised complex $[EuL^{44a}]^{3+}$ should possess a high degree of structural homology to that of $[EuL^{24}]^{3+}$, in order to retain the favourable binding preferences and affinities with target anions.

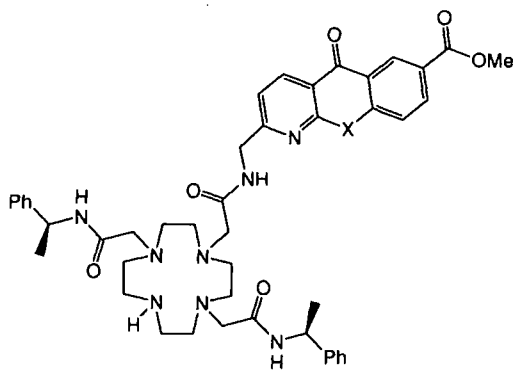

44a (X = O)
44b (X = S)

The structure of the proposed complex retains the N_4O_3 coordination environment around the Ln(III) ion, as in $[EuL^{24}]^{3+}$. Only the peripheral segment of one amide arm was modified to incorporate the azaxanthone sensitiser. The fourth ring *N*-atom was left unsubstituted. In previous work it had been observed that *N*-methylated

* All complexes synthesised in this chapter were isolated and analysed as their chloride salts, except $[GdL^{44b}]^{3+}$ which was isolated and analysed as its acetate salt. $[EuL^{52}]^{3+}$ was analysed as its triflate salt.

complexes tend to favour chelated structures over phosphate-bound adducts.[66] The azaxanthone sensitiser was chosen following earlier work that established the suitability of these chromophores for sensitising Eu(III) and Tb(III) emission.[54] In addition, the carboxymethyl substituent of the azaxanthone provides a functionality through which further conjugation of synthesised complexes could be accommodated.

The synthesis of $\mathbf{L}^{44a}$ involved amide bond formation between a protected cyclen ligand bearing a carboxylic acid arm (**46**), and an azaxanthone derivative with a pendant primary amine (**47**), Figure 2.3.

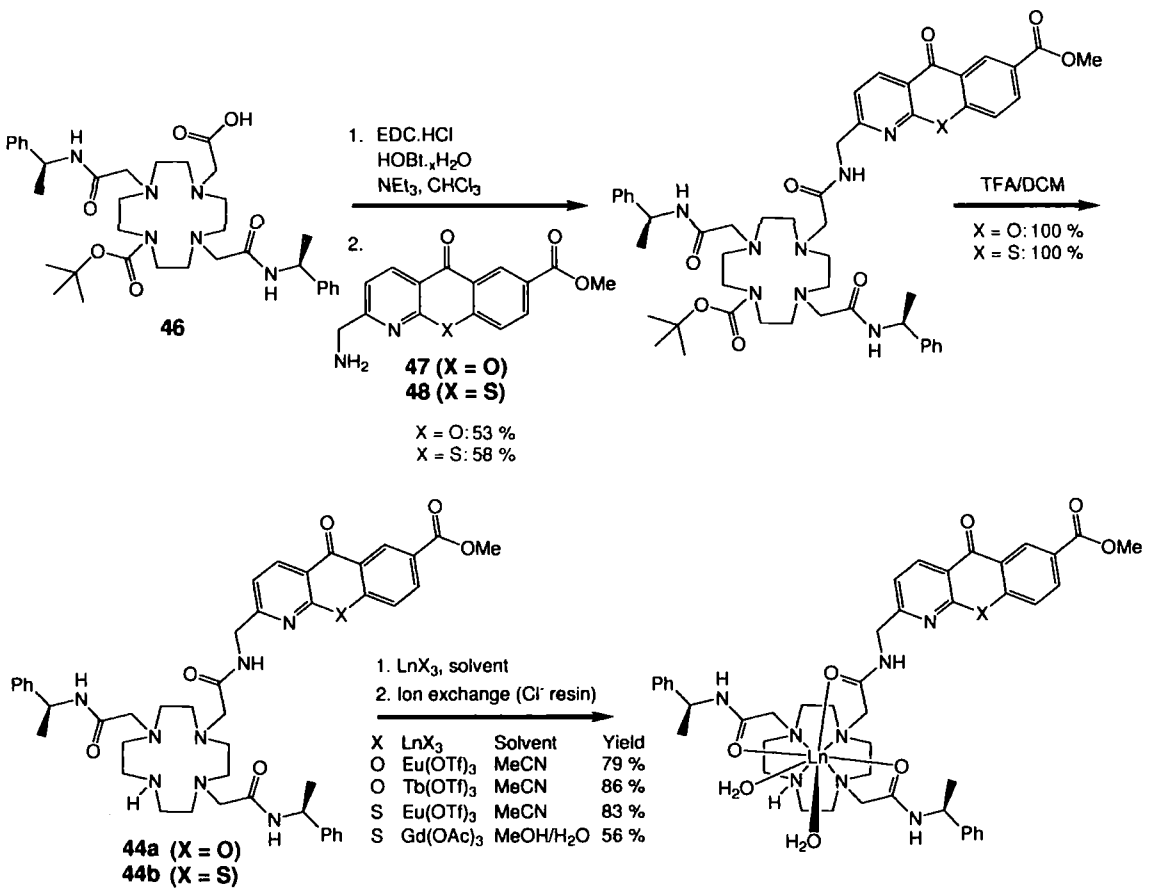

Figure 2.3 – Outline of the synthetic route used for the synthesis of $\mathbf{L}^{44a}$ and $\mathbf{L}^{44b}$.

The acid **46** was synthesised as shown in Figure 2.4. Selective *N*-protection of cyclen at the 1,7-positions was achieved following established literature procedures using benzyl chloroformate.[85] The introduction of the two chiral pendant amide arms was

achieved by *N*-alkylation of the remaining two cyclen secondary amines, followed by standard deprotection conditions to remove the Cbz-groups. Mono-protection of one of the free ring nitrogens was carried out using BOC_2O. However, synthesis of the tetra-substituted side product could not be easily avoided and column chromatography was required to separate the desired product. The tetra-substituted side product (di-BOC) could be transformed back to the starting 1,7-disubstituted precursor through standard BOC deprotection chemistry and washing steps. Alkylation of **45** with ethyl bromoacetate, followed by hydrolysis, yielded the desired protected ligand bearing a pendant acid arm.

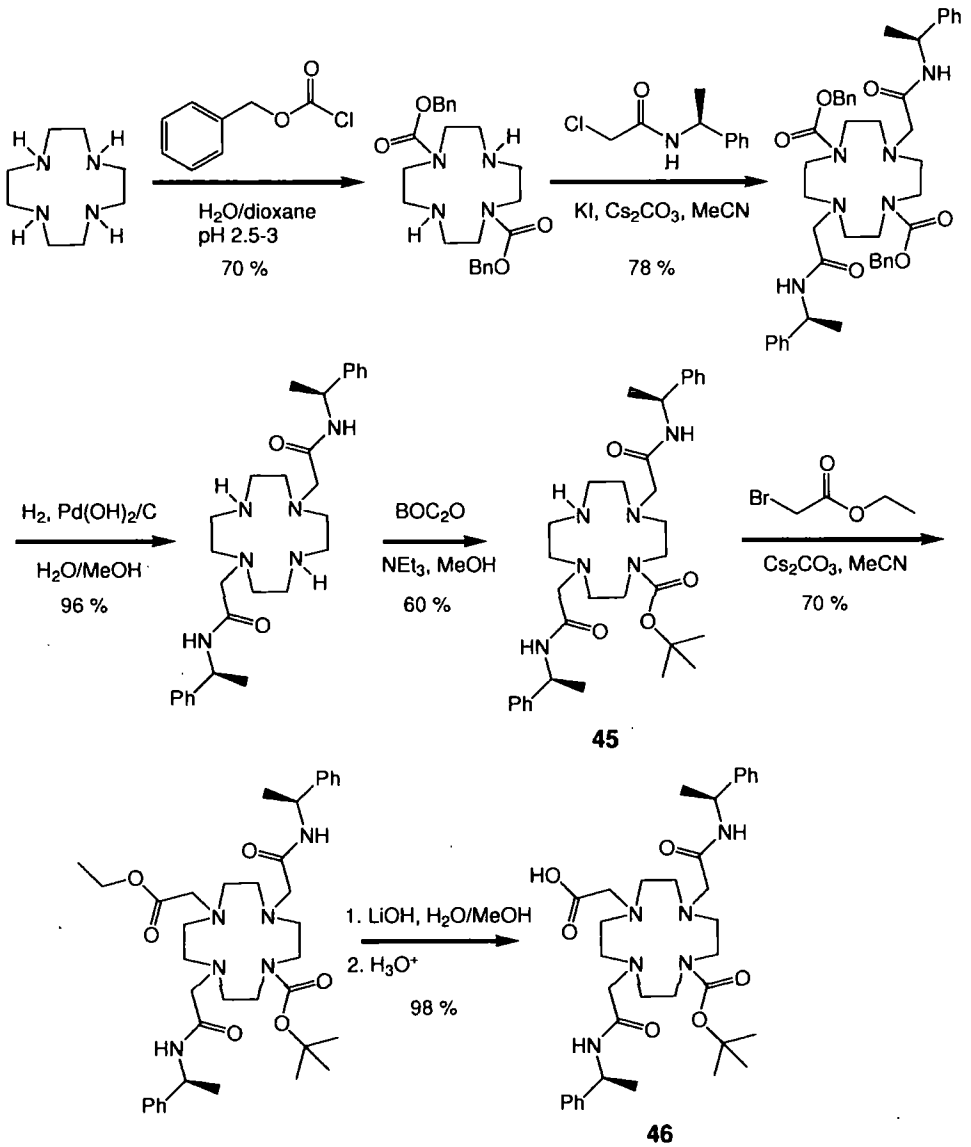

Figure 2.4 – Outline of the synthetic route taken to achieve the synthesis of **46**.

The acid, **46**, proved to be a versatile intermediate in the synthesis of several other complexes reported in this thesis. These complexes will be discussed in later chapters.

The 2-aminomethylazaxanthone derivative (**47**) was prepared in good yield from the bromomethyl precursor via a Gabriel reaction, Figure 2.5. Initial attempts to introduce the amine group via reaction of 7-methoxycarbonyl-2-bromomethyl-1-azaxanthone with sodium azide proved unsuccessful. The synthesis of 7-methoxycarbonyl-2-bromomethyl-1-azaxanthone was undertaken following previously reported procedures.[54] This involved deprotonation of methyl-4-hydroxybenzoate with sodium methoxide, followed by coupling with 2-chloro-6-methylnicotinic acid in molten methyl-4-hydroxybenzoate. Electrophilic cyclisation of the resulting intermediate in PPA yielded 7-methoxycarbonyl-2-methyl-1-azaxanthone. Benzylic bromination with NBS using an AIBN initiator yielded the desired product.

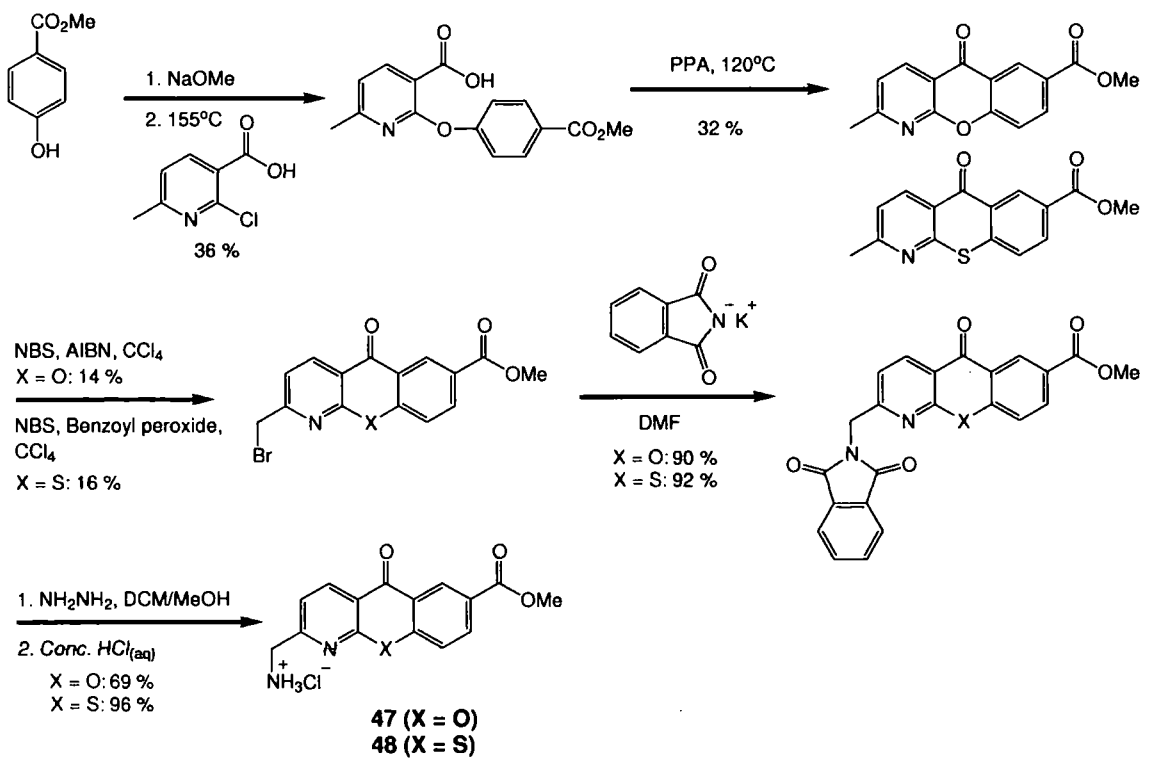

Figure 2.5 – Outline of the synthetic route used to synthesise **47** and **48**.

Problems associated with this synthetic route related to the competitive hydrolysis of the methyl ester during work up of the electrophilic cyclisation step, forming an

acid that proved difficult to isolate. However, this problem was alleviated when using MeOH instead of H_2O to quench PPA. A further limitation was the formation of the dibrominated side product during the benzylic bromination step. However, methodology has been established utilising diethyl phosphite to convert this side product back to the mono-brominated and non-brominated precursors.[86] In any case, each of these steps significantly reduced the overall reaction yield.

Coupling of **46** and **47** was achieved by activation of **46** using carbodiimide chemistry, followed by amide formation in good yield upon addition of **47**, Figure 2.3. Deprotection of the ligand using TFA, followed by complexation yielded the desired complex. Ion-exchange chromatography was carried out to convert the complexes to their chloride salts, thereby enhancing their water solubility. It should be noted that typical methodology used in the research group is to use a slight excess of Ln(III) salt over the free ligand during complexation reactions. Excess Ln(III) salt is then removed by adjusting the pH of an aqueous complex solution to 10 to precipitate insoluble $Ln(OH)_3$. The solution is then filtered and the pH is adjusted back to neutral. In this work, a slight excess of ligand was used during complexation reactions as it was discovered that uncomplexed ligand could be easily removed by washing the crude reaction product with CH_2Cl_2. This removed the need for harsh basic conditions and ensured NaCl/KCl did not contaminate the final product.

The azathioxanthone analogue, $\mathbf{L}^{44b}$, was also synthesised, Figures 2.3 and 2.5. Each reaction proceeded in a similar fashion as described previously. During the synthesis of **48** the crystal structure of the intermediate 2-phthalimidomethyl-7-methoxycarbonyl-1-azathioxanthone was obtained, Figure 2.6.

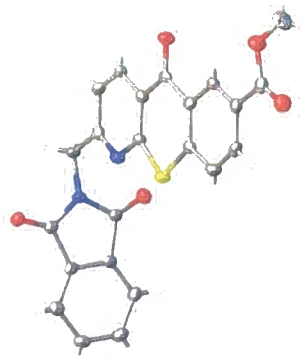

Figure 2.6 – Molecular structure of 2-phthalimidomethyl-7-methoxycarbonyl-1-azathioxanthone, showing the phthalimide unit to be twisted perpendicular with respect to the azathioxanthone.

The acid analogue of $[EuL^{44a}]^{3+}$, $[EuL^{49}]^{2+}$, was also synthesised, Figure 2.7. The free acid group of the complex structure was intended to allow conjugation of the complex using standard coupling methods.

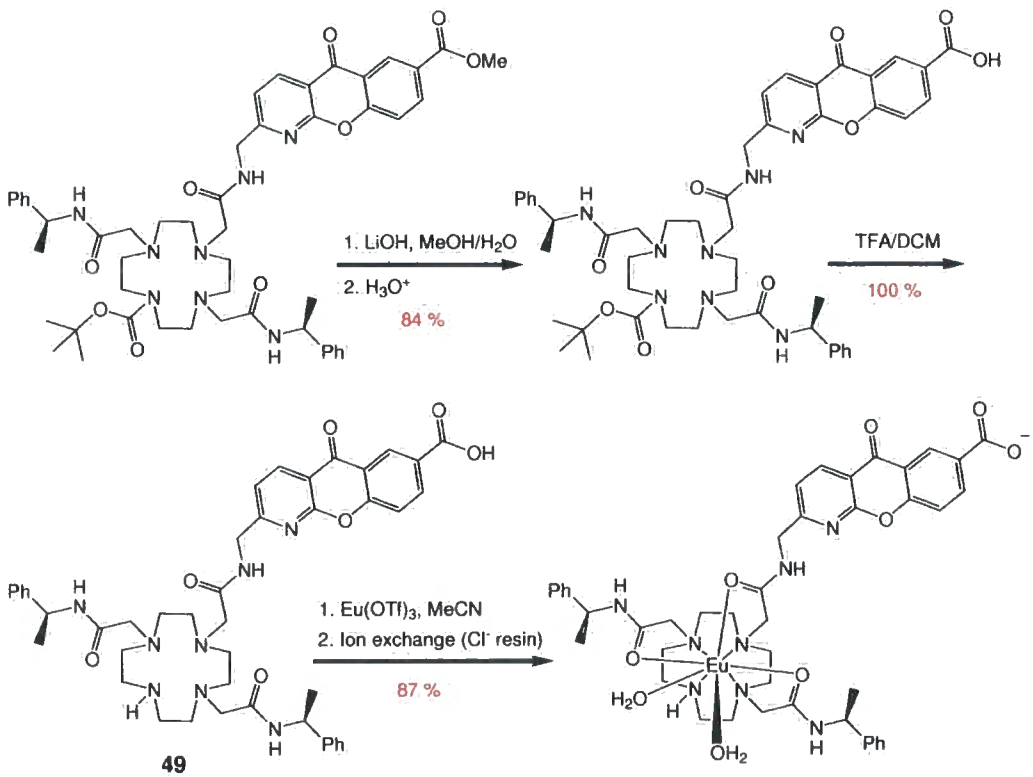

Figure 2.7 – Outline of the synthetic route used for the synthesis of L^{49}.

The simplest envisaged method by which $[EuL^{49}]^{2+}$ could be synthesised involved mild base hydrolysis of $[EuL^{44a}]^{3+}$. However, this method proved problematic and

decomplexation of the Eu(III) ion was observed. Whilst hydrolysis of complexes with octadentate ligands has previously proved to be a successful strategy towards the synthesis of Ln(III) conjugates,[86,87] the lower coordination environment around $[EuL^{49}]^{2+}$ gives rise to a less kinetically stable complex that cannot tolerate such basic conditions. Other routes towards the synthesis of L^{49}, via the hydrolysis of the parent sensitiser, ultimately did not allow access to the desired ligand.[88] Finally, synthesis of the desired ligand was achieved through base catalysed hydrolysis of BOC protected L^{44a}, Figure 2.7. The hydrolysis and all subsequent steps were high yielding. No undesired side products were detected or isolated. Complexation of the resulting ligand, L^{49}, proceeded as described earlier to yield the desired Eu(III) complex.

The octadentate analogue of L^{44a}, L^{50}, was also synthesised as part of wider studies examining the mechanism of cellular uptake of Ln(III) complexes, Figure 2.8. The ligand L^{50} was one of a series examined in which the resulting complexes differed in the nature of the pendant arms or the link between the sensitiser and the macrocycle.

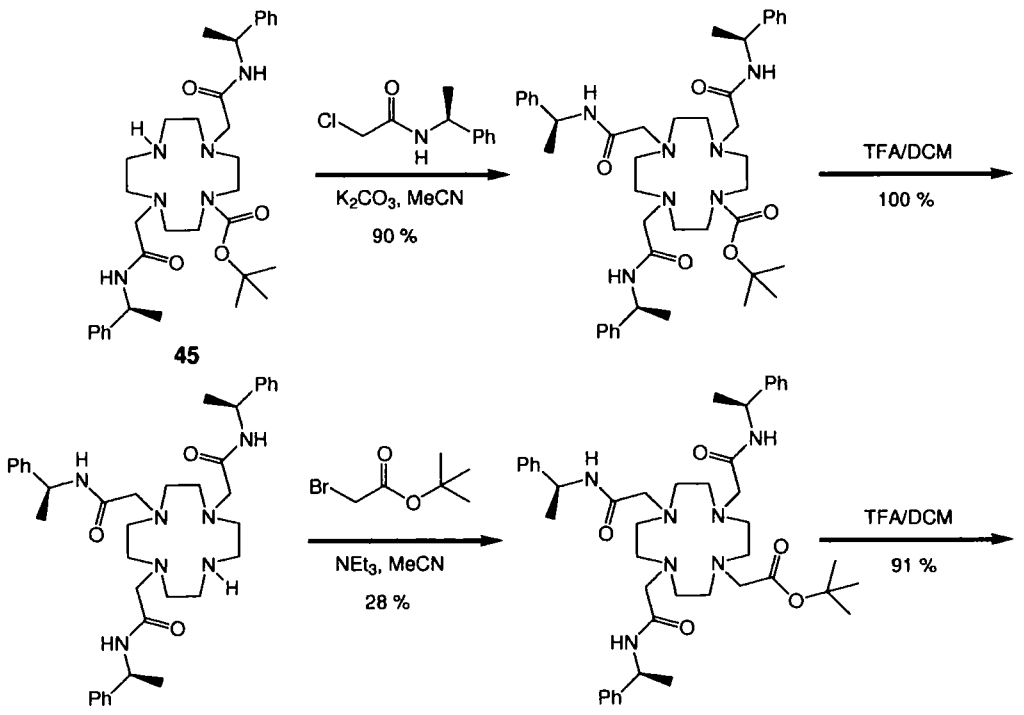

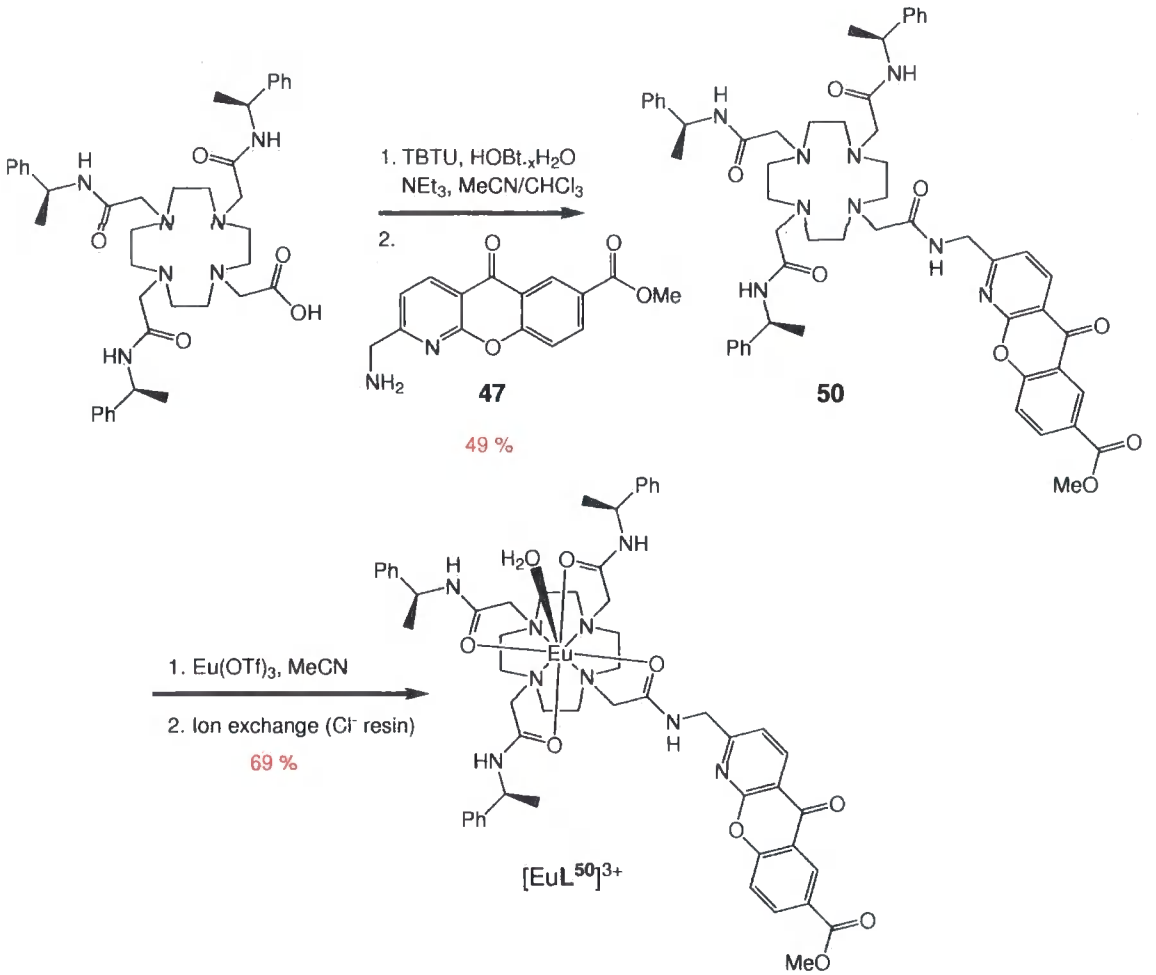

Figure 2.8 – Outline of the synthesis of complex $[EuL^{50}]^{3+}$.

The synthesis of $[EuL^{50}]^{3+}$ involved the intermediate **45**, and followed procedures outlined previously. The key step involved the introduction of a protected acid followed by its unmasking, Figure 2.8. In this case, acid activation was achieved using TBTU followed by amide formation using the azaxanthone sensitiser **47**. Complexation of the subsequent ligand proceeded as described earlier, using a slight excess of ligand. All complexes and precursors were rigorously characterised by standard spectroscopic techniques. In addition, the purity of the complexes was assessed by reverse phase HPLC to ensure that any uncomplexed ligand had been fully removed.

2.2.2 Design and synthesis of an analogue of $[EuL^{36}]^{3+}$

In light of the citrate selectivity reported for $[EuL^{36}]^{3+}$,[79] it was decided to probe the effect of modulating the ligand amide substituents on the anion binding properties of

this complex. The proposed ligands ($\mathbf{L}^{51a}/\mathbf{L}^{51b}$) were designed so that the resulting complex retained the coordinated chromophore and conserved vacant coordination sites, so that labile water molecules could be displaced on anion binding.

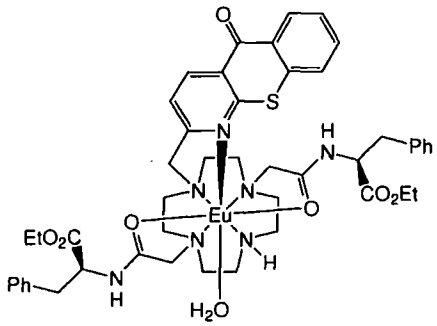

$[EuL^{36}]^{3+}$

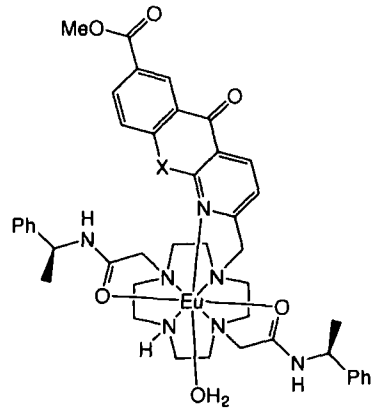

$[EuL^{51a}]^{3+}$ **(X = O)**
$[EuL^{51b}]^{3+}$ **(X = S)**

The synthetic route chosen involved the tri-substituted cyclen intermediate, **45**, Figure 2.4. Alkylation of **45** with either 7-methoxycarbonyl-2-bromomethyl-1-azaxanthone or 2-bromomethyl-7-methoxycarbonyl-1-azathioxanthone, followed by column purification on alumina, yielded the desired protected ligand. Subsequent deprotection (TFA/DCM) yielded $\mathbf{L}^{51a}/\mathbf{L}^{51b}$, Figure 2.9. Complexation with $Eu(OTf)_3$ followed by ion-exchange utilised identical methodology as described earlier. Both ligands were rigorously characterised by standard spectroscopic techniques. Complexes were also analysed by reverse phase HPLC.

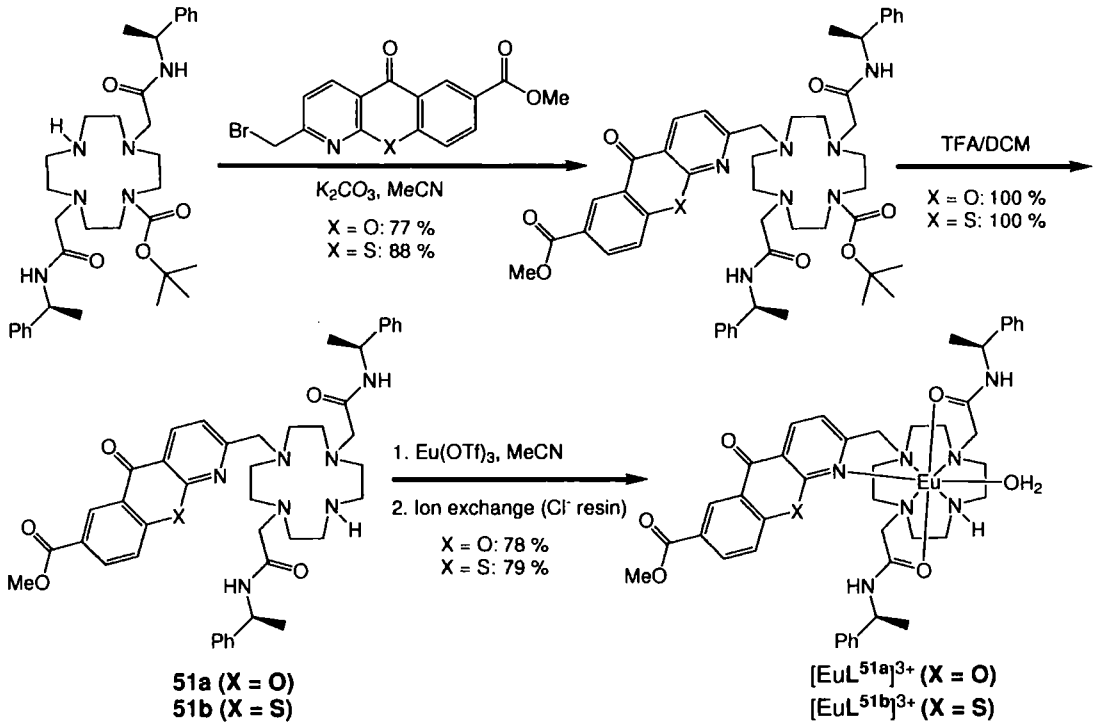

Figure 2.9 – Outline of the synthetic route towards ligands $\mathbf{L}^{51a}$ and $\mathbf{L}^{51b}$.

2.3 Solution studies with coordinatively unsaturated complexes

2.3.1 Characterisation of complex solution structure

The series of 7-coordinate complexes was examined in solution to determine the coordination environment about each Ln(III) ion. The Eu(III) complexes $[\mathrm{EuL}^{44a/b}]^{3+}$ and $[\mathrm{EuL}^{51a/b}]^{3+}$ were characterised by ^{1}H-NMR. As outlined in section 1.5.3, the chemical shifts of the axial macrocycle protons can be used to probe complex solution structure. The NMR spectra of $[\mathrm{EuL}^{44a}]^{3+}$ and $[\mathrm{EuL}^{44b}]^{3+}$ were virtually identical. The spectra, in particular the shifts of the axial macrocyclic protons, are very similar to that of $[\mathrm{EuL}^{24}]^{3+}$, Figure 2.10. This indicates a high degree of structural similarity between the complexes and suggests a constant axial donor ligand (D_2O).

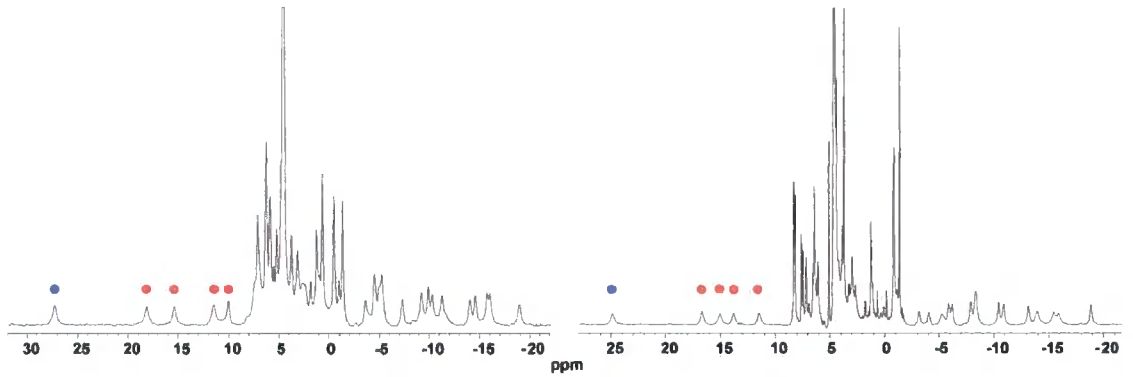

Figure 2.10 – ^{1}H-NMR spectra for $[EuL^{24}]^{3+}$ (200 MHz) (left) and $[EuL^{44a}]^{3+}$ (500 MHz) (right) (D_2O, 295 K, pD 7.8, 1 mM complex). Resonances marked with • are assigned to the cyclen NH proton, resonances marked with • are assigned to cyclen H_{ax} protons.

In contrast, the ^{1}H-NMR spectra of $[EuL^{51a}]^{3+}$ and $[EuL^{51b}]^{3+}$ were suprisingly different to each other (Figure 2.11), and were far less well defined than those of $[EuL^{44a/b}]^{3+}$. The broad resonances observed suggest a far greater degree of complex conformational mobility on the NMR timescale. In addition, the differences between the spectra of $[EuL^{44a/b}]^{3+}$ and $[EuL^{51a/b}]^{3+}$ highlight the effect of varying the functionality linking the macrocycle and sensitiser on the ligand environment about the Eu(III) ion. It should be noted that the magnitude of the chemical shifts in each spectrum suggests a constant axial donor ligand (D_2O).

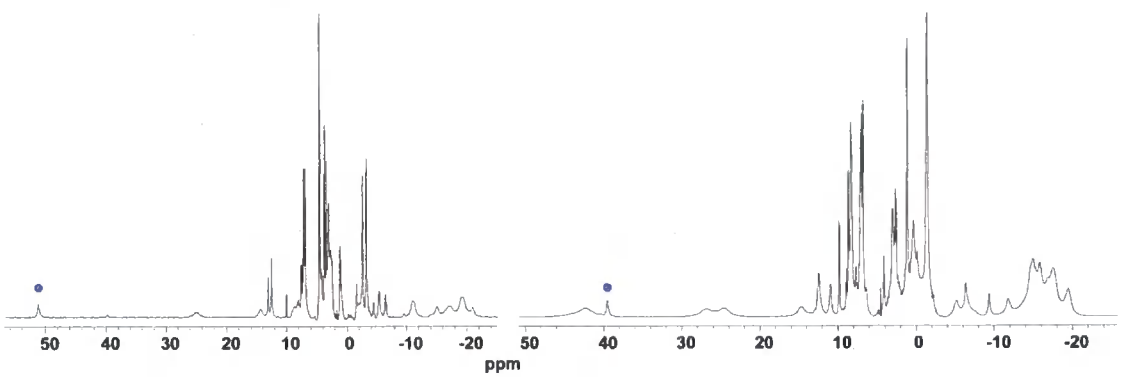

Figure 2.11 – ^{1}H-NMR spectra for $[EuL^{51a}]^{3+}$ (left) and $[EuL^{51b}]^{3+}$ (right) (500 MHz, D_2O, 295 K, pD 7.8, 1 mM complex). Resonances marked with • are assigned to the cyclen NH proton.

A further technique by which the solution structure of the complexes may be compared, and related to that of $[EuL^{24}]^{3+}$, is circularly polarised luminescence (CPL)

spectroscopy. In CPL spectroscopy the degree of chirality sensed by an electronic transition is represented by the emission dissymmetry factor (g_{em}) (eqn. 2).

$$g_{em} = \frac{2(I_L - I_R)}{(I_L + I_R)} \qquad \text{(eqn. 2)}$$

I_L and I_R are the intensities of the left or right circularly polarised components of the transition, respectively. Accordingly, the sum of the two is the total luminescence intensity of the transition. Conformationally rigid chiral Ln(III) complexes may therefore be structurally probed by CPL. The sign and magnitude of g_{em} are determined by the degree of helical twist about the principal axis of the complex and the nature of the ligand field.[89] Comparison of the CPL spectra of $[EuL^{44a}]^{3+}$ and $[EuL^{44b}]^{3+}$ with that of $[EuL^{24}]^{3+}$ revealed a similarity in form, supporting the suggestion of structural homology, Figure 2.12. Additionally, comparison of g_{em} values at specific wavelengths also highlights similarities and differences within these spectra. For example, g_{em} values for $[EuL^{44b}]^{3+}$ are lower in magnitude than those of $[EuL^{24}]^{3+}$, but are of the same sign, Table 2.1. This may suggest increased conformational flexibility of the sensitised complex, compared to $[EuL^{24}]^{3+}$, on the experimental timescale. This may average the effective local helicity, as reflected by the lower g_{em} values. Therefore, from the ^{1}H-NMR and CPL evidence obtained it may be concluded that (*SS*)-$[EuL^{44a/b}]^{3+}$ retains the Δ-(λλλλ) configuration (Figure 1.7) exhibited by $[(SSS)\text{-}EuL^{24}]^{3+}$.[58]

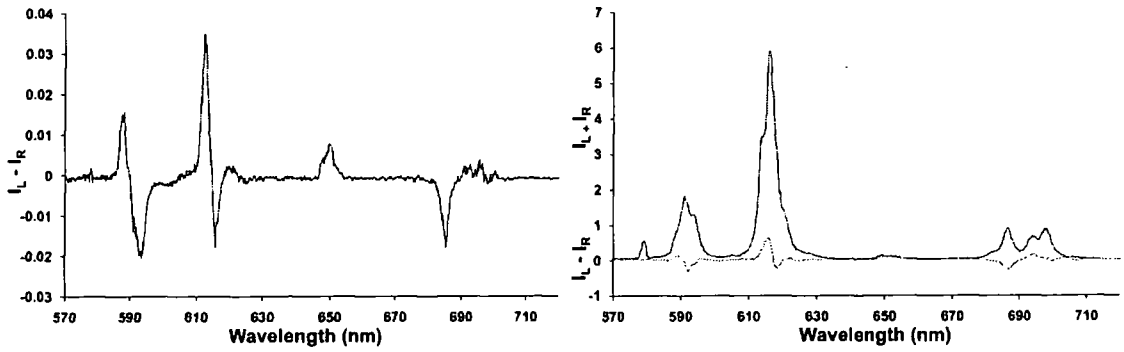

Figure 2.12 – CPL spectra of $[EuL^{24}]^{3+}$ (H_2O, 1 mM, 295 K, λ_{exc} = 255 nm) (left);[89] total luminescence and CPL spectra (x 18) of $[EuL^{44b}]^{3+}$ (D_2O, 0.05 mM, 295 K, λ_{exc} = 275 nm) (right).

Complex	$\Delta J = 1$ (λ)	$\Delta J = 2$ (λ)
$[EuL^{24}]^{3+}$	-0.05 (593)	+0.03 (612)
$[EuL^{44b}]^{3+}$	-0.022 (593)	+0.012 (616)

Table 2.1 – Emission dissymmetry values (g_{em}) at specified wavelengths (D_2O, 295 K); $[EuL^{24}]^{3+}$ in H_2O.[89]

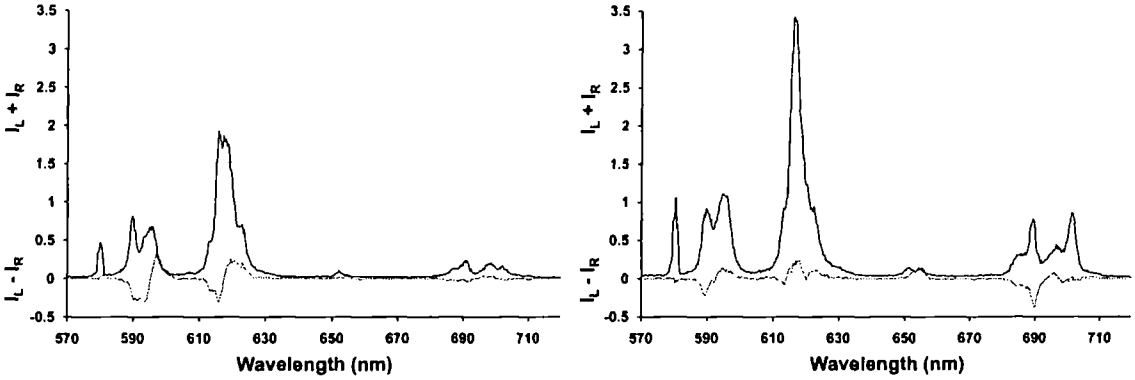

Figure 2.13 – Total luminescence and CPL spectra (x 18) of $[EuL^{51a}]^{3+}$ (left) and $[EuL^{51b}]^{3+}$ (right) (D_2O, 0.05 mM, 295 K, λ_{exc} = 235 nm and 275 nm respectively).

The form and relative intensity of the CPL spectra of $[EuL^{51a}]^{3+}$ and $[EuL^{51b}]^{3+}$ differed, Figure 2.13, and contrasted with those observed above, Figure 2.12. This difference was reflected by the reversal in sign of the ΔJ=1 and ΔJ=2 transitions of both complexes, showing that $[EuL^{51a}]^{3+}$ and $[EuL^{51b}]^{3+}$ are of opposite local helicity at Eu(III) compared to $[EuL^{44a}]^{3+}$, $[EuL^{44b}]^{3+}$ and $[EuL^{24}]^{3+}$. Analysis of the ^{1}H-NMR spectra of $[EuL^{51a}]^{3+}$ and $[EuL^{51b}]^{3+}$ suggest they retain the SAP geometry, as complexes with a TSAP geometry have been shown to possess a comparatively reduced spectral width.[58,90] It is therefore likely that $[EuL^{51a}]^{3+}$ and $[EuL^{51b}]^{3+}$ possess the diastereomeric configuration as that of $[EuL^{44a}]^{3+}$ and $[EuL^{44b}]^{3+}$, i.e. $\Lambda(\delta\delta\delta\delta)$ (Figure 1.7). The difference in the NMR and CPL spectra of $[EuL^{51a}]^{3+}$ and $[EuL^{51b}]^{3+}$ is intriguing; obviously they differ in constitution only at one heteroatom of the sensitiser. The proton resonances of the $[EuL^{51b}]^{3+}$ ^{1}H-NMR spectra appear broader than those of $[EuL^{51a}]^{3+}$. This may be attributed to a greater degree of ligand conformational exchange on the NMR timescale and may be tentatively related to a reduced presence of a stabilising hydrogen bond network with this ligand.

Measurements of the radiative lifetime of each complex in H_2O and D_2O were

taken to allow an estimation of the number of coordinated water molecules, q (Table 2.2).[57] Values of q were estimated to be 2 for complexes with an O-containing ligand ($[EuL^{44a}]^{3+}/[EuL^{51a}]^{3+}$). Those with an S-containing ligand possessed a q value closer to unity ($[EuL^{44b}]^{3+}/[EuL^{51b}]^{3+}$), suggesting these may either be mono-aqua complexes or mixtures of mono or diaqua species. As suggested above, the change from O to S in the ligand will presumably reduce the degree of hydration of the ligand, as reflected in the q values obtained.

2.3.2 Anion binding studies

Studies examining the binding of simple anions to the complexes $[EuL^{44a/b}]^{3+}$ and $[EuL^{51a/b}]^{3+}$ were examined using emission spectroscopy. Initially, a series of limiting emission spectra were acquired. This involved examination of a solution of complex (0.05 mM) in the presence of 10 eqs. of added anion at pH 7.4.

Anion binding studies with $[EuL^{44a}]^{3+}$ and $[EuL^{44b}]^{3+}$

Emission spectra for $[EuL^{44a/b}]^{3+}$ in the presence of HCO_3^- and various phospho-anions exhibited features previously noted for structurally related complexes.[66,72,73] In particular, limiting emission spectra possessed a ΔJ=2/ΔJ=1 intensity ratio distinctive for that particular class of anion. Binding of the HCO_3^- anion, for example, induced a ratio change that was 100 % greater than that of the aqua complex. The form of the ΔJ=2 and ΔJ=4 transitions was distinctive in each of the spectra with phospho-anions. Phosphate ligation induced a shoulder to appear at 621 nm in the ΔJ=2 emission manifold, Figure 2.14, consistent with earlier observations.[66,72,73]

With $[EuL^{44a}]^{3+}$ in the presence of $(O$-P-Tyr$)^{2-}$, lanthanide emission appeared to be severely quenched relative to the emission of the aqua complex, Figure 2.15. Emission was also weak when excitation was attempted at 275 nm, the λ_{max} of Tyr. Quenching of emission with $[EuL^{44a}]^{3+}$ was also observed in the presence of Tyr or HSA, albeit not as strongly as in the case of $(O$-P-Tyr$)^{2-}$. This presumably reflects the weaker binding of Tyr itself to the complex.

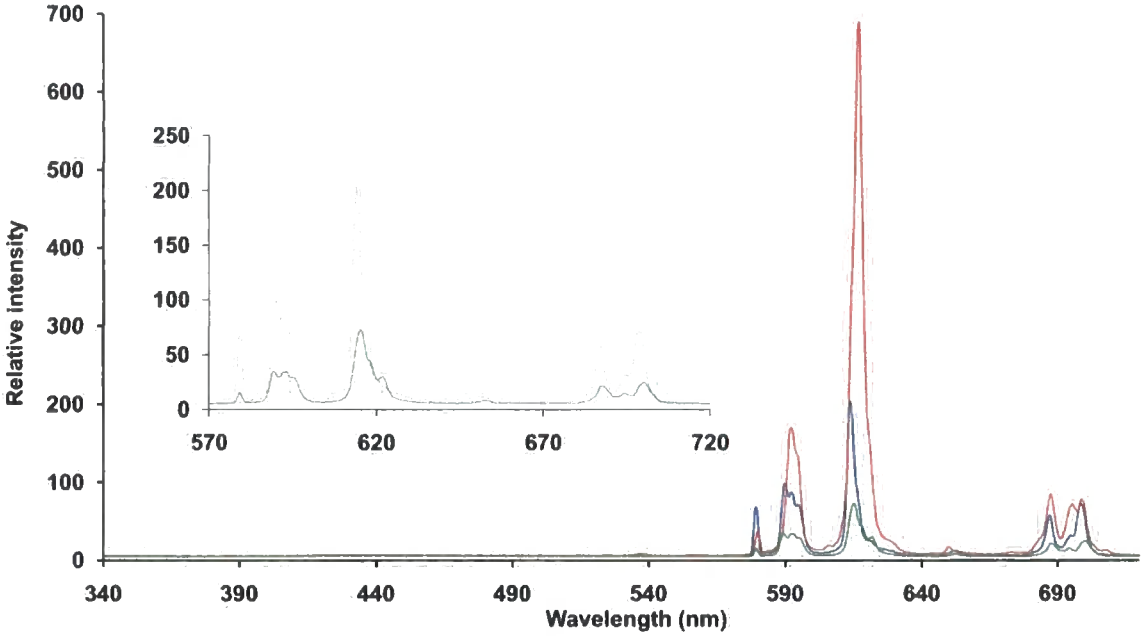

Figure 2.14 – Emission spectra of $[EuL^{44a}]^{3+}$ (blue) and with 10 eqs. HCO_3^- (red) and 10 eqs. HPO_4^{2-} (green) (H_2O, pH 7.4, 0.05 mM complex, 298 K, λ_{exc} = 335 nm). These spectra also highlight the fast rate of intersystem crossing in azaxanthone based systems as ligand-based fluorescence is not seen. Inset is an enlargement of the Eu(III) emission of $[EuL^{44a}]^{3+}$ (blue) and with 10 eqs. HPO_4^{2-} (green).

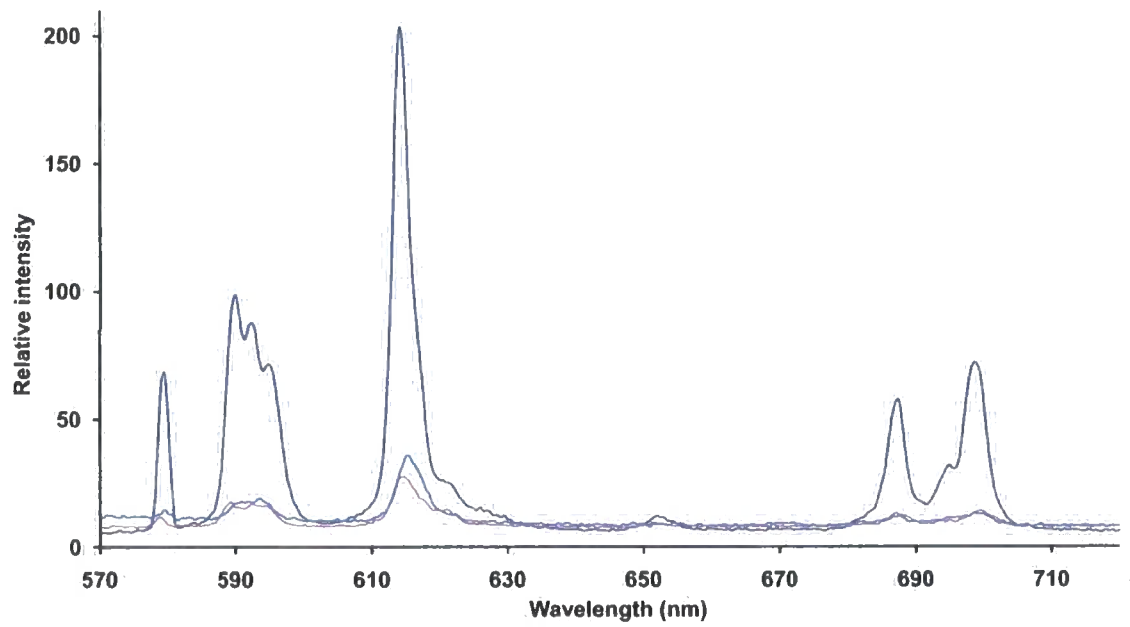

Figure 2.15 – Emission spectra of $[EuL^{44a}]^{3+}$ (upper, blue) and with 10 eqs. *O*-P-Tyr)$^{2-}$ (red) and 0.35 mM HSA (lower, blue) (H_2O, pH 7.4, 0.05 mM complex, 298 K, λ_{exc} = 335 nm).

Complex/anion	$k_{(H_2O)}/ms^{-1}$	$k_{(D_2O)}/ms^{-1}$	$\Delta k/ms^{-1}$	$q^{a,b}$
$[EuL^{44a}]^{3+}/Cl^-$	3.85	1.56	2.29	2.18
(O-P-Tyr)$^{2-}$	2.70	1.69	1.01	0.67
HCO_3^-	2.44	1.35	1.09	0.77
HSA	2.63	1.85	0.78	0.35
$[TbL^{44a}]^{3+}/Cl^-$	0.85	0.48	0.37	1.5
(O-P-Tyr)$^{2-}$	0.63	0.55	0.08	0.12
$[EuL^{44b}]^{3+}/Cl^-$	3.03	1.54	1.49	1.24
(O-P-Tyr)$^{2-}$	2.63	1.64	0.99	0.65
HCO_3^-	2.38	1.56	0.82	0.47
HSA	2.70	1.67	1.03	0.72
Citrate	2.63	1.75	0.88	0.52
Lactate	2.70	1.59	1.11	0.77
HPO_4^{2-}	2.78	1.54	1.24	0.9
$[EuL^{49}]^{2+}/Cl^-$	3.33	1.67	1.66	1.5
(O-P-Tyr)$^{2-}$	2.63	1.72	0.91	0.53
HCO_3^-	2.44	1.61	0.83	0.41
HSA	2.63	1.64	0.99	0.62
HPO_4^{2-}	2.56	1.61	0.95	0.6
(O-P-Ser)$^{2-}$	2.56	1.72	0.84	0.43
(Glc-6-P)$^{2-}$	2.56	1.59	0.97	0.61
Tyr	2.63	1.67	0.96	0.56
$[EuL^{51a}]^{3+}/Cl^-$	3.85	1.67	2.18	2.09
HCO_3^-	2.56	1.47	1.09	0.79
$[EuL^{51b}]^{3+}/Cl^-$	3.13	1.61	1.52	1.25
HCO_3^-	2.94	1.45	1.49	1.26
HSA	2.17	1.59	0.58	0.12
HPO_4^{2-}	2.17	1.28	0.89	0.52
Citrate	1.79	1.52	0.27	0
Lactate	2.13	1.41	0.72	0.34

Table 2.2 – Effect of added anions on the rate constants (k) (± 10 %) for radiative decay of the excited states of $[EuL^{44a}]^{3+}$, $[TbL^{44a}]^{3+}$, $[EuL^{44b}]^{3+}$, $[EuL^{49}]^{2+}$, $[EuL^{51a}]^{3+}$ and $[EuL^{51b}]^{3+}$ (295 K, 0.05 mM complex, 0.5 mM anion except HSA (0.35 mM)) and derived hydration numbers, q (± 20 %). [a] $q^{Eu} = 1.2[(k_{(H_2O)}\text{-}k_{(D_2O)})\text{-}(0.25+0.07x)]$ (x = number of carbonyl-bound amide NH oscillators) [b] $q^{Tb} = 5(k_{(H_2O)}\text{-}k_{(D_2O)}\text{-}0.06)$.[57]

Several measurements were taken to investigate which excited state was being quenched, i.e. sensitiser singlet, triplet or the Eu(III) excited state. The emission lifetime of $[EuL^{44a}]^{3+}$ increased upon addition of (O-P-Tyr)$^{2-}$ and HSA, consistent with displacement of a Eu(III) coordinated water molecule. This confirms that the quenching was not caused by a reduction in Eu(III) excited state lifetime, Table 2.2. These results were supported by the observation that $[TbL^{44a}]^{3+}$ emission lifetime also in-

creased upon $(O\text{-P-Tyr})^{2-}$ binding, whilst emission intensity was severely reduced, suggesting that perturbation of the sensitiser was the most likely cause of quenching.

Given the likelihood of sensitiser-based quenching, the sulfur analogue of the Eu(III) complex, $[\mathrm{EuL}^{44b}]^{3+}$, was also examined. For $[\mathrm{EuL}^{44b}]^{3+}$, the parent azathioxanthone sensitiser possesses a triplet energy of 23800 cm^{-1}, compared to 24900 cm^{-1} in $[\mathrm{EuL}^{44a}]^{3+}$ for the related azaxanthone sensitiser.[54] This allows a comparison to see whether the differing triplet energies might affect the susceptibilty to quenching. Upon addition of $(O\text{-P-Tyr})^{2-}$ to $[\mathrm{EuL}^{44b}]^{3+}$, emission was quenched, Figure 2.16; a similar result was observed with Tyr and HSA. Importantly, it was observed that residual ligand fluorescence possessed by $[\mathrm{EuL}^{44b}]^{3+}$ wasn't quenched to any significant degree compared to the quenching of Eu(III) emission.

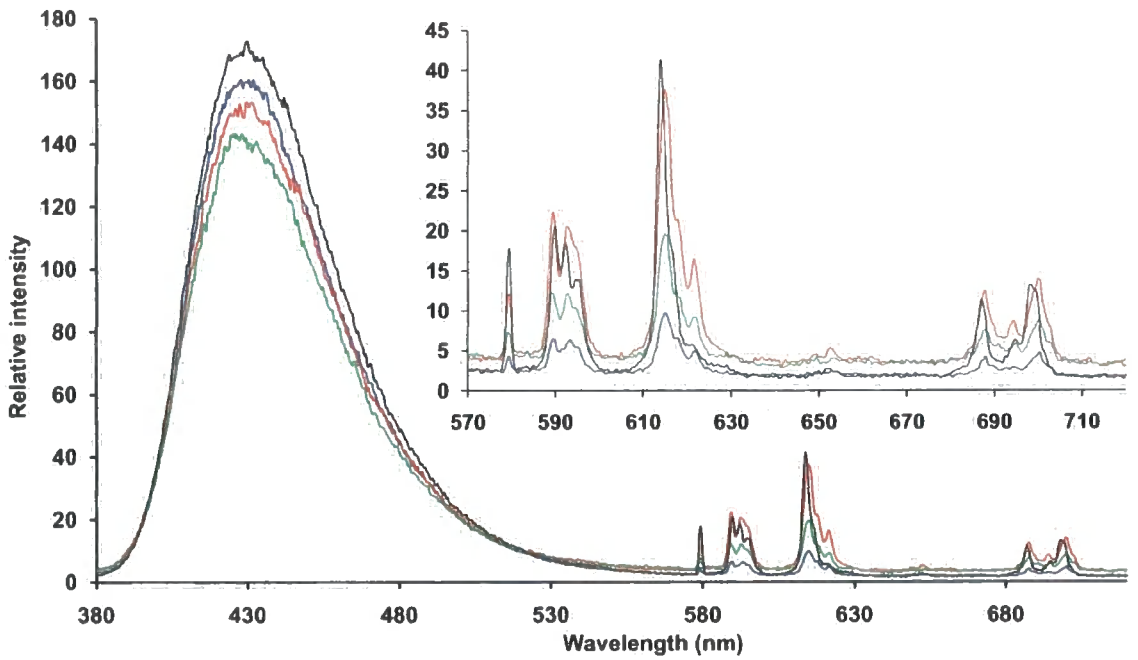

Figure 2.16 – Emission spectra of $[\mathrm{EuL}^{44b}]^{3+}$ (black) and with 10 eqs. $(O\text{-P-Tyr})^{2-}$ (blue), 10 eqs. $(O\text{-P-Ser})^{2-}$ (red) and 5 eqs. $(O\text{-P-Tyr})^{2-}$/10 eqs. $(O\text{-P-Ser})^{2-}$ (green). Inset is an enlargement of Eu(III) emission for each adduct and the aqua complex (H_2O, pH 7.4, 0.05 mM complex, 298 K, λ_{exc} = 372 nm.)

These results suggest that the quenching process does not perturb the singlet excited state of the sensitiser. If this was the route through which quenching occurred, the fluorescence of $[\mathrm{EuL}^{44b}]^{3+}$ would also be expected to decrease. As a theoretical

value of 24600 cm^{-1} for Tyr T_1 to S_0 emission has been cited,[91] alongside our own observation of 29000 cm^{-1} ($\pm$ 400cm^{-1}) with ^{t}Bu-Tyr (EPA glass, 77 K) it would appear that sensitiser-Tyr triplet-triplet energy transfer is unlikely as a source of quenching. In particular, it might be expected that a reduced degree of quenching of $[EuL^{44b}]^{3+}$, compared to that of $[EuL^{44a}]^{3+}$, would be observed if this was the case due to the larger energy gap between the sensitiser and Tyr triplet states. Therefore, the most likely mechanism of quenching is by a charge transfer process involving the chromophore excited state. Binding of (*O*-P-Tyr)$^{2-}$ to the Ln(III) centre brings an electron rich Tyr site close to the sensitiser.

The original binding preference of $[LnL^{24}]^{3+}$ for (*O*-P-Tyr)$^{2-}$ over (*O*-P-Ser)$^{2-}$/ (*O*-P-Thr)$^{2-}$ was also observed in competitive emission spectra with both $[EuL^{44a}]^{3+}$ and $[EuL^{44b}]^{3+}$. This preference was signalled by a marked reduction in emission intensity following addition of 5 eqs. (*O*-P-Tyr)$^{2-}$ to a solution of $[EuL^{44a}]^{3+}$/$[EuL^{44b}]^{3+}$ containing 10 eqs. (*O*-P-Ser)$^{2-}$, Figure 2.16. Further competition experiments revealed a selectivity for (*O*-P-Tyr)$^{2-}$ over HCO_3^-. This selectivity was characterised by the appearance of the distinctive shoulder at 624 nm in the ΔJ=2 manifold, and a severe reduction in emission intensity, upon addition of equimolar quantities of (*O*-P-Tyr)$^{2-}$ to a solution of $[EuL^{44a}]^{3+}$/$[EuL^{44b}]^{3+}$ and HCO_3^-. In addition, the quenched emission of $[EuL^{44a}]^{3+}$/$[EuL^{44b}]^{3+}$ in the presence of HSA (0.35 mM) was partially restored upon the addition of $NaHCO_3^-$ (30 mM), Figure 2.17. Conversely, the Eu(III) emission intensity of the complex carbonate adduct was reduced upon addition of HSA.

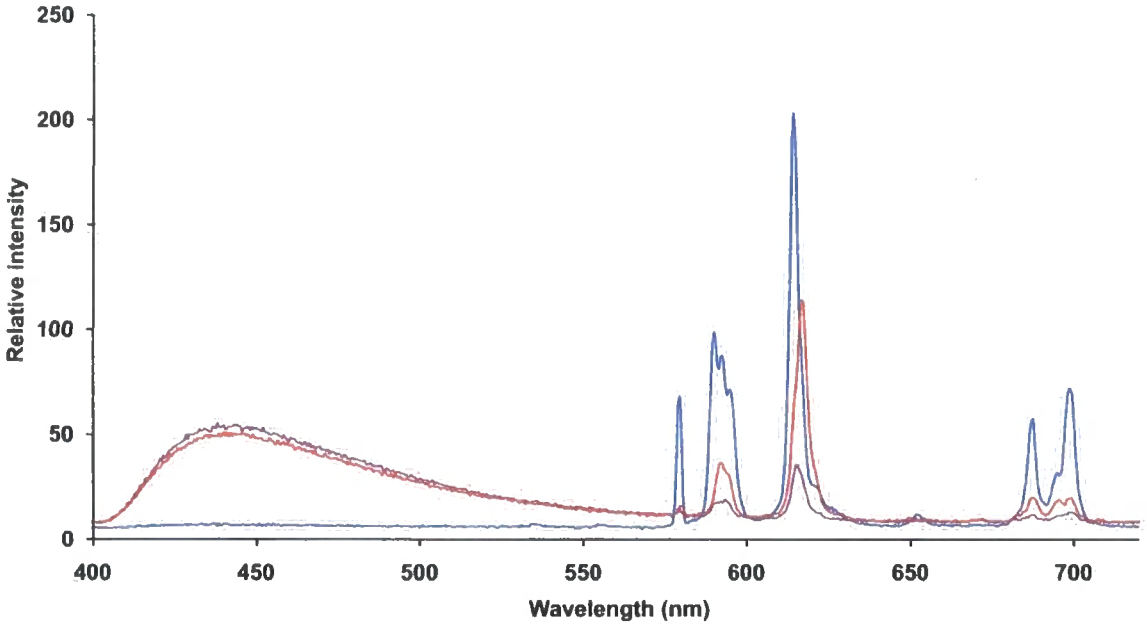

Figure 2.17 – Emission spectra of $[EuL^{44a}]^{3+}$ (blue), with HSA (0.35 mM) (purple) and with HSA (0.35 mM) and $NaHCO_3$ (30 mM) (red) (H_2O, pH 7.4, 0.05 mM complex, 298 K, λ_{exc} = 335 nm.)

The ratio of the intensity of the ΔJ=2/ΔJ=1 Eu(III) emission bands in these limiting emission spectra varied, depending upon the species present within solution. For example, the ratio with the aqua complex (pH 7.4) was ~2; which was conserved upon the addition of HSA. With the carbonate-only bound adduct this ratio was ~4 (Figure 2.14); while upon addition of HSA to this adduct, the ratio decreased slightly to ~3.2. These limiting spectra demonstrate that the complex is signalling the binding of HCO_3^- in the presence of extracellular concentrations of HSA. It is clear that bicarbonate binding is competitive, as reflected by the 'averaged' ΔJ=2/ΔJ=1 ratio containing the contributions of both the carbonate and HSA bound species.

Changes in ^{1}H-NMR spectra were also used to confirm anion binding and distinguish differing ternary anion complexes. For example, the addition of an excess of $NaHCO_3$ to $[EuL^{44b}]^{3+}$ in D_2O resulted in dramatic changes in the observed spectrum, Figure 2.18. Some resonances shifted by up to 15 ppm; consistent with the replacement of the hard 'axial' D_2O donor molecule with the more polarisable oxygen atom of the chelated carbonate anion.[66]

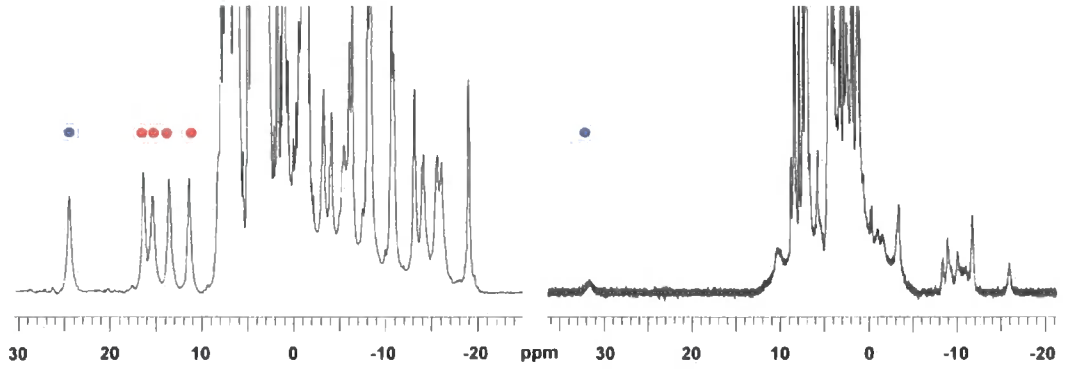

Figure 2.18 – ^{1}H-NMR spectra for $[EuL^{44b}]^{3+}$ in the absence (left) and presence (right) of 30 mM $NaHCO_3$ (D_2O, 500 MHz, 295 K, pD 7.5, 1 mM complex). Resonances marked with • are assigned to the cyclen NH proton, resonances marked with • are assigned to cyclen H_{ax} protons.

Finally, binding of selected anions was monitored by CPL spectroscopy, Figure 2.19. Bound $(O\text{-P-Thr})^{2-}$ resulted in a spectrum whose form at the $^5D_0$-$^7F_1$ transition resembled that of CPL spectra reported previously of $[EuL^{24}]^{3+}$ with HPO_4^{2-} and $(Glc\text{-}6\text{-}P)^{2-}$, but was distinctly different to that with $(O\text{-P-Tyr})^{2-}$.[66] The spectrum with added sodium lactate closely resembled that of the aqua complex. $NaHCO_3$ addition modulated the form of CPL emission in the $^5D_0$-$^7F_1$ transition whilst spectra recorded in the presence of HSA resembled the aqua complex, but with reduced intensity.

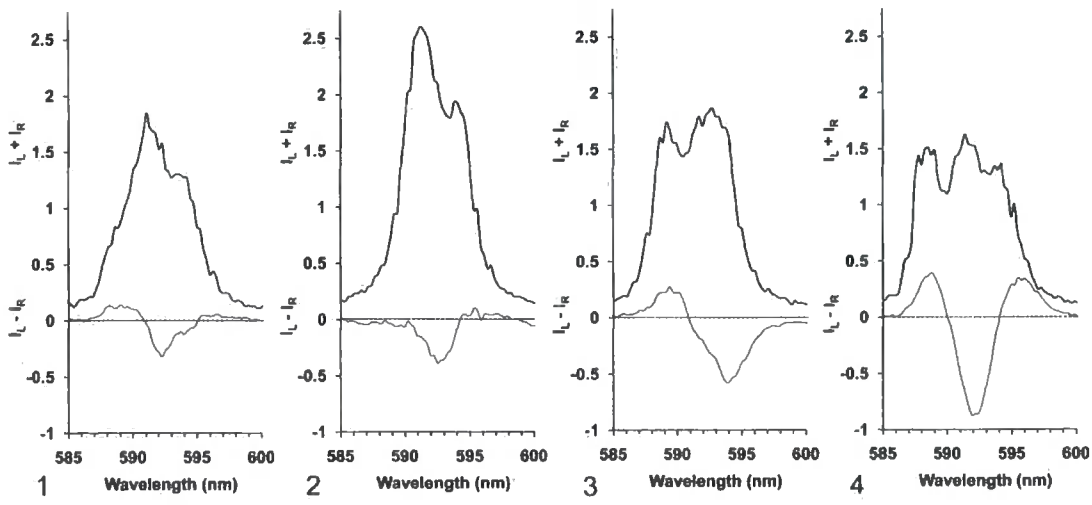

Figure 2.19 – CPL spectra (x 18) for: (1) $[EuL^{44b}]^{3+}$; (2) plus 10 eqs. HCO_3^- ; (3) plus 10 eqs. lactate; (4) plus 10 eqs. $(O\text{-P-Thr})^{2-}$. Total luminescence also shown (0.05 mM complex, 295 K, λ_{exc} = 275 nm).

It was observed that in limiting emission spectra the acid analogue of $[EuL^{44a}]^{3+}$,

$[EuL^{49}]^{2+}$, exhibited identical anion binding properties to the parent system. However, an interesting feature of this complex was the apparent pH dependent self-association. The ^{1}H-NMR spectrum of this complex (pD 7.8) was different to that of $[EuL^{44a}]^{3+}$. It was noted that a broader set of resonances shadowed the sharp resonances attributed to the complex, Figure 2.20.

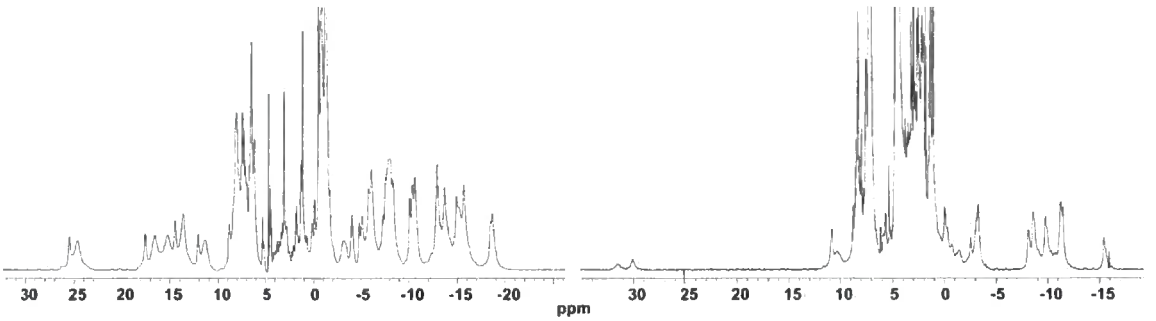

Figure 2.20 – ^{1}H-NMR spectra for $[EuL^{49}]^{2+}$ in the absence (left) and presence (right) of 30 mM $NaHCO_3$ (D_2O, 500 MHz, 295 K, pD 7.8, 1 mM complex).

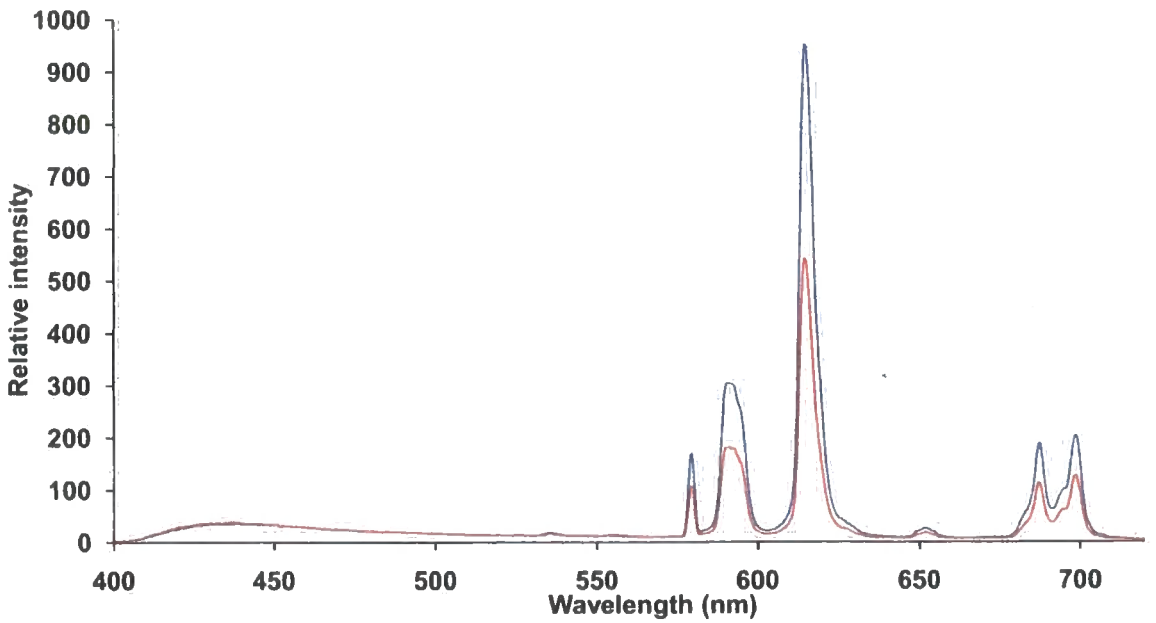

Figure 2.21 – Emission spectra of $[EuL^{49}]^{2+}$ at pH 6.25 (blue) and pH 3.65 (red) (H_2O, 0.05 mM complex, 298 K, $\lambda_{exc} = 332$ nm). Also observable is ligand fluorescence, contrasting with the spectra of $[EuL^{44a}]^{3+}$ where none was present.

In addition, the q value estimated for $[EuL^{49}]^{2+}$ was 1.5. This is lower than the value of 2.2 estimated for $[EuL^{44a}]^{3+}$. To test the hypothesis that the complex was weakly self-associating through chelation of the sensitiser carboxylate group, HCO_3^- was

introduced to the NMR solution. The resulting ^{1}H-NMR spectrum, Figure 2.20, resembled that of [Eu**L**^{44b}]$^{3+}$, in the presence of 30 mM $NaHCO_3$, Figure 2.18. This suggests that competitive chelation of carbonate is displacing the sensitiser acid. The emission spectrum of [Eu**L**^{49}]$^{2+}$ was recorded at pH 3.65 and pH 6.25, Figure 2.21. Emission intensity was reduced in the acidic conditions, consistent with hydration of the Eu(III) ion following protonation of the sensitiser carboxylate.

Evidence for self-association was also found in HRMS (ES$^+$) analyses. Mass spectra gave peaks whose mass and isotopic profile corresponded to [2M - 2H]$^{4+}$ and [2M - 4H]$^{2+}$ adducts.

Anion binding studies with [Eu**L**^{51b}]$^{3+}$

Limiting spectra for [Eu**L**^{51b}]$^{3+}$ in the presence of anions revealed a similar binding preference with the (*O*-P-amino acids)$^{2-}$; (*O*-P-Tyr)$^{2-}$ was the preferred anion in the presence of equimolar concentrations of (*O*-P-Ser)$^{2-}$/(*O*-P-Thr)$^{2-}$, Figure 2.22. Binding of (*O*-P-Tyr)$^{2-}$ to this complex, however, resulted in emission that was quenched, but not to such an extent as observed with [Eu**L**$^{44a/b}$]$^{3+}$.

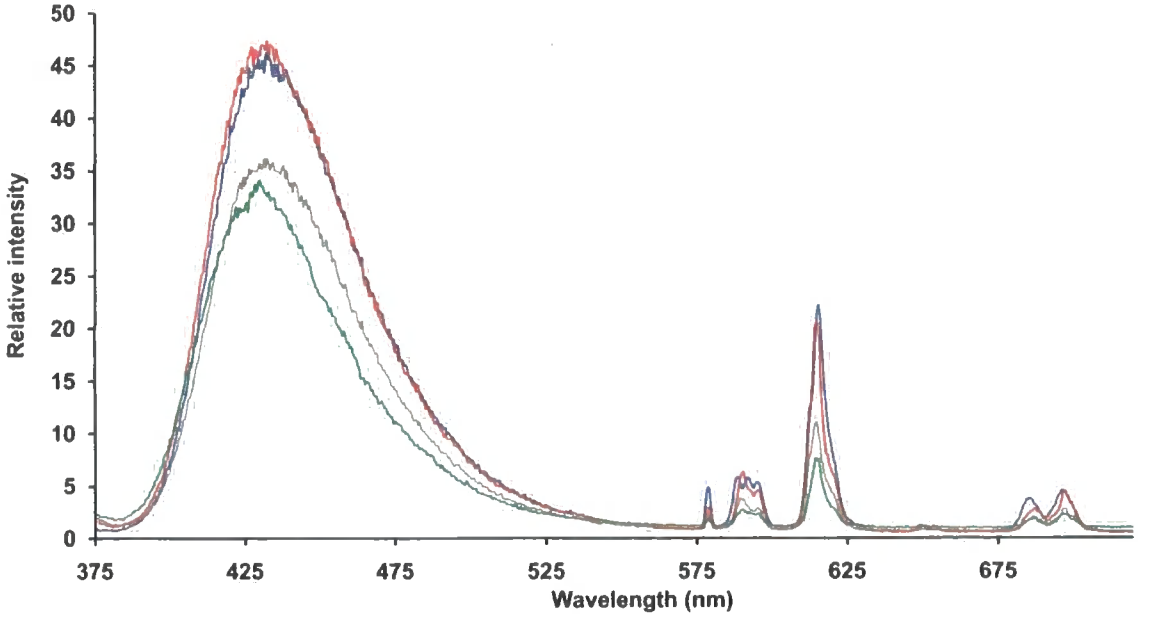

Figure 2.22 – Emission spectra of [Eu**L**^{51b}]$^{3+}$ (blue) and with 10 eqs. (*O*-P-Tyr)$^{2-}$ (brown), 10 eqs. (*O*-P-Ser)$^{2-}$ (red) and 10 eqs. (*O*-P-Tyr)$^{2-}$/10 eqs. (*O*-P-Ser)$^{2-}$ (green) (H_2O, pH 7.4, 0.05 mM complex, 298 K, λ_{exc} = 372 nm).

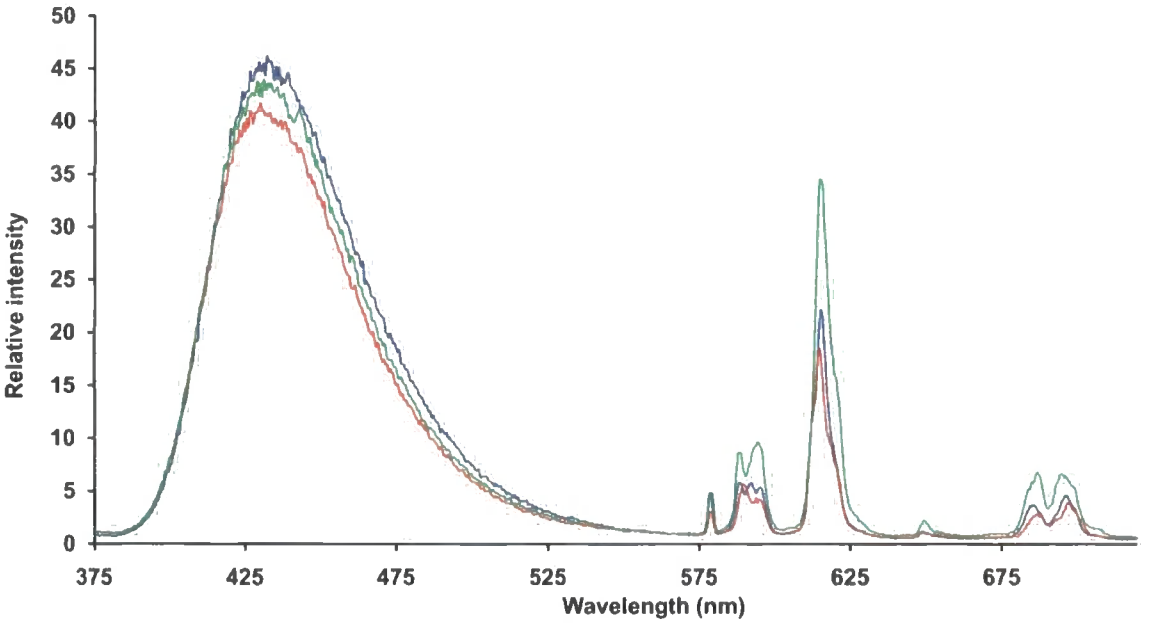

Figure 2.23 – Emission spectra of $[EuL^{51b}]^{3+}$ (blue) and with 10 eqs. HPO_4^{2-} (red) and 10 eqs. HCO_3^- (green) (H_2O, pH 7.4, 0.05 mM complex, 298 K, λ_{exc} = 372 nm).

The form of the spectra in the presence of phosphates was not as distinctive for this complex, compared to $[EuL^{44a/b}]^{3+}$. For example, addition of HPO_4^{2-} did not result in further broadening of the ΔJ=2 emission manifold, Figure 2.23. On addition of HCO_3^- the ratio of the ΔJ=2/ΔJ=1 emission bands remained close to that exhibited by the aqua complex, although total emission intensity did increase.

No anion binding information for $[EuL^{51a/b}]^{3+}$ could be gleaned from ^{1}H-NMR experiments, due to the kinetic instability of the complexes in solution. In the presence of $NaHCO_3$ or NaH_2PO_4 at concentrations of $\geq$10 mM, precipitation was observed. This is consistent with slow decomplexation of Eu(III) from the ligand. Unfortunately this instability restricted the scope of anion binding analyses.

CPL spectra of $[EuL^{51b}]^{3+}$ in the presence of selected anions were also recorded, Figure 2.24. The $^5D_0$-$^7F_1$ transition was observed to change in form upon addition of $NaHCO_3$ and sodium lactate. In particular, upon addition of the anion a more intense CPL transition was observed. The g_{em} value increased from -0.027 at 590 nm for the aqua complex to -0.077 with sodium lactate and -0.080 with $NaHCO_3$. This

may reflect the change in axial donor polarisability upon anion chelation, but may also suggest enhanced rigidification of the ligand, associated with anion ligation.

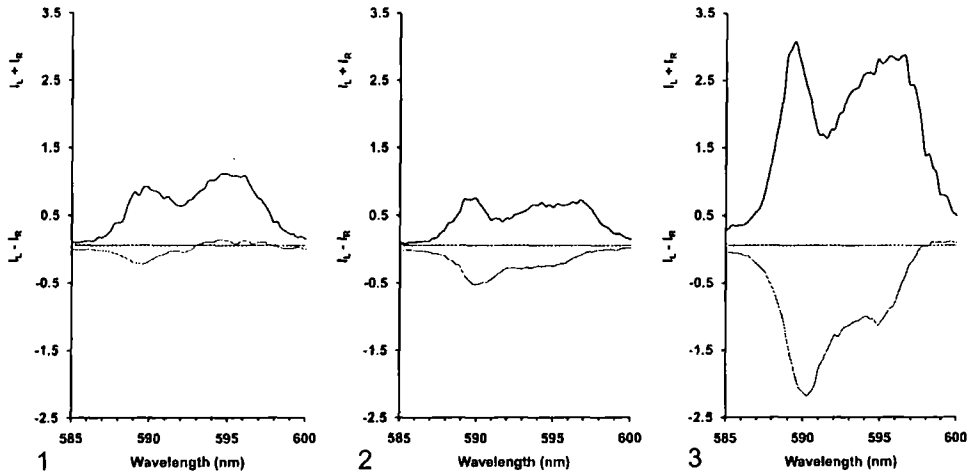

Figure 2.24 – CPL spectra (x 18) for: (1) $[EuL^{51b}]^{3+}$; (2) plus 10 eqs. lactate; (3) plus 10 eqs. HCO_3^-. Total luminescence also shown (black) (0.05 mM complex, 295 K, λ_{exc} = 275 nm).

Further comparative anion binding studies with $[EuL^{44b}]^{3+}$ and $[EuL^{51b}]^{3+}$

In light of the selectivities observed with $[EuL^{44a/b}]^{3+}$ and $[EuL^{51b}]^{3+}$, selected anions were studied in more detail.[92] The association of $[EuL^{44b}]^{3+}$ and $[EuL^{51b}]^{3+}$ with HCO_3^-, HPO_4^{2-}, lactate and citrate was investigated by a series of luminescence titrations.

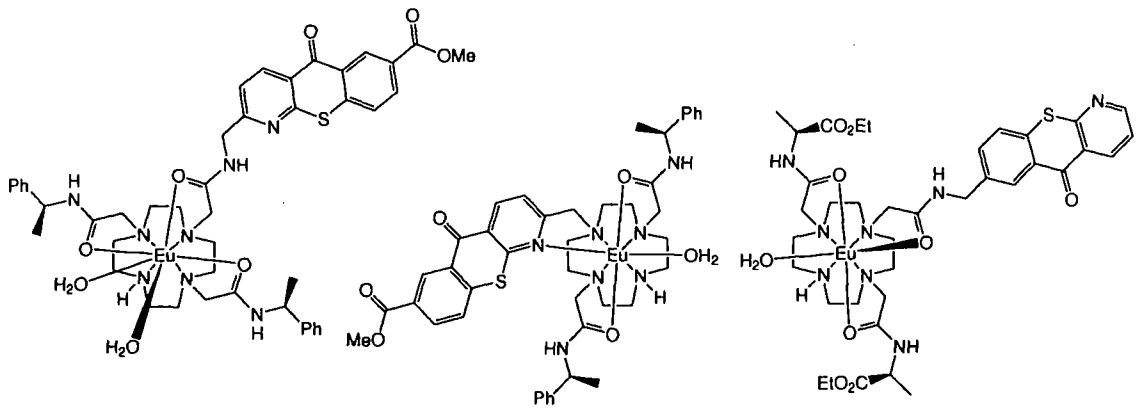

$[EuL^{44b}]^{3+}$ $[EuL^{51b}]^{3+}$ $[EuL^{52}]^{3+}$

Eu(III) emission spectra were recorded in the presence of varying anion concentrations at constant pH. In addition, the binding of specific anions, at a constant

concentration, was monitored as a function of pH. The anion binding properties of a structurally related complex reported in previous studies,[93,94] $[EuL^{52}]^{3+}$ (q = 0.92), was also investigated, these results are included here for comparison purposes.

Changes in emission spectral form enabled anion binding to be monitored, examining the change in the intensity ratio of a pair of emission bands (e.g. 616/614 nm, 700/687 nm or 594/592 nm). A plot of this ratio against anion concentration was fitted to a 1:1 binding model, allowing affinity constants to be calculated, Table 2.3.

Complex	Citrate (pH 7.4)	Lactate (pH 6)	HCO_3^- (pH 7.4)	HPO_4^{2-} (pH 7.4)
$[EuL^{44b}]^{3+}$	6.02(03)	2.73(02)	3.50(03)	3.95(03)
$[EuL^{51b}]^{3+}$	5.24(03)	2.98(02)	2.08(02)	2.60(03)
$[EuL^{52}]^{3+}$	4.33(02)	2.67(02)	3.01(02)	3.14(02)

Table 2.3 – Affinity constants of $[EuL^{44b}]^{3+}$, $[EuL^{51b}]^{3+}$ and $[EuL^{52}]^{3+}$ with anions (298 K, 0.1 M NaCl). The pH regime used was based upon preliminary experiments examining the pH dependence of the emission profile at a fixed anion concentration, (30 mM HCO_3^-, 2.3 mM lactate, 0.9 mM HPO_4^{2-} and 0.1 mM citrate with 10 μM complex) seeking a relatively 'flat' part of the spectral response/pH profile.

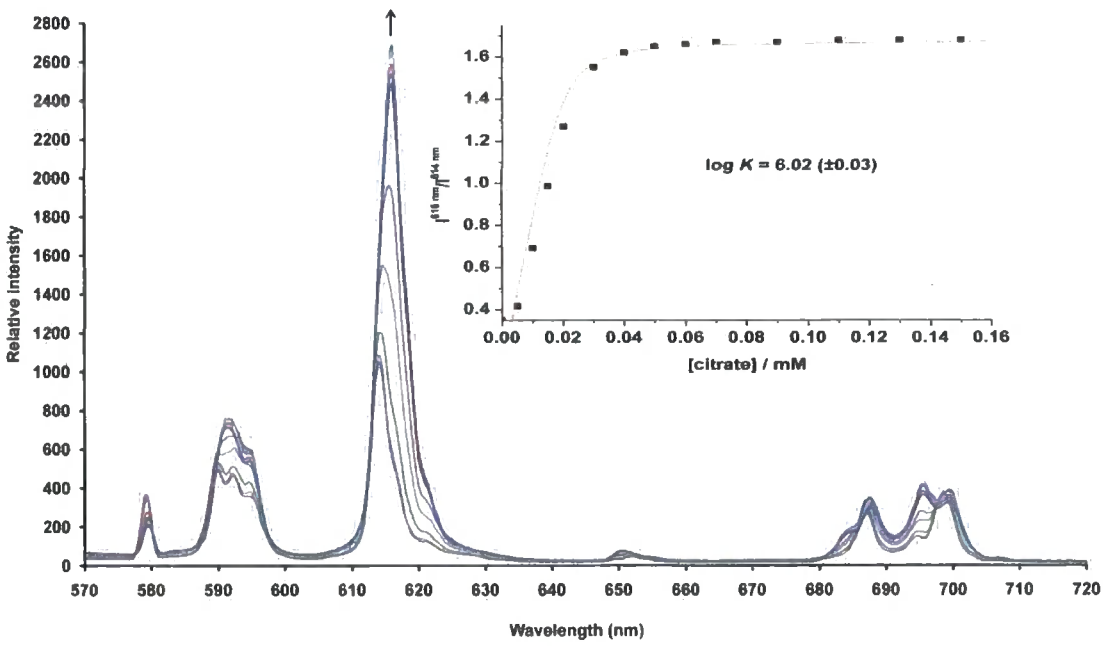

Figure 2.25 – Variation of the Eu(III) emission spectra for $[EuL^{44b}]^{3+}$, following addition of sodium citrate (H_2O, pH = 7.4 (±0.05), 0.025 mM complex, 298 K, I = 0.1 M NaCl, λ_{exc} = 375 nm). Inset is a plot of the intensity ratio (616/614 nm) with [citrate], allowing calculation of the apparent binding constant.

Binding of citrate and lactate to $[EuL^{44b}]^{3+}$ induced distinctive changes in emission spectral form. For example, lactate binding resulted in a increase in relative emission intensity at 624 nm whilst the spectral response to citrate binding included a 70 % increase in the ΔJ=2/ΔJ=1 ratio and the appearence of an isoemissive point at 698 nm, Figure 2.25.

Binding of lactate and HPO_4^{2-} to $[EuL^{51b}]^{3+}$ resulted in minor changes in Eu(III) spectral form, as seen earlier for HCO_3^- binding. On addition of citrate, a dramatic change to the Eu(III) spectral form was seen, Figure 2.26. For example, a 100 % increase in the ΔJ=2/ΔJ=1 ratio was observed, alongside changes to the form and relative intensity of the ΔJ=0 and ΔJ=1 transitions.

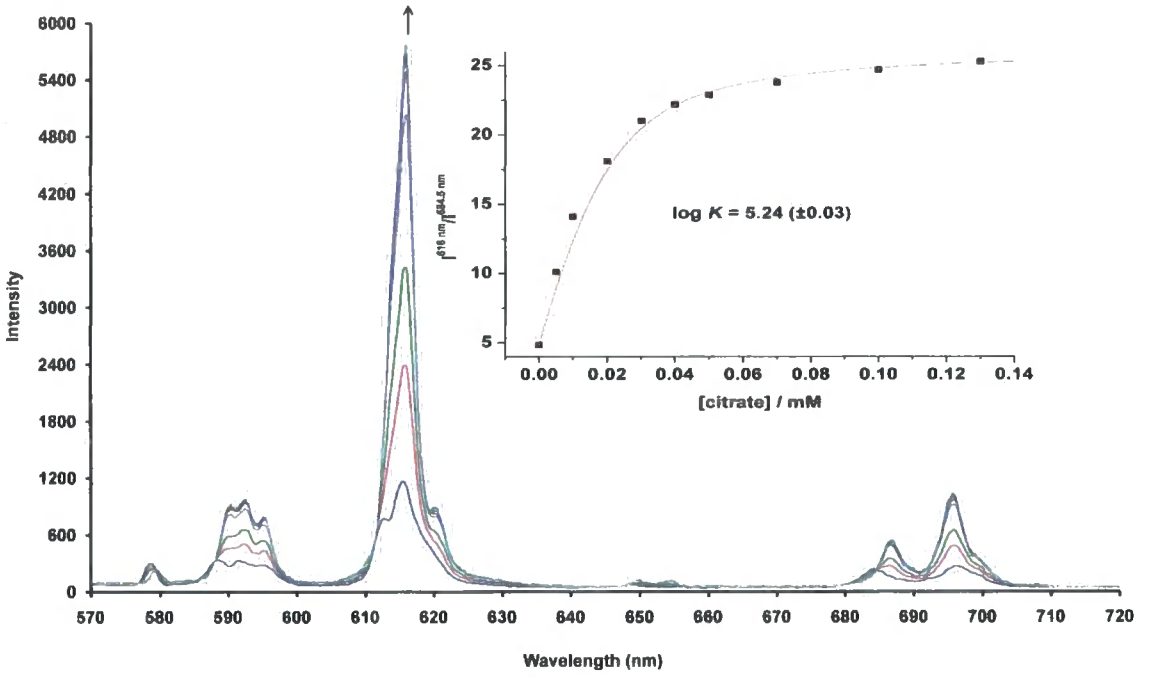

Figure 2.26 – Variation of the Eu(III) emission spectra for $[EuL^{51b}]^{3+}$ following addition of sodium citrate (H_2O, pH = 7.4 (±0.05), 0.02 mM complex, 298 K, I = 0.1 M NaCl, λ_{exc} = 375 nm. Inset is a plot of the intensity ratio (616/684.5 nm) with [citrate], allowing calculation of the apparent binding constant.

In stark contrast, the Eu(III) emission response of $[EuL^{52}]^{3+}$ with the anions investigated was minimal. Changes were just sufficient to allow calculation of apparent affinity constants. In addition, ^{1}H-NMR spectra of $[EuL^{52}]^{3+}$ (5 mM, pD 7.8, 295 K, 200 MHz) alone were compared to those obtained in the presence of added $NaHCO_3$

(30 mM). Addition of HCO_3^- resulted in the sharpening of the observed complex resonances but no major differences in the ^{1}H-NMR spectra were observed.

Of the structurally related complexes $[EuL^{44b}]^{3+}$ and $[EuL^{52}]^{3+}$, affinity constants were higher with $[EuL^{44b}]^{3+}$. This can be attributed to the extra enthalpic and entropic benefit of displacing two water molecules in citrate, lactate and bicarbonate binding. With $[EuL^{44b}]^{3+}$ in the presence of anions at their common 'extracellular' concentrations, HCO_3^- competes with citrate for Eu(III) coordination. A titration of $[EuL^{44b}]^{3+}$ with sodium citrate, in a $NaHCO_3$ background (30 mM), revealed a decrease in the affinity constant from log K = 6.02 to log K = 3.33 ($\pm$0.02). This allows an estimate of the ratio of the $[EuL^{44b}]^{3+}$ citrate adduct to the $[EuL^{44b}]^{3+}$ carbonate adduct. This is calculated to be 7:1.

The lower affinity of $[EuL^{51b}]^{3+}$ for HCO_3^- and phosphate follows the trend observed in similar complex structures, such as $[EuL^{36}]^{3+}$.[79,95] In addition, separate protein titration experiments, using HSA, with each of the three complexes were carried out to determine relative protein affinity constants. Assuming 1:1 binding, an apparent HSA affinity constant of log K = 3.71 ($\pm$0.03) was calculated for $[EuL^{51b}]^{3+}$. The value recorded with $[EuL^{52}]^{3+}$ was log K = 3.10 ($\pm$0.03). The affinity of $[EuL^{44b}]^{3+}$ with HSA could not be determined due to the severity of quenching of the Eu(III) emission. A independent method, monitoring the variation in the relaxivity of $[GdL^{44b}]^{3+}$ as a function of added protein, also did not permit a protein affinity constant to be estimated.[96]

The binding studies presented highlight the significant differences in anion selectivity exhibited by these complexes, notwithstanding the small pertubation in ligand structure. An explanation for this differing behaviour may be reached through consideration of the differing coordination geometries of the major solution species. All evidence obtained for $[EuL^{44b}]^{3+}$ suggests that this complex possesses the coordination environment exhibited by $[EuL^{24}]^{3+}$, the structure of which has been probed through X-ray analyses of crystals of $[YbL^{24}]^{3+}$ and citrate, lactate and carboxylate

adducts of $[EuL^{24}]^{3+}$.[64] In each of these complexes a water molecule has been shown to occupy the 'axial' coordination site (upper diagram, Figure 2.27). Upon binding to carbonate, this water molecule is displaced by an oxygen atom of the anion. As explained in section 1.5.3, this results in a change of the second order crystal field coefficient, which gives rise to changes in ^{1}H-NMR and Eu(III) emission spectra.

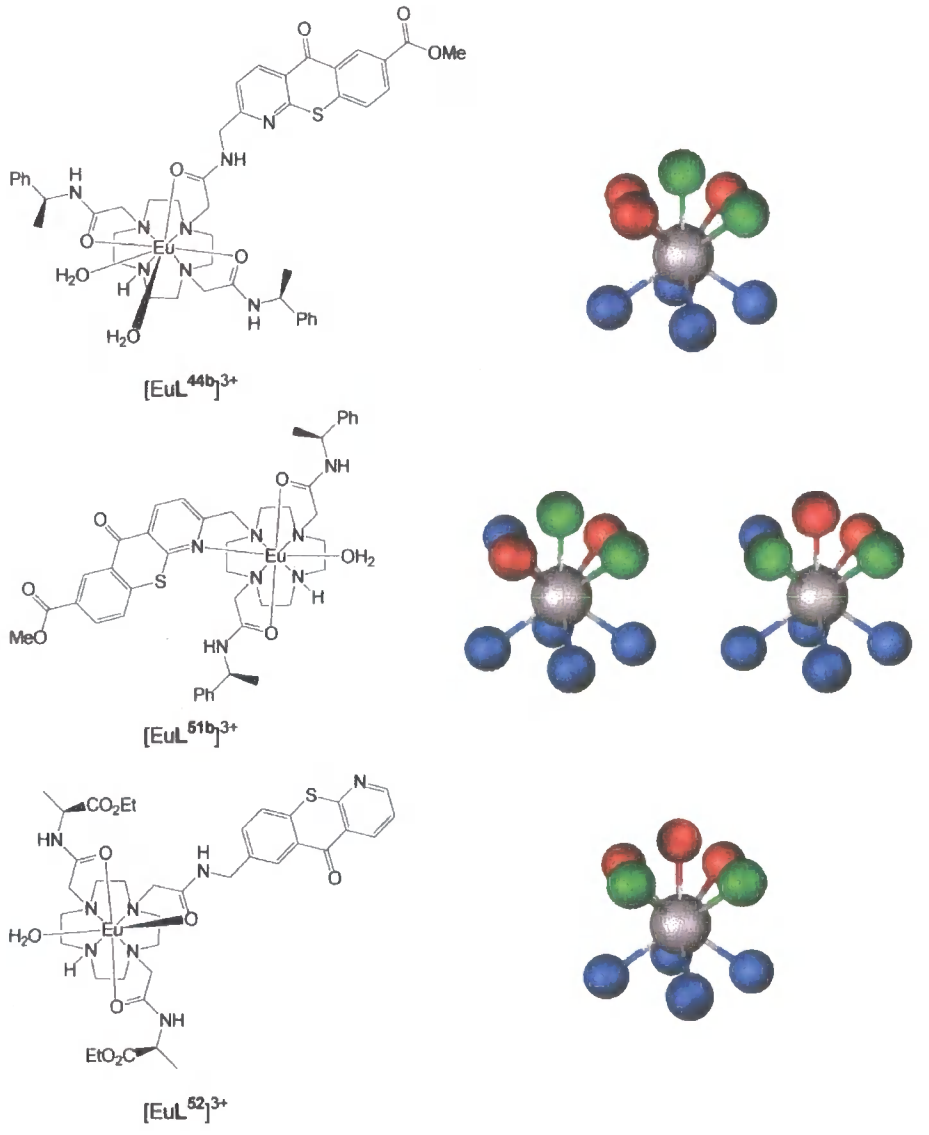

Figure 2.27 – A representation of the hypothesised coordination geometries of $[EuL^{44b}]^{3+}$, $[EuL^{51b}]^{3+}$ and $[EuL^{52}]^{3+}$. Coordinating cyclen N-atoms are seen in the lower plane (blue), pendant amide arm carbonyl O-atoms (red) and 'vacant' coordination sites (green) which may or may not be occupied by water (solvent). For $[EuL^{51b}]^{3+}$, the coordinating pyridyl N-atom is shown in blue, above the plane of the cyclen N-atoms.

The minimal response in ^{1}H-NMR and Eu(III) emission spectra following anion binding to $[EuL^{52}]^{3+}$ suggests that a benzylic amide carbonyl oxygen must occupy the 'axial' capping site in both the aqua complex and in its various anion adducts (lower diagram, Figure 2.27). Hence, the axial donor ligand, and therefore the second order crystal field coefficient remain constant. This may occur with a distorted square anti-prismatic or bicapped trigonal prismatic coordination environment. Considering the former model, anion chelation could occur at two sites in the plane of the square antiprism. Finally, the 'intermediate' behaviour of $[EuL^{51b}]^{3+}$, where citrate binding results in large changes in the emission spectra whilst other anion binding does not, can be rationalised by consideration of the fluxional nature of the coordination environment of this complex. It is possible that the position of anion coordination is dependent upon the steric demand of the anion itself. Small anions may be able to bind in the plane of the square antiprism resulting in a minimal spectral response, whilst the larger citrate anion must be able to chelate to axial and equatorial positions (centre diagram, Figure 2.27). This would be in keeping with the hypothesis of a weakly bound pyridyl *N*-atom of the sensitiser.

2.3.3 Luminescence microscopy and cellular cytotoxicity studies

As stated at the outset, these Eu(III) probes could be used to monitor the spatial distribution and concentrations of selected anions, in live cells in real time. It is therefore important that such probes are not significantly toxic to the cells in which they are to be examined. One relative indicator of complex cytotoxicity is the MTT assay.[97] This assay utilises the conversion of 3-(4,5-dimethylthiazol-2-yl)-2,5-diphenyltetrazolium bromide to a purple 'formazan' product by mitochondrial dehydrogenase enzymes of viable cells. The 'formazan' product is insoluble in water but can be solubilised with DMSO; it is then quantified spectrophotometrically. Typically, 24 h incubations of varying concentrations of complex or ligand with at least 10000 cells were analysed to obtain an IC_{50} value. This is defined as the concentration of complex required to reduce the absorbance to 50 % of that in the untreated cells.

Complex or ligand	$IC_{50}/\mu M$
$[EuL^{44a}]^{3+}$	164(±31)
L^{44a}	99.3(±11.8)
$[EuL^{44b}]^{3+}$	>270
L^{44b}	>350
$[EuL^{49}]^{3+}$	109(±16)
$[EuL^{50}]^{3+}$	>240
L^{50}	173(±17)
$[EuL^{51a}]^{3+}$	173(±34)
L^{51a}	180(±15)
$[EuL^{51b}]^{3+}$	5.62(±0.34)
L^{51b}	4.87(±1.26)

Table 2.4 – Cell toxicity profiles (IC_{50} in NIH-3T3 cells) for Eu(III) complexes and ligands.

It is seen that the only significant toxicity was observed with $[EuL^{51b}]^{3+}$. This behaviour contrasted with every other Eu(III) complex tested. In addition, the complex cytotoxicity was also reflected in the IC_{50} value of the corresponding ligand, L^{51b}. The correlation of these values is consistent with the dissociation of the complex *in cellulo*, over the incubation period. The origins of the toxicity of $[EuL^{51b}]^{3+}$ were examined through the measurement of IC_{50} values of 2-methylazaxanthone (>240 μM), 2-methylazathioxanthone (72.5(±6.3) μM) and the corresponding sulfoxide (>240 μM) and sulfone (21.1(±0.2) μM) analogues, Figure 2.28. These results provide a tentative link between IC_{50} values and oxidative metabolism of L^{51b}. Similar cytotoxicity profiles were observed in Chinese Hamster Ovarian (CHO) cells.

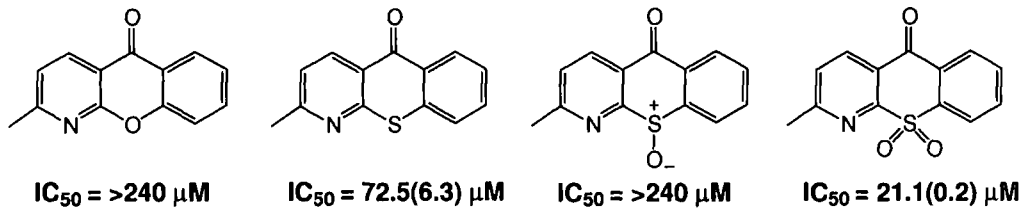

Figure 2.28 – Structures of 2-methylazaxanthone, 2-methylazathioxanthone and its derivatives and their corresponding IC_{50} values in NIH-3T3 cells.

Cellular uptake of the Eu(III) complexes was examined by fixed cell imaging in NIH-3T3 and CHO cells. Incubation of cells grown on glass cover-slips for periods of 20 m to 24 h was carried out in the presence of complex concentrations of

10 μM to 100 μM. The ligand fluorescence (where possible) and Eu(III) emission was monitored by fluorescence microscopy after excitation at the sensitiser λ_{max}. Untreated control cells showed no luminescence at wavelengths monitored whilst luminescence was observed in treated cells at a variety of optical sections, showing that the complex was internalized within the cell and not just associated with the cell membrane. Localisation profiles were observed in cells at various points on the slide. The localisation behaviour of $[EuL^{44a}]^{3+}$, $[EuL^{44b}]^{3+}$ and $[EuL^{49}]^{2+}$ was examined in each cell line. Fluorescence microscopy revealed that within 5 minutes of cell incubation with a 50 μM complex solution, the complex was localised within the mitochondria. This observation was supported by co-localisation experiments with Mitotracker Green™ (Invitrogen) in which merged images corresponded well, Figure 2.29. When longer incubation times were used, the complex was observed to migrate from the mitochondria to late endosomes/lysosomes.

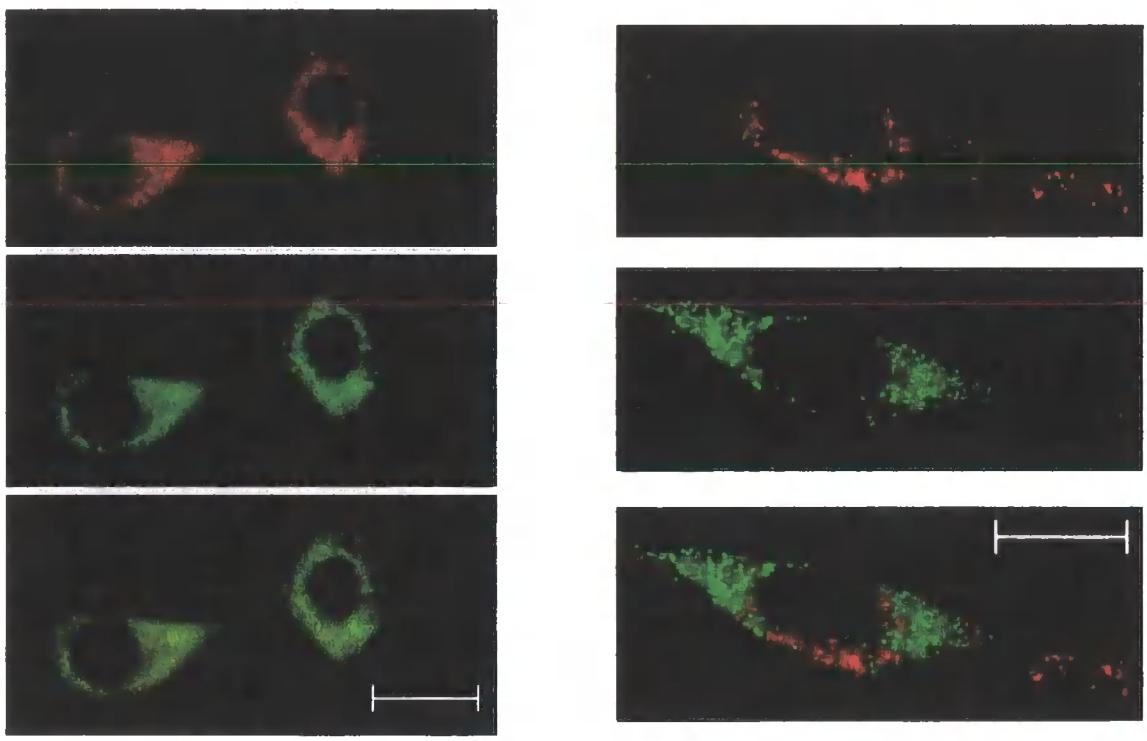

Figure 2.29 – Epifluorescence microscopy images for $[EuL^{44b}]^{3+}$: 50 μM complex, 4 h incubation (left set of images); 50 μM complex, 24 h incubation (right set of images). Images reveal a mitochondrial localisation profile after 4 h and a profile consistent with migration of the complex from the mitochondria to the perinuclear endosomes/lysosomes after 24 h. Upper images: Eu(III) complex; centre images: Mitotracker Green™; lower images: merged image (scale bars 20 microns).

The interesting localisation profiles of $[EuL^{44a/b}]^{3+}$ warranted further preliminary investigation. In particular, the known quenching of these complexes in the presence of protein, and the observation that the complexes were still highly luminescent when localised within the mitochondrial environment posed interesting questions as to the nature of their coordination environment. Given the mitochondrial localisation of these complexes, and their affinity for carbonate and citrate, it was hypothesised that the majority of intracellular complex adducts would be those of carbonate or citrate. To study this hypothesis, an experiment was carried out that monitored the relative luminescence intensity of the mitochondrially localised complex, under varying atmospheric CO_2 concentrations, Figure 2.30.

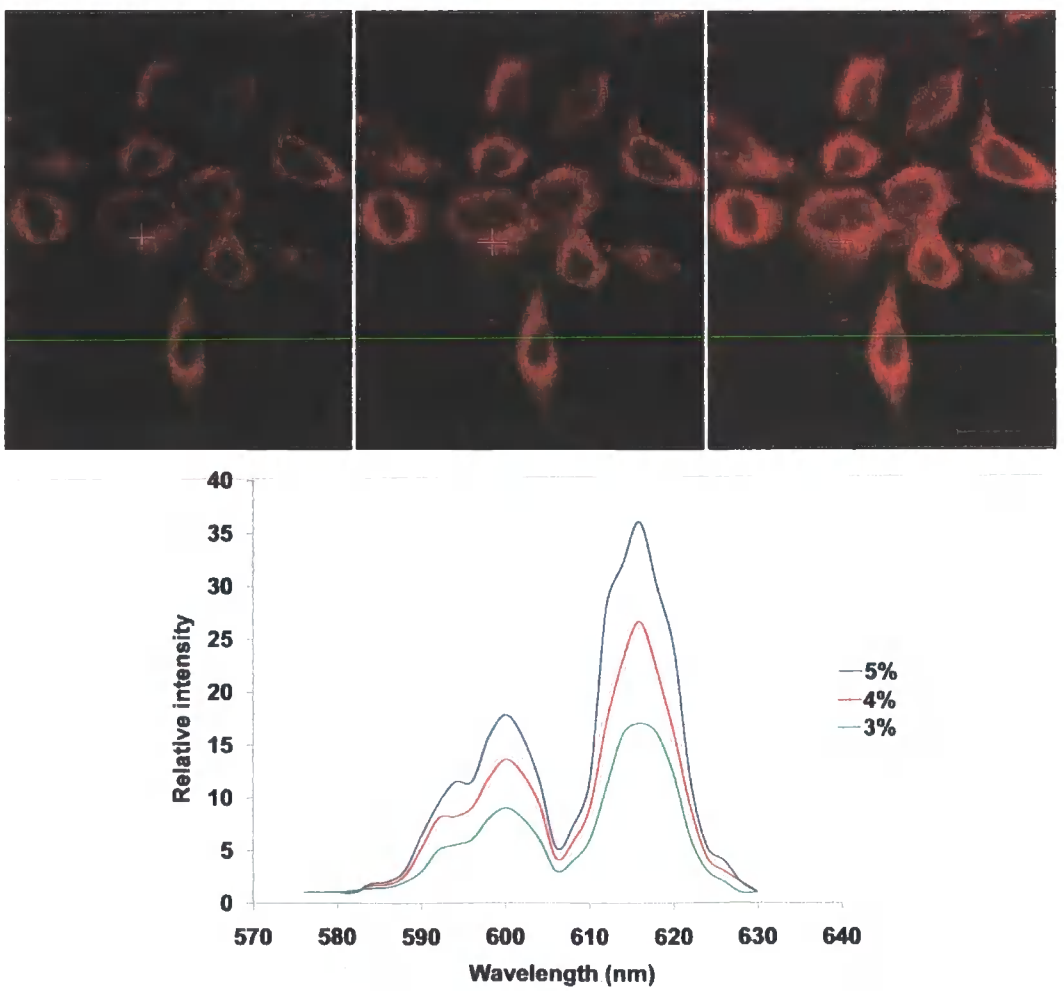

Figure 2.30 – Confocal microscopy images for $[EuL^{44a}]^{3+}$ (50 μM complex, 2-3.5 h incubation, λ_{exc} = 360 nm) in HeLa cells at 3 % (left image), 4 % (centre image) and 5 % (right image) atmospheric CO_2 (scale bar 20 microns). The graph shows a plot of the relative intensities of complex emission as a function of pCO_2.

As can be observed, $[EuL^{44a}]^{3+}$ emission intensity decreased as the level of atmospheric CO_2, and consequentially mitochondrial HCO_3^- concentration, was reduced. Earlier experiments with consistent CO_2 levels had suggested no significant modulation of Eu(III) emission intensity, over the time course of this experiment. This preliminary result is encouraging as it offers the possibility that future work involving this complex, or related structures, may be able to relay spatial concentrations of HCO_3^- in real time.

The complexes $[EuL^{51a}]^{3+}$ and $[EuL^{51b}]^{3+}$ were examined within both NIH-3T3 and CHO cell lines, and exhibited similar localisation profiles. In each case rapid transport of the complex to the perinuclear lysosomes was observed to occur by monitoring Eu(III) emission and examining co-staining experiments with Lysotracker Green™, Figure 2.31.

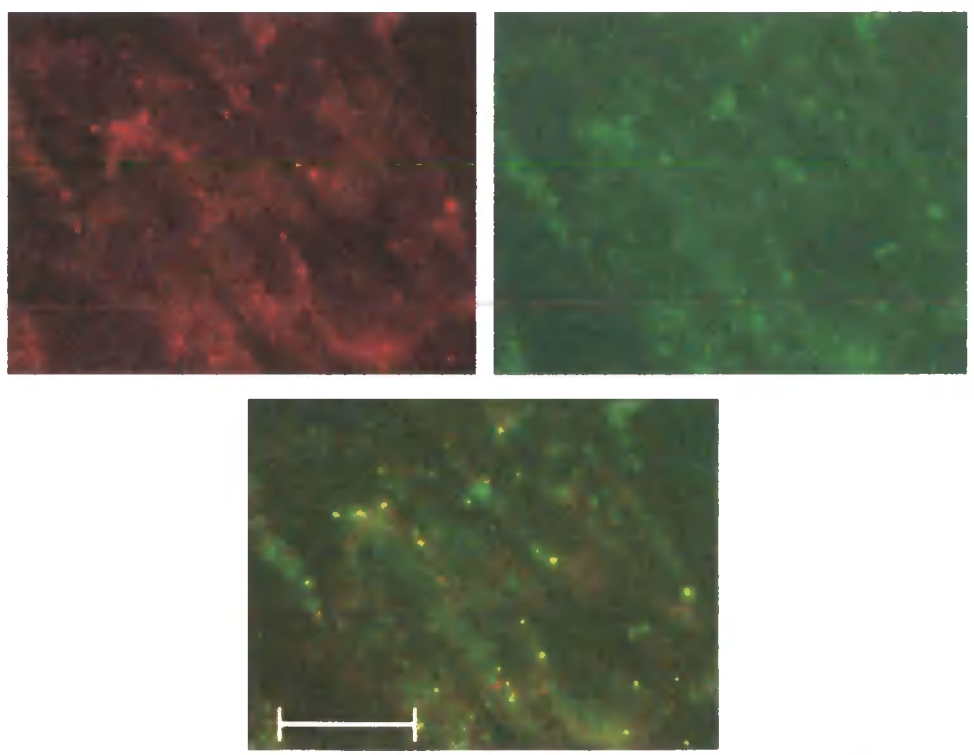

Figure 2.31 – Epifluorescence microscopy images for $[EuL^{51b}]^{3+}$. 50 μM complex, 1 h incubation, co-staining experiments with Lysotracker Green™: upper left image: Eu(III) complex (575-625 nm); upper right image: Lysotracker Green™ (FITC filter set); lower image: merged image (scale bar 20 microns). After 1 h Eu(III) emission and Lysotracker Green™ largely correspond, consistent with a common lysosomal localisation profile.

The use of appropriate filter sets allowed Eu(III) emission and ligand fluorescence to be separately observed, Figure 2.32. It was noted that they did not spatially correspond as ligand fluorescence was observed in the mitochondria after 1 h (50 μM complex), 4 h (20 μM complex) and 24 h (10 μM complex) incubation periods. Such an observation is consistent with complex dissociation within the cell, and is also consistent with the cytotoxicity profiles of $[EuL^{51b}]^{3+}$ and L^{51b} reported above. The high toxicity of the complex, due to its dissociation, resulted in images of lower quality being obtained, compared to the other complexes examined.

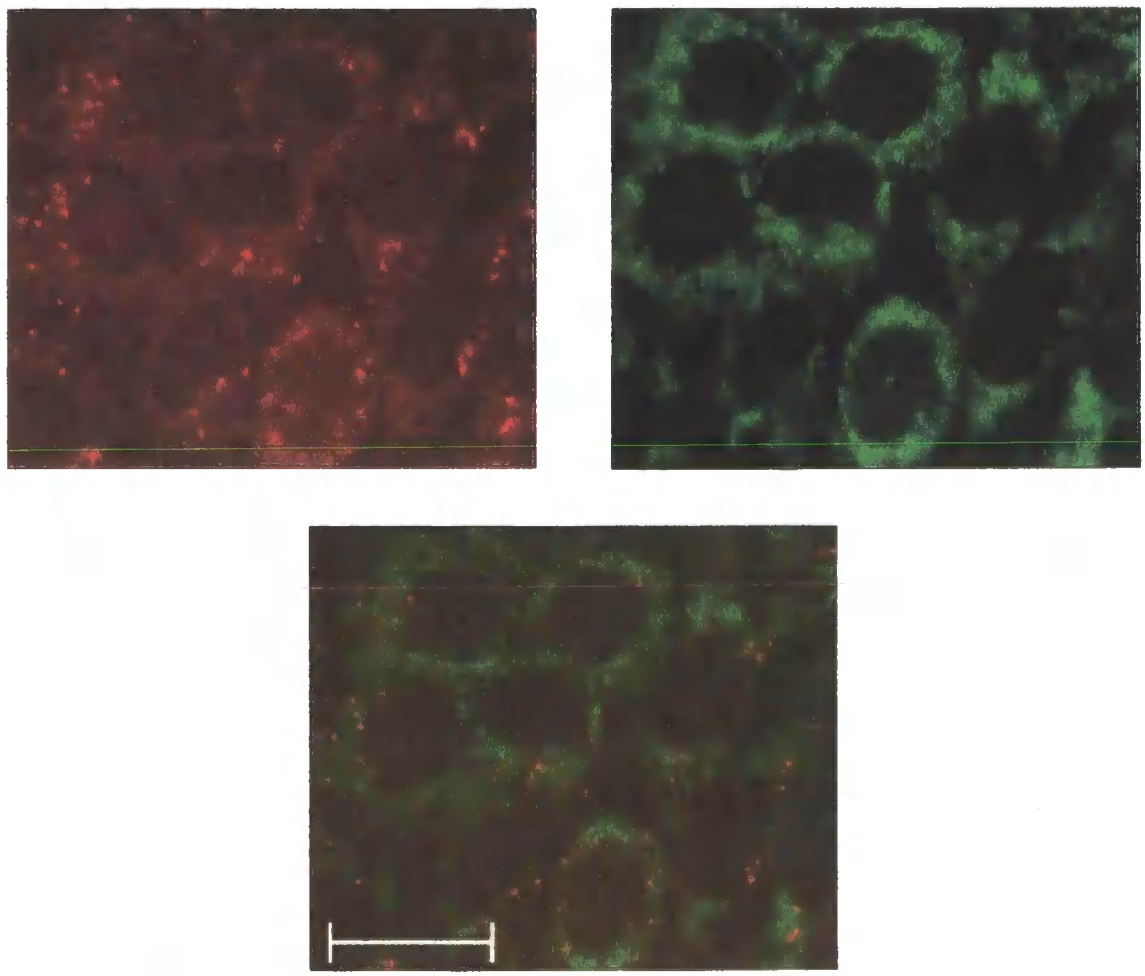

Figure 2.32 – Epifluorescence microscopy images for $[EuL^{51b}]^{3+}$. 50 μM complex, 1 h incubation, comparing localisation of ligand fluorescence and Eu(III) emission: upper left image: Eu(III) complex (575-625 nm); upper right image: ligand fluorescence (450 ± 50 nm); lower image: merged image (scale bar 20 microns). Images reveal ligand fluorescence and Eu(III) emission begin not to spatially correspond after 1 h, indicating complex dissociation.

2.4 Studies with $[EuL^{50}]^{3+}$

As described in section 2.2.1, the octadentate complex $[EuL^{50}]^{3+}$ was synthesised as part of studies examining the cellular uptake of a wide series of Ln(III) complexes. In light of the differing cellular localisation profiles of $[EuL^{44a/b}]^{3+}$ and $[EuL^{51a/b}]^{3+}$ it was appropriate to probe whether the linkage between the sensitiser and complex dictated the localisation profile of the complex. $[EuL^{50}]^{3+}$ possesses a similar ligand structure to that of $[EuL^{44a/b}]^{3+}$. The only difference is the extra pendant amide arm, which may be expected to reduce the conformational mobility of the ligand compared to $[EuL^{44a/b}]^{3+}$. The amide linkage between the sensitiser and complex may be expected to be orientated around the metal ion in a similar fashion to that present in $[EuL^{44a/b}]^{3+}$. Therefore, the complex was considered as a good target for such a comparative study.

The ^{1}H-NMR spectrum of the complex showed the presence of a well defined major isomer, Figure 2.33. In addition, a small amount (<10 %) of a second isomer was also observed.

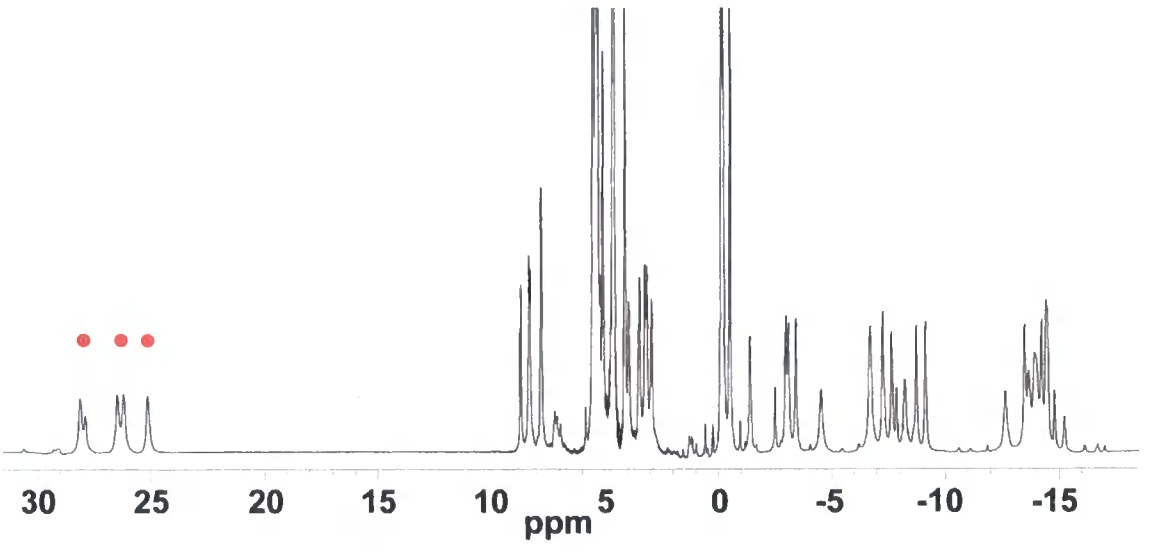

Figure 2.33 – ^{1}H-NMR spectra for $[EuL^{50}]^{3+}$ (500 MHz, D_2O, 295 K, pD 7.8, 1 mM). Resonances marked with • are assigned to cyclen H_{ax} protons.

The emission spectrum of the complex was acquired in the absence and presence of HSA, Figure 2.34. As expected, Eu(III) emission was quenched in the presence of

protein. This result provides further support for the hypothesis of a charge transfer quenching process. Evidently, the octadentate complex cannot directly bind to the protein through the Eu(III) centre.

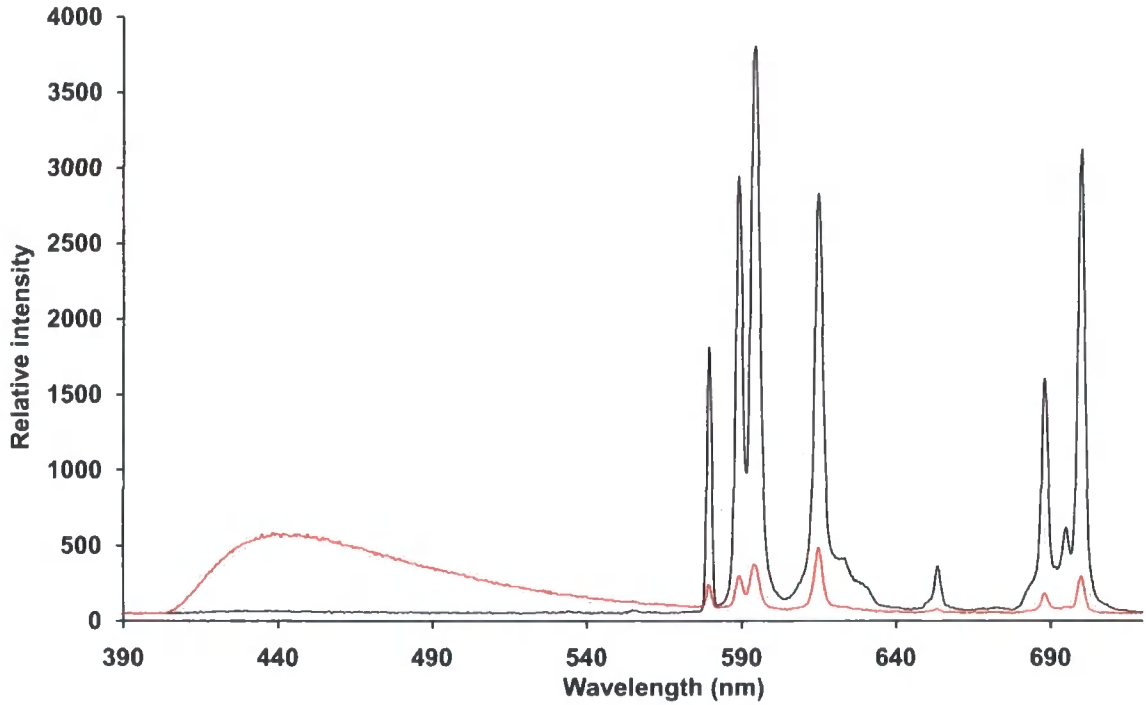

Figure 2.34 – Eu(III) emission spectra for $[EuL^{50}]^{3+}$ alone (black) and in the presence of HSA (0.35 mM) (red) (H_2O, pH = 7.4, 0.05 mM complex, 298 K, λ_{exc} = 335 nm).

The Eu(III) excited state lifetimes were recorded in H_2O and D_2O and in the presence of HSA, Table 2.5. These revealed the direct Eu(III) coordination of one water molecule in aqueous solution. On addition of HSA, the q value of the complex decreased. This indicates shielding of the complex from the bulk solvent by HSA, thereby reducing quenching of the Eu(III) excited state.

Complex/anion	$k_{(H_2O)}/ms^{-1}$	$k_{(D_2O)}/ms^{-1}$	$\Delta k/ms^{-1}$	q^a
$[EuL^{50}]^{3+}/Cl^-$	1.72	0.44	1.28	0.86
HSA	1.35	0.58	0.77	0.26

Table 2.5 – The rate constants (k) (± 10 %) for radiative decay of the excited state of $[EuL^{50}]^{3+}$ (0.05 mM) (± 10 %) as the aqua complex and in the presence of HSA (0.35 mM) (295 K, pH 7.4) and derived hydration numbers, q (± 20 %). [a] $q^{Eu} = 1.2[(k_{(H_2O)}\text{-}k_{(D_2O)})\text{-}(0.25+0.07x)]$ (x = number of carbonyl-bound amide NH oscillators).[57]

2.4.1 Luminescence microscopy and cellular cytotoxicity studies

The IC_{50} value of >240 μM obtained for $[EuL^{50}]^{3+}$ shows that this complex is non-toxic to cells, Table 2.4. Cellular uptake of $[EuL^{50}]^{3+}$ was examined by fixed cell imaging as described above.

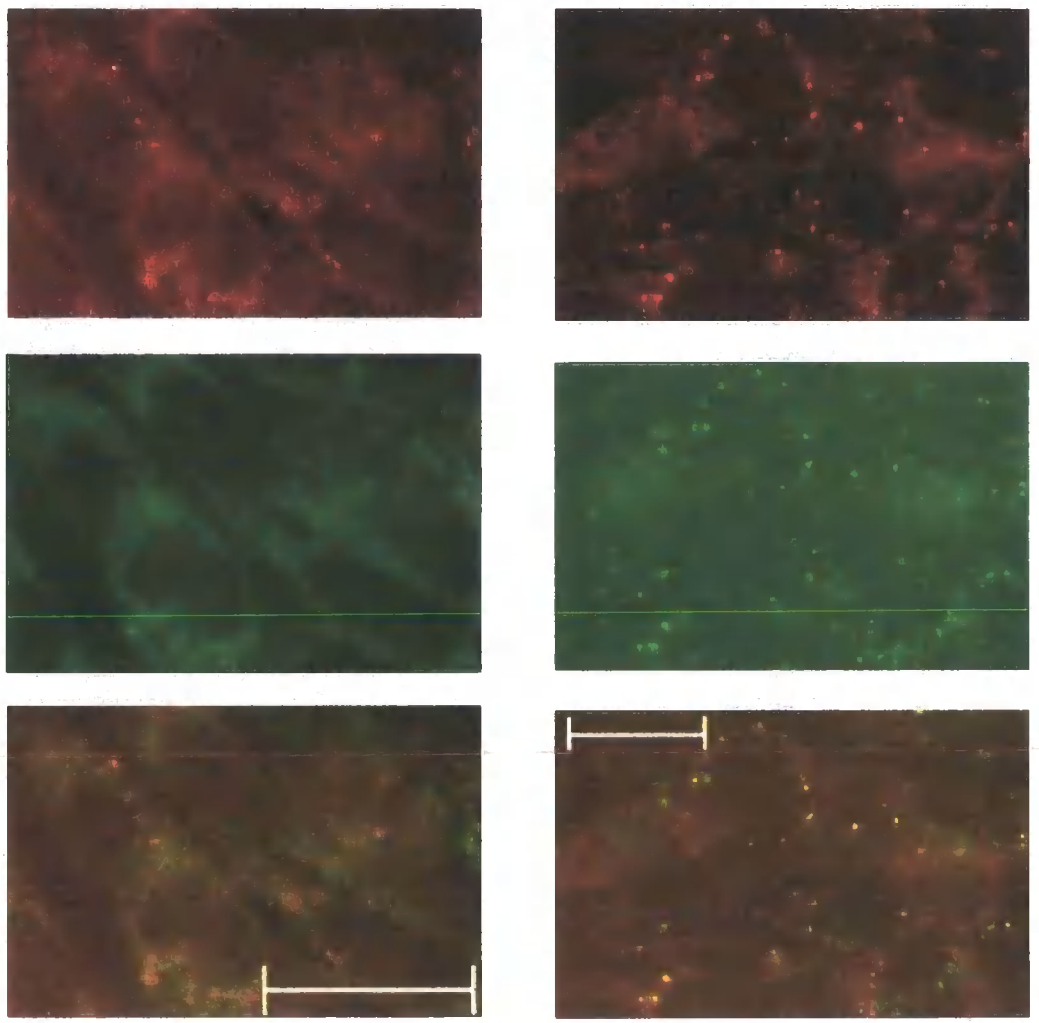

Figure 2.35 – Epifluorescence microscopy images for $[EuL^{50}]^{3+}$. Left set of images (50 μM complex, 4 h incubation, examining mitochondrial localisation): Upper image: Eu(III) complex; centre image: Mitotracker Green™; lower image: merged image (scale bar 20 microns). Right set of images (50 μM complex, 4 h incubation, examining lysosomal localisation): Upper image: Eu(III) complex; centre image: Lysotracker Green™; lower image: merged image (scale bar 20 microns). Images reveal a localisation profile split between the mitochondria and lysosomes.

Fluorescence microscopy revealed that within 15 min, in NIH-3T3 and CHO cell lines, $[EuL^{50}]^{3+}$ was localised within the mitochondria and late endosomes/lysosomes.

Localisation was confirmed by appropriate co-staining experiments with Mitotracker Green^{TM} and Lysotracker Green^{TM} (Invitrogen), Figure 2.35. Similar localisation was also observed after incubation times of 4 h and 24 h, the relative distribution does not appear to change over time.

These observations suggest that the intra-cellular localisation of complexes of this structure type may not be dictated solely by the nature of the functionality between the macrocycle and sensitiser. However, the complexes reported here form only a very small data set and any relationships drawn between complex structure and their intracellular localisation are extremely tentative. Ongoing work is attempting to compare a wider range of structures.

2.5 Conclusions

A variety of Eu(III) complexes have been synthesised that bind preferentially to selected anions in aqueous media. The complexes report on their local coordination environment either through modulation of Eu(III) emission or ^{1}H-NMR spectra. The syntheses of the complexes were achieved through a variety of common synthetic intermediates, providing routes by which subtly different ligand structures could be prepared expediently. The combined wealth of spectral information that was gained in these anion binding studies allowed the effect of these subtle ligand changes on the anion binding properties of the respective complexes to be probed. It was found that the anion binding selectivities of the complexes could generally be 'predicted' for certain classes of anions, based on previous studies. This work further demonstrates that knowledge of the behaviour of these cyclen based complexes is certainly sufficient to allow the creation of receptors that target specific anions in aqueous media. One common feature of each complex was their preference to bind to (O-P-Tyr)$^{2-}$ in the presence of equimolar equivalents of any other anion examined. This preference is still tentatively attributed to the high charge density and reduced level of hydration of (O-P-Tyr)$^{2-}$, compared to related phospho-anions.

Cellular localisation profiles of the complexes were also examined. The most well defined complexes e.g. $[EuL^{44a/b}]^{3+}$ proved to be non-toxic to the cells. Complexes of low kinetic stability proved toxic and this was tentatively related to the oxidative metabolism products of the ligand. $[EuL^{44a/b}]^{3+}$ possessed a very interesting localisation profile, remaining within the mitochondrial environment for extended incubation periods before being shuttled along a lysosomal path. Furthermore, these complexes remained luminescent within the mitochondrial environment, despite the quenching of the complex by protein as revealed *in vitro*. It is likely that the complex is binding to anionic species within the cell. This was backed up by a preliminary study that revealed a dependence of $[EuL^{44a}]^{3+}$ emission intensity on atmospheric pCO_2. Adducts with anions will probably be in exchange with protein bound complex, as observed *in vitro*. Aside from carbonate adducts, it is likely that a significant proportion of luminescent species within the mitochondrial environment will be citrate adducts. The resulting emission spectra of $[EuL^{44a}]^{3+}$ in the mitochondrial environment will therefore be a convoluted average of all the species present.

Notwithstanding the carbonate/citrate selectivity issues, the reported results augur well for the future development of a chemoselective probe that can relay the concentration of essential anion concentrations such as HCO_3^- or citrate on the Eu(III) emission timescale, within specific cellular organelles.

2.6 Future work

The mitochondrial localisation of $[EuL^{44a/b}]^{3+}$ and $[EuL^{49}]^{2+}$ is unprecedented for such responsive Ln(III) complexes. Future work should fully exploit this feature. An initial experiment would be to repeat the experiment examining the emission intensity of mitochondrially localised $[EuL^{44a}]^{3+}$ as a function of pCO_2. In this repeat, one new aspect would be to examine the reversibility of the changes in complex emission intensity upon the raising and lowering of pCO_2, hence establishing whether or not this is a dynamic signalling process.

To enable intracellular emission spectra to relay the concentration of bicarbonate, a calibration would need to be established, based upon the ratiometric analysis of two wavelengths, for example, of the ΔJ=1 and ΔJ=2 manifolds. However, a further method could be to examine the utility of using $[Eu\mathbf{L}^{44a}]^{3+}$ and $[Tb\mathbf{L}^{44a}]^{3+}$ in tandem as a bicarbonate probe. In theory, the ratio of emission at 545 nm ($[Tb\mathbf{L}^{44a}]^{3+}$) and 616 nm ($[Eu\mathbf{L}^{44a}]^{3+}$) would change as a function of $pHCO_3^-$. As each complex shares a common ligand, any competing anionic species and protein quenching would affect each complex equally, notwithstanding their differing anion affinities, and therefore the recorded ratio would include an intrinsic correction for these factors. This therefore means that in a competitive anionic environment, such as within the mitochondria, any changes in the ratio of both emission intensities could be related back, through a calibration plot, to the concentration of bicarbonate. Before tandem probe methodology could be established, the response of $[Tb\mathbf{L}^{44a}]^{3+}$ to bicarbonate and protein concentrations would have to be thoroughly examined through a series of luminescent binding titrations. This is because the different charge density of Tb(III) means that its anion and protein affinity will be slightly different to that of Eu(III), and because Tb(III) emission is not as sensitive to its coordination environment as Eu(III) emission.

Another interesting exercise would be to determine the variation of mitochondrial pH as a function of pCO_2. The probe could be based on $[Eu\mathbf{L}^{44a}]^{3+}$ to try and conserve cellular localisation properties. The free cyclen amine group would be substituted by a pH sensitive functionality that over the physiological pH range will ligate to the Eu(III) ion. The resulting emission profile of the complex would be related back to the local pH. A previously reported example is that of a sensitised Eu(III) complex incorporating an *N*-methylsulfonamide moiety.[98,99] This complex enabled the measurement of pH in the range of 6-8. An initial step to determine the effect of *N*-substitution on the cellular localisation of $[Eu\mathbf{L}^{44a}]^{3+}$ could be to synthesise the *N*-methylated analogue. In addition, the association of bicarbonate and citrate with the *N*-methylated analogue could be examined to determine if any further selectivity between these two anions could be established with this

complex. It would be expected that association constants for these two anions with *N*-methylated $[EuL^{44a}]^{3+}$ would be greater than for $[EuL^{44a}]^{3+}$, because of the reduced free energy of hydration of the former complex, as postulated for related complexes such as $[LnL^{25}]^{3+}$.[66]

Another route may be to tune complex selectivity more towards either bicarbonate or citrate. Because cellular localisation profiles of complexes can not yet be reliably predicted, initial work may address the issue of anion selectivity through the synthesis of complexes related to $[EuL^{44a/b}]^{3+}$ that are of lower global charge, Figure 2.36. As an initial step the affinity constants of $[EuL^{49}]^{2+}$ for HCO_3^- or citrate could be estimated to determine the effect of the reduction in global positive charge on anion affinity. If this complex proved to possess a lower selectivity for citrate compared to carbonate then such complexes may be evaluated also. Such a strategy would lead to a Eu(III) complex that exhibits enhanced carbonate affinity/reduced citrate affinity, retains the mitochondrial localisation profile and remains non-toxic.

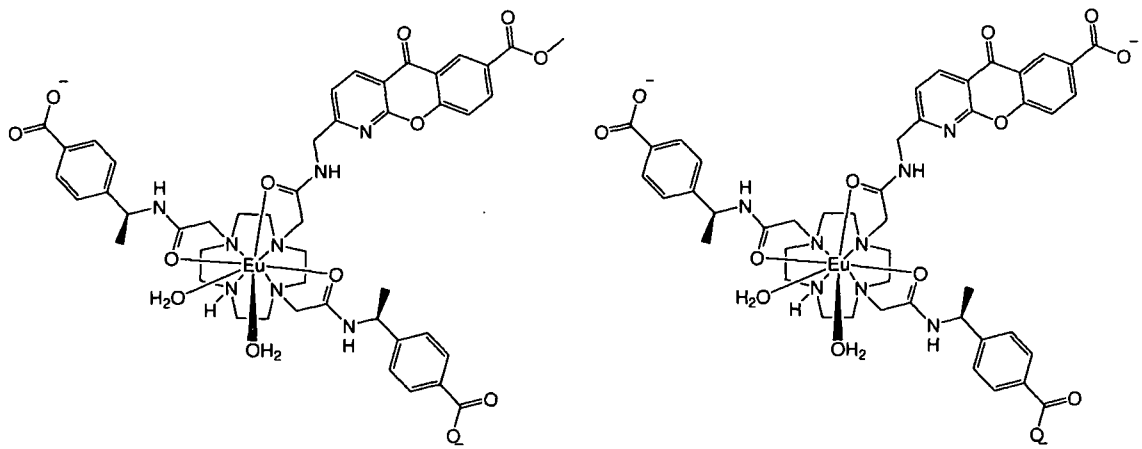

Figure 2.36 – Proposed complexes structurally related to $[EuL^{49}]^{2+}$ bearing a global charge of +1 (left) and 0 (right).

Chapter 3

Anion binding studies with dimeric Ln(III) complexes

3.1 Novel dimeric Ln(III) complexes

3.1.1 Background

The chemoselective ligation of $[EuL^{24}]^{3+}$ to the phosphate functionalities of phosphopeptides **43b-43d**, and the regioselectivity of the complex for binding to residue 9 of the triphosphorylated peptide (**43d**) has been described (section 2.1).

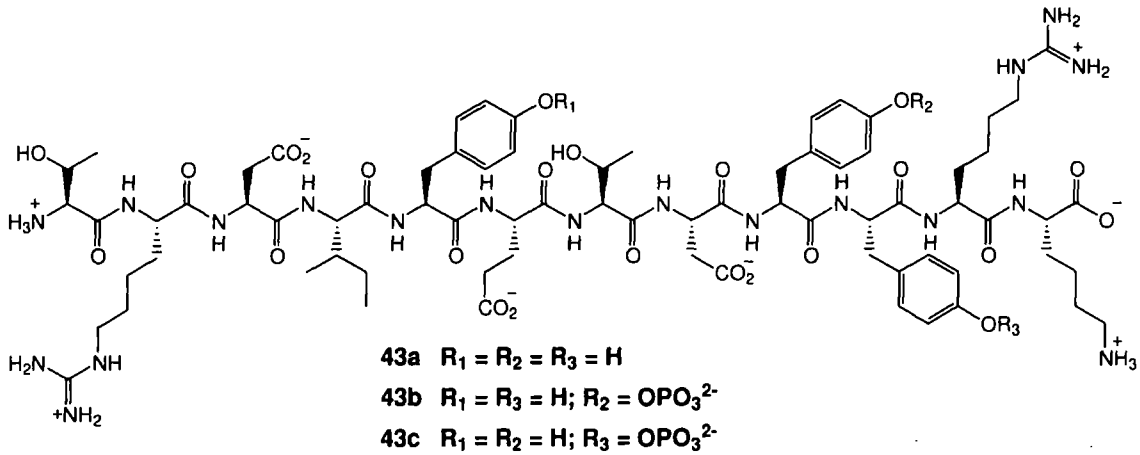

43a $R_1 = R_2 = R_3 = H$
43b $R_1 = R_3 = H$; $R_2 = OPO_3^{2-}$
43c $R_1 = R_2 = H$; $R_3 = OPO_3^{2-}$
43d $R_1 = R_2 = R_3 = OPO_3^{2-}$

In light of these observations, the design and synthesis of closely related dimeric Ln(III) complexes was proposed. The long-term aim of this work was to assess if dimeric complexes could be synthesised that bound to multi-phosphorylated peptide fragments, such as **43d**, in a regioselective manner. For example, binding of a dimeric Ln(III) complex to **43d** could occur at adjacent phospho-tyrosine residues

at positions 9 and 10. Intra-peptide cross-linking could also occur due to complex binding at residues 5 and 9 or 5 and 10. Finally, inter-peptide crosslinking could take place via binding of the complex to phospho-tyrosine residues of different phospho-peptides. In addition, the affinity of dimeric complexes for the phospho-peptides could be estimated and compared to that of the monomeric complex $[EuL^{24}]^{3+}$, to establish if any cooperativity occurred in the binding process.

Several examples of dinuclear Ln(III) complexes have been reported in the literature. Some recently reported structurally related examples are shown below.

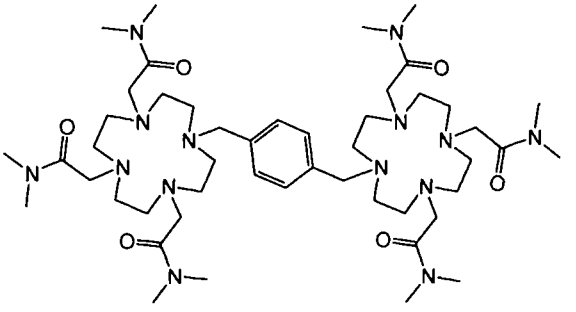

52

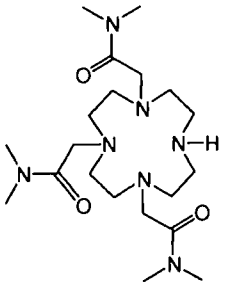

39

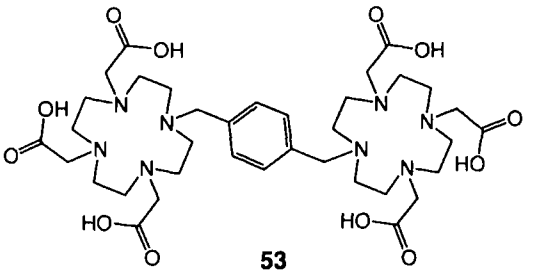

53

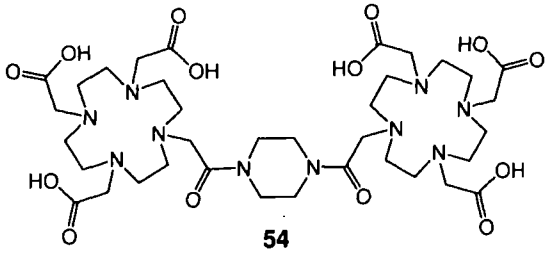

54

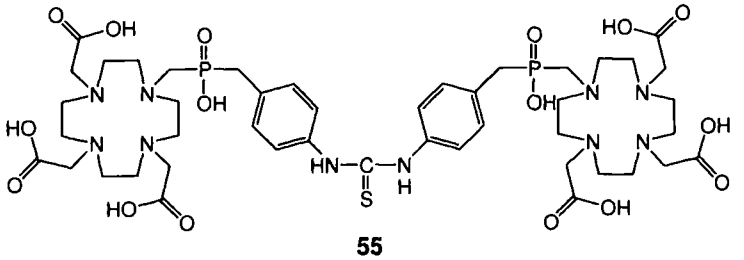

55

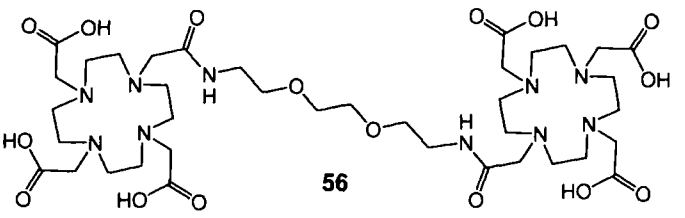

56

One of the most recent reports the dimeric Tb(III) complex, $[Tb_2\mathbf{L}^{52}]^{6+}$.[100] This coordinatively unsaturated complex possesses a *p*-xylylene bridge between the two macrocycles allowing the association of the complex with a range of mono- and bis(carboxylates) to be probed. The design of the dimeric complex was based on the corresponding monomer, $[Tb\mathbf{L}^{39}]^{3+}$ ($[Eu\mathbf{L}^{39}]^{3+}$ was discussed in section 1.6.3), that had been examined in earlier binding studies with aromatic carboxylates.[101] Through analysis of binding titrations, the preference of binding to a range of bridging bis(carboxylates) and mono(carboxylates) was established in neutral, aqueous conditions. The Eu(III), Tb(III) and Yb(III) DO3A analogues of $\mathbf{L}^{52}$, $[Ln_2\mathbf{L}^{53}]$, had been examined in separate earlier work reporting the potential utility of such systems as anion receptors or contrast agents.[102] Other studies have also examined several dimeric Gd(III) complexes as potential MRI contrast agents, $\mathbf{L}^{54}$-$\mathbf{L}^{56}$.[103,104]

3.1.2 Ligand design

The proposed ligands, $\mathbf{L}^{57}$ and $\mathbf{L}^{58}$, are simple extensions of the parent ligand, $\mathbf{L}^{24}$, in which the coordination environment around each Ln(III) ion of the resulting complexes is predicted to be conserved, along with the anion binding properties of the complex.

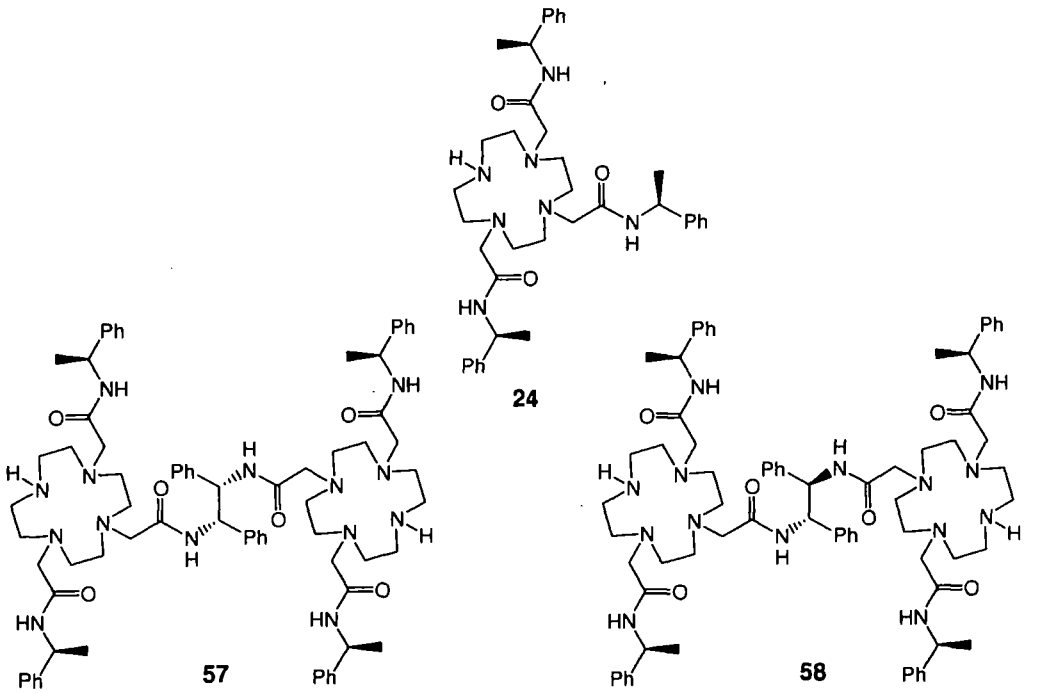

The dimeric ligands were designed so that they possessed a rigid linker backbone in order to reduce the conformational flexibility of the molecule. Two amide bonds and two adjacent Ph groups were incorporated into the linker of the two cyclen units. Such a design was expected to restrict rotation around the central bond. The populations of the ligand conformations were expected to be controlled by the relative stereochemistry at the *C*-atom either side of the central linking bond. For example, the use of a linking molecule possessing (*R*,*R*) or (*S*,*S*) stereochemistry may be expected to result in the formation of stereoisomeric dimeric ligands with concave conformations. The use of a linking molecule of (*R*,*S*) (*meso*) stereochemistry would be expected to result in a complex with a more open structure. These conformations may be considered through analysis of Newman projections, looking down the central bond of the linking unit, Figure 3.1.

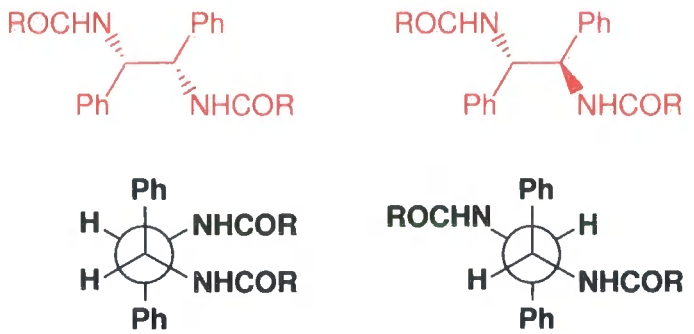

Figure 3.1 – Newman projection of the central linking units of $\mathbf{L}^{57}$ (*S*,*S*) (left) and of $\mathbf{L}^{58}$ (*R*,*S*) (right), highlighting the expected conformations based on consideration of steric demand.

Modulation of the central stereocentres allows the effect of complex conformation on binding to a multi-phosphorylated phospho-peptide to be examined. A concave conformation would therefore be expected to be more likely to bind to two phosphate residues of the same peptide, whilst a more open structure might be expected to result in interpeptide cross-linking. The overall complex rigidity is further enforced by the pendant chiral amide arms of the macrocycle which serve to favour one major solution phase isomer. This is beneficial in the analysis of receptor-anion binding, as multiple isomers can complicate subsequent spectral analysis.

3.1.3 Ligand and complex synthesis

Ligands $\mathbf{L}^{57}$ or $\mathbf{L}^{58}$ were synthesised following the strategy used in the synthesis of $\mathbf{L}^{44a/b}$, i.e. modification of the parent ligand $\mathbf{L}^{24}$ at the peripheral segment of one amide arm. The acid intermediate, **46**, was utilised in the synthesis of $\mathbf{L}^{57}$ and $\mathbf{L}^{58}$, Figure 3.2 . Activation of **46** followed by addition of the simple diamines (1*S*,2*S*)-(-)-1,2-diphenylethylenediamine or *meso*-1,2-diphenylethylenediamine resulted in amide formation, yielding the desired protected ligands. It is interesting to note that when (1*S*,2*S*)-(-)-1,2-diphenylethylenediamine was used as the central linking unit the coupling agent, EDC.HCl, proved to be effective at facilitating the formation of the desired BOC protected ligand. It was observed, however, when *meso*-1,2-diphenylethylenediamine was used as the linking unit and EDC.HCl as the coupling agent only one amine group of the linker reacted. Despite variation of the reagent stoichiometries, reaction temperature and solvent, the mono-amide remained the major product. Upon changing the coupling agent to TBTU, the desired product was obtained in reasonable yield, suggesting a possible steric barrier hindering the approach of the mono-amide intermediate toward the active ester of **46**, when EDC.HCl was used. Subsequent BOC removal using TFA/DCM yielded the desired ligands as their TFA salts.

The complexation of $\mathbf{L}^{57}$ or $\mathbf{L}^{58}$ was initially attempted with 2 equivalents of Ln(III) salt. However, alongside the desired product, this resulted in predominant formation of a mono-Ln(III) species, as determined by ESMS analysis. To drive complexation to completion typically 6 equivalents of Ln(III) salt were used, resulting in the desired dimeric complexes. The excess of Ln(III) salt was initially removed by gel filtration chromatography, but this resulted in the loss of large amounts of complex. As a result, the utility of dialysis tubing was investigated. It was observed that passing large volumes of H_2O over a solution of complex (as its chloride/acetate salt) in benzoylated tubing, with a 1200 MW cut-off, resulted in the removal of $LnCl_3$ from the samples, leaving the desired product as determined by ^{1}H-NMR, HPLC,

high resolution ESMS analysis and preliminary X-ray analysis.[105*]

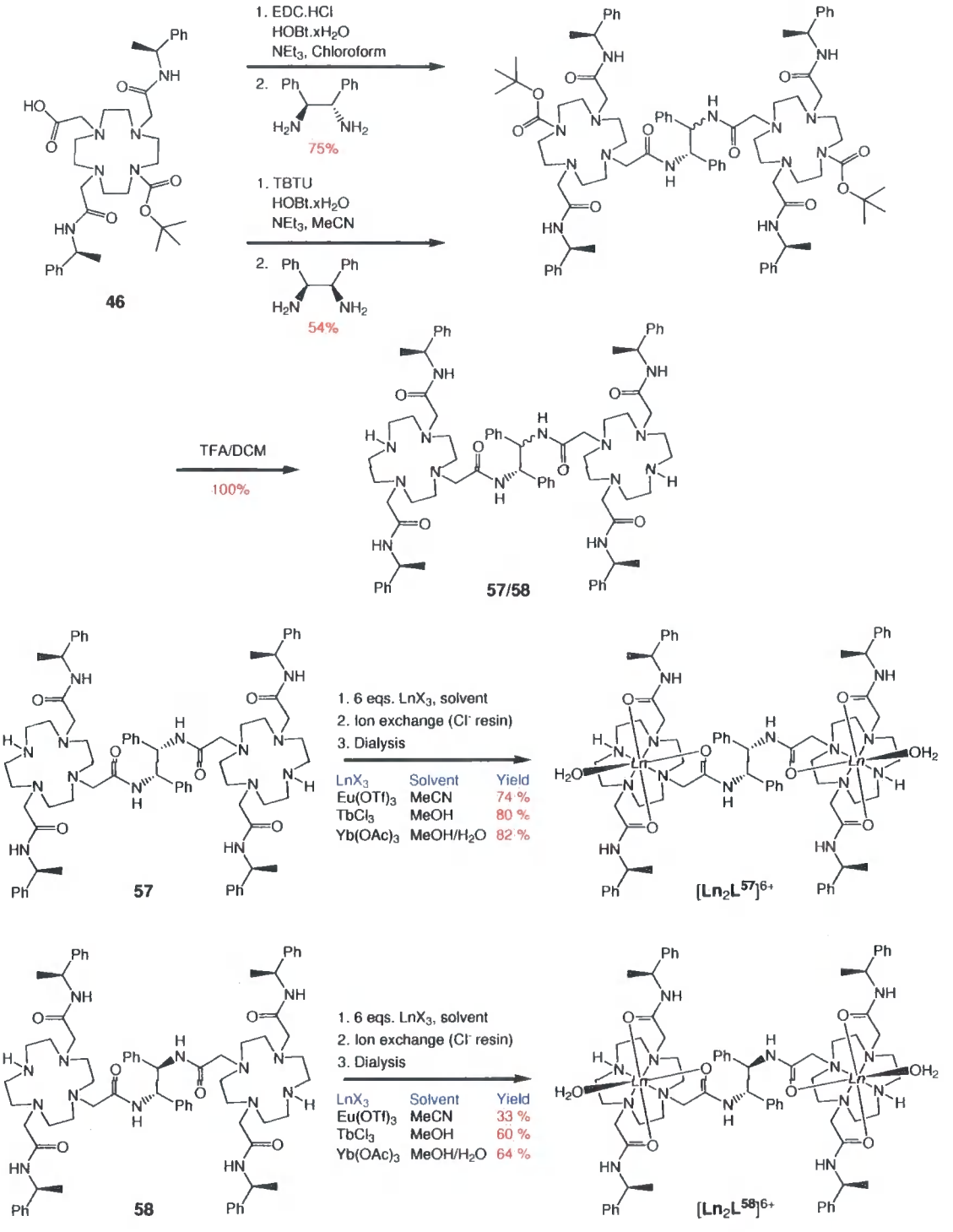

Figure 3.2 – The synthetic route used for the synthesis of $[Ln_2\mathbf{L}^{57}]^{6+}$ and $[Ln_2\mathbf{L}^{58}]^{6+}$.

All complexes and precursors were rigorously characterised by standard spectro-

* All dimeric Eu(III) and Tb(III) complexes synthesised in this chapter were isolated and analysed as their chloride salts and all dimeric Yb(III) complexes as their acetate salts. $[Ln\mathbf{L}^{24}]^{3+}$ complexes were analysed as their triflate salts.

scopic techniques. In addition, complexes were characterised by HPLC in order to confirm complexation reactions had proceeded to completion. HRMS (ES^+) analysis revealed the rich isotopic fingerprint of the dimeric complexes, Figure 3.3. Such isotope patterns proved invaluable in identifying product MS peaks and provided a method by which the progress of complexation reactions could be followed. Complex ESMS spectra were recorded in the presence of a large excess of ammonium acetate, acting as an ionization aid, resulting in more intense complex peaks compared to spectra of complexes in the presence of their chloride or triflate counterions only.

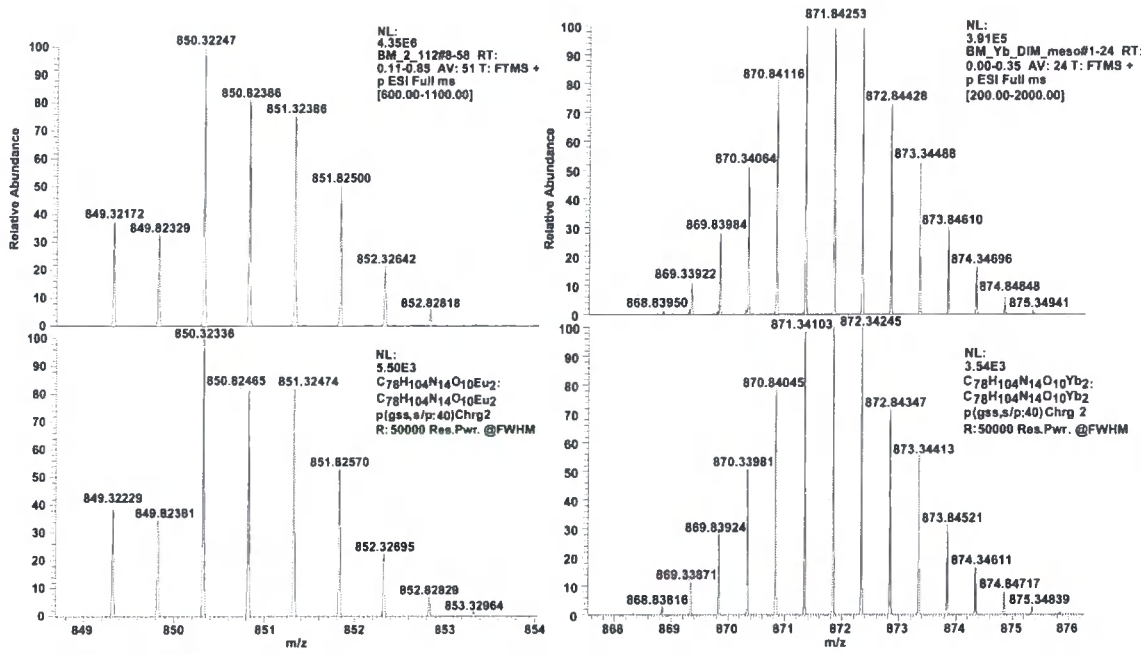

Figure 3.3 – The observed (upper) and theoretical (lower) isotopic distribution profiles for the di-acetate ($[M + 2(OAc)^- - 2H^+]^{2+}$) adducts of $[Eu_2\mathbf{L}^{57}]^{6+}$ (left) and $[Yb_2\mathbf{L}^{58}]^{6+}$ (right).

The MS analysis of all dimeric complexes, in the presence of excess ammonum acetate, detected solely adducts with two acetate anions per dimeric complex, i.e. one acetate per metal ion. Adducts were detected as either doubly or triply charged species and were formed through the loss of either one or two protons in addition to the two acetate anions associated with the complex. The observed 2:1 anion:complex stoichiometry clearly indicates that each metal centre can accommodate only one anion, this is consistent with the previously reported crystal structure of the $[Yb\mathbf{L}^{24}]^{3+}$ acetate adduct.[64] The crystal structure showed chelated 1:1 association of acetate

at the Yb(III) ion, chelation had displaced both metal-bound H_2O molecules.

3.1.4 Characterisation of ligand and complex solution structure

Analysis of the partial ^{1}H-NMR spectra of the two ligands $\mathbf{L}^{57}$ and $\mathbf{L}^{58}$ immediately reveals their structural non-equivalence, Figure 3.4.

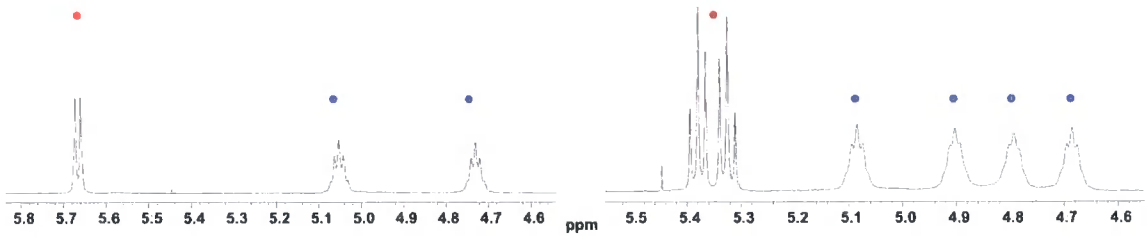

Figure 3.4 – Partial ^{1}H-NMR spectra of $\mathbf{L}^{57}$ (left) and $\mathbf{L}^{58}$ (right) as their TFA salts (MeCN, 700 MHz, 295 K, 3 mM ligand) Resonances marked with • are assigned to the linker CH protons, resonances marked with • are assigned to amide arm CH protons.

The clarity of these spectra is associated with protonation of the macrocycles by residual TFA used in BOC removal. This restricts the conformational mobility of the ligand and results in relatively sharper spectra being obtained. With $\mathbf{L}^{57}$, the two linker CH protons are homotopic, as a result they do not couple with each other but do couple with adjacent amide protons, resulting in the observed doublet. In the case of $\mathbf{L}^{58}$, the two linker CH protons are diastereotopic. As a result, these two protons couple with each other and also to the adjacent amide protons, resulting in two overlapping doublet of doublets. In a similar manner, two resonances were observed for the four amide arm CH protons of $\mathbf{L}^{57}$, whilst four resonances were observed for the four amide arm CH protons of $\mathbf{L}^{58}$. Because $\mathbf{L}^{58}$ possesses no central symmetry each amide arm CH proton is rendered non-equivalent on the timescale of the acquisition. For $\mathbf{L}^{57}$, possessing C_2 symmetry, each proton has an equivalent twin on the adjacent macrocycle, resulting in two distinct amide arm CH proton environments.

For each dimeric Eu(III) and Yb(III) complex a ^{1}H-NMR spectrum was obtained, Figure 3.5. The spectra obtained are broader than those of the parent complexes

$[LnL^{24}]^{3+}$, and there are noteable differences between the spectra of $[Ln_2L^{57}]^{6+}$ and $[Ln_2L^{58}]^{6+}$ (where Ln = Eu or Yb).

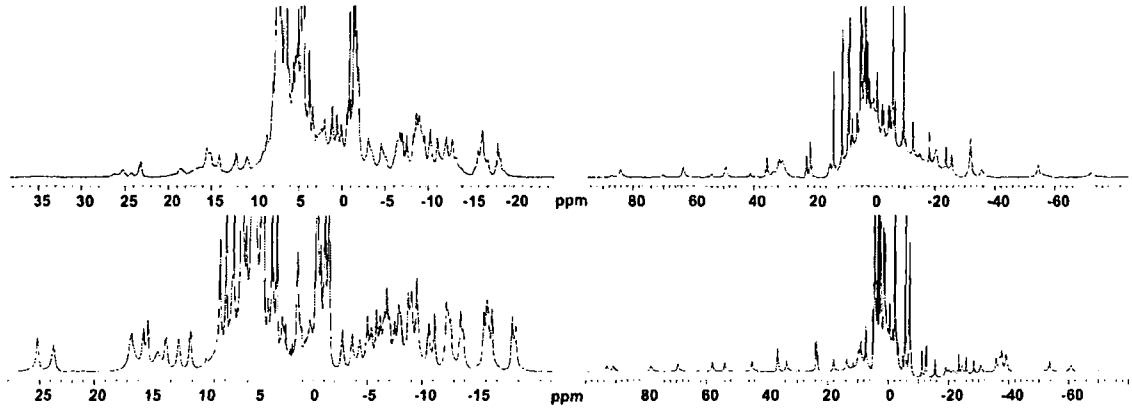

Figure 3.5 – ^{1}H-NMR spectra of $[Eu_2L^{57}]^{6+}$ (upper, left), $[Yb_2L^{57}]^{6+}$ (upper, right), $[Eu_2L^{58}]^{6+}$ (lower, left) and $[Yb_2L^{58}]^{6+}$ (lower, right) (D_2O, pD 7.8, 500 MHz, 295 K, 2 mM complex).

The spectra of complexes with the *meso* linker, $[Eu_2L^{58}]^{6+}$ and $[Yb_2L^{58}]^{6+}$, are the simplest, revealing the protons of the two macrocycles to be non-equivalent and the presence of only one conformer on the 500 MHz NMR timescale. In contrast, the spectra of the complexes with the *SS* linker, $[Eu_2L^{57}]^{6+}$ and $[Yb_2L^{57}]^{6+}$, exhibited a distribution of a similar number of paramagnetically shifted resonances; the relative ratio of which indicated the presence of at least one minor and one major conformer on the NMR timescale. Attempts to simplify the spectrum of $[Eu_2L^{57}]^{6+}$ by recording it at 50°C proved unsuccessful, resulting in an extremely broad spectrum.

The CPL spectra of $[Eu_2L^{57}]^{6+}$ and $[Eu_2L^{58}]^{6+}$ were recorded, alongside their total luminescence spectra. In each case, the form of the total luminescence spectra was virtually identical; suggesting that each complex retained a constant axial donor ligand (D_2O), and possessed a consistent coordination environment around the central Eu(III) ions. The CPL spectra of $[Eu_2L^{57}]^{6+}$ and $[Eu_2L^{58}]^{6+}$ were distinctly different. Whereas the spectrum obtained for $[Eu_2L^{58}]^{6+}$ was very similar to that of the parent monomer, $[EuL^{24}]^{3+}$, the spectrum obtained for $[Eu_2L^{57}]^{6+}$ was significantly different in form, Figure 3.6.

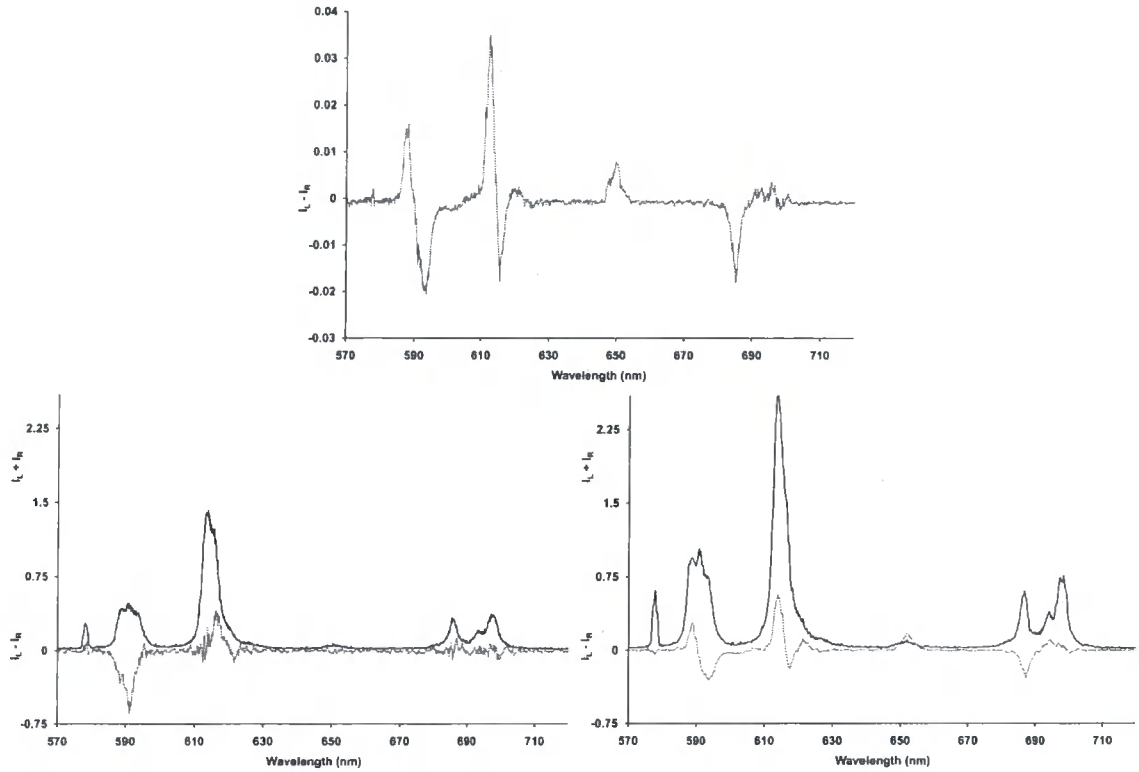

Figure 3.6 – CPL spectra of $[EuL^{24}]^{3+}$ (H_2O, 1 mM, 295 K, $\lambda_{exc} = 255$ nm) (upper);[89] total luminescence and CPL spectra (x 60) of $[Eu_2L^{57}]^{6+}$ (D_2O, 1 mM, 295 K, λ_{exc} = 255 nm) (lower left) and total luminescence and CPL spectra (x 18) of $[Eu_2L^{58}]^{6+}$ (D_2O, 1 mM, 295 K, λ_{exc} = 255 nm) (lower right).

Comparison of g_{em} values at specific wavelengths of the three spectra highlights the difference in form of the two dimeric complex spectra and the similarity between the spectra of $[Eu_2L^{58}]^{6+}$ and $[EuL^{24}]^{3+}$, Table 3.1.

Complex	**$\Delta J = 1$ (λ)**	**$\Delta J = 1$ (λ)**	**$\Delta J = 2$ (λ)**
$[EuL^{24}]^{3+}$	+0.04 (588)	-0.05 (593)	+0.03 (612)
$[Eu_2L^{57}]^{6+}$	-0.03 (588)	-0.04 (591)	+0.003 (614)
$[Eu_2L^{58}]^{6+}$	+0.03 (588)	-0.04 (593)	+0.025 (614)

Table 3.1 – Emission dissymmetry values (g_{em}) at specified wavelengths (D_2O, 295 K); $[EuL^{24}]^{3+}$ in H_2O.[89]

The differences in the CPL spectra of $[Eu_2L^{57}]^{6+}$ and $[Eu_2L^{58}]^{6+}$ suggest that there may be opposing local helicities at the two Eu(III) centres of $[Eu_2L^{57}]^{6+}$. This results in a degree of averaging of the CPL originating from each Eu(III) ion, culminating in a reduced nett CPL. This is reflected by the g_{em} values of various transitions being either of lower magnitude or opposite sign to those of $[EuL^{24}]^{3+}$ and $[Eu_2L^{58}]^{6+}$. In

contrast, the form of the CPL spectra of $[Eu_2\mathbf{L}^{58}]^{6+}$ can be explained in terms of each Eu(III) centre behaving as an independent complex, each with the same helicity at Eu(III), as found in $[Eu\mathbf{L}^{24}]^{3+}$. This results in no averaging of the global CPL signal, rendering the CPL spectrum (and thus the g_{em} values) virtually identical to that of $[Eu\mathbf{L}^{24}]^{3+}$.

The magnitude of the paramagnetic shifts observed in the ^{1}H-NMR spectra of all complexes, and the similarity in the CPL spectra of $[Eu_2\mathbf{L}^{58}]^{6+}$ and $[Eu\mathbf{L}^{24}]^{3+}$ suggests that the dimeric complexes retain the SAP prismatic geometry around each Ln(III) ion as observed previously for $[Eu\mathbf{L}^{24}]^{3+}$[58] and $[Yb\mathbf{L}^{24}]^{3+}$.[64]

Finally, the hydration states of the complexes were estimated through analysis of the radiative decay rate constants of the excited states of the Eu(III) and Tb(III) complexes.

Complex/anion	$k_{(H_2O)}/ms^{-1}$	$k_{(D_2O)}/ms^{-1}$	$\Delta k/ms^{-1}$	$q^{a,b}$
$[Eu_2\mathbf{L}^{57}]^{6+}/Cl^-$	2.78	1.22	1.56	1.28
$[Tb_2\mathbf{L}^{57}]^{6+}/Cl^-$	0.72	0.47	0.25	0.94
(*O*-P-Tyr)$^{2-}$	0.77	0.65	0.12	0.30
Lactate	0.58	0.49	0.09	0.14
$[Eu_2\mathbf{L}^{58}]^{6+}/Cl^-$	2.86	1.22	1.64	1.42
$[Tb_2\mathbf{L}^{58}]^{6+}/Cl^-$	0.79	0.48	0.31	1.26
(*O*-P-Tyr)$^{2-}$	0.68	0.49	0.19	0.67
Lactate	0.59	0.47	0.12	0.3

Table 3.2 – Effect of added anions on the rate constants (k) (± 10 %) for radiative decay of the excited states of $[Eu_2\mathbf{L}^{57}]^{6+}$, $[Tb_2\mathbf{L}^{57}]^{6+}$, $[Eu_2\mathbf{L}^{58}]^{6+}$ and $[Tb_2\mathbf{L}^{58}]^{6+}$ (295 K, 0.05 mM complex, 0.5 mM anion) and derived hydration numbers, q (± 20 %). [a] $q^{Eu} = 1.2[(k_{(H_2O)}-k_{(D_2O)})-(0.25+0.07x)]$ (x = number of carbonyl-bound amide NH oscillators) [b] $q^{Tb} = 5(k_{(H_2O)}-k_{(D_2O)}-0.06)$.[57]

Whereas the parent complexes $[Eu\mathbf{L}^{24}]^{3+}$ and $[Tb\mathbf{L}^{24}]^{3+}$ were shown to possess two directly coordinating H_2O molecules (i.e. $q = \sim 2$) in aqueous solution,[106] estimates suggest the dimeric complexes each possess a lower q value. This indicates that for each complex there may either be a mixture of $q = 1$ and $q = 2$ systems or solely $q = 1$ systems. This may be related to the micro-environments around the metal centres being more hydrophobic and sterically demanding than that for the parent

complexes, resulting in the lower non-integer values of q observed.

3.2 Anion binding studies

The binding of $[Ln_2\mathbf{L}^{57}]^{6+}$ and $[Ln_2\mathbf{L}^{58}]^{6+}$ (Ln = Eu, Tb, Yb) to selected anions was probed through analysis of ^{1}H-NMR, ^{31}P-NMR, Ln(III) luminescence spectra and mass spectrometry data. It was decided to determine the binding stoichiometries of the dimeric systems to probe whether each encapsulated Ln(III) ion could reversibly bind to anions, and to determine whether or not the conformation of each dimeric complex restricted the access of anions to the metal centres. In addition, it was also considered appropriate to determine the individual binding constants for anion binding at each Ln(III) centre, or at least estimate a global affinity constant for anion binding, by analysis of either NMR or luminescence titrations.

3.2.1 NMR and CPL anion binding studies

Binding titrations of the dimeric Eu(III) complexes $[Eu_2\mathbf{L}^{57}]^{6+}$ and $[Eu_2\mathbf{L}^{58}]^{6+}$ with $(O$-P-Tyr$)^{2-}$, monitored through acquisition of ^{1}H-NMR and ^{31}P-NMR spectra, yielded disappointing results. Analysis of the data was hampered by severe line broadening in the spectra, in the presence of ≤ 1 eq. added $(O$-P-Tyr$)^{2-}$. Moreover, precipitation occurred in the presence of ≥ 1.4 eqs. added $(O$-P-Tyr$)^{2-}$, suggesting a degree of insolubility of 1:2 adduct between the complex and $(O$-P-Tyr$)^{2-}$. Despite these limitations, the shifts of the H_{ax} resonances in the limiting spectra (in the presence ≥ 2.4 eqs. $(O$-P-Tyr$)^{2-}$) were consistent with a Eu(III) bound $(O$-P-Tyr$)^{2-}$ species.[66] In addition, the number and ratio of resonances in the limiting spectra suggests the presence of two conformers, as observed in spectra of the aqua complex. Unfortunately, due to exchange broadening on the NMR timescale no phosphorus signal was observable until over 1 eq. $(O$-P-Tyr$)^{2-}$ had been added. This signal corresponded to unbound $(O$-P-Tyr$)^{2-}$. Presumably, the signal associated with bound $(O$-P-Tyr$)^{2-}$ was too broad to be observed. In addition, in all subsequent NMR studies, including those mentioned below, no bound phosphorus signal was observed. Previous work in monomeric systems had observed such shifted, broad ^{31}P-NMR signals at -136 ppm ($\omega_{1/2} \approx 200$ Hz, 298 K, H_2O, 162 MHz, pH 7.4).[73,84]

Despite the adduct solubility issues discussed above, the limiting ^{1}H-NMR spectra of $[Yb_2\mathbf{L}^{57}]^{6+}$ and $[Yb_2\mathbf{L}^{58}]^{6+}$ were recorded in the presence of a range of anions, Figure 3.7. The Yb(III) complexes were examined due to the greater spectral range of their ligand resonances, aiding the analysis of shifted H_{ax} resonances. In addition, limiting ^{1}H-NMR spectra of $[Eu_2\mathbf{L}^{57}]^{6+}$ and $[Eu_2\mathbf{L}^{58}]^{6+}$ were recorded in the presence of D-glucose-6-(dihydrogen phosphate) $(Glc\text{-}6\text{-}P)^{2-}$ or α-D-glucose 1,6-bisphosphate potassium salt $(Glc\text{-}1,6\text{-}P)^{4-}$, Figure 3.8.

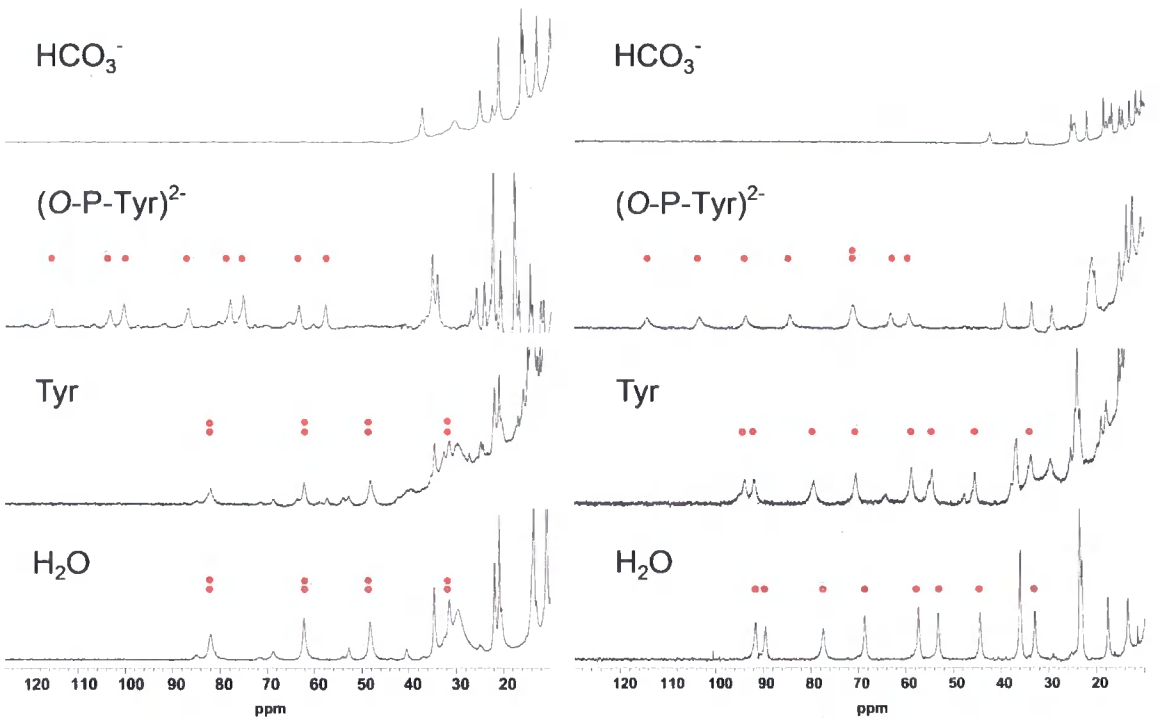

Figure 3.7 – Partial ^{1}H-NMR spectra (500 MHz, D_2O, 295 K, pD 7.8, 2 mM complex, 10 mM added anion) of $[Yb_2\mathbf{L}^{57}]^{6+}$ (left spectra set) and $[Yb_2\mathbf{L}^{58}]^{6+}$ (right spectra set) of the anion adducts of HCO_3^-, $(O\text{-P-Tyr})^{2-}$, L-Tyrosine (Tyr) and chloride (unbound), showing the most paramagnetically shifted resonances (H_{ax} protons marked by •).

For both Yb(III) dimeric complexes, where possible, the mean shift (average of 8) of the most shifted macrocycle proton (H_{ax}) was calculated, Table 3.3. As described in chapter 1, the chemical shift of this resonance is extremely sensitive to the local coordination environment, in particular the nature of the 'pseudo-axial' donor atom. The mean chemical shift values allow comparisons to be made with $[Yb\mathbf{L}^{24}]^{3+}$, for which such values had been reported previously.[66]

Anion[a]	$[YbL^{24}]^{3+}$	$[Yb_2L^{57}]^{6+}$	$[Yb_2L^{58}]^{6+}$
Cl^-	n.d.	56	65
$CF_3SO_3^-$	75	n.d.	n.d.
$(O\text{-P-Tyr})^{2-}$	95(40)	85	80
Tyr	39	55	64

Table 3.3 – Mean chemical shifts[b] (295 K, pD = 7.8, 500 MHz) of the most shifted axial ring protons in ternary anion adducts. [a] The value in parenthesis refers to a minor chelated species; with chloride or triflate as the counter-ion, there is no bound anion.;[64] [b] Values for $[YbL^{24}]^{3+}$ obtained previously.[66]

The most striking observation in these binding studies is that the spectrum of $[YbL^{24}]^{3+}$ in the presence of Tyr was dramatically different to that of the aqua complex, highlighted by the differences in mean shift of the H_{ax} protons, Table 3.3. The differences in shift were explained by the formation of a chelate when in the presence of Tyr, the amino *N*-atom capping the square-antiprism with the carboxylate *O*-atom binding in an equatorial position. Such chelated systems were established through X-ray analysis of amino acid ternary adducts of $[YbL^{24}]^{3+}$.[64] However, comparison of the spectra of $[Yb_2L^{57}]^{6+}$ and $[Yb_2L^{58}]^{6+}$ as the aqua complexes and Tyr adducts suggest that formation of this chelate was inhibited, as the spectra remained virtually unchanged. The only evidence of interaction was the broadening of the resonances and the appearence of some minor resonances (<15 %) that may possibly be attributed to a chelated binding mode. Furthermore, with $[YbL^{24}]^{3+}$ in the presence of added $(O\text{-P-Tyr})^{2-}$ the chelated species was observed to compete with phosphate ligation in a ratio of ~1:3.[66] With $[Yb_2L^{57}]^{6+}$ and $[Yb_2L^{58}]^{6+}$, in the presence of $(O\text{-P-Tyr})^{2-}$, only phosphate ligation was observed.

The addition of $NaHCO_3$ to aqueous solutions of both $[Yb_2L^{57}]^{6+}$ and $[Yb_2L^{58}]^{6+}$ induced a significant spectral contraction, as observed for $[YbL^{24}]^{3+}$,[66] consistent with the replacement of the axial D_2O with the *O*-atom of a chelating carbonate. The ability of each dimeric Yb(III) complex to bind to the phosphate functionality of $(O\text{-P-Tyr})^{2-}$ selectively, coupled with an apparent suppression of the competing chelated amino acid binding mode is promising for future peptide studies. Although the broad nature of the spectra hinders analysis, it appears that there are the same

number of conformers in each adduct spectra as in the parent aqua spectra. The suppression of chelate formation with the dimeric systems is intriguing. It is possible that the chelate of the amino acid (possibly formed in a stepwise manner through displacement of labile water through equatorial ligation of a carboxylate oxygen then axial ligation of the protonated amine)[64] may be trapped at the intermediate stage where the protonated amine is stabilised in a hydrogen bonding network incorporating the ligand and second-sphere solvent, preventing chelation. It may be that the more sterically demanding metal site restricts formation of the 5-membered chelate. In these studies the $(O\text{-P-Tyr})^{2-}$ adducts exhibited partial insolubility, the carbonate adducts less so, whilst no precipitation was observed with the complex and Tyr mixture.

Analysis of the ^{1}H-NMR spectra $[Eu_2\mathbf{L}^{57}]^{6+}$ and $[Eu_2\mathbf{L}^{58}]^{6+}$ in the presence of $(Glc\text{-}6\text{-}P)^{2-}$ and $(Glc\text{-}1,6\text{-}P)^{4-}$ suggested that binding of the phospho-anions occurred. The ternary adducts of $(Glc\text{-}6\text{-}P)^{2-}$ and $(Glc\text{-}1,6\text{-}P)^{4-}$ gave rise to somewhat different spectra.

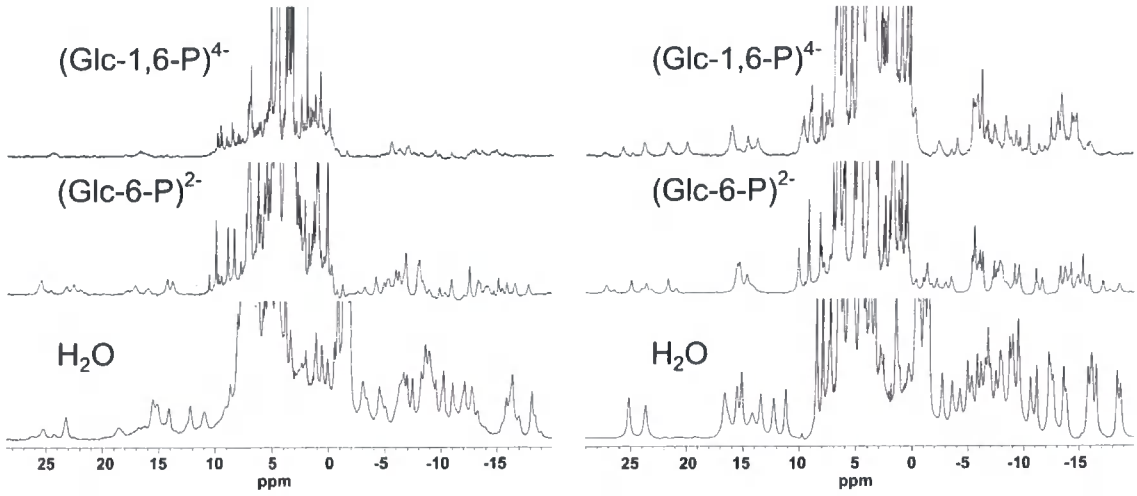

Figure 3.8 – ^{1}H-NMR spectra (500 MHz, D_2O, 295 K, pD 7.8, 2 mM complex, 10 mM added anion) of $[Eu_2\mathbf{L}^{57}]^{6+}$ (left spectra set) and $[Eu_2\mathbf{L}^{58}]^{6+}$ (right spectra set) of the anion adducts of D-glucose-6-(dihydrogen phosphate) $(Glc\text{-}6\text{-}P)^{2-}$, α-D-glucose 1,6-bisphosphate potassium salt $(Glc\text{-}1,6\text{-}P)^{4-}$ and chloride (unbound), showing the most paramagnetically shifted resonances.

The broad spectra obtained with $[Eu_2\mathbf{L}^{57}]^{6+}$ and $(Glc\text{-}1,6\text{-}P)^{4-}$ may be indicative of multiple binding modes (e.g. 1:1 and 2:1 anion:complex adducts, depending upon

complex conformation) and the presence of conformational exchange. In contrast, the spectrum obtained with $[Eu_2\mathbf{L}^{58}]^{6+}$ and $(Glc\text{-}1,6\text{-}P)^{4-}$ is considerably sharper, consistent with a lower number of more conformationally rigid solution species. It should be borne in mind that the complexity of these spectra in part may arise from the formation of diastereoisomeric saccharide complexes, as previously observed.[66]

The CPL spectra of $[Eu_2\mathbf{L}^{57}]^{6+}$ and $[Eu_2\mathbf{L}^{58}]^{6+}$ adducts with $(Glc\text{-}6\text{-}P)^{2-}$ and $(Glc\text{-}1,6\text{-}P)^{4-}$ were recorded and compared to spectra of the aqua complexes and those previously recorded for the $[Eu\mathbf{L}^{24}]^{3+}$ aqua complex and $(Glc\text{-}6\text{-}P)^{2-}$ adduct, Figure 3.9.

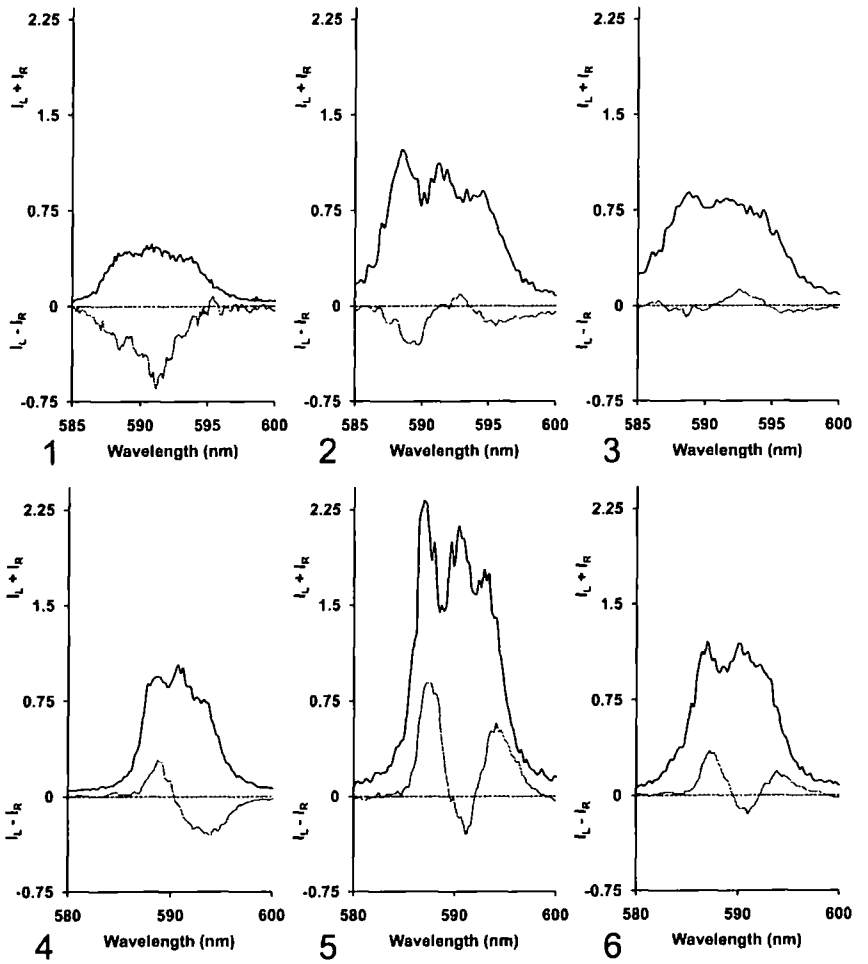

Figure 3.9 – CPL spectra for: (1) $[Eu_2\mathbf{L}^{57}]^{6+}$ (x 60); (2) $[Eu_2\mathbf{L}^{57}]^{6+}$ plus 10 eqs. $(Glc\text{-}6\text{-}P)^{2-}$ (x 60); (3) $[Eu_2\mathbf{L}^{57}]^{6+}$ plus 10 eqs. $(Glc\text{-}1,6\text{-}P)^{4-}$ (x 60); (4) $[Eu_2\mathbf{L}^{58}]^{6+}$ (x 18); (5) $[Eu_2\mathbf{L}^{58}]^{6+}$ plus 10 eqs. $(Glc\text{-}6\text{-}P)^{2-}$ (x 18); (6) $[Eu_2\mathbf{L}^{58}]^{6+}$ plus 10 eqs. $(Glc\text{-}1,6\text{-}P)^{4-}$ (x 18). Total luminescence spectra are also shown (black) (1 mM complex, 295 K, λ_{exc} = 255 nm).

For each dimeric complex, the form and sign of the transitions for their (Glc-6-P)$^{2-}$ and (Glc-1,6-P)$^{4-}$ adducts were identical and were markedly different to that of the aqua complex. The $[Eu_2\mathbf{L}^{58}]^{6+}$ (Glc-6-P)$^{2-}$ and (Glc-1,6-P)$^{4-}$ adduct CPL spectra mirrored the CPL spectrum of the $[Eu\mathbf{L}^{24}]^{3+}$ (Glc-6-P)$^{2-}$ adduct reported previously.[66] This indicates a homology in the central helicity around the Eu(III) ions of the dimeric complex anion adducts, as exhibited by monomer anion adducts. In contrast, the $[Eu_2\mathbf{L}^{57}]^{6+}$ (Glc-6-P)$^{2-}$ and (Glc-1,6-P)$^{4-}$ adduct CPL spectra were weak and markedly different to that of the $[Eu\mathbf{L}^{24}]^{3+}$ (Glc-6-P)$^{2-}$ adduct CPL spectra, reinforcing the hypothesis that this dimeric complex exhibits different helicities at each Eu(III) centre.

In the binding studies described above with the dimeric complexes and (*O*-P-Tyr)$^{2-}$/HCO_3^-, small amounts of precipitate were immediately observable. In spite of this insolubility, NMR studies of complex binding to the phopeptides (**43a-43d**) were undertaken. Unfortunately upon addition of $\geq$0.5 eq. of any phosphopeptide to either $[Eu_2\mathbf{L}^{57}]^{6+}$ or $[Eu_2\mathbf{L}^{58}]^{6+}$ immediate precipitation occurred; the residual solution yielding no useful spectra. Despite the hydrophillic nature of this particular peptide, the insolubility of the resultant adduct at the concentration range required for ^{1}H and ^{31}P-NMR analysis precluded any further NMR investigations.

Whilst the NMR and CPL data obtained did not allow definite binding stoichiometries and anion affinites of the dimeric complexes to be obtained, the spectral information highlights the conformational differences between the two dimeric complexes, allowing a comparison to be made with the monomer complexes, $[Ln\mathbf{L}^{24}]^{3+}$. As a result, luminescence studies of the dimeric complexes with selected anions were undertaken to probe further the binding of anions with these complexes.

3.2.2 Luminescence studies of anion binding

Initially, luminescence studies were attempted with $[Eu_2\mathbf{L}^{57}]^{6+}$ and $[Eu_2\mathbf{L}^{58}]^{6+}$. It was envisaged that anion binding to the Ln(III) centres, with the concomitant displacement of a water molecule, would lead to an increase in the luminescence inten-

sity of the $\Delta J = 2$ band, following excitation at 255 nm. However, upon addition of $(O\text{-P-Tyr})^{2-}$ the changes in luminescent intensity were small.* It was therefore decided to utilise the analogous Tb(III) complexes $[Tb_2\mathbf{L}^{57}]^{6+}$ and $[Tb_2\mathbf{L}^{58}]^{6+}$ in luminescent titrations. As tyrosine is known to sensitise Tb(III) emission efficiently,[107,108] it was decided to monitor the binding of $(O\text{-P-Tyr})^{2-}$ to the metal by excitation of the $(O\text{-P-Tyr})^{2-}$ chromophore that would sensitise the Tb(III) emission. Therefore, binding could be monitored by following the intensity increase of Tb(III) luminescence at 545 nm. Accordingly, luminescent binding titrations of $[Tb_2\mathbf{L}^{57}]^{6+}$ and $[Tb_2\mathbf{L}^{58}]^{6+}$ with $(O\text{-P-Tyr})^{2-}$ were carried out. In addition, binding titrations with $[Tb\mathbf{L}^{24}]^{3+}$ and $(O\text{-P-Tyr})^{2-}$ were recorded for comparison purposes.

Upon addition of $(O\text{-P-Tyr})^{2-}$ to the complexes, Tb(III) emission was clearly enhanced, Figure 3.10. These enhancements indicate population of the $^5D_4$ excited state of Tb(III) through coordination of the $(O\text{-P-Tyr})^{2-}$ sensitiser, and also reflect a contribution to emission enhancement from displacement of the quenching OH oscillators of the metal bound water molecules. Job plots established a 2:1 binding stoichiometry for the association of $(O\text{-P-Tyr})^{2-}$ with $[Tb_2\mathbf{L}^{57}]^{6+}$ and $[Tb_2\mathbf{L}^{58}]^{6+}$, and a 1:1 binding stoichiometry with $[Tb\mathbf{L}^{24}]^{3+}$, Figure 3.10. These results further are corroborated by the HRMS (ES^+) spectra of the dimeric complexes (section 3.1.3) in which two acetate anions are bound per complex in the gas phase, i.e. one per metal ion. It was possible to fit the titration data to appropriate binding models using the programme SPECFIT, to obtain binding curves and speciation distribution diagrams (Figure 3.10) and estimated affinity constants, Table 3.4. This work was carried out in conjunction with Dr. C. dos Santos (Trinity College Dublin).

* This is likely to be due to competitive sensitisation of Eu(III) by the added $(O\text{-P-Tyr})^{2-}$, a process in which the excited S_1 state of $(O\text{-P-Tyr})^{2-}$ is quenched by electron transfer to Eu(III)

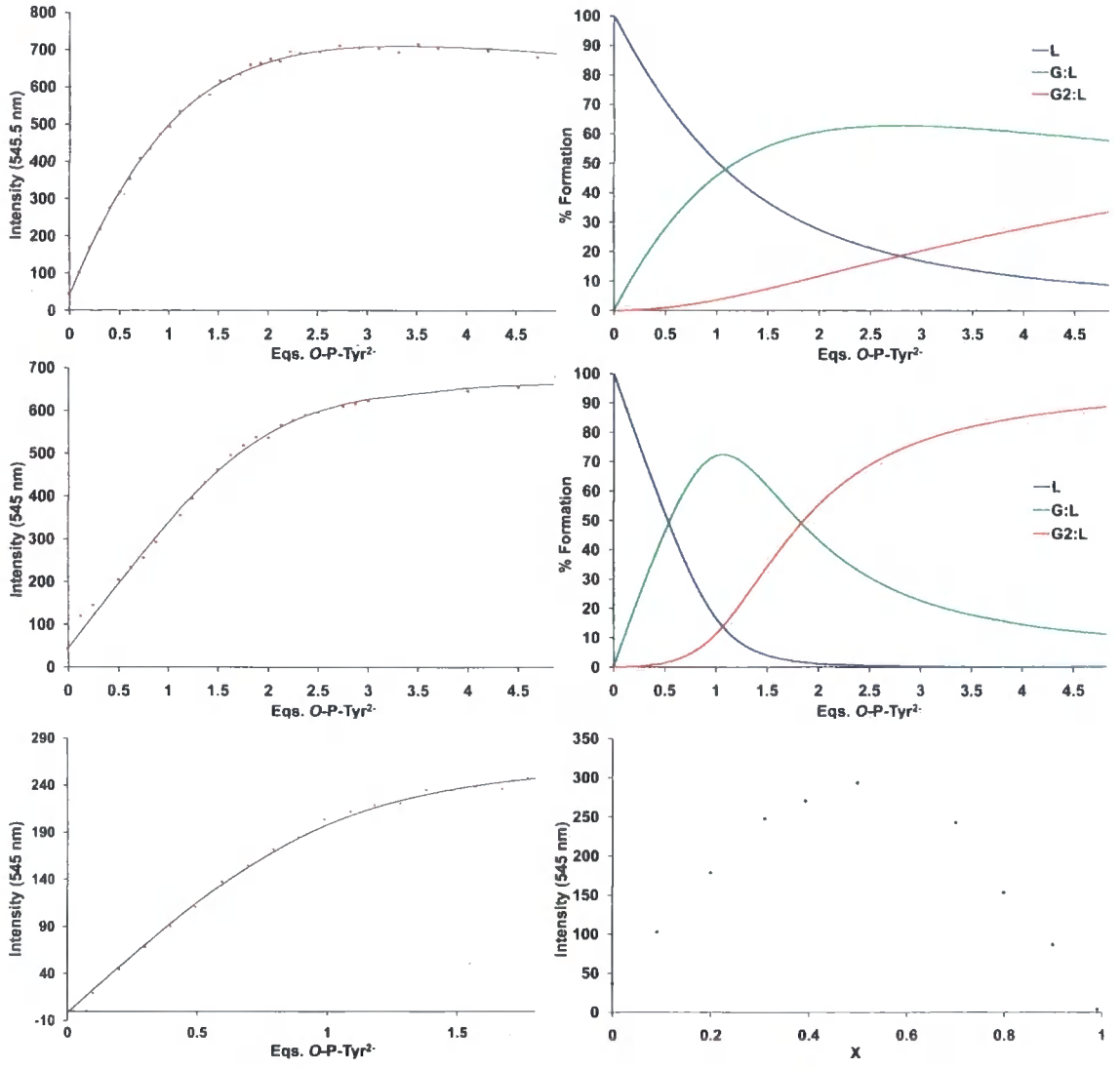

Figure 3.10 – Binding curves and speciation distribution diagrams (295 K, pH 7.4, λ_{exc} = 275 nm) for the association of $(O\text{-P-Tyr})^{2-}$. Upper: $[Tb_2\mathbf{L}^{57}]^{6+}$ (0.05 mM); Centre: $[Tb_2\mathbf{L}^{58}]^{6+}$ (0.05 mM); Lower: binding curve for $[Tb\mathbf{L}^{24}]^{3+}$ (0.11 mM) association with $(O\text{-P-Tyr})^{2-}$ and Job plot establishing 1:1 stoichiometry for its association with $(O\text{-P-Tyr})^{2-}$ (295 K, pH 7.4, λ_{exc} = 275 nm), X = $[(O\text{-P-Tyr})^{2-})]/([(O\text{-P-Tyr})^{2-}] + [[Tb\mathbf{L}^{24}]^{3+}])$.

The binding curve for $[Tb_2\mathbf{L}^{57}]^{6+}$ shows that Tb(III) emission intensity reached a maximum after the addition of 2 eqs. of $(O\text{-P-Tyr})^{2-}$. Similar behaviour was observed with $[Tb_2\mathbf{L}^{58}]^{6+}$. However, in this case the emission intensity reached a maximum more gradually. The difference in form of the binding curves is reflected in the magnitude of the step-wise binding constants. With $[Tb_2\mathbf{L}^{57}]^{6+}$, each step-wise binding constant (and therefore the global affinity constant) was lower than the corresponding value estimated for $[Tb_2\mathbf{L}^{58}]^{6+}$. The speciation distribution dia-

	$[TbL^{24}]^{3+}$	$[Tb_2L^{57}]^{6+}$	$[Tb_2L^{58}]^{6+}$
G:L log β	4.88	4.60	5.67
G:L Log K	4.88 (±0.10)	4.60 (±0.03)	5.67 (±0.30)
G_2:L log β	-	8.14	10.45
G_2:L log K	-	3.54 (±0.10)	4.78 (±0.29)

Table 3.4 – Affinity constants estimated for the association of $(O$-P-Tyr$)^{2-}$ with $[TbL^{24}]^{3+}$, $[Tb_2L^{57}]^{6+}$ and $[Tb_2L^{58}]^{6+}$. G = $(O$-P-Tyr$)^{2-}$, L = complex, values in parenthesis are the estimated standard deviations.

grams show that the formation of a 2:1 G:L adduct with $[Tb_2L^{58}]^{6+}$ is rapid after the addition of >2 eqs. $(O$-P-Tyr$)^{2-}$. In contrast, the formation of a 1:1 adduct with $[Tb_2L^{57}]^{6+}$ is the predominant solution species even after the addition of >4 eqs. $(O$-P-Tyr$)^{2-}$. These differences can be explained by the greater steric barrier towards initial and secondary $(O$-P-Tyr$)^{2-}$ binding at the Tb(III) centres of $[Tb_2L^{57}]^{6+}$, compared to the more open structure of $[Tb_2L^{58}]^{6+}$. Further analysis of anion binding is provided by analysis of the radiative decay rate constants of the Tb(III) excited state. In the presence of an excess of $(O$-P-Tyr$)^{2-}$ the derived hydration number for each dimeric complex is reduced compared to that of the aqua complex. In each case, the change in q is a non-integer value, and most likely reflects a complex of mixed hydration states; a situation that can be accounted for by the hydrophobic nature of the resultant adduct. For each dimeric complex the initial binding constant is one order of magnitude higher than that of the second binding constant. This behaviour is consistent with a decrease in overall complex positive charge upon initial $(O$-P-Tyr$)^{2-}$ binding, and the effect of increased steric hindrance.

The binding curve obtained for $(O$-P-Tyr$)^{2-}$ association with $[TbL^{24}]^{3+}$ was subjected to the iterative data fitting process used in previous work, to allow comparison with earlier binding studies with $[EuL^{27}]$ and $(O$-P-Tyr$)^{2-}$.[66] These results revealed an association constant of log K = 4.88 (±0.10), greater than the value of log K = 4.2 (±0.2) obtained with $[EuL^{27}]$. However, this latter association constant was recorded in the presence of a 5 mM $NaHCO_3^-$ background, so the greater magnitude of the former is not suprising.

A similar analysis of the association of lactate with $[Tb_2\mathbf{L}^{57}]^{6+}$, $[Tb_2\mathbf{L}^{58}]^{6+}$ and $[Tb\mathbf{L}^{24}]^{3+}$ was undertaken.

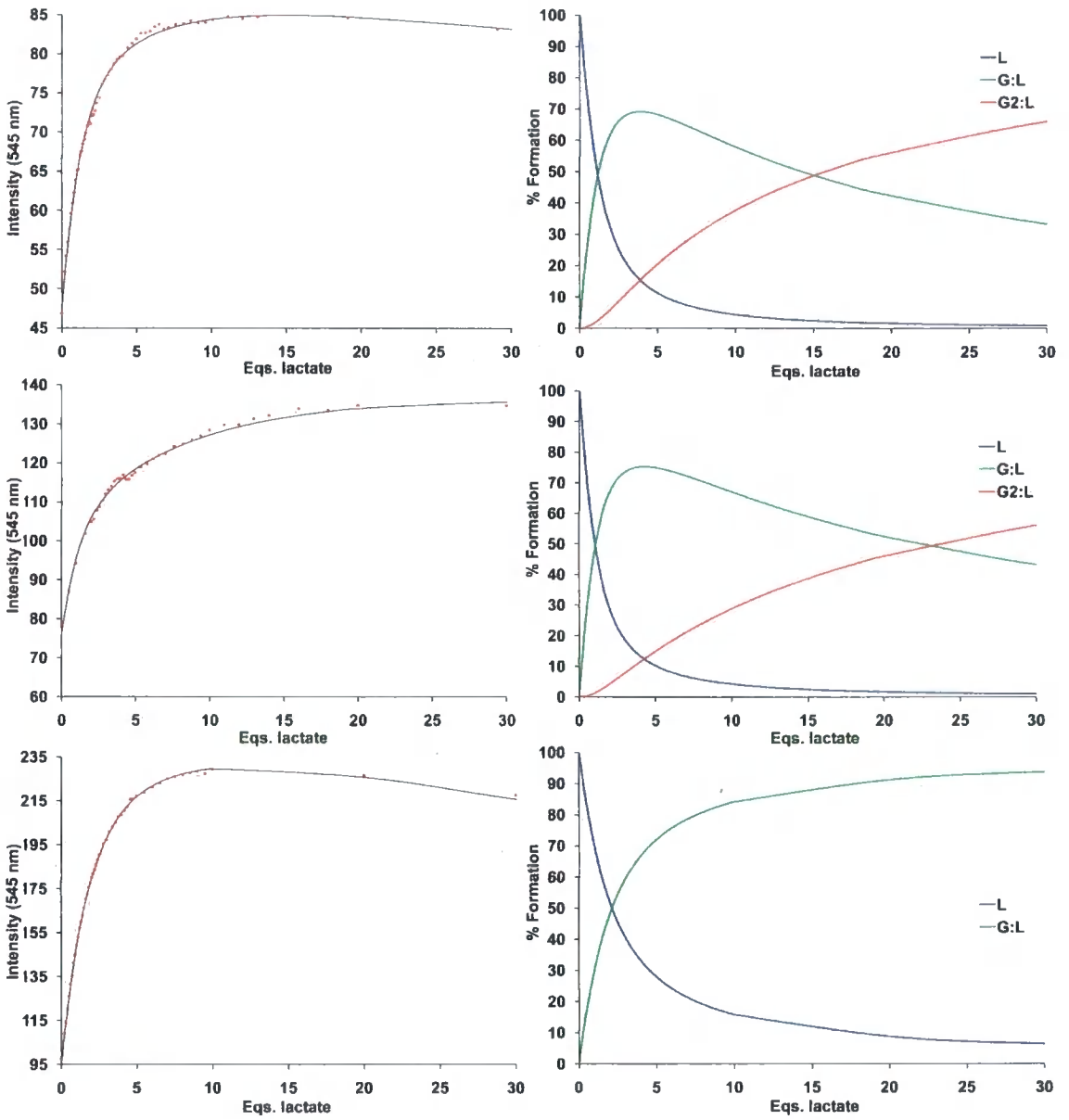

Figure 3.11 – Binding curves and speciation distribution diagrams (295 K, pH 7.4, λ_{exc} = 255 nm, 3.0 ms delay time) for the association of lactate: Upper; $[Tb_2\mathbf{L}^{57}]^{6+}$ (0.049 mM), Centre; $[Tb_2\mathbf{L}^{58}]^{6+}$ (0.049 mM): Lower; $[Tb\mathbf{L}^{24}]^{3+}$ (0.097 mM) (lower diagrams).

The affinity constants defining lactate binding were estimated to be lower than those for $(O\text{-P-Tyr})^{2-}$, Table 3.5. This primarily reflects the lower charge of lactate compared to $(O\text{-P-Tyr})^{2-}$.

	$[TbL^{24}]^{3+}$	$[Tb_2L^{57}]^{6+}$	$[Tb_2L^{58}]^{6+}$
G:L log β	3.80	4.50	4.58
G:L Log K	3.80 (±0.01)[a]	4.50 (±0.10)	4.58 (±0.13)
G_2:L log β	-	7.70	7.60
G_2:L log K	-	3.20 (±0.27)	3.02 (±0.19)

Table 3.5 – Affinity constants estimated for the association of lactate with $[TbL^{24}]^{3+}$, $[Tb_2L^{57}]^{6+}$ and $[Tb_2L^{58}]^{6+}$. G = lactate, L = complex, values in parenthesis are the estimated standard deviations. [a] The iterative data fitting process used in the analysis of $(O$-P-Tyr$)^{2-}$ association with $[TbL^{24}]^{3+}$ was also used to estimate lactate association with this complex. A log K value of 3.95 (±0.01) was estimated using this method.

The lower affinity constants across the series were reflected in the form of the binding curves. The intensity increase in Tb(III) emission, as a function of added lactate, was observed to reach a maximum after addition of about 20 eqs. of anion. Very similar affinity constants were estimated for both dimeric complexes, through fitting of the data to a 2:1 G:L binding model. This contrasts with the behaviour in binding to $(O$-P-Tyr$)^{2-}$, in which the values for were different for each dimeric complex. The simplest explanation for this differing behaviour is that the relatively smaller lactate anion has equal access to the equivalent metal centres of $[Tb_2L^{57}]^{6+}$ and $[Tb_2L^{58}]^{6+}$, with steric factors and differing complex conformations influencing the binding free energy very little. As a result, each affinity constant is of a similar magnitude. In each case, the second affinity constant is lower, as expected for an asociation to a complex of lower overall charge. In contrast, the association of the more sterically demanding $(O$-P-Tyr$)^{2-}$ anion with $[Tb_2L^{57}]^{6+}$ and $[Tb_2L^{58}]^{6+}$ is influenced much more by steric factors and complex conformation, as noted above. The estimated association constant for lactate with $[TbL^{24}]^{3+}$ was lower than that estimated for the initial association of lactate with the dimeric complexes, this is consistent with the greater positive charge of the dimeric complexes. The estimated q values of 0.14 and 0.3 for the $[Tb_2L^{57}]^{6+}$ and $[Tb_2L^{58}]^{6+}$ lactate adducts respectively, were also lower than those estimated with the $(O$-P-Tyr$)^{2-}$ adducts. Such behaviour is consistent with the tendency of the lactate anion to bind to the metal centre in a chelated manner, as observed in the X-ray crystal structure of the related monomeric $[YbL^{24}]^{3+}$ lactate adduct.[64]

3.3 Conclusions

The synthesis of dimeric Ln(III) complexes with stereoisomeric structures was achieved through a synthetic route allowing the conformation of the resultant complex to be modulated through the variation of stereochemistry of the central linking group. The stereoisomeric complexes were synthesised via a common intermediate, that facilitates the synthesis of analogues in which the bridging group is varied.

The differing conformers of the stereoisomeric complexes and ligands were able to be successfully probed by a variety of spectroscopic techniques. These included the application of CPL spectroscopy that highlighted the difference in the local chirality at the Ln(III) centres of the complexes. The binding of anions to the dimeric complexes was examined, with clear differences being observed between the two stereoisomeric structures in the form of the binding curves and the estimated stepwise affinity constants for association with $(O\text{-P-Tyr})^{2-}$. Differences between the association of the dimeric complexes with the smaller lactate anion proved to be insignificant. These differences have been rationalised by consideration of the preferred complex conformation and relative steric bulk of the anions. Unfortunately, some adducts at the 2 mM concentration level proved to be partially insoluble, particularly with phosphopeptide adducts. This prevented more detailed NMR analysis from being carried out, and limited studies to luminescence methods at higher dilution.

This work therefore indicates that dimeric coordinatively unsaturated Ln(III) complexes are appropriate candidates for the synthesis of selective ditopic receptors. The modulation of the bridging linker determines guest binding affinities and selectivity for certain anionic guests.

3.4 Future work

The stereoisomeric complexes outlined here may be considered suitable targets for the phopho-peptide series **43b-43d**, although the insolubility of complex adducts

precluded detailed analysis of the interactions of these species. Future work may revolve around MS analysis of dimeric complex phospho-peptide adducts. Initial MS analyses of 1:1 solutions of $[LnL^{24}]^{3+}$ (Ln = Eu(III), Tb(III), Yb(III)) and **43b**, at μM concentrations, resulted in the detection of 1:1 adducts. Electron-capture dissociation (ECD) of these adducts sequenced the peptide, locating the site of complex ligation at the phospho-tyrosine residue.[109] As noted earlier, the solubility of the dimeric complex phospho-peptide adducts, at mM concentrations, was extremely poor. Preliminary MS studies have detected 1:1 adducts of $[Eu_2L^{57}]^{6+}$ or $[Eu_2L^{58}]^{6+}$ and **43b** from 1:1 solutions at μM concentrations. Future work includes further MS analysis, using ECD to sequence the peptide and locate the site of ligation of the dimeric complex. An extension of this preliminary study would be the MS analysis and ECD sequencing of adducts of $[Ln_2L^{57}]^{6+}$ or $[Ln_2L^{58}]^{6+}$ with **43d** to determine any regioselectivity of binding of the complex to the peptide.

Innumerable closely related analogues of L^{57} and L^{58} may be envisaged that would be expected to increase the water solubility of resultant adducts, selected examples are shown below.[110]

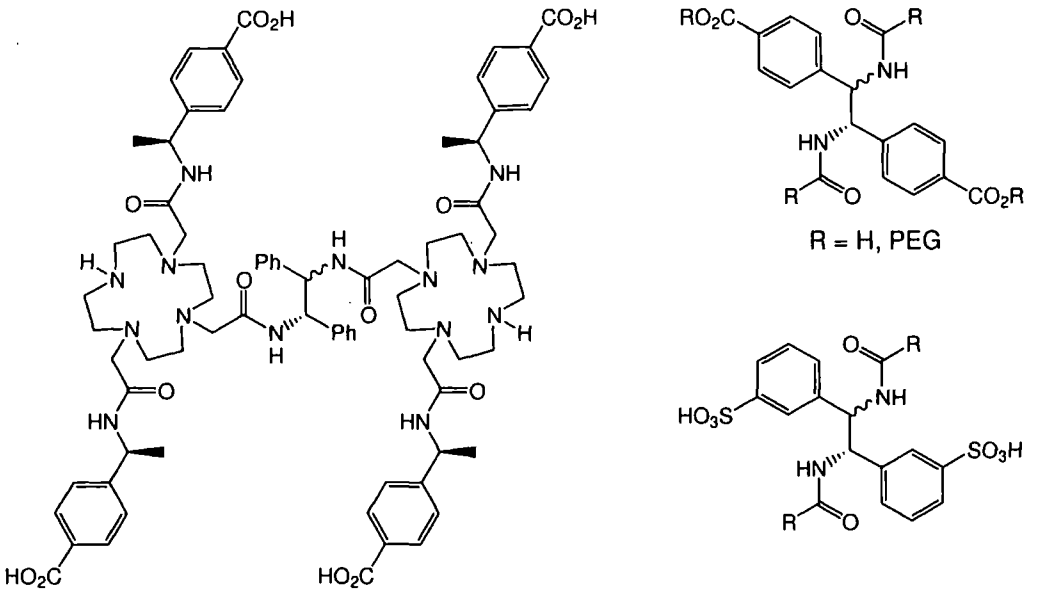

If anionic functionalities were to be introduced to the ligand the reduced global charge of the resultant complexes would be expected to reduced their affinity for

anionic species, therefore a balance would have to be struck between solubility and affinity. In addition, modulation of the central linker group may alter the conformation of the complex. Each complex would therefore have to be examined in detail to determine the relative orientation of the Ln(III) ions.

The synthesis of complexes, such as the few examples suggested, could allow the desired binding studies to be undertaken. In the longer term, if ditopic anion receptors could be identified that exhibited significantly enhanced selectivity for specific sequences of multiphosphorylated phospho-peptides, then the concept could be examined of a probe (or phosphatase inhibitor) selective for specific phosphate residues.

Chapter 4

Immobilised Ln(III) complexes

4.1 Phospho-peptide enrichment techniques

The biological significance of protein phosphorylation was mentioned in section 1.4.1. Phospho-proteins are estimated to constitute between 10-35 % of the proteome but influence virtually all cell signalling processes.[111,112] Phosphorylation of proteins is a dynamic post-translational modification, controlled through the interplay of protein kinases and protein phosphatases.[113,114] In addition, it is becoming increasingly clear that the abnormal regulation of amino acid phosphorylation plays a role in human disease. For example, the dysregulation of tyrosine phosphorylation is known to play a key role in a wide range of diseases including diabetes and cancer.[112,115,116] The ability to establish the sites of phosphorylation within substrate proteins has huge medical potential, and also carries significant academic interest. Recent years have seen intensive academic research and increased efforts by the pharmaceutical industry toward identifying phosphorylation sites, in order to create inhibitors of specific kinases and phosphatases. In the case of tyrosine kinases, several specific inhibitory drugs have been developed and have yielded promising results in the inhibition of tumour cell proliferation.[115,116]

The analytical method of choice for the identification of phosphate sites on phosphorylated proteins is mass spectrometry.[111] Modern MS techniques, utilising MALDI-TOF and/or ESI, enable the sequencing of proteins through analysis of protein digests and therefore the identification of phosphorylation sites. However,

before analysis of digests is undertaken, the phospho-peptides need to be purified to enable them to be detected. This is due to the low stoichiometric ratio of phospho-proteins, resulting in signals due to phosphorylated fragments being swamped by the non-phosphorylated background signal. In addition, phospho-peptides (particularly multi-phosphorylated fragments) often exhibit a low response in MS analysis due to the negative charge of the phosphate functionality. Both of these factors ensure that phospho-protein enrichment is a prerequisite in order to increase the levels of phospho-peptides to detectable levels.

Many methods have been reported that enrich phospho-peptide fragments, Figure 4.1.

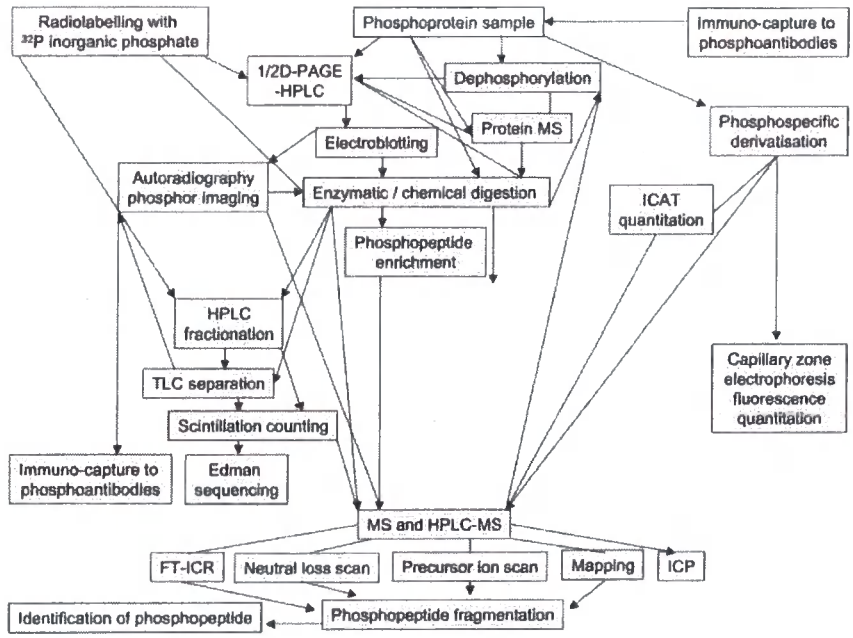

Figure 4.1 – A schematic[111] overview highlighting several approaches to phospho-protein analysis through radiolabelling and mass spectrometric techniques.

However, these enrichment methods are largely residue specific and very few procedures are applicable to all phospho-proteins. The vast majority of these methods are aimed at the enrichment of peptides containing *O*-phosphorylated amino acid residues. The relative abundance of phospho-amino acids within vertebrate cells has been estimated at approximately 92.5:7.45:0.05 for (*O*-P-Ser)$^{2-}$/(*O*-P-Thr)$^{2-}$/(*O*-P-Tyr)$^{2-}$.[117] However, further phosphorylated amino acids exist at significant levels,

such as the *N*-phosphorylated amino acids where phosphorylation of the amino acid occurs through phosphoramidate bond formation. Kinases and phosphatases are known that act on His, Lys, and Arg,[118,119] and phospho-histidine has been estimated to be between 10 and 100 times more abundant than $(O\text{-P-Tyr})^{2-}$.[118] These phosphorylated amino acid residues are not detected using conventional enrichment techniques due to the lability of the phosphoramidate bond in the moderately acidic conditions often used. These will be described below. However, given the estimated abundance of phospho-histidine residues relative to phospho-tyrosine, and the lack of enrichment techniques designed for *N*-phosphorylated residues, suitable analytical techniques may reveal much information on their role within the cellular environment.

The enrichment of phospho-peptides by immobilized metal ion affinity chromatography (IMAC) is well established and several literature reports have described the use of this technology.[111,120–125] The basis of IMAC is that metal ions loaded inside a host matrix will selectively interact with the phosphate functionality of phospho-peptides present within a protein digest. The 'beads' may then be washed to remove unbound material followed by phospho-peptide elution, normally using a competitive buffer at acidic pH. The enriched sample may then be analysed using MS. Reports have detailed various types of IMAC media, including amongst many others, the use of Fe^{3+} and Ga^{3+} loaded nitrilotriacetic agarose,[123,124] Fe^{3+} immobilized on magnetic nanoparticles[120] and iminodiacetic acid functionalised silica particles loaded with Fe^{3+}.[122] The IMAC enrichment method does not discriminate between different phosphate residues, so that $(O\text{-P-Ser})^{2-}$, $(O\text{-P-Thr})^{2-}$ and $(O\text{-P-Tyr})^{2-}$ containing residues may be identified. The metal, matrix and loading levels of an IMAC material may be modulated easily to allow the optimisation for specific concentrations and conditions. In addition, extremely low concentrations of phospho-peptide have been detected using IMAC coupled with MALDI-TOF detection (5×10^{-11} M for 100 μL of a purified standard).[120] Disadvantages of this technique include non-specific retention of non-phosphorylated residues rich in acid functionalities (Asp, Glu), although this may be circumvented by quantitative

methylation of acid residues.[121] Furthermore, multi-phosphorylated peptide fragments have been shown to be difficult to elute from IMAC media. Thus, variation of the metal ion and modulation of phosphate affinity may be required for each sample, in order to identify every phosphorylated residue.[123,124] Additionally, the use of high salt eluants may also be required, which then makes de-salting essential prior to MS analysis, and the use of acidic buffers may catalyse the hydrolysis of any *N*-phosphorylated amino acids present.

One technique which may be classed as 'residue specific' includes the β-elimination of the phosphate residue, followed by the introduction of a tag that enables the modified peptide to be isolated from untagged species, Figure 4.2. Solid phase and affinity based methods have been utilised to enrich tagged peptides.[126,127] The released phospho-peptide fragment is then typically analysed by MS. $(O\text{-P-Tyr})^{2-}$ residues do not undergo β-elimination and so may not be modified using this technique.

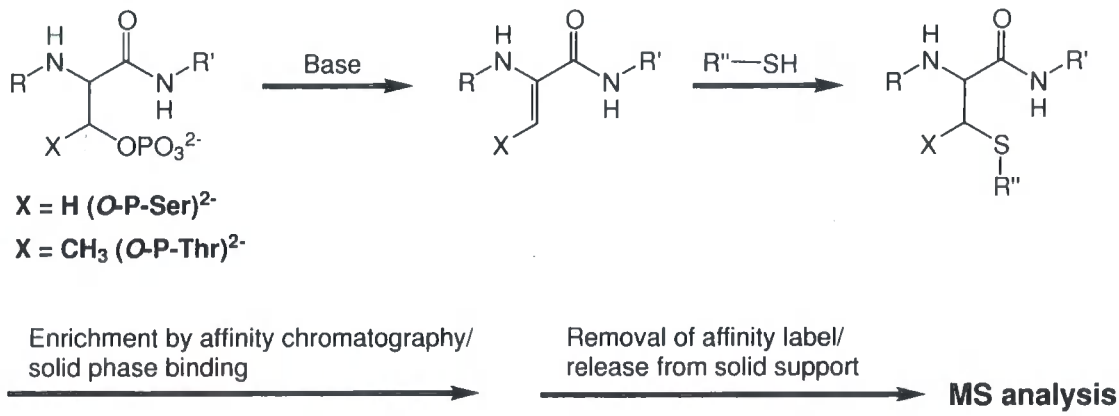

Figure 4.2 – A general schematic showing base mediated β-elimination followed by Michael addition of a thiol-tag for $(O\text{-P-Ser})^{2-}$ and $(O\text{-P-Thr})^{2-}$.

Several disadvantages to the β-elimination process have been identified. These include the slow β-elimination of the $(O\text{-P-Thr})^{2-}$ phosphate (up to 6 h for quantitative elimination) and competitive hydrolysis of the phosphate ester.[126] In addition, it is reported that β-elimination and subsequent Michael addition can occur at cysteine, glycosylated serine and glycosylated threonine residues, potentially resulting in the identification of false phosporylation sites.[128] One specific advantage of the

β-elimination method is the removal of the phosphate functionality that hinders MS analysis.

Combined IMAC separation followed by on-resin β-elimination and Michael addition has been reported.[128] This approach was designed to allow peptides containing $(O$-P-Tyr$)^{2-}$ residues to be retained through to the analysis step, and to reduce the number of false phosphorylation sites to be identified from glycosylated serine and threonine residues. In addition, it was expected that liberation of retained peptides from the IMAC bead by β-elimination would reduce the number of contaminating non-phosphorylated peptides in the final analysis sample, attributed to binding through acidic residues. Promising results were recorded, such as no glycosylation sites being detected in the final sample. However, the basic conditions required for effective β-elimination of phosphate residues also resulted in the non-specific elution of peptides from the resin, and incomplete β-elimination resulted in lower than expected signal intensities.

The immunoprecipitation of $(O$-P-Tyr$)^{2-}$ containing proteins and peptides has been demonstrated through the use of $(O$-P-Tyr$)^{2-}$ specific antibodies.[129,130] Because of the specificity of antibodies for particular targets, often more than one antibody has to be used in global studies of a whole cell lystate, for results to be representative.[129] Following isolation, phospho-proteins are often digested and subjected to further IMAC enrichment. The immunoprecipitation enrichment of proteins containing $(O$-P-Ser$)^{2-}$ and $(O$-P-Thr$)^{2-}$ residues, however, has been seldom demonstrated.[131,132] A chemoenzymatic technique for enrichment of peptides containing $(O$-P-Tyr$)^{2-}$ residues has been reported.[133] Based on tyrosinase oxidation of dephosphorylated $(O$-P-Tyr$)^{2-}$ residues to an *ortho*-quinone followed by their tagging and purification, this methodology was shown to enrich the desired peptide, but involves multiple-steps that make it impractical in its current form.

It is clear that despite the wide range of enrichment techniques available there are no methods that may be regarded as universally applicable across the whole range of

phosphorylated residues that may be encountered within a cell lysate, whilst remaining simple, selective and high yielding. In particular, the coupling of an improved enrichment technique with mass spectrometric analysis would further improve this range of powerful tools for identification of protein phosphorylation sites.

4.2 Immobilised Lanthanide Affinity Chromatography (ILAC)

4.2.1 Designing novel ILAC media

The complex $[EuL^{24}]^{3+}$ was considered for incorporation into a novel chromatographic media, defined as immobilised lanthanide affinity chromatography (ILAC).

The binding of $[EuL^{24}]^{3+}$ to phospho-peptides has been shown to be selective for side-chain ligation at *O*-P-sites of tyrosine/serine/threonine. Competitive *C*- or *N*-chelation was shown to be significantly less favoured.[66,72,73] Furthermore, the preference of $[EuL^{24}]^{3+}$ and related complexes for binding to $(O\text{-P-Tyr})^{2-}$ residues over $(O\text{-P-Ser})^{2-}/(O\text{-P-Thr})^{2-}$ (log K = 4.2 vs. 2.7 respectively for $[EuL^{27}]$; 298K, 5 mM $NaHCO_3$, pH 7.4)[66] may favour discrimination of $(O\text{-P-Tyr})^{2-}$ sites.

It was envisaged that, given appropriate conjugation to a suitable solid phase support, the complex would retain the binding properties and selectivity profile observed in solution studies. This would result in a material that would have a much higher specific retention than currently available IMAC materials, thus reducing the leakage of non-phosphorylated fragments into the final analysis sample. Additionally, the use of an acidic buffer solution to remove the sample from the solid support would not be needed with an ILAC material. The phospho-peptide can be eluted selectively through the addition of a competitive anion, e.g. by using aqueous ammonium carbonate solution (30 - 50 mM) under ambient pH conditions. The eluted phospho-peptide solution could then simply be evaporated and the volatile ammonium carbonate removed under reduced pressure to leave the enriched phospho-peptide, without contamination from residual salt. An additional advantage that

may be envisaged is that separate elution of $(O\text{-P-Ser})^{2-}/(O\text{-P-Thr})^{2-}$ from $(O\text{-P-Tyr})^{2-}$ could be possible, if a gradient elution was used with the aqueous carbonate solution. The higher affinity of $[\text{Eu}\mathbf{L}^{24}]^{3+}$ for $(O\text{-P-Tyr})^{2-}$ suggests that $(O\text{-P-Ser})^{2-}$ and $(O\text{-P-Thr})^{2-}$ would be eluted first, under these conditions.

The design of novel media suitable for ILAC has to take into consideration two key points. The first is the choice of solid support to which the Eu(III) complex would be conjugated; the second is the method and point of complex conjugation to the chosen solid support. A general representation of the envisaged material is shown in Figure 4.3.

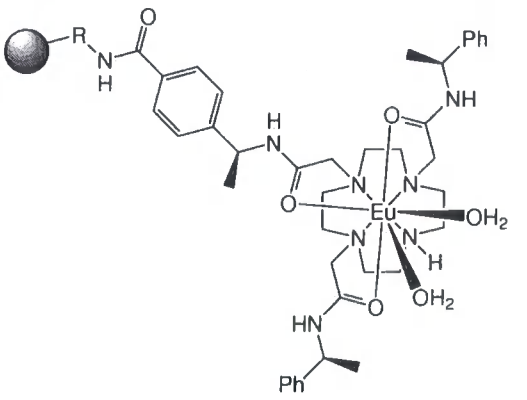

Figure 4.3 – Proposed general structure for a resin bound Eu(III) complex for use in ILAC.

Numerous polymeric resins and nano-particles are commercially available. Materials are available in a range of dimensions and are derivatised to various extents with a choice of functionalities. Given the past experience of the research group with the conjugation of Ln(III) complexes,[86,87] it was decided to couple the chosen support and complex by amide formation, with the solid support being chosen to carry the amine functionality. TentaGel^{TM} S-NH_2 (crosslinked polystyrene matrix to which is grafted amine functionalized PEG spacers) and Affi-Gel® 102 (amino-terminal crosslinked agarose gel) were chosen due to their favourable swelling/solubility characteristics in water. SiMAG-Amino (amine functionalized non-porous silica matrix) was also chosen as the magnetic properties of these amine functionalized nanoparticles facilitate isolation of bound phospho-peptides, Figure 4.4.

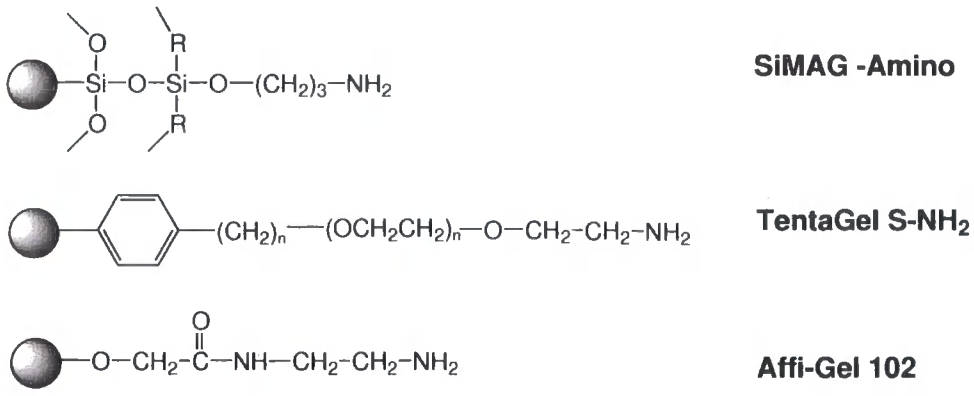

Figure 4.4 – The chemical structure of the spacer groups linking the terminal amine groups and the bulk matrix of the selected support. Structures are as described in the manufacturers specifications.

4.2.2 Synthesis of immobilised complexes

The designed ligand, $\mathbf{L}^{61}$, incorporated a simple conjugation point at the peripheral *C*-atom of the central amide arm. As structurally related complexes (e.g. $[Eu\mathbf{L}^{44a}]^{3+}$, $[Eu\mathbf{L}^{44b}]^{3+}$, $[Eu\mathbf{L}^{49}]^{3+}$, section 2.3.1) had retained a high degree of structural homology to the 'parent complex', $[Eu\mathbf{L}^{24}]^{3+}$, it was expected that a relatively minor modulation of the periphery of the central amide arm would also not change the coordination properties of $[Eu\mathbf{L}^{62}]^{2+}$ compared to $[Eu\mathbf{L}^{24}]^{3+}$. The incorporation of the modified amide arm into the cyclen framework proceeded through the acid intermediate, **46** (section 2.2.1), utilising amide formation between the acid functionality and the amine, **59** (Figure 4.5). The intermediate, **60**, was isolated by column chromatography on alumina.

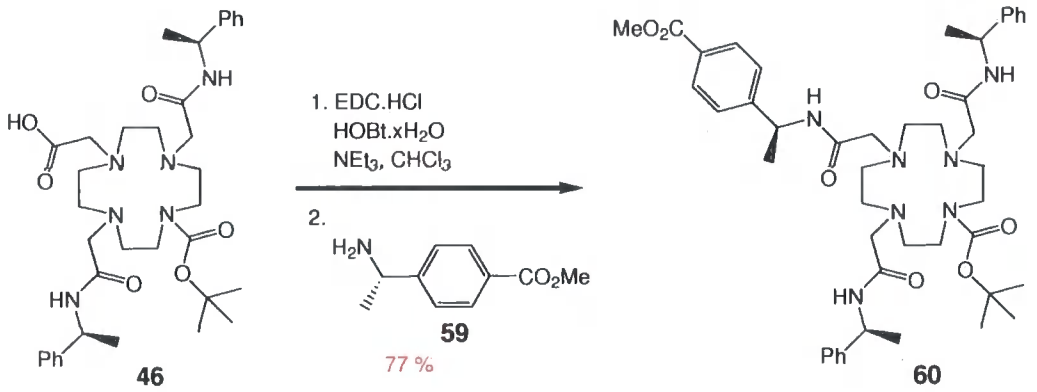

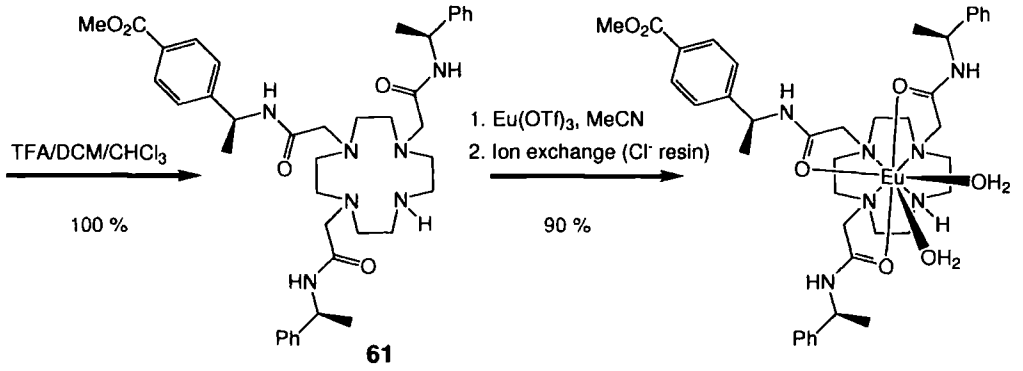

Figure 4.5 – Outline of the synthesis of $[EuL^{61}]^{3+}$.

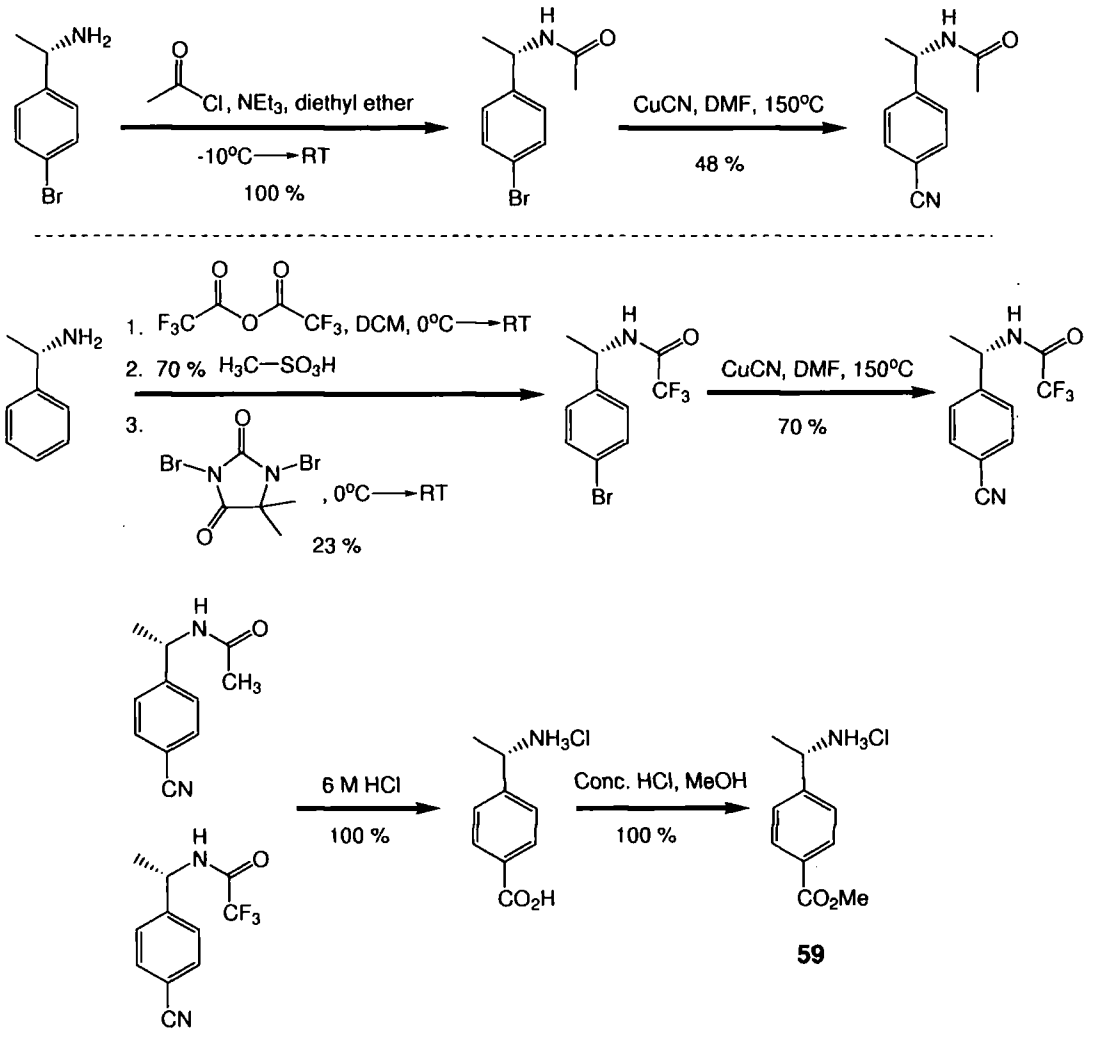

Figure 4.6 – Outline of the synthesis of the pendant amide arm intermediate, **59**.

The synthesis of **59** (Figure 4.6) commenced with the N-protection of commercially available (*S*)-(-)-1-(4-bromophenyl)ethylamine, followed by its conversion to the nitrile. However, subsequent syntheses of **59** proceeded through the one-pot

protection and bromination of (*S*)-(-)-α-methylbenzylamine, via protonated 1,3-dibromo-5,5-dimethylhydantoin, as described previously.[134] The latter route was considerably less expensive than the former. At each stage, the required product could be easily recrystallised, negating the need for column chromatography.

Following the isolation of the desired complex, $[EuL^{61}]^{3+}$,* the methyl ester of the central amide arm was hydrolysed to unmask the acid. However, a small amount of precipitate was observed via this synthetic route, possibly due to Eu(III) decomplexation, resulting in the precipitation of the free ligand. Therefore, to circumvent possible competing decomplexation and to confirm the purity of the final acid complex, $[EuL^{62}]^{2+}$, the methyl ester of the intermediate, **60**, was hydrolysed so that no post-complexation transformations were required, Figure 4.7.

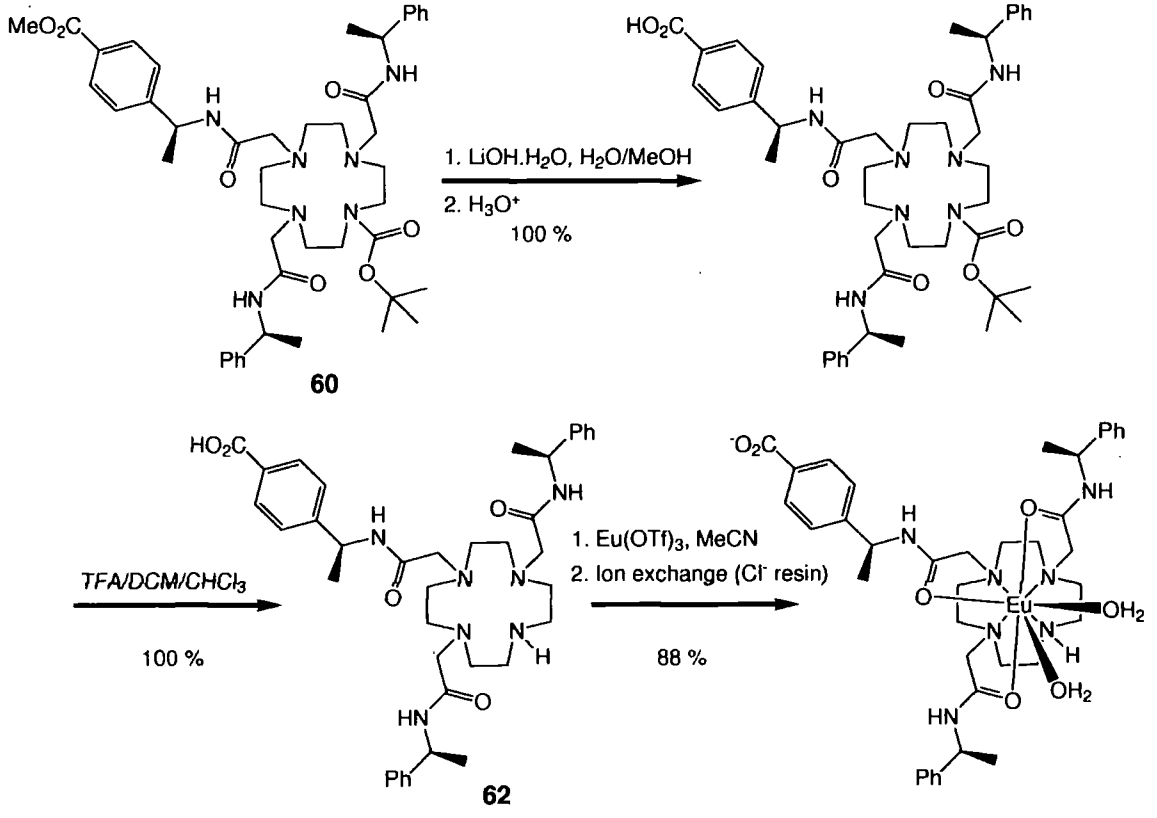

Figure 4.7 – Outline of the synthesis of $[EuL^{62}]^{2+}$.

The chosen solid supports and $[EuL^{62}]^{2+}$ were coupled together using standard amide coupling chemistry, Figure 4.8. The carboxyl group in $[EuL^{62}]^{2+}$ was activated

* All complexes described within this chapter were isolated as their chloride salts.

in situ, using either pH controlled aqueous reactions or changing to organic based amide formation, if required, when in aqueous media yields were poor.[135] After each coupling reaction was completed, the remaining free amine groups of the support were capped using the NHS ester of acetic acid. A small amount of uncapped material was retained for comparison purposes. In each case, the materials were subjected to several washing steps to ensure all unreacted complex has been removed from the samples.

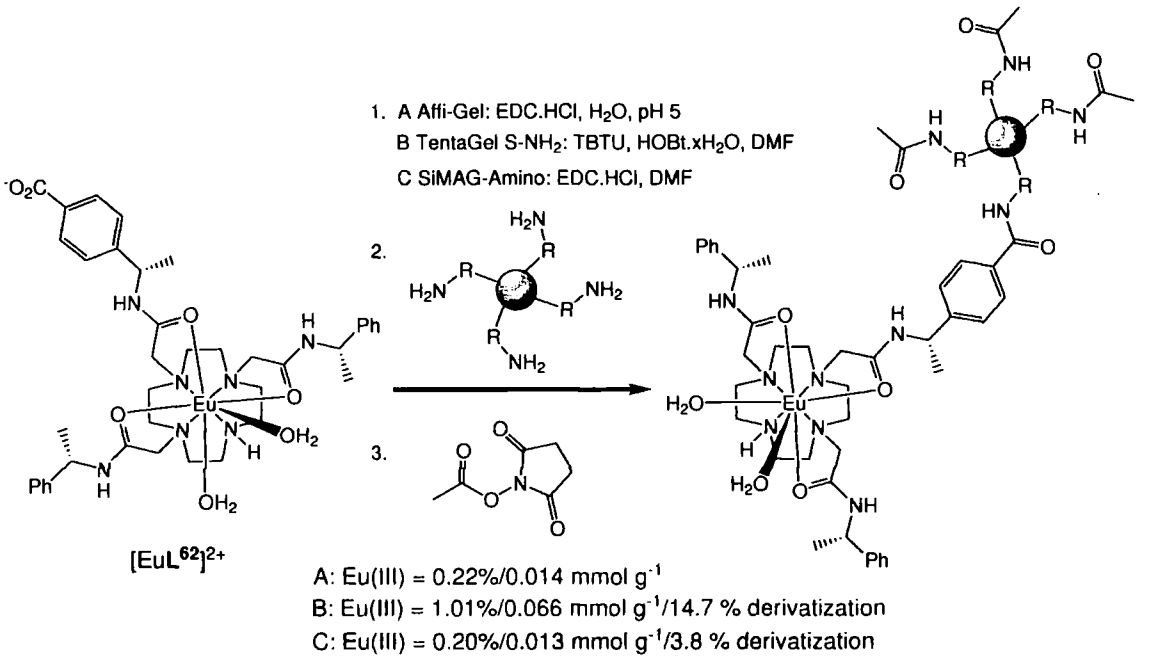

Figure 4.8 – Outline of the coupling of $[EuL^{62}]^{2+}$ with various solid supports, followed by capping of the free amines. Derivatization yields refer to the maximum loadings obtained. The percentage level of Affi-Gel® 102 derivatization is not given. This is because this material was supplied in its gel form with NH_2 levels indicated as a concentration, and the exact dilution of the starting material being unknown.

In a separate experiment, amide formation was used to couple $[EuL^{49}]^{2+}$ (section 2.2.1) with TentaGel™ S-NH_2, to allow luminescence measurements to be used to probe the complex environment around the Eu(III) ion in the resin, Figure 4.9.

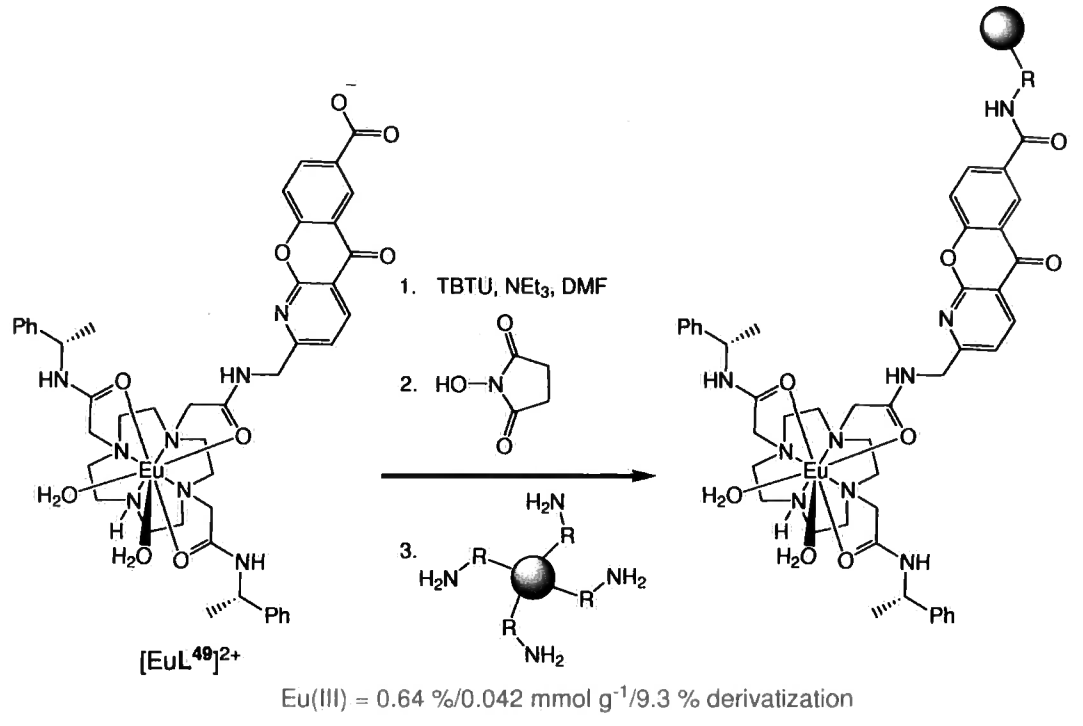

Figure 4.9 – Outline of the coupling of $[EuL^{49}]^{2+}$ with TentaGel^{TM} S-NH_2.

4.2.3 Characterisation of $[EuL^{62}]^{2+}$ and ILAC media

All complexes and intermediates were rigorously characterised by standard spectroscopic techniques. The ^{1}H-NMR spectra of $[EuL^{61}]^{3+}$ and $[EuL^{62}]^{2+}$ were acquired, Figure 4.10. Each spectrum exhibited very similar paramagnetically shifted resonances. Both were also virtually identical to that of the 'parent' $[EuL^{24}]^{3+}$ spectrum, Figure 2.10, consistent with their high degree of structural homology.

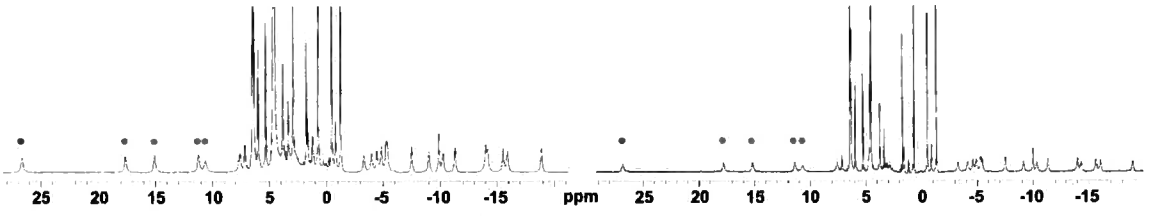

Figure 4.10 – ^{1}H-NMR spectra for $[EuL^{61}]^{3+}$ (left) and $[EuL^{62}]^{2+}$ (right) (500 MHz, D_2O, 295 K, pD 7.8, 1 mM complex). Resonances marked with • are assigned to the cyclen NH proton, resonances marked with • are assigned to cyclen H_{ax} protons.

The rate constants for the radiative decay of the excited state of $[EuL^{61}]^{3+}$ in H_2O and D_2O were 3.60 and 1.64 ms^{-1} respectively, giving a q value of 1.8. This is

consistent with the value of $q = 2$, estimated for $[EuL^{24}]^{3+}$.[106]

Following the solid phase immobilization of $[EuL^{62}]^{2+}$ the level of Eu(III) loading was determined through combustion analysis, using ICP-MS measurements. Eu(III) loadings varied widely depending upon the support and reaction conditions used. Samples of $[EuL^{62}]^{2+}$ loaded TentaGel™ S-NH_2 and $[EuL^{62}]^{2+}$ loaded Affi-Gel® 102 were submitted for MAS ^{1}H-NMR analysis. Whilst spectra obtained with the latter proved to be too broad for any paramagnetically shifted resonances to be observed, broadened complex resonances were clearly observable with the sample of the former, alongside a sharp peak attributed to capping acetyl groups. This provides further evidence for the covalent linkage of $[EuL^{62}]^{2+}$ to TentaGel™ S-NH_2.

4.3 Preliminary phospho-anion separation studies with ILAC media

4.3.1 Luminescence studies of immobilized $[EuL^{49}]^{2+}$

In preliminary work, several samples of $[EuL^{49}]^{2+}$ immobilised on TentaGel™ S-NH_2 have been examined. It was desirable to observe the binding of anions to the immobilized complex through observation of changes to the complex lifetime and spectral emission profile. Samples were typically prepared through the mixing of 2-3 mg of the resin on a glass slide with 10 µl of a sample solution, followed by the sealing of the mixture under a glass-cover slip. Samples examined were the Eu(III) resin bead alone, the Eu(III) resin mixed with H_2O (pH 7.4) and the Eu(III) resin mixed with $NaHCO_3$ solution (30 mM, pH 7.4). The radiative decay curves of each sample were recorded (using a long pass filter) following laser excitation at 355 nm. It was interesting to note that the sample of the dry Eu(III) resin and the Eu(III) resin immersed in H_2O possessed similar luminescent decay curves. These were best fitted to a biexponential decay profile, indicating the presence of two luminescent species in each sample. The complex lifetimes recorded were 0.04 ms and 0.25 ms, present in the ratio 1:0.9. The decay curve obtained for the Eu(III) resin with bicarbonate fitted well to a monoexponential decay, consistent with one

major species that could involve a bound carbonate anion at the Eu(III) centre. The observed lifetime was 0.15 ms. These results may be explained by considering that the Eu(III) complex is conjugated to a resin consisting of flexible PEG chains and free amine groups that would be protonated at pH 7.4. It is therefore likely that there will be various species trapped by these PEG chains such as metal ions, water molecules and anions that may bind to the complex or quench its emission, resulting in the two luminescent species observed. The lifetimes of the immobilized complex and its anionic adducts are lower than those of the untethered complex (Table 2.2) suggesting that additional quenching of the Eu(III) ion is occurring, possibly through an electron transfer process.

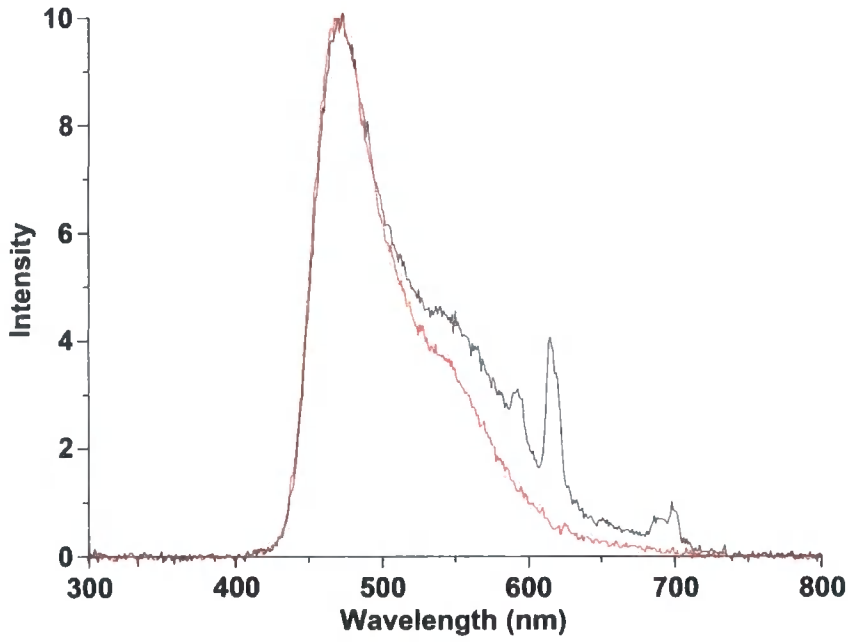

Figure 4.11 – A graph comparing emission of $[EuL^{49}]^{2+}$ immobilised on TentaGel^{TM} S-NH_2 (black) to that of the underivatised resin alone (red) (resins in H_2O, 298 K, λ_{exc} = 355 nm).

In addition to the lifetime measurements recorded, the emission spectrum of the immobilised Eu(III) ion in both H_2O (Figure 4.11) and bicarbonate solution was acquired. It was hoped that analysis of the $\Delta J = 2/\Delta J = 1$ ratio would reveal the coordination environment around the central Eu(III) ion. Unfortunately, residual fluorescence from the polystyrene resin overlapped with metal based emission inhibiting ratiometric analysis. Attempts to normalize the emission proved unsuc-

cessful.

In conclusion, the modulation of the complex lifetime upon the addition of bicarbonate indicates that the immobilised complex was associating with the added anions. It may expected that the analogous complex $[EuL^{62}]^{2+}$ should also still associate with anionic species when immobilised on the resin. The emission spectra obtained may be in future simplified through the use of time gated acquisition.

4.3.2 Trial phospho-anion separation experiments

The indication that the lifetime of immobilised $[EuL^{49}]^{2+}$ was being modulated in the presence of anionic species encouraged the examination of $[EuL^{62}]^{2+}$, immobilised on TentaGel^{TM} S-NH_2, for selective retention of phospho-anions. The simplest way to initially study the resin was to examine its ability to retain $(O$-P-Tyr$)^{2-}$ selectively, when present in a mixture with tyrosine. An experimental procedure was designed to investigate the retention capabilities of the immobilized complex, Figure 4.12. The aim of the experiment was to examine if the ILAC media could selectively retain $(O$-P-Tyr$)^{2-}$ residues in a mixture also containing tyrosine residues in excess, then liberate the complex bound residues using aqueous ammonium carbonate solution.

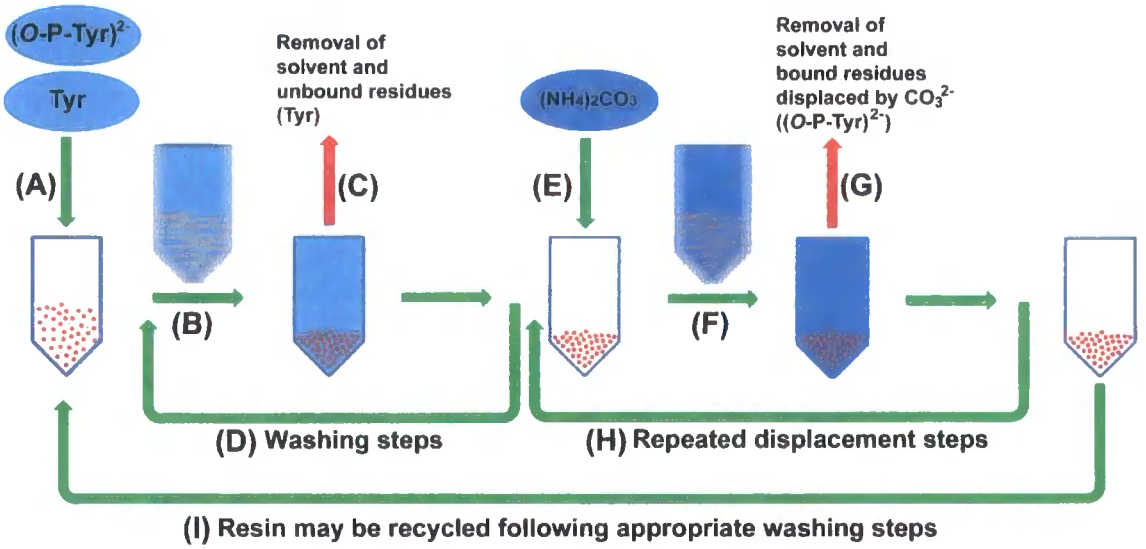

Figure 4.12 – A schematic detailing the trial separation of $(O\text{-P-Tyr})^{2-}$ from tyrosine. Steps detailed are: **(A)** addition of a mixed solution of $(O\text{-P-Tyr})^{2-}$ and Tyr (H_2O, pH 7.4) to the resin contained within an eppendorf; **(B)** vortex mixing (3 min) of the sample followed by centrifugation (2 min, 3000 rpm); **(C)** removal of solution containing unbound residues; **(D)** addition of further H_2O to wash the resin; **(E)** addition of ammonium carbonate solution to the resin (H_2O, 30 mM, pH 8.1); **(F)** as step **(B)**; **(G)** removal of solution containing displaced $(O\text{-P-Tyr})^{2-}$ residues; **(H)** addition of further ammonium carbonate solution to the resin to displace $(O\text{-P-Tyr})^{2-}$ residues still bound; **(I)** following displacement steps the resin may be washed for re-use.

Initial experiments utilised $[\mathrm{EuL}^{62}]^{2+}$ immobilised on TentaGel$^{\mathrm{TM}}$ S-NH_2 (261 mg, 4.4 % derivatization, 0.0052 mmol Eu(III) binding sites, remaining amine groups were acetyl capped), pre-soaked in H_2O overnight. Typically, experiments have examined separations of mixed solutions of $(O\text{-P-Tyr})^{2-}$ and tyrosine (1 ml, pH 7.4) in the region of ~0.5 mg/ml final amino acid concentrations. The total number of amino acid molecules loaded onto the resin was always lower than the total number of Eu(III) binding sites available. In each experiment, the procedure outlined in Figure 4.12 was followed. The resin was subjected to one further washing step with H_2O (1 ml, step **(D)**), followed by displacement of bound residues with ammonium carbonate solution (1 ml, 30 mM, pH 8.1, step **E**) with one additional displacement step (step **(H)**). Each solution was collected by a syringe needle, then lyophilized under reduced pressure to remove solvent and the volatile ammonium carbonate. Control $(O\text{-P-Tyr})^{2-}$/tyrosine separation experiments, utilising resins that were not conjugated to the Eu(III) complex, were also carried out. The two resins used

were 'uncapped' TentaGel^{TM} S-NH_2 and 100 % '*N*-acetyl capped' TentaGel^{TM} S-NH_2. These control separation experiments followed the procedure described above and in Figure 4.12. The relative concentration of $(O$-P-Tyr$)^{2-}$ and tyrosine in each isolated solution was determined, as described in detail within the experimental chapter, through quantification using LCMS analysis. A typical result set obtained for separation of $(O$-P-Tyr$)^{2-}$ and tyrosine with $[EuL^{62}]^{2+}$ immobilised on TentaGel^{TM} S-NH_2 is shown in Figure 4.13.

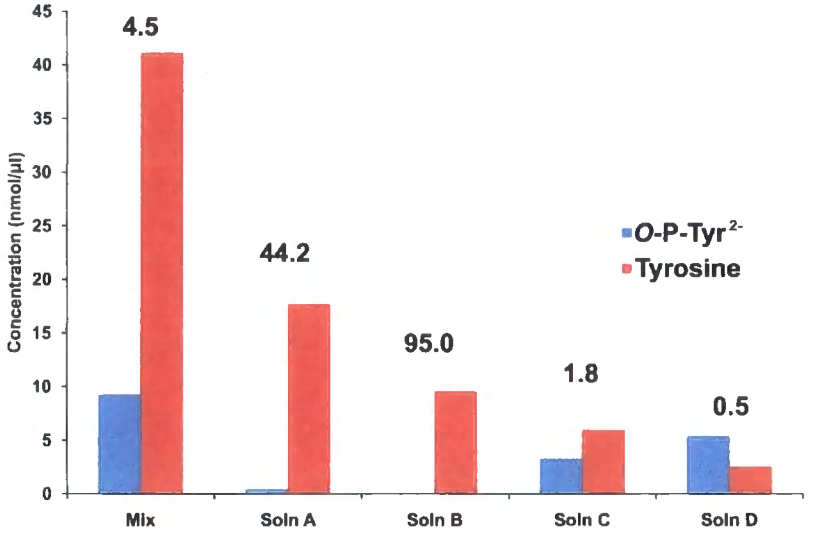

Figure 4.13 – A representation of the relative concentrations of $(O$-P-Tyr$)^{2-}$ and tyrosine solutions at each stage of the separation experiment. The solutions are named as; **Mix**: The concentration of $(O$-P-Tyr$)^{2-}$ and tyrosine in the 1 ml solution initially loaded onto the resin in stage (A) (Figure 4.12); **Soln A**: The concentration of $(O$-P-Tyr$)^{2-}$ and tyrosine in the solution removed from the resin in stage **(C)**; **Soln B**: The concentration of $(O$-P-Tyr$)^{2-}$ and tyrosine in the solution removed from the resin in stage **(C)** after one further washing step (stage **(D)**); **Soln C**: The concentration of $(O$-P-Tyr$)^{2-}$ and tyrosine in the solution removed from the resin in stage **(G)**; **Soln D**: The concentration of $(O$-P-Tyr$)^{2-}$ and tyrosine in the solution removed from the resin in stage **(G)** after one further displacement step (stage **(H)**). The number above each pair of bar graphs is the ratio of the tyrosine/$(O$-P-Tyr$)^{2-}$ concentrations.

It is seen from the results, after loading the initial amino acid mixture (tyrosine in 4.5 fold excess) onto the resin, followed by mixing and removal of the solvent, that the tyrosine/$(O$-P-Tyr$)^{2-}$ ratio increased to ~44 in the isolated solution, consistent with the selective retention of $(O$-P-Tyr$)^{2-}$ residues. A second H_2O wash of the resin removed virtually only tyrosine residues. The molar ratio (tyrosine/$(O$-P-Tyr$)^{2-}$) of this solution was ~95. The two washing steps accounted for the removal

of ~75 % of the initially added tyrosine residues, whilst <5 % of the initially added (O-P-Tyr)$^{2-}$ residues were removed. Step-wise additions of ammonium carbonate solution were observed to displace bound (O-P-Tyr)$^{2-}$ residues, indicated by the consecutive decrease in the tyrosine/(O-P-Tyr)$^{2-}$ ratio of abstracted solutions to 1.8 then 0.5. The latter analysis indicating that (O-P-Tyr)$^{2-}$ was now in excess over tyrosine. The latter two washing steps accounted for the recovery of >90 % of the initially loaded (O-P-Tyr)$^{2-}$ residues, whilst ~20 % of initially loaded tyrosine was also recovered in these steps.

Analysis of data from the control experiments showed that when using the 'uncapped' resin a minor amount of non-specific retention of residues was observed. In contrast, neither tyrosine or (O-P-Tyr)$^{2-}$ were significantly retained on the 100 % 'N-acetyl-capped' resin. For example, ~95 % of recovered (O-P-Tyr)$^{2-}$ residues were collected in the first two water washing steps.

4.4 Conclusions

The synthetic methodology described within this chapter afforded a simple route to the desired complex, $[EuL^{62}]^{2+}$, followed by conjugation to a variety of solid supports. The conjugation of the sensitiser-bearing complex, $[EuL^{49}]^{2+}$, enabled luminescence methods to be used to probe the interaction of the immobilized complex with the carbonate anion. In addition, luminescence spectra of the immobilized complex were also obtained,. Although Eu(III) emission was partially masked by fluorescence attributed to the resin, this technique hinted that time-gated acquisition of Eu(III) emission spectra would reveal much about the coordination environment of this complex.

Preliminary separation studies showed that the derivatised resin ($[EuL^{62}]^{2+}$ immobilized on TentaGel^{TM} S-NH_2) selectively retained phospho-amino acid residues over non-phosphorylated residues. Subsequent displacement procedures yielded so-

lutions where the relative concentration of $(O\text{-P-Tyr})^{2-}$ was significantly enhanced compared to that of the initial amino acid mixture. Control experiments revealed that the retention of $(O\text{-P-Tyr})^{2-}$ residues was due to their binding to immobilized Eu(III) complexes, as the *N*-acetyl capped resin exhibited no retention capability. The same control experiments revealed the need for the capping of residual NH_2 groups on the resin, as this functionality, when protonated, was observed to play a minor role in non-specific amino acid retention. In summary, the results show that there is a promising future for immobilized Ln(III) complexes as chromatographic materials that can selectively bind phosphate fragments, hence aiding their subsequent separation, analysis and identification.

4.5 Future work

There are a great many possibilities for future work within the area of synthesis and evaluation of novel ILAC media. The results reported herein constitute the first step in the evaluation of this particular ILAC methodology. Much work needs to be done to identify its scope and utility in the enrichment of phospho-peptides. In the longer term, its utility in isolating phospho-peptide fragments from protein digests needs to be addressed. Factors such as the reproducibility of separation results with a particular media, the working lifetime of the resin (number of useful separation cycles per resin sample, stability of the complex), and the analyte concentration ranges in which effective separations and analysis can be achieved, need to be examined and established. All of these conditions may be examined through analysis of mixtures of various amino acids. Next, conditions would need to be shown to be reproducible with peptide samples, containing certain phosphorylated residues.

It is to be expected that different solid supports will uniquely influence the behaviour of the resulting functionalised resin, and that identical solid supports of different Eu(III) loadings will likewise behave differently. It will therefore be essential to examine each system in detail, to determine its utility in phospho-peptide separations. Because of the innumerable variations of solid support and Eu(III) loadings

possible, it will be necessary to judiciously select suitable resins and Eu(III) loadings at the outset. Once the most promising resin has been identified, in terms of synthetic behaviour, handling and separation utility, variations of Eu(III) loadings can be examined to identify the most applicable system for the widest range of samples. Eu(III) loadings could be easily modulated, as required. Of the novel conjugated media presented within this thesis, the samples of $[EuL^{62}]^{2+}$ loaded Affi-Gel® 102 and $[EuL^{62}]^{2+}$ loaded SiMAG-Amino remain to be tested.

The longer term aim of this work is to create ILAC media that can be used to isolate phospho-peptide fragments from digests of cell lysates. Further to the early characterisation experiments, the selectivity of retention between the various *O*-phosphorylated amino acids would need to be examined through similar separation experiments, as described earlier. In particular, the use of a phospho-peptide elution flow-system, using a buffer of increasing concentration to selectively displace weaker bound phospho-peptide fragments, should be investigated. Such a system can be tested initially with corresponding phosphorylated amino acid residues to determine the levels of discrimination likely to be achieved. As outlined in section 4.1, a whole cell lysate is likely to contain significant levels of *N*-phosphorylated amino acids, for which methods of retention and analysis are under-represented. The mild elution conditions used with ILAC media may make the retention of these *N*-phosphorylated amino acids more likely, as they are less likely to decompose than in the more acidic IMAC buffers. Because of this possibility, the association of the parent complex, $[EuL^{24}]^{3+}$, with these *N*-phosphorylated amino acids needs to be examined to determine if the retention of such species is significant.

Chapter 5

Experimental

5.1 Experimental procedures

5.1.1 General procedures

All commercially available reagents were used as received, from their respective suppliers. Solvents were dried using an appropriate drying agent when required ((CH_3CN over CaH_2, CH_3OH over $Mg(OMe)_2$). Reactions requiring anhydrous conditions were carried out using Schlenk-line techniques under an atmosphere of dry argon. Water and H_2O refer to high purity water with conductivity ≤ 0.04 μS cm^{-1} obtained from the 'PuriteSTILL Plus' purification system.

Thin-layer chromatography was carried out on neutral alumina plates (Merck Art 5550) or silica plates (Merck 5554) and visualised under UV (254 nm) or by staining with iodine. Preparative column chromatography was carried out using neutral alumina (Merck Aluminium Oxide 90, activity II-III, 70230 mesh), pre-soaked in ethyl acetate, or silica (Merck Silica Gel 60, 230400 mesh).

^1H and ^{13}C-NMR spectra were recorded on a Varian VXR-400 (^1H at 399.97 MHz, ^{13}C at 100.57 MHz), Varian Inova-500 (^1H at 499.78 MHz, ^{13}C at 125.67 MHz, ^{19}F at 470.25 MHz, ^{31}P at 202.31 MHz) or a Varian VNMRS-700 (^1H at 699.73 MHz, ^{13}C at 175.95 MHz, ^{19}F at 658.41 MHz) spectrometer. Spectra were referenced internally to the residual protio-solvent resonances. Immobilized Eu(III) complex ^1H-NMR spectra were recorded on the Varian Inova-500 machine using a 4 mm GHX

NanoProbe fitted with a MAS rotor.

Electrospray mass spectra were recorded on a Thermo-Finnigan LTQ FT, Fisons VG Platform II or Waters Micromass LCT instrument, operating in positive or negative ion mode as stated, with methanol as the carrier solvent. MALDI mass spectra were recorded on the Thermo-Finnigan LTQ FT instrument. Accurate mass spectra were recorded using the Thermo Finnigan LTQ FT mass spectrometer.

Melting points were recorded using a Reichart-Köfler block and are uncorrected.

pH measurements used a Jenway 3020 or a Jenway 3320 pH meter attached to an Aldrich Chemical Company micro-pH combination electrode (three point calibration using pH = 4.0 ±0.02, pH = 7.00 ±0.02 and pH = 10.00 ±0.02 (T = 20°C) buffer solution supplied by Aldrich. The adjustment of pH was carried out using conc. NaOH and conc. HCl (or NaOD and DCl if required) solution to avoid any significant increase in sample volume. For measurements carried out in D_2O the pD was calculated using the actual pH meter reading and the equation: pD = pH (meter reading) + 0.41.

Exchange of complex counterions to chloride anions was performed using 'DOWEX® 1x8 200-400 mesh Cl' ion exchange resin (Sigma-Aldrich®). Typically the resin (1 g) was prepared by boiling in MeOH (50 ml) overnight followed by washing with H_2O (500 ml). The resin was then stirred in $HCl_{(aq)}$ (1 M, 50 ml) for 2 h then washed with H_2O until the washings were pH 7. Suction dried resin was then added to a solution of the complex (H_2O:MeOH, 50:50), the mixture was stirred for 2 h followed by filtration. MeOH was removed under reduced pressure, the aqueous phase was again filtered then dried under reduced pressure to yield the desired chloride salt of the complex.

Excess $LnCl_3$ or $Ln(OAc)_3$ was removed from dimeric complex samples using benzoylated dialysis tubing (9 mm flat width, MWCO 2000) (Sigma-Aldrich®). Typically

the dialysis tubing was washed with H_2O, the solid complex was dissolved in H_2O (1 ml) and the solution was transferred to the tubing that was sealed by clamping at both ends. The tubing was submerged in stirring H_2O (500 ml) and the H_2O was exchanged 4 times over 72 h followed by the removal and filtering of the tubing contents. The aqueous solution was then frozen and lyophilized to yield the desired complex.

5.1.2 Relaxivity measurements

Relaxivity measurements were carried out at 37°C and 60 MHz on a BrukerMinispec mq60 instrument. The mean value of three separate measurements was recorded.

5.1.3 HPLC analysis of Ln(III) complexes

Reverse phase HPLC analysis were performed at 298 K on a Perkin Elmer system, comprising of a Perkin Elmer Series 200 Pump, Perkin Elmer Series 200 Autosampler, Perkin Elmer Series 200 Diode array detector and Perkin Elmer Series 200 Fluorescence detector. Columns used were a 4.6 x 150 mm 4 μm Phenomenex Synergi Fusion RP 80Å analytical column or a 4.6 x 150 mm 4 μm Phenomenex Synergi Polar-RP 80Å analytical column. In each case an H_2O + 0.1 % HCOOH/MeCN + 0.1 % HCOOH or H_2O + 0.1 % CF_3COOH/MeCN + 0.1 % CF_3COOH solvent system was used (gradient elution) with a run time of 20 minutes. In each case, a single major product was observed in >95 % purity using a diode array UV-Vis detector operating at 255 nm, 335 nm or 375 nm. This corresponds to the absorption band of the appropriate aryl ring, azaxanthone or azathioxanthone used as the sensitizing moiety for each Eu(III) or Tb(III) complex, and, for the latter two wavelengths, is to longer wavelength of any organic contaminant. Such behaviour indicated that each of the species that was eluted bore this chromophore. A fluorescence detector was also connected to the HPLC, monitoring eluent from the column at a wavelength corresponding to the Eu(III) or Tb(III) centred emission (616 nm or 545 nm respectively); again emission was seen for each of these peaks, suggesting that each peak corresponding to a chromophore bound species also was coordinated to Eu(III) or Tb(III), in such a way that it was efficiently sensitized. For each Yb(III) or Gd(III)

complex, a UV-Vis detector was used operating with a LP 250 nm detection filter. Individual solvent systems are stated in Appendix A.

5.1.4 Optical techniques

UV/Vis absorbance spectra were recorded either on a Perkin Elmer Lambda 900 UV/Vis/NIR spectrometer (using FL Winlab software) or a Unicam UV/Vis UV2.

Emission spectra were measured on a ISA Joblin-Yvon Spex Fluorolog-3 luminescent spectrometer (using DataMax v2.20 software) or a Perkin Elmer LS55 luminescence spectrometer (using FL Winlab software), while lifetimes were measured on the Perkin Elmer LS55 luminescence spectrometer. All samples were contained in quartz cuvettes with a path length of 1 cm and polished base. Measurements were recorded at 298 K and were obtained relative to a reference of pure solvent contained in a matched cell, following indirect excitation of the Ln(III) ion at the stated wavelength. An integration time of 0.5 seconds, increment of 0.5 nm and excitation and emission slit widths of 2 and 1 nm, respectively, were employed throughout. Luminescent titrations were carried out by normalising the emission spectra with the absorption spectra in each point, in order to revise the decrease in the sample concentration caused by pH adjustment or addition of an anion stock solution, where appropriate.

Lifetimes of Eu(III) and Tb(III) complexes were measured by excitation of the sample using a short pulse of light (255, 335, 372 nm depending on the nature of the complex) followed by monitoring the integrated intensity of light (for Eu(III) 612-618 nm, for Tb(III) 543-546 nm; depending on the measured species and the pH) emitted during a fixed gate time, t_g, after a delay time, t_d. At least 20 delay times were used covering 3 or more lifetimes. A gate time of 0.1 ms was used, and the excitation and emission slits were set to 10 nm and 2.5 nm band-pass respectively. The obtained exponential decay curves were fitted to the equation below, using Origin 6.0 software (Data Analysis & Technical Graphics):

$$I = A_0 + A_1 * \exp(-kt) \qquad \text{(eqn. 3)}$$

where: I: intensity at time t after the flash; A_0: intensity after the decay has finished; A_1: pre-exponential factor; k: rate constant for decay of the excited state.

A low temperature phosphorescence spectrum of (*O*-P-Tyr)$^{2-}$ was recorded to enable the triplet energy to be determined. An Oxford Instruments optical cryostat operating at 77 K and LS 55B spectrometer were used. The sample was dissolved in EPA (diethyl ether-isopentane-ethanol, 5 : 5 : 2) and contained in 10 mm cuvettes. The triplet energy was considered as the highest energy (shortest wavelength) observed phosphorescence band, corresponding to the 0-0 transition, using time-gated detection.

CPL spectra were recorded on a custom modified Spex Fluoromax-2 spectrometer at the University of Glasgow, with the assistance of Dr. Bob Peacock.

5.1.5 Determination of binding constants

To examine the influence of some biologically common anions on Eu(III) and Tb(III) complexes, luminescent titrations were carried out examining separate solutions containing either *O*-phospho-L-tyrosine, Na_2CO_3, sodium lactate, NaH_2PO_4 or trisodium citrate. All of these measurements were carried out by adding the selected anion as liquid concentrated stock solution where the addition at each point was approx. 0.1-0.5 % in volume of the original solution observed to avoid significant increase in sample volume. HSA was added as a solid. Each Eu(III) emission spectrum was corrected for dilution. The apparent binding constant of the selected anion was calculated using eqn. 4 in Origin 6.0 software (Data Analysis & Technical Graphics):

$$[X] = \frac{[(F - F_0)/(F_1 - F_0)]/K + [EuL] * (F - F_0)/(F_1 - F_0)}{1 - [(F - F_0)/(F_1 - F_0)]} - \frac{[EuL] * [(F - F_0)/(F_1 - F_0)]^2}{1 - [(F - F_0)/(F_1 - F_0)]} \qquad \text{(eqn. 4)}$$

where: X: the total concentration of anion in solution; K: binding constant; F: the ratio or intensity of the selected peak(s); F_0: ratio or intensity of the selected peak(s) at the beginning of the titration; F_1: the final ratio or intensity of the se-

lected peak(s); [EuL]: the total concentration of Eu(III) complex in solution.

Alternatively, binding constants have been determined, where stated, by using the nonlinear least-squares program SPECFIT/32^{TM}.[136] The fitting methodology, which relies on the use of various mathematical parameters, uses the Levenberg-Marquardt procedure to minimise the least-squares residuals between the data set and the model system.[137,138] This work was undertaken by Dr. Cidália dos Santos (Trinity College Dublin).

5.1.6 Cellular microscopy

Epifluorescence images were taken on a Zeiss Axiovert 200M epifluorescence microscope with objectives 63x/1.40 oil DIC and 40x/1.40 oil DIC respectively, equipped with an Axiocam CCD camera. For excitation a 340-390 nm (90 % transmission) band-pass (BP) filter was used. Ligand fluorescence were observed using a BP 445-465 nm filter (80 % transmission), while Eu(III) emission was observed using a 570 nm long-pass (LP) filter (85 % transmission).

5.1.7 Cell Culture and Toxicity

Two cell lines were selected for cell culture studies: CHO (Chinese Hamster Ovary) cells and NIH 3T3, mouse skin fibroblast (connective tissue) cells. Each line is transformed, and compromise adherent cells, which grow in a monolayer. These cell lines were cultured in a copper jacket incubator at 37°C, average 20 % humidity and 5 % (v/v) CO_2 in 50 mL volume plastic grow plates. Cells for microscopy were grown in a 24 well-plate using d = 13 mm glass cover slips (average thickness l = 0.1 mm). DMEM (Dulbeccos Modified Eagle Media), and F-12 (Ham) medias were used for NIH 3T3 and CHO cells respectively, each containing 10 % (v/v) NCS (Newborn Calf Serum) and 1 % (v/v) penicillin-streptomycin. Complexes were loaded onto cells using the appropriate growth medium. For flow cytometry measurements, cells were detached from the glass surface using 1 % (v/v) trypsin solution at 37°C for 5 min. The solutions and washings were analysed in separate ICP-MS measurements to measure any possible Eu(III) complex egress. IC_{50} values were determined

using the MTT assay, as described by Carmichael *et al*[97] which makes use of the conversion of MTT (3-(4,5-dimethylthiazol-2-yl)-2,5-diphenyltetrazolium bromide) to a purple formazan product by the mitochondrial dehydrogenase of viable cells. This insoluble formazan was quantified spectrophotometrically upon dissolution in DMSO. Approximately 5 x 10^3 NIH 3T3 cells in 100 μL DMEM were seeded into each well of flat-bottomed 96-well plates and allowed to attach overnight. Complex solutions were added to triplicate wells to give final concentrations over a 2-log range. Following 24 h incubation, MTT (1.0 mM) was added to each well, and the plates incubated for a further 4 h. The culture medium was removed, and DMSO (150 μL) was added. The plates were shaken for 20 seconds and the absorbance measured immediately at 540 nm in a microplate reader. IC_{50} values were determined as the drug concentration required to reduce the absorbance to 50 % of that in the untreated, control wells, and represent the mean for data from three independent experiments.

5.1.8 Microscopy under variable atmospheric CO_2 levels

The dependence of $[EuL^{44a}]^{3+}$ emission intensity, localised within the mitochondria of HeLa cells, as a function of atmospheric CO_2 concentration, was examined by Dr. Ga-Lai Law, using facilities at the Department of Biology and Chemistry, City University of Hong Kong. The cells were grown in 60 x 15 mm culture dishes at 2 ml/dish, and were allowed to attach overnight. The cells were imaged in a tissue culture chamber (5 % to 3 % (v/v) CO_2, 37°C) through a Zeiss 510 LSM (upright configuration) confocal microscope equipped with a femtosecond-pulsed Ti:Sapphire laser (Libra II, Coherent). The excitation beam produced by the second harmonic generation of the femtosecond laser (λ_{exc} = 360 nm, ~ 4 mW) was passed through the LSM 510 microscope with HFT 650 dichroic (Carl Zeiss, Inc.) and focused onto the coverslip-adherent cells using a 63 x oil immersion objective. The images were obtained as a time series and cut by a band pass filter at 580-620 nm. The CO_2 level (as a percentage value) was controlled by an interface programme with each image and emission spectrum being obtained after 30 min of modifying the CO_2 level inside the tissue chamber. Images were selected at 30 min time intervals after the change

in CO_2 level to ensure total equilibrium of the gas. The first time point was 30 min after addition of the complex starting with 5 % of CO_2. The total duration of the time series was within 1h 45 min, with images chosen at 30 min, 60 min, and 90 min intervals, corresponding to CO_2 levels of 5 %, 4 % and 3 % respectively.

5.1.9 Resin microscopy

Resin samples (~2 mg) were mixed with H_2O or aqueous anion solution (10 µl, pH 7.4), spread onto a glass slide then sealed under a glass cover slip. Slides were then mounted on a XY microscope stage. Following laser excitation (Nd:YAG, UVFQ-100-1-Y-335 - Elforlight, 5 ns pulses at a 30 Hz repetition rate, λ_{exc} = 355 nm), Eu(III) emission was detected through a fibre-coupled charge coupled device (CCD, Imagex-nannoCCD - Photonic research systems) camera connected to a Zeiss Axio vert inverted microscope. In a similar manner, the radiative decay curves of each sample were recorded, using a long pass filter to isolate Eu(III) emission. Mono-exponential and bi-exponential decay curves were fitted to eqns. 3 and 5 respectively using Origin 6.0 software (Data Analysis & Technical Graphics):

$$I = A_0 + A_1 * \exp(-kt) \qquad \text{(eqn. 3)}$$

$$I = A_0 + A_1 * \exp(-k/t_1) + A_2 * \exp(-k/t_2) \qquad \text{(eqn. 5)}$$

5.1.10 Inductively Coupled Plasma Mass Spectrometry

All ICP-MS determination, including all Eu(III) concentrations from cells and growth media, were carried out by Dr. Chris Ottley in the Department of Earth Sciences at Durham University using a Thermo Finningan ELEMENT$_2$ High Resolution Select Field ICPMS.

5.1.11 LCMS quantification of (*O*-P-Tyr)$^{2-}$ and tyrosine

All amino acid calibration plots were determined using an LCMS method on a Thermo-Finnigan LTQ FT mass spectrometer coupled with a 20 x 150 mm 4 µm Phenomenex Synergi Polar-RP 80Å analytical column. A dilution series of (*O*-P-Tyr)$^{2-}$ and tyrosine solutions at concentrations of 50 pg µl^{-1}, 500 pg µl^{-1}, 5 ng µl^{-1},

50 ng μl^{-1} and 500 ng μl^{-1} were created from 1 mg ml^{-1} stock solutions. Solutions were injected onto the column at a flow rate of 200 μl min^{-1} and resolved using the following elution system:

Time	A	B	Gradient
0 - 5 min	100 %	0 %	N/A
5 - 8 min	100 % → 5 %	0 % → 95 %	Linear
8 - 13 min	5 %	95 %	N/A
13 - 20 min	100 %	0 %	N/A

Table 5.1 – Solvent **A**: H_2O + 0.1 % HCOOH; Solvent **B**: MeCN.

Eluted amino acids were detected using absorbance measurements at 214 nm, 254 nm and 280 nm. $(O\text{-P-Tyr})^{2-}$ elution centred at ~2.2 min and tyrosine elution centred at ~3.3 min.

Post-column MS detection was performed using three scan events: 1: Full scan in negative ion mode (100 - 500 m/z); 2: Negative ion mode (70-190 m/z) with MSMS on ions detected at 180 ± 2 m/z; 3: Negative ion mode (70-270 m/z) with MSMS on ions detected at 260 ± 2 m/z. Each ion chromatogram was extracted and the area under each region of interest was determined.

Calibration plots were created using the UV or MS peak areas found. Each calibration point was recorded three times and at a different injection volume (2 μl, 5 μl or 10 μl). Corresponding calibration plots were determined using the average of each of these three points.

Each unknown sample was run alongside the calibration points and its constituent amino acid concentrations determined using the calibration plot.

5.1.12 Single crystal X-ray diffraction

The crystal structure of 2-phthalimidomethyl-7-methoxycarbonyl-1-azathioxanthone was determined. Data was collected using graphite monochromated Mo Kα radiation (λ=0.71073 Å) on a Bruker SMART 6K CCD area detector. A series of

narrow ω-scans (0.3°), each run at a different ϕ-angle, were carried out to cover approximately a full sphere of data. Cell parameters were determined and refined using SMART software,[139] and raw frame data were integrated using the SAINT program.[140] The structure was solved by direct methods and refined by full-matrix least squares on F^2 using SHELXTL software.[141] Further crystal data is given in Appendix C.

5.2 Synthetic procedures

5.2.1 Sensitised complexes and precursors

2-Chloro-*N*-[(S)-1-phenylethyl]ethanamide[142]

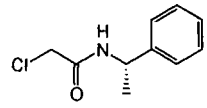

Chloroacetyl chloride (12.47 ml, 156.6 mmol) was added dropwise to a vigorously stirring solution of (S)-(-)-α-methylbenzylamine (10.63 ml, 82.5 mmol) and NEt_3 (12.56 ml, 90.5 mmol) in dry Et_2O (200 ml) at -78°C. Following complete addition the solution was allowed to warm to room temperature over the course of 2 h yielding a yellow tinged solution containing a white precipitate. The suspension was washed with $HCl_{(aq)}$ (1M, 2 x 40 ml) followed by H_2O (2 x 100 ml) to yield a clear yellow tinged organic phase that was cooled at 4°C to precipitate the crude product as off-white needle-like crystals. The desired product was purified by recrystallisation from Et_2O and isolated as white needle-like crystals (14.52 g, 73.5 mmol, 89 %); m.p. 101-103°C (Lit.[143] 101-102°C); ^{1}H-NMR ($CDCl_3$, 400 MHz) δ 7.32-7.38 (m, 5H, Ar), 6.82 (br, 1H, NH), 5.15 (m, 1H, CH), 4.06 (m, 2H, CH_2), 1.55 (d, 3H, J=6.5 Hz, CH_3); ^{13}C-NMR ($CDCl_3$, 100 MHz, ^{1}H decoupled 400 MHz) δ 165.3 (1C, C=O), 142.6 (1C, $Ar_{(q)}$), 129.1 (2C, $Ar_{(m)}$), 128.0 (1C, $Ar_{(p)}$), 126.4 (2C, $Ar_{(o)}$), 49.6 (1C, CH), 43.0 (1C, CH_2), 22.0 (1C, CH_3); MS (ES^+) m/z 220.1 $[M + Na]^+$ 100 %.

1,4,7,10-Tetraaza-cyclododecane-1,7-dicarboxylic acid dibenzyl ester[85]

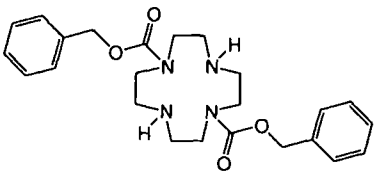

Disodium hydrogen phosphate (14 g, 98.62 mmol) was added to a solution of cyclen (5 g, 29.02 mmol) in distilled water:dioxane (50:20, 70 ml), followed by adjustment of the pH to between 2.5-3 with conc. $HCl_{(aq)}$. Benzyl chloroformate (10.0 ml, 70.05 mmol) in dioxane (20 ml) was added dropwise to the solution over 2.5 h at room temperature, followed by stirring for a further 18 h to yield a colourless solution containing a white precipitate. Solvent was removed from the crude mixture under reduced pressure to leave a viscous white gum. The gum was dissolved in water (100 ml) followed by adjustment of the pH to 7 with conc. $KOH_{(aq)}$. The resultant solution was extracted with diethyl ether (3 x 50 ml) to remove reaction side products. The aqueous phase was then extracted with dichloromethane (3 x 50 ml) followed by the organic phase being dried under reduced pressure to give the desired product as a colourless viscous oil. The oil was redissolved in DCM (5 ml) followed by precipitation of the desired product via the addition of cold ether (60 ml) to give a coarse white powder that was collected by centrifugation (8.97 g, 20.36 mmol, 70 %); m.p. 113-116°C; ^{1}H-NMR ($CDCl_3$, 500 MHz) δ 7.33-7.40 (m, 10H, Ar), 5.18 (s, 4H, Cbz CH_2), 3.47-3.79 (m br, 8H, cyclen CH_2), 2.86-3.12 (m br, 8H, cyclen CH_2), 2.05 (s br, 2H, 2 x NH); ^{13}C-NMR ($CDCl_3$, 125 MHz, ^{1}H decoupled 500 MHz) δ 156.5, 156.4 (2C, C=O), 136.2, 136.1 (2C, $Ar_{(q)}$), 129.1, 129.0, 128.8, 128.7, 128.4, 128.3 (10C, Ar), 68.2, 68.1 (2C, Cbz CH_2), 50.9, 50.7, 50.5, 50.1, 49.9, 49.4, 49.2 (16C, cyclen CH_2); MS (ES^+) m/z 441.4 $[M + H]^+$ 100 %.

4,10-Bis-[((S)-1-phenyl-ethylcarbamoyl)-methyl]-1,4,7,10-tetraaza-cyclododecane-1,7-dicarboxylic acid dibenzyl ester[94]

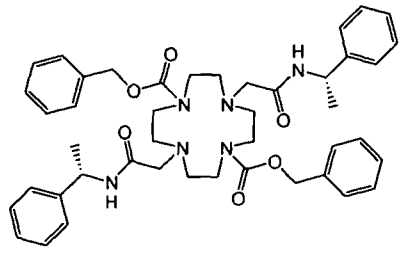

A stirring mixture of 1,4,7,10-tetraaza-cyclododecane-1,7-dicarboxylic acid dibenzyl ester (1.25 g, 2.84 mmol), 2-chloro-*N*-[(*S*)-methylbenzyl]ethanamide (1.23 g, 6.22 mmol), Cs_2CO_3 (1.84 g, 5.65 mmol) and KI (10 mg) was boiled under reflux in dry MeCN for 24 h. The resultant orange tinged solution was allowed to cool to room temperature then dried under reduced pressure. The orange residue was taken up in DCM (15 ml), washed with sodium thiosulfate solution (0.01 M, 10 ml) then H_2O (2 x 15 ml). The orange tinged organic layer was dried under reduced pressure to leave a viscous oil. The oil was sonicated in diethyl ether (2 x 20 ml), the insoluble material was collected by centrifugation, dissolved in DCM (10 ml) then dried under vacuum to give the desired product as a off-white glassy solid (1.70 g, 2.23 mmol, 78 %); m.p. 64-66°C; ^{1}H-NMR ($CDCl_3$, 500 MHz) δ 7.59 (s br, 2H, NH), 7.20-7.35 (m, 20H, amide arm and Cbz Ar), 5.11 (m, 2H, CH), 4.97 (s br, 4H, Cbz CH_2), 3.43 (m br, 8H, cyclen CH_2), 3.15 (s br, 4H, CH_2CO), 2.75 (m br, 8H, cyclen CH_2), 1.44 (s br, 6H, CH_3); ^{13}C-NMR ($CDCl_3$, 125 MHz, ^{1}H decoupled 500 MHz) δ 170.2 (2C, amide arm C=O), 157.0 (2C, Cbz C=O), 143.8 (2C, amide arm $Ar_{(q)}$), 136.5 (2C, Cbz $Ar_{(q)}$), 128.8, 128.5, 128.4, 2 x 127.4, 126.5 (20C, amide arm and Cbz Ar), 67.5 (2C, Cbz CH_2), 59.2 (2C, CH_2CO), 54.9-56.3 (br, 4C, cyclen CH_2), 48.7 (2C, CH), 47.8-49.0 (br, 4C, cyclen CH_2), 22.0 (2C, CH_3); MS (ES^+) *m/z* 763.5 $[M + H]^+$ 100 %; HRMS (ES^+) *m/z* found 763.4187 $[M + H]^+$ $C_{44}H_{55}O_6N_6$ requires 763.4178.

***N*-((S)-1-Phenyl-ethyl)-2-(7-[((S)-1-phenyl-ethylcarbamoyl)-methyl]-1,4,7,10-tetraaza-cyclododec-1-yl)-acetamide[94]**

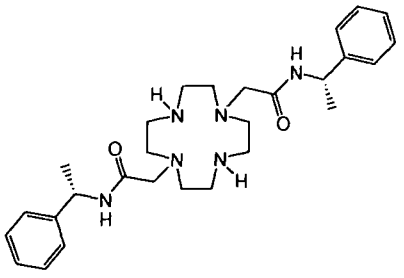

4,10-Bis-[((S)-1-phenyl-ethylcarbamoyl)-methyl]-1,4,7,10-tetraaza-cyclododecane-1,7-dicarboxylic acid dibenzyl ester (1.69 g, 2.22 mmol) in H_2O:MeOH (1:3, 30 ml) was shaken in a Parr hydrogenation flask at 40 psi H_2 over $Pd(OH)_2/C$ (0.15 g) for 24 h. The resulting mixture was filtered through celite to leave a clear solution that was dried under reduced pressure to yield the desired product as a glassy white solid (1.05 g, 2.12 mmol, 96 %); m.p. 140-143°C; ^{1}H-NMR (CD_3OD, 500 MHz) δ 7.28-7.32 and 7.21-7.23 (m, 10H, Ar), 5.04 (m, 2H, CH), 3.54 (d, 2H, J=17.0 Hz, CHCO), 3.41 (d, 2H, J=16.5 Hz, CHCO), 2.88-3.18 (m br, 16H, cyclen CH_2), 1.46 (d, 6H, J=7.0 Hz, CH_3); ^{13}C-NMR (CD_3OD, 125 MHz, ^{1}H decoupled 500 MHz) δ 172.7 (2C, C=O), 145.8 (2C, $Ar_{(q)}$), 130.5, 129.0, 128.0 (10C, Ar), 57.2 (2C, CH_2CO), 52.4 (2C, CH), 51.1, 50.7, 45.2 (br, 8C, cyclen CH_2), 23.5 (2C, CH_3); MS (ES^+) m/z 495.3 $[M + H]^+$ 100 %; HRMS (ES^+) m/z 495.3447 $[M + H]^+$ $C_{28}H_{43}O_2N_6$ requires 495.3442.

4,10-Bis-[((S)-1-phenyl-ethylcarbamoyl)-methyl]-1,4,7,10-tetraaza-cyclododecane-1-carboxylic acid *tert*-butyl ester (45)[94]

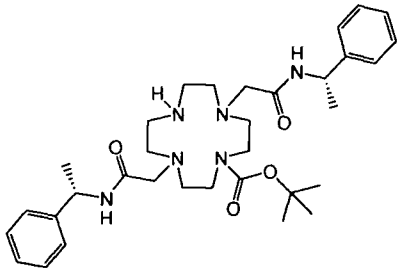

A solution of di-*tert*-butyl dicarbonate (0.353 g, 1.61 mmol) in dry MeOH (6 ml) was added dropwise over 1 h, at room temperature, to a stirring solution of *N*-((S)-1-phenyl-ethyl)-2-(7-[((S)-1-phenyl-ethylcarbamoyl)-methyl]-1,4,7,10-tetraaza-cyclododec-1-yl)-acetamide (0.998 g, 2.02 mmol) and NEt_3 (0.560 ml, 4.04 mmol) in dry MeOH (30 ml). The reaction mixture was left to stir overnight then dried under reduced pressure. The crude yellow tinged viscous oil was purified by column chromatography on alumina (utilising an incremental solvent system of DCM/MeOH starting from 100 % DCM with 0.1 % MeOH increments) to yield, after drying, the desired product as a glassy white solid (0.573 g, 0.963 mmol, 60 %); R_F (Alumina, DCM-MeOH, 49:1) : 0.46; m.p. 98-101°C; ^{1}H-NMR ($CDCl_3$, 500 MHz) δ 7.86 (s br, 1H, cyclen NH), 7.20-7.33 (m, 10H, Ar), 5.13 (m br, 2H, CH), 3.09 (m br, 4H, CH_2CO), 2.53-3.37 (m br, 16H, cyclen CH_2), 1.50 (d, 6H, J=7.0 Hz, amide arm CH_3), 1.39-1.41 (m br, 9H, ^{t}Bu CH_3); ^{13}C-NMR ($CDCl_3$, 125 MHz, ^{1}H decoupled 500 MHz) δ 170.5 (2C, amide C=O), 156.7 (1C, ^{t}Boc C=O), 143.8 (2C, $Ar_{(q)}$), 128.8, 127.5, 126.8 (10C, Ar), 80.3 (1C, ^{t}Boc$_{(q)}$), 59.6 (2C, CH_2CO), 49.0-53.8 (m br, 8C, cyclen CH_2), 48.7 (2C, CH), 28.8 (3C, ^{t}Boc CH_3), 22.0 (2C, amide arm CH_3); MS (ES^+) m/z 595.4 $[M + H]^+$ 100 %; HRMS (ES^+) m/z found 595.3972 $[M + H]^+$ $C_{33}H_{51}O_4N_6$ requires 595.3966.

7-Ethoxycarbonylmethyl-4,10-bis-[((S)-1-phenyl-ethylcarbamoyl)-methyl]-1,4,7,10-tetraaza-cyclododecane-1-carboxylic acid *tert*-butyl ester[94]

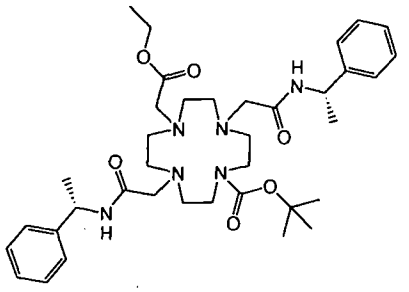

A mixture of 4,10-bis-[((S)-1-phenyl-ethylcarbamoyl)-methyl]-1,4,7,10-tetraaza-cyclododecane-1-carboxylic acid *tert*-butyl ester (0.224 g, 0.377 mmol), ethyl bromoacetate (0.035 ml, 0.316 mmol) and Cs_2CO_3 (0.123 g, 0.378 mmol) in MeCN (10 ml) was heated at reflux and stirred vigorously for 12 h then allowed to cool to room temperature. The mixture was dried under reduced pressure, dissolved in DCM then extracted with saturated $NaHCO_{3(aq)}$ solution (10 ml) followed by H_2O (2 x 10 ml). The yellow tinged organic layer was dried under reduced pressure to leave a yellow tinged oil. The desired product was isolated from the oil by column chromatography on alumina (using DCM/MeOH starting from 100 % DCM with 0.1 % MeOH increments) as a clear glassy solid (0.151 g, 0.222 mmol, 70 %); R_F (Alumina, DCM-MeOH, 95:5) : 0.61; m.p. 39-41°C; ^{1}H-NMR ($CDCl_3$, 500 MHz) δ 7.87 (s br, 1H, NH), 7.59 (s br, 1H, NH), 7.21-7.33 (m, 10H, Ar), 5.16 (m, 2H, CH), 4.07 (m, 2H, ethyl CH_2), 2.18-3.36 (m, 22H, cyclen CH_2, amide arms CH_2 and ester arm CH_2), 1.51 (d br, 6H, J=13.0 Hz, amide arm CH_3), 1.42 (m br, 9H, ^{t}Bu CH_3), 1.24 (t, 3H, J=7 Hz, ethyl CH_3); ^{13}C-NMR ($CDCl_3$, 125 MHz, ^{1}H decoupled 500 MHz) δ 171.0 (1C, ethyl ester C=O), 170.9, 170.3 (2C, amide C=O), 156.2 (1C, ^{t}Boc C=O), 144.2, 143.1 (2C, $Ar_{(q)}$), 129.0, 128.8, 127.9, 127.3, 127.0, 126.6 (10C, Ar), 80.1 (1C, ^{t}Boc$_{(q)}$), 60.7 (1C, ethyl CH_2), 59.5 (1C, ethyl ester CH_2CO), 53.3-55.0 (m br, 8C, cyclen CH_2), 54.3 (2C, amide arm CH_2CO), 48.5, 48.3 (2C, CH), 28.8 (3C, ^{t}Boc CH_3), 22.3, 21.2 (2C, amide arm CH_3), 14.6 (1C, ethyl CH_3); MS (ES^+) m/z 344.1 $\frac{1}{2}[M + H + Li]^{2+}$ 100 %, 681.4 $[M + H]^+$ 10 %; HRMS (ES^+) m/z found 681.4341 $[M + H]^+$ $C_{37}H_{57}O_6N_6$ requires 681.4334.

7-Carboxymethyl-4,10-bis-[((S)-1-phenyl-ethylcarbamoyl)-methyl]-1,4,7,10-tetraaza-cyclododecane-1-carboxylicacid *tert*-butyl ester (46)[94]

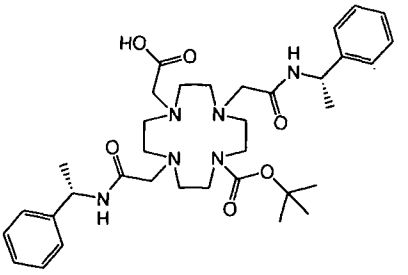

7-Ethoxycarbonylmethyl-4,10-bis-[((S)-1-phenyl-ethylcarbamoyl)-methyl]-1,4,7,10-tetraaza-cyclododecane-1-carboxylic acid *tert*-butyl ester (0.135 g, 0.198 mmol) and $LiOH.H_2O$ (0.025 g, 0.596 mmol) in H_2O:MeOH (100 ml, 50:50) were heated at reflux for 12 h. The solution was allowed to cool then MeOH was removed under reduced pressure. The aqueous solution was neutralised with dilute $HCl_{(aq)}$ then extracted with DCM (3 x 20 ml) after the addition of brine (20 ml). The combined organic washings were dried under reduced pressure to leave the desired product as a glassy white solid (0.127 g, 0.195 mmol, 98 %). ^{1}H-NMR ($CDCl_3$, 400 MHz) δ 7.18-7.32 (m, 10H, Ar), 5.10 (m br, 2H, CH), 2.31-3.22 (m br, 22H, cyclen CH_2, amide arms CH_2CO and acid arm CH_2CO), 1.46 (d, 6H, J=4.8 Hz, amide arm CH_3), 1.35 (m br, 9H, ^{t}Bu CH_3); ^{13}C-NMR ($CDCl_3$, 100 MHz, ^{1}H decoupled 400 MHz) δ 170.7 (br, 2C, amide C=O), 159.9 (br, 1C, ^{t}Boc C=O), 143.9 (br, 2C, $Ar_{(q)}$), 128.9, 127.4, 126.8 (10C, Ar), 80.4 (1C, ^{t}Boc$_{(q)}$), 58.4 (1C, acid arm CH_2CO), 53.7 (m br, 10C, cyclen CH_2 and amide arm CH_2CO), 49.1 (2C, CH), 28.7 (3C, ^{t}Boc CH_3), 22.2 (2C, amide arm CH_3); MS (ES^+) m/z 653.4 $[M + H]^+$ 100 %; HRMS (ES^+) m/z found 653.4029 $[M + H]^+$ $C_{35}H_{53}O_6N_6$ requires 653.4021.

Methyl-4-hydroxybenzoate[144]

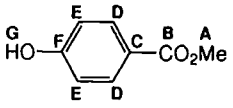

H_2SO_4 (7 ml) was slowly added dropwise to a solution of 4-hydroxybenzoic acid (10 g, 72.4 mmol) in dry methanol (50 ml). The solution was heated to reflux (65°C) with stirring for 2 h, then allowed to cool. The pH of the cooled solution was carefully adjusted to 5 by the addition of 40% $NaOH_{(aq)}$ solution, at which point a white precipitate formed. The white precipitate was isolated on a sinter then washed thoroughly with water. The white solid obtained was dissolved in ethyl acetate, the solution was dried with magnesium sulfate then filtered. The filtrate was dried under reduced pressure to yield the title compound as a crystalline white solid (8.5 g, 55.9 mmol, 77%); m.p. 127-129°C (Lit.[145] 123-124°C); ^{1}H-NMR (CD_3OD, 500 MHz) δ 7.89 (d, 2H, J=7.0 Hz, H_D), 6.85 (d, 2H, J=6.5 Hz, H_E), 4.93 (s br, 1H, H_G), 3.86 (s, 3H, H_A); ^{13}C-NMR (CD_3OD, 125 MHz, ^{1}H decoupled 500 MHz) δ 169.5 (1C, C_B), 164.3 (1C, C_F), 133.6 (2C, C_D), 123.0 (1C, C_C), 117.0 (2C, C_E), 53.1 (1C, C_A); MS (ES^-) m/z 151.1 $[M\text{-}H]^-$ 100 %.

2-(4-Methoxycarbonylphenoxy)-6-methylnicotinic acid[54]

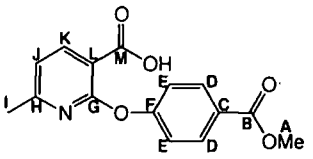

Methyl-4-hydroxybenzoate (12.6 g, 82.8 mmol) was added to a solution of sodium metal (0.84 g, 36.54 mmol) in dry methanol (15 ml) to form a viscous light yellow solution. Methanol was removed from the solution under reduced pressure to leave a white glassy solid. 2-Chloro-6-methylnicotinic acid (3.00 g, 17.48 mmol) was added to the solid which was heated for 25 h at 155°C to form a brown solution. After 25 h the mixture was allowed to cool to 120°C then poured into water (80 ml) to form a yellow tinged solution containing an insoluble brown residue. The aqueous

suspension was extracted with ether (3 x 50 ml) then acidified with glacial acetic acid to precipitate the crude product. The precipitate was isolated by filtration, washed thoroughly with water then dried under vacuum to yield the desired product as a fibrous white solid (1.8 g, 6.27 mmol, 36%); m.p. 122-123°C (Lit.[54] 118-120°C); ^{1}H-NMR ($CDCl_3$, 500 MHz) δ 8.38 (d, 1H, J=7.5 Hz, H_K), 8.11 (d, 2H, J=9.0 Hz, H_D), 7.22 (d, 2H, J=8.5 Hz, H_E), 7.06 (d, 1H, J=8.0 Hz, H_J), 3.94 (s, 3H, H_A), 2.42 (s, 3H, H_I); ^{13}C-NMR ($CDCl_3$, 125 MHz, ^{1}H decoupled 500 MHz) δ 166.8 (1C, C_B), 166.8 (1C, C_M), 163.5 (1C, C_H), 160.5 (1C, C_G), 157.2 (1C, C_F), 143.8 (1C, C_K), 131.6 (2C, C_D), 127.3 (1C, C_C), 121.5 (2C, C_E), 119.8 (1C, C_J), 111.2 (1C, C_L), 52.5 (1C, C_A), 24.7 (1C, C_I); MS (ES$^+$) m/z 288.1 $[M + H]^+$ 90 %.

7-Methoxycarbonyl-2-methyl-1-azaxanthone[54]

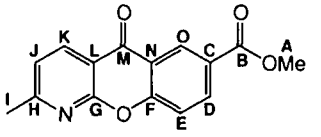

Polyphosphoric acid (70 g) and 2-(4-methoxycarbonylphenoxy)-6-methylnicotinic acid (1.30 g, 4.53 mmol) were heated together for 18 h, at 120°C, under argon. The resulting brown liquid was cooled to 0°C followed by the addition of cold methanol (100 ml) with stirring until the mixture homogenised. The apparent pH of the resulting brown solution was adjusted to 7 by the addition of concentrated $KOH_{(aq)}$ solution, at 0°C, to yield an off-white suspension. The suspension was extracted with dichloromethane (4 x 25 cm^3), the solvent was removed from the combined organic washings to yield the desired product as a yellow solid (0.391 g, 1.45 mmol, 32%). m.p. 198-199°C (Lit.[54] 194-196°C); ^{1}H-NMR ($CDCl_3$, 500 MHz) δ 8.99 (d, 1H, J=2.0 Hz, H_O), 8.60 (d, 1H, J=8.0 Hz, H_K), 8.41 (dd, 1H, J=9.0, 2.0 Hz, H_D), 7.65 (d, 1H, J=9.0 Hz, H_E), 7.34 (d, 1H, J=8.0 Hz, H_J), 3.98 (s, 3H, H_A), 2.72 (s, 3H, H_I); ^{13}C-NMR ($CDCl_3$, 125 MHz, ^{1}H decoupled 500 MHz) δ 177.2 (1C, C_M), 166.0 (1C, C_B), 166.0 (1C, C_H), 160.2 (1C, C_G), 158.6 (1C, C_F), 137.8 (1C, C_K), 136.3 (1C, C_D), 129.5 (1C, C_O), 127.0 (1C, C_C), 122.1 (1C, C_J), 121.7 (1C, C_N), 119.3 (1C, C_E), 114.6 (1C, C_L), 52.8 (1C, C_A), 25.5 (1C, C_I); MS (ES$^+$) m/z 291.9

$[M + Na]^+$ 50 %, 561.4 $[2M + Na]^+$ 100 %.

7-Methoxycarbonyl-2-bromomethyl-1-azaxanthone[54]

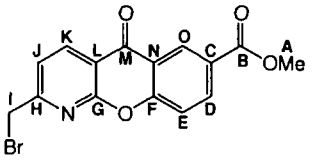

7-Methoxycarbonyl-2-methyl-1-azaxanthone (1.12 g, 4.16 mmol) was stirred in CCl_4 (10 ml) under reflux (100°C). NBS (0.37 g, 2.08 mmol) and AIBN (2 mg) were added to the mixture, at reflux, to form a sparingly soluble suspension of the reactants in CCl_4 (an identical addition was repeated 2 h later) and the reaction micture was left to stir and reflux. After 12 h the yellow solution was allowed to cool to room temperature then filtered, solvent was removed from the filtrate under reduced pressure to leave a yellow powder. The desired product was isolated from the crude reaction mixture by column chromatography on silica gel (DCM with 0.1% increments of MeOH per 50 ml of solvent) as a fine white powder (200 mg, 0.57 mmol, 14 %); m.p. 172-173°C (Lit.[54] 156-158°C); R_F (SiO_2, DCM-MeOH, 93:7) : 0.45; ^{1}H-NMR ($CDCl_3$, 400 MHz) δ 8.92 (dd, 1H, J=2.0, 0.5 Hz, H_O), 8.68 (d, 1H, J=8.0 Hz, H_K), 8.38 (dd, 1H, J=9.0, 2.0 Hz, H_D), 7.62 (dd, 1H, J=9.0, 0.5 Hz, H_E), 7.59 (d, 1H, J=8.0 Hz, H_J), 4.59 (s, 2H, H_I), 3.95 (s, 3H, H_A); ^{13}C-NMR ($CDCl_3$, 100 MHz, ^{1}H decoupled 400 MHz) δ 176.7 (1C, C_M), 165.8 (1C, C_B), 162.7 (1C, C_H), 159.8 (1C, C_G), 158.4 (1C, C_F), 139.1 (1C, C_K), 136.6 (1C, C_D), 129.4 (1C, C_O), 127.3 (1C, C_C), 121.6 (1C, C_J), 121.5 (1C, C_N), 119.2 (1C, C_E), 116.2 (1C, C_L), 52.8 (1C, C_A), 32.3 (1C, C_I); MS (ES^+) m/z 371.2 $[M + Na]^+$ 100 %, 719.0 $[2M + Na]^+$ 45 %.

7-Methoxycarbonyl-2-phthalimidomethyl-1-azaxanthone[92]

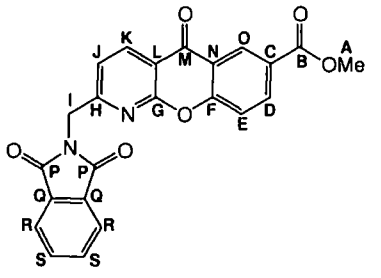

7-Methoxycarbonyl-2-bromomethyl-1-azaxanthone (0.061 g, 0.175 mmol) and potassium phthalimide (0.130 g, 0.702 mmol) in DMF (5 ml) were stirred, under argon, for 12 h at room temperature. The resulting solution was poured into ice water (500 ml) to yield a yellow/orange precipitate that was isolated by centrifugation. The filtrate was further cooled in the fridge yielding further precipitate which too was isolated. The solids were combined and recrystallised from DCM:Ether to yield the product as a yellow/orange crystalline solid (0.065 g, 0.157 mmol, 90 %); m.p. >250°C; ^{1}H-NMR ($CDCl_3$, 500 MHz) δ 8.96 (d, 1H, J=2.0, H_O), 8.68 (d, 1H, J=8.0 Hz, H_K), 8.39 (dd, 1H, J=9.0, 2.0 Hz, H_D), 7.93 (dd, 2H, J=5.5, 3.0 Hz, H_R), 7.79 (dd, 2H, J=5.5, 3.0 Hz, H_S), 7.60 (d, 1H, J=9.0 Hz, H_E), 7.42 (d, 1H, J=8.0 Hz, H_J), 5.14 (s, 2H, H_I), 3.97 (s, 3H, H_A); ^{13}C-NMR ($CDCl_3$, 125 MHz, ^{1}H decoupled 500 MHz) δ 177.0 (1C, C_M), 168.2 (2C, C_P), 165.9 (1C, C_B), 162.1 (1C, C_H), 160.3 (1C, C_G), 158.5 (1C, C_F), 138.8 (1C, C_K), 136.5 (1C, C_D), 134.7 (2C, C_S), 132.4 (2C, C_Q), 129.5 (1C, C_O), 127.2 (1C, C_C), 124.1 (2C, C_R), 121.6 (1C, C_N), 119.5 (1C, C_J), 119.3 (1C, C_E), 116.1 (1C, C_L), 52.9 (1C, C_A), 43.1 (1C, C_I); MS (ES^+) m/z 437.3 $[M + Na]^+$ 100 %, 851.2 $[2M + Na]^+$ 50 %; HRMS (ES^+) m/z found 437.0741 $[M + Na]^+$ $C_{23}H_{14}O_6N_2Na$ requires 437.0744. $C_{23}H_{14}N_2O_6.\frac{1}{6}CH_2Cl_2$ (%): calcd C 64.93 H 3.37 N 6.54; found C 65.09 H 3.34 N 6.48.

7-Methoxycarbonyl-2-aminomethyl-1-azaxanthone (47)[92]

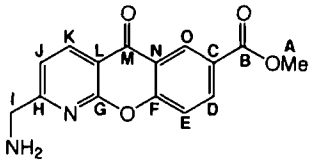

A solution of 7-methoxycarbonyl-2-phthalimidomethyl-1-azaxanthone (0.061 g, 0.147 mmol) and $NH_2NH_2.H_2O$ (0.014 ml, 0.297 mmol) in DCM:MeOH (50:50, 8 ml) was heated at 50°C followed by further additions of $NH_2NH_2.H_2O$ (0.014 ml, 0.297 mmol) at 3 h intervals until TLC analysis showed all starting 7-methoxycarbonyl-2-phthalimidomethyl-1-azaxanthone to have been consumed. The clear yellow solution was allowed to cool followed by the addition of conc. $HCl_{(aq)}$ until a pH of 2 was reached. The resultant solution containing a white precipitate was heated at 50°C for 2 h then allowed to cool to room temperature, the solution was filtered followed by the drying of the yellow filtrate under vacuum to yield a yellow powder. Immediately prior to use the solid was dissolved in H_2O containing 1 eq. NaOMe then extracted with DCM (5 ml), the organic phase was dried under reduced pressure to leave the title product as a pale green solid (0.029 g, 0.102 mmol, 69 %) ; ^{1}H-NMR ($CDCl_3$, 500 MHz) δ 9.00 (d, 1H, J=2.0 Hz, H_O), 8.69 (d, 1H, J=8.0 Hz, H_K), 8.43 (dd, 1H, J=9.0, 2.5 Hz, H_D), 7.60 (d, 1H, J=8.5 Hz, H_E), 7.52 (d, 1H, J=8.0 Hz, H_J), 4.16 (s, 2H, H_I), 3.99 (s, 3H, H_A), 1.84 (s br, 2H, NH_2); ^{13}C-NMR ($CDCl_3$, 125 MHz, ^{1}H decoupled 500 MHz) δ 177.2 (1C, C_M), 169.3 (1C, C_H), 166.0 (1C, C_B), 160.4 (1C, C_G), 158.5 (1C, C_F), 138.1 (1C, C_K), 136.2 (1C, C_D), 129.3 (1C, C_O), 127.0 (1C, C_N), 121.5 (1C, C_C), 119.4 (1C, C_J), 119.0 (1C, C_E), 115.3 (1C, C_L), 52.7 (1C, C_A), 45.0 (1C, C_I); MS (ES^+) m/z 285.2 $[M + H]^+$ 100 %; HRMS (ES^+) m/z found 285.0869 $[M + H]^+$ $C_{15}H_{13}O_4N_2$ requires 285.0870.

2-[(2-(7-*tert*-Butoxycarbonyl-4,10-bis-[((S)-1-phenyl-ethylcarbamoyl)-methyl]-1,4,7,10-tetraaza-cyclododec-1-yl)-acetylamino)-methyl]-10-oxo-10*H*-9-oxa-1-aza-anthracene-6-carboxylic acid methyl ester[92]

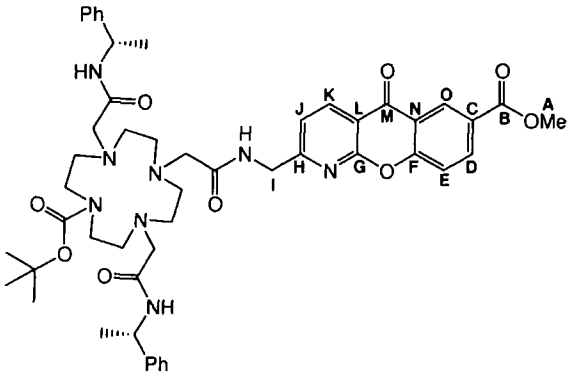

7-Carboxymethyl-4,10-bis-[((S)-1-phenyl-ethylcarbamoyl)-methyl]-1,4,7,10-tetra- aza-cyclododecane-1-carboxylic acid *tert*-butyl ester (0.128 g, 0.196 mmol), EDC.HCl (0.037 g, 0.193 mmol), HOBt.H_2O (10 mg) and NEt_3 (0.082 ml, 0.588 mmol) in chloroform (2 ml) were stirred for 20 min at room temperature to form a yellow tinged solution. 7-Methoxycarbonyl-2-aminomethyl-1-azaxanthone (0.042 g, 0.148 mmol) in chloroform (3 ml) was then added to form a orange solution that was left to stir for 12 h at room temperature. The resulting yellow solution was extracted with sat. $NaHCO_3$ solution (2 x 15 ml) then H_2O (10 ml), the organic phase was dried under reduced pressure to leave an orange foam. The desired product was purified via alumina column chromatography (using a graduated solvent system starting from 100% DCM with 0.1% MeOH increments every 100 ml) yielding a glassy orange residue (0.073 g, 0.079 mmol, 53 %); m.p. 70-72°C; R_F (alumina, DCM-MeOH, 99:1) : 0.16; ^{1}H-NMR ($CDCl_3$, 500 MHz) δ 8.95 (d, 1H, J=2.5 Hz, H_O), 8.60 (d, 1H, J=8.0 Hz, H_K), 8.39 (dd, 1H, J=8.5, 2.0 Hz, H_D), 8.00 (s br, 1H, linker amide NH), 7.58 (d, 1H, J=8.5 Hz, H_E), 7.32 (d, 1H, J=6.5 Hz, H_J), 7.19-7.25 (m, 10H, amide arm Ar), 5.08 (m, 2H, arm CH), 4.54 (m, 2H, H_I), 3.97 (s, 3H, H_A), 2.40-3.16 (m br, 22H, cyclen CH_2 and amide arms CH_2CO), 1.43 (d, 6H, J=6.5 Hz, amide arms CH_3), 1.37-1.41 (m br, 9H, ^{t}Bu CH_3); ^{13}C-NMR ($CDCl_3$, 125 MHz, ^{1}H decoupled 500 MHz) δ 176.8 (1C, C_M), 171.4 (1C, linker amide C=O), 170.4 (2C br, amide arm C=O), 165.8 (1C, C_B),

163.9 (1C, C_H), 160.1 (1C, C_G), 158.3 (1C, C_F), 156.0 (1C, ^{t}Boc C=O), 143.7, 143.1 (2C br, amide arm $Ar_{(q)}$), 138.3 (1C, C_K), 136.5 (1C, C_D), 129.4 (1C, C_O), 126.5-128.8 (10C, amide arm Ar), 127.5 (1C, C_N), 121.6 (1C, C_C), 120.1 (1C, C_J), 119.0 (1C, C_E), 115.6 (1C, C_L), 80.3 (1C, $^t Boc_{(q)}$), 60.0, 59.4, 54.6, 53.4 (8C, cyclen CH_2), 52.8 (1C, C_A), 48.7 (2C, amide arms CH), 47.8 (3C, amide arms and linker CH_2CO), 44.6 (1C, C_I), 28.7 (3C, ^{t}Boc CH_3), 21.9, 21.5 (2C, amide arms CH_3); MS (ES^+) *m/z* 919.7 $[M + H]^+$ 100 %; HRMS (ES^+) *m/z* found 919.4726 $[M + H]^+$ $C_{50}H_{63}O_9N_8$ requires 919.4713.

2-[(2-(4,10-Bis-[((S)-1-phenyl-ethylcarbamoyl)-methyl]-1,4,7,10-tetraaza-cyclododec-1-yl)-acetylamino)-methyl]-10-oxo-10*H*-9-oxa-1-aza-anthracene-6-carboxylic acid methyl ester (L^{44a})[92]

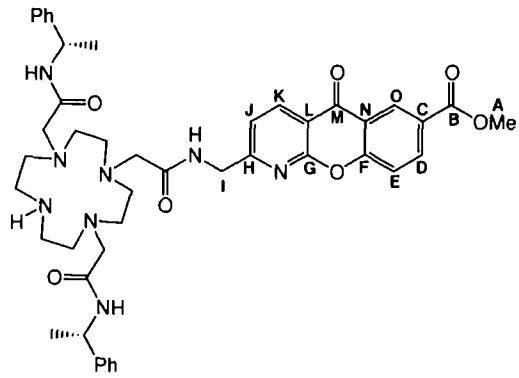

2-[(2-(7-*tert*-Butoxycarbonyl-4,10-bis-[((S)-1-phenyl-ethylcarbamoyl)-methyl]-1,4,7,10-tetraaza-cyclododec-1-yl)-acetylamino)-methyl]-10-oxo-10*H*-9-oxa-1-aza-anthracene-6-carboxylic acid methyl ester (72 mg, 0.078 mmol) in DCM:TFA (50:50, 4 ml) was stirred in a sealed flask for 12 h yielding a yellow solution. Solvent was then removed under reduced pressure to yield the desired product as its TFA salt as a glassy yellow solid in quantitative yield; ^{1}H-NMR ($CDCl_3$, 500 MHz) δ 9.39 (s, 1H, linker NH), 8.86 (d, 1H, J=1.5 Hz, H_O), 8.56 (d, 1H, J=8.0 Hz, H_K), 8.34 (dd, 1H, J=8.5 Hz 1.5 Hz, H_D), 8.10 (s br, 1H, arm NH), 7.87 (s br, 1H, arm NH), 7.54 (d, 1H, J=9.0 Hz, H_E), 7.36 (d, 1H, J=8.0 Hz, H_J), 7.15-7.23 (m br, 10H, arm Ar), 4.85-4.95 (m br, 2H, arm CH), 4.59 (m br, 2H, H_I), 3.94 (s, 3H, H_A), 3.00-3.66 (m br, 22H, cyclen, arm and linker CH_2), 1.40 (s br, 6H, arm CH_3); ^{13}C-NMR ($CDCl_3$, 125 MHz, ^{1}H decoupled 500 MHz) δ 176.9 (1C, C_M), 171.1, 170.1 (3C, amide arm C=O

and linker arm C=O), 165.9 (1C, C_B), 163.6 (1C, C_H), 161.6 (q, 1C, TFA C=O), 160.1 (1C, C_G), 158.3 (1C, C_F), 143.6 (2C, arm $Ar_{(q)}$), 138.5 (1C, C_K), 136.5 (1C, C_D), 129.3 (1C, C_O), 128.9, 127.7, 126.5, 126.4 (10C, arm Ar), 127.1 (1C, C_N), 121.5 (1C, C_C), 119.4 (1C, C_J), 119.2 (1C, C_E), 115.7 (1C, C_L), 115.4 (q, 1C, TFA CF_3), 55.4, 53.8, 52.4 (br, 8C, cyclen CH_2), 52.9 (1C, C_A), 49.8 (br, 2C, arm CH), 45.0 (br, 1C, C_I), 43.5 (br, 3C, arm and linker CH_2), 22.2, 21.9 (br, 2C, amide arm CH_3); MS (ES^+) *m/z* 819.5 $[M + H]^+$ 100 %, 841.5 $[M + Na]^+$ 40 %; HRMS (ES^+) *m/z* found 819.4198 $[M + H]^+$ $C_{45}H_{55}O_7N_8$ requires 819.4188.

Eu(III) complex of 2-[(2-(4,10-bis-[((S)-1-phenyl-ethylcarbamoyl)-methyl]-1,4,7,10-tetraaza-cyclododec-1-yl)-acetylamino)-methyl]-10-oxo-10*H*-9-oxa-1-aza-anthracene-6-carboxylic acid methyl ester ($[EuL^{44a}]^{3+}$)[92]

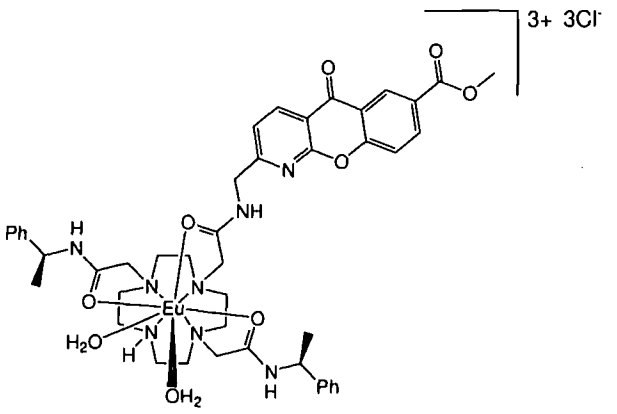

A solution of 2-[(2-(4,10-bis-[((S)-1-phenyl-ethylcarbamoyl)-methyl]-1,4,7,10-tetraaza-cyclododec-1-yl)-acetylamino)-methyl]-10-oxo-10*H*-9-oxa-1-aza-anthracene-6-carboxylic acid methyl ester as its TFA salt (46 mg, 0.049 mmol) and $Eu(OTf)_3$ (26 mg, 0.043 mmol) in MeCN (1 ml) was heated at reflux under argon, in Schlenk apparatus, for 48 h. Solvent was removed under reduced pressure to leave a orange glassy solid. DCM (5 ml) was added to the solid which was sonicated for 5 min, solvent was then decanted to leave a orange residue. The sonication process was repeated followed by drying of the remaining residue, under reduced pressure, to yield the triflate salt of the desired product as a fine cinder coloured powder (50 mg, 0.034 mmol, 79 %). The solid was made water soluble by the exchange of triflate anions for chloride anions using DOWEX 1x8 200-400 mesh Cl ion exchange resin,

as described earlier, to yield the complex as a cinder coloured powder in quantitative yield; ^{1}H-NMR (as tri-chloride salt, D_2O, 500 MHz, partial data and assignment) δ 25.1 (1H, NH), 16.9 (1H, H_{ax}), 15.2 (1H, H_{ax}), 14.0 (1H, H_{ax}), 11.7 (1H, H_{ax}); MS (ES^+) m/z 508.3 $[M + HCO_2]^{2+}$ 100 %, 1015.2 $[M + HCO_2 - H]^+$ 10 %; HRMS (ES^+) m/z found 1027.3359 $[M + CH_3CO_2 - H]^+$ $C_{47}H_{56}O_9N_8{}^{151}Eu$ requires 1027.3363; $\lambda_{abs}(H_2O)$: 333 nm; $\tau_{(H_2O)}$: 0.38 ms, $\tau_{(D_2O)}$: 0.60 ms; HPLC (solvent system B, 4.6 x 150 mm 4 μm Phenomenex Synergi Fusion RP 80Å analytical column): t_R = 10.8 min.

Tb(III) complex of 2-[(2-(4,10-bis-[((S)-1-phenyl-ethylcarbamoyl)-methyl]-1,4,7,10-tetraaza-cyclododec-1-yl)-acetylamino)-methyl]-10-oxo-10*H*-9-oxa-1-aza-anthracene-6-carboxylic acid methyl ester ($[TbL^{44a}]^{3+}$)[92]

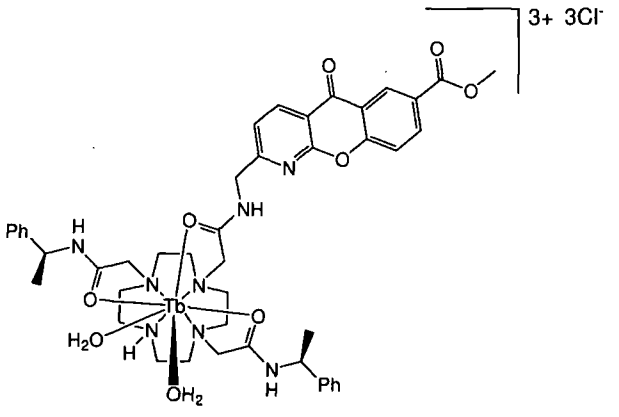

A solution of 2-[(2-(4,10-bis-[((S)-1-phenyl-ethylcarbamoyl)-methyl]-1,4,7,10-tetraaza-cyclododec-1-yl)-acetylamino)-methyl]-10-oxo-10*H*-9-oxa-1-aza-anthracene-6-carboxylic acid methyl ester (28 mg, 0.034 mmol) and $Tb(OTf)_3$ (17 mg, 0.028 mmol) in MeCN (1 ml) was heated at reflux under argon, in Schlenk apparatus, for 48 h. Solvent was removed under reduced pressure to leave a orange glassy solid. DCM (5 ml) was added to the solid which was sonicated for 5 min, solvent was then decanted to leave a orange residue. The sonication process was repeated followed by drying of the remaining residue, under reduced pressure, to yield the triflate salt of the desired product as a fine cinder coloured powder (34 mg, 0.024 mmol, 86 %). The solid was made water soluble by the exchange of triflate anions for chloride anions using DOWEX 1x8 200-400 mesh Cl ion exchange resin, as described previously,

to yield the cinder coloured complex in quantitative yield; MS (ES^+) *m/z* 511.3 $[M + HCO_2]^{2+}$ 100 %, 1021.2 $[M + HCO_2 - H]^+$ 25 %; HRMS (ES^+) *m/z* found 1035.3409 $[M + CH_3CO_2 - H]^+$ $C_{47}H_{56}O_9N_8{}^{159}Tb$ requires 1035.3418; $\lambda_{abs}(H_2O)$: 332 nm; $\tau_{(H_2O)}$: 1.17 ms, $\tau_{(D_2O)}$: 2.07 ms; HPLC (solvent system A, 4.6 x 150 mm 4 μm Phenomenex Synergi Polar-RP 80Å analytical column): t_R = 9.5 min.

2-[(2-(7-*tert*-Butoxycarbonyl-4,10-bis-[((S)-1-phenyl-ethylcarbamoyl)-methyl]-1,4,7,10-tetraaza-cyclododec-1-yl)-acetylamino)-methyl]-10-oxo-10*H*-9-oxa-1-aza-anthracene-6-carboxylic acid

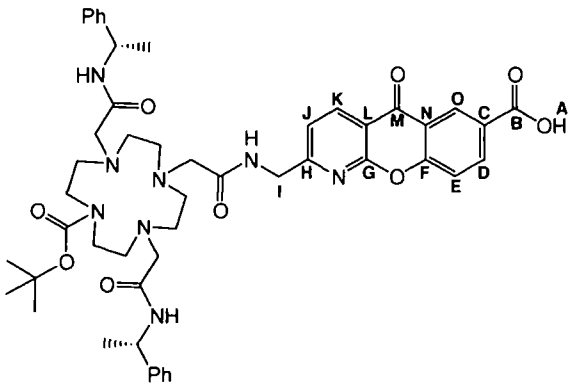

A sparingly soluble solution of 2-[(2-(7-*tert*-butoxycarbonyl-4,10-bis-[((S)-1-phen- yl-ethylcarbamoyl)-methyl]-1,4,7,10-tetraaza-cyclododec-1-yl)-acetylamino)-methyl]-10-oxo-10*H*-9-oxa-1-aza-anthracene-6-carboxylic acid methyl ester (0.053 g, 0.058 mmol) and $LiOH.H_2O$ (0.005 g, 0.119 mmol) in $MeOH:H_2O$ (2:1, 3 ml) was stirred overnight in a sealed flask to form a dark orange solution. The pH of the solution was subsequently adjusted to 5 with $HCl_{(aq)}$ (1 M) followed by removal of MeOH under reduced pressure to yield a light yellow solution. The aqueous solution was extracted with $CHCl_3$ (2 x 5 ml), the orange organic phases were combined then dried under reduced pressure to leave the desired product as a glassy dark orange solid (0.044 g, 0.049 mmol, 84 %); ^{1}H-NMR ($CDCl_3$, 500 MHz) δ 8.85 (s br, 1H, amide NH), 8.49, 8.30 (m br, 3H, azaxanthone protons), 7.20-7.32 (m br, 14H, amide arm Ar, azaxanthone protons and amide NH protons), 5.08 (m, 2H, arm CH), 4.69 (br, 1H, H_I), 4.36 (br, 1H, H_I), 2.48-3.47 (m br, 22H, cyclen CH_2 and amide arms CH_2CO), 1.50 (d, 6H, J=7.0 Hz, amide arms CH_3), 1.41 (s, 9H, ^{t}Bu CH_3); ^{13}C-NMR ($CDCl_3$, 125 MHz, ^{1}H decoupled 500 MHz) δ 176.5 (1C, C_M), 171.0 (1C, linker amide

C=O), 169.8 (2C br, amide arm C=O), 164.1, 159.4, 156.9 (3C, azaxanthone C), 155.7 (1C, ^{t}BOC C=O), 143.4 (2C br, amide arm $Ar_{(q)}$), 137.8, 136.8, 128.8 (3C, azaxanthone C), 126.4, 127.6, 128.8 (10C, amide arm Ar), 127.8, 120.4, 118.3, 118.2, 114.8 (5C, azaxanthone C), 80.8 (1C, $^{t}BOC_{(q)}$), 59.1, 57.7, 52.9 (8C, cyclen CH_2), 49.1 (2C, amide arms CH), 46.8 (3C, amide arms and linker CH_2CO), 44.8 (1C, C_I), 28.6 (3C, ^{t}BOC CH_3), 21.8 (2C, amide arms CH_3); MS (ES^-) *m/z* 903.5 $[M - H]^-$ 100 %; HRMS (ES^-) *m/z* found 903.4411 $[M - H]^-$ $C_{49}H_{59}O_9N_8$ requires 903.4411.

2-[(2-(4,10-Bis-[((S)-1-phenyl-ethylcarbamoyl)-methyl]-1,4,7,10-tetraaza-cyclododec-1-yl)-acetylamino)-methyl]-10-oxo-10*H*-9-oxa-1-aza-anthracene-6-carboxylic acid (L^{49})

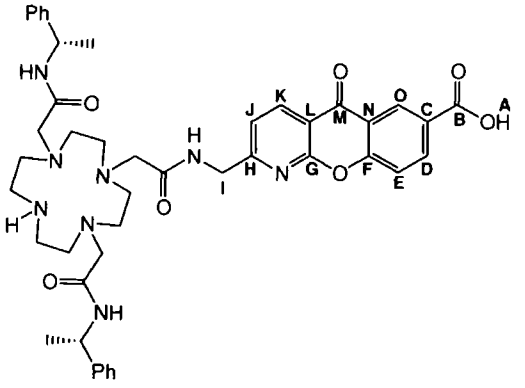

2-[(2-(7-*tert*-Butoxycarbonyl-4,10-bis-[((S)-1-phenyl-ethylcarbamoyl)-methyl]-1,4,7,10-tetraaza-cyclododec-1-yl)-acetylamino)-methyl]-10-oxo-10*H*-9-oxa-1-aza-anthracene-6-carboxylic acid (0.030 g, 0.033 mmol) in DCM:TFA (1:1, 2 ml) was stirred in a sealed flask for 2 h. The resultant dark yellow solution was dried under reduced pressure to yield the TFA salt of the desired product, as a orange glassy solid, in quantitative yield; ^{1}H-NMR (CD_3CN, 700 MHz) δ 8.67 (d, 1H, J=1.5 Hz, H_O), 8.52 (d, 1H, J=8.0 Hz, H_K), 8.32 (dd, 1H, J=8.5, 2.0 Hz, H_D), 7.90-8.01 (s br, 3H, arm NH), 7.62 (d, 1H, J=9.0 Hz, H_E), 7.44 (d, 1H, J=8.5 Hz, H_J), 7.17-7.32 (m br, 10H, arm Ar), 4.96 (m, 1H, arm CH), 4.88 (m, 1H, arm CH), 4.58 (m, 2H, H_I), 3.91 (m, 2H, linker arm CH_2CO), 2.93-3.59 (m br, 20H, cyclen and amide arm CH_2), 1.38 (d br, 3H, J=6.0 Hz, arm CH_3), 1.35 (d br, 3H, J=5.5 Hz, arm CH_3); ^{13}C-NMR (CD_3CN, 175 MHz, ^{1}H decoupled 700 MHz) δ 177.5 (1C, C_M), 171.0 (br, 2C, amide arm C=O), 166.6 (1C, C_B), 165.6 (1C, linker C=O), 164.4 (1C, C_H), 160.8 (1C,

C_G), 160.3 (q, 1C, TFA C=O), 159.1 (1C, C_F), 144.7, 144.5 (2C, arm $Ar_{(q)}$), 138.7 (1C, C_K), 137.0 (1C, C_D), 127.0, 128.0, 129.5 (10C, arm Ar), 129.3 (1C, C_L), 127.9 (1C, C_O), 122.3 (1C, C_C), 120.5 (1C, C_J), 120.0 (1C, C_E), 116.4 (1C, C_N), 117.0 (q, 1C, TFA CF_3), 56.3, 55.8, 53.2, 51.1 (br, 8C, cyclen CH_2), 49.8 (1C, Arm CH), 45.6 (1C, C_I), 43.9 (br, 3C, arm and linker CH_2), 22.6, 22.2 (br, 2C, amide arm CH_3); MS (ES^+) *m/z* 805.4 $[M + H]^+$ 100 %; HRMS (ES^+) *m/z* found 805.4029 $[M + H]^+$ $C_{44}H_{53}O_7N_8$ requires 805.4032.

Eu(III) complex of 2-[(2-(4,10-bis-[((S)-1-phenyl-ethylcarbamoyl)-methyl]-1,4,7,10-tetraaza-cyclododec-1-yl)-acetylamino)-methyl]-10-oxo-10*H*-9-oxa-1-aza-anthracene-6-carboxylic acid ($[EuL^{49}]^{2+}$)

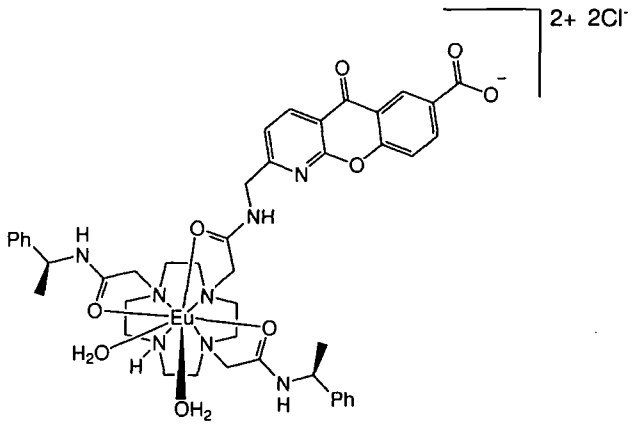

A solution of 2-[(2-(4,10-bis-[((S)-1-phenyl-ethylcarbamoyl)-methyl]-1,4,7,10-tetraaza-cyclododec-1-yl)-acetylamino)-methyl]-10-oxo-10*H*-9-oxa-1-aza-anthracene-6-carboxylic acid (34.8 mg, 0.038 mmol) and $Eu(OTf)_3.5H_2O$ (16.5 mg, 0.023 mmol) in MeCN (1 ml) was heated at reflux for 48 h. The resultant yellow solution was cooled followed by removal of solvent under reduced pressure. The resultant yellow residue was sonicated in DCM (2 x 10 ml) with the solid collected each time by centrifugation. The isolated complex was made water soluble by the exchange of triflate anions for chloride anions using DOWEX 1x8 200-400 mesh Cl ion exchange resin, as described earlier, to yield the complex as a pale yellow solid (22 mg, 0.020 mmol, 87 %); MS (ES^+) *m/z* 478.1 $[2M - 2H]^{4+}$ 100 %; HRMS (ES^+) *m/z* found 477.1535 $[2M - 2H]^{4+}$ $C_{88}H_{102}O_{14}N_{16}{}^{151}Eu_2$ requires 477.1534; $\lambda_{abs}(H_2O)$: 336 nm; $\tau_{(H_2O)}$: 0.30 ms, $\tau_{(D_2O)}$: 0.60 ms; HPLC (solvent system A, 4.6 x 150 mm 4 μm

Phenomenex Synergi Fusion RP 80Å analytical column): t_R = 8.0 min.

Solid phase supported Eu(III) complex of 2-[(2-(4,10-bis-[((S)-1-phenyl-ethylcarbamoyl)-methyl]-1,4,7,10-tetraaza-cyclododec-1-yl)-acetylamino)-methyl]-10-oxo-10*H*-9-oxa-1-aza-anthracene-6-carboxylic acid

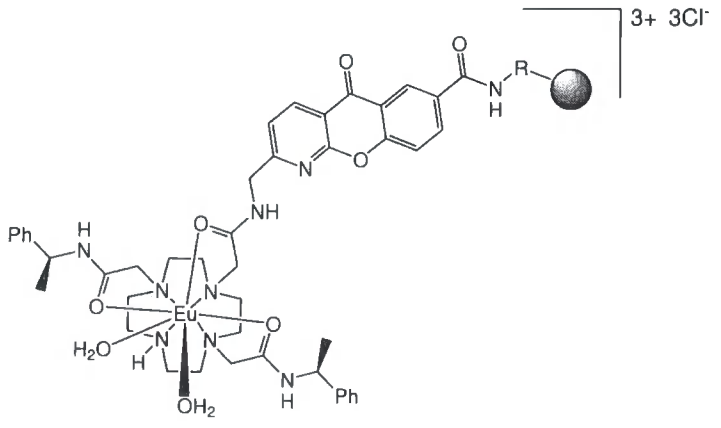

Eu(III) complex of 2-[(2-(4,10-bis-[((S)-1-phenyl-ethylcarbamoyl)-methyl]-1,4,7,10-tetraaza-cyclododec-1-yl)-acetylamino)-methyl]-10-oxo-10*H*-9-oxa-1-aza-anthracene-6-carboxylic acid (18 mg, 0.016 mmol), TBTU (7 mg, 0.022 mmol) and NEt_3 (0.0049 ml, 0.035 mmol) were stirred for 5 min in anhydrous DMF (0.5 ml). *N*-Hydroxysuccinimide (2.5 mg, 0.021 mmol) was then added and the yellow solution was allowed to stir for 30 min. TentaGel^{TM} S-NH_2 (44 mg) was added to the solution and the suspension was stirred for 2 h followed by the removal of solvent under reduced pressure. The crude resin was washed with H_2O (2 x 2 ml) and MeOH (2 x 2 ml), each time the resin was isolated by centrifugation, then dried under reduced pressure. Elemental analysis determined Eu(III) content to be 0.64 % or 0.042 mmol g^{-1}, this corresponds to 9.3 % derivatization as the resin NH_2 content is stated as ~0.45 mmol g^{-1}.

2-Bromomethyl-7-methoxycarbonyl-1-azathioxanthone[54]

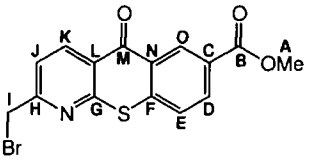

7-Methoxycarbonyl-2-methyl-1-azathioxanthone (594 mg, 2.08 mmol) and NBS (370 mg, 2.08 mmol) were heated to reflux in CCl_4 (10 ml), under argon, followed by the addition of dibenzoyl peroxide (5 mg) after 0, 3 and 6 h. After reflux for a total of 24 h the bright orange solution was allowed to cool then CCl_4 was removed under reduced pressure. The desired mono-brominated product was isolated from the crude orange residue by column chromatography on silica gel (DCM with 0.05% increments of MeOH per 50 ml of solvent) as a fine white powder (125 mg, 0.34 mmol, 16 %); m.p. 194-196°C (Lit.[54] sublimes 186-190°C); R_F (SiO_2, DCM-MeOH, 96:4) : 0.7; ^{1}H-NMR ($CDCl_3$, 500 MHz) δ 9.23 (d, 1H, J=1.5 Hz, H_O), 8.85 (d, 1H, J=8.0 Hz, H_K), 8.30 (dd, 1H, J=8.5, 2.0 Hz, H_D), 7.74 (d, 1H, J=8.5 Hz, H_E), 7.62 (d, 1H, J=8.0 Hz, H_J), 4.61 (s, 2H, H_I), 4.00 (s, 3H, H_A); ^{13}C-NMR ($CDCl_3$, 125 MHz, ^{1}H decoupled 500 MHz) δ 180.0 (1C, C_M), 166.2 (1C, C_B), 161.7 (1C, C_H), 158.1 (1C, C_G), 142.5 (1C, C_F), 139.5 (1C, C_K), 133.3 (1C, C_D), 131.9 (1C, C_O), 129.2 (1C, C_N), 129.1 (1C, C_C), 127.2 (1C, C_E), 125.8 (1C, C_L), 122.4 (1C, C_J), 52.9 (1C, C_A), 32.5 (1C, C_I); MS (ES^+) m/z 418.1 $[M + Na + MeOH]^+$ 95 %; HRMS (ES^+) m/z found 417.9723 $[M + Na + MeOH]^+$ $C_{16}H_{14}O_4N^{79}BrNa^{32}S$ requires 417.9719.

2-Phthalimidomethyl-7-methoxycarbonyl-1-azathioxanthone[94]

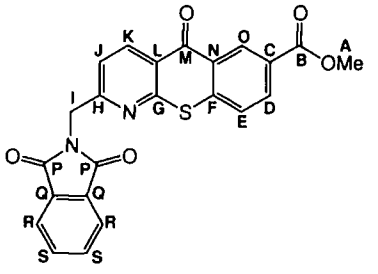

2-Bromomethyl-7-methoxycarbonyl-1-azathioxanthone (0.125 g, 0.343 mmol) and potassium phthalimide (0.191 g, 1.03 mmol) in DMF (10 ml) were stirred, under argon, for 12 h at room temperature. The resulting brown product mixture was poured onto ice water (200 ml) forming a brown solution containing a yellow oily precipitate that was extracted with DCM (5 x 50 ml). The crude organic extracts were combined and dried under reduced pressure yielding the desired product as a crude yellow-brown solid. The crude solid was dissolved in boiling ethyl acetate (50 ml) then hot filtered, the solution volume was reduced (10 ml) then left to cool to room temperature. The desired product precipitated as a crystalline yellow solid that was collected by filtration, washed with cold ethyl acetate (3 ml), then dried under reduced pressure (0.136 g, 0.316 mmol, 92 %); m.p. 246-247°C; ^{1}H-NMR ($CDCl_3$, 500 MHz) δ 9.19 (d, 1H, J=2.0 Hz, H_O), 8.79 (d, 1H, J=8.0 Hz, H_K), 8.26 (dd, 1H, J=8.5, 2.0 Hz, H_D), 7.93 (dd, 2H, J=5.5, 3.0 Hz, H_R), 7.79 (dd, 2H, J=5.5, 3.0 Hz, H_S), 7.65 (d, 1H, J=8.5 Hz, H_E), 7.40 (d, 1H, J=8.0 Hz, H_J), 5.13 (s, 2H, H_I), 3.98 (s, 3H, H_A); ^{13}C-NMR ($CDCl_3$, 125 MHz, ^{1}H decoupled 500 MHz) δ 180.1 (1C, C_M), 168.3 (2C, C_P), 166.2 (1C, C_B), 160.5 (1C, C_H), 158.3 (1C, C_G), 142.7 (1C, C_F), 139.1 (1C, C_K), 134.7 (2C, C_S), 133.2 (1C, C_D), 132.4 (2C, C_Q), 131.8 (1C, C_O), 129.1 (2C, $C_{C,N}$), 127.1 (1C, C_E), 125.7 (1C, C_L), 124.1 (2C, C_R), 120.1 (1C, C_J), 52.9 (1C, C_A), 43.1 (1C, C_I); MS (MALDI, pencil matrix, FTMS$^+$) m/z 430.9 $[M + H]^+$, 452.9 $[M + Na]^+$; HRMS (MALDI, pencil matrix, FTMS$^+$) m/z found 431.0700 $[M + H]^+$ $C_{23}H_{15}O_5N_2{}^{32}S$ requires 431.0696; $C_{23}H_{14}N_2O_5S.\frac{1}{6}C_4H_8O_2$ (%): calcd C 63.86 H 3.47 N 6.29; found C 63.70 H 3.26 N 6.25; Structure confirmed by single crystal X-ray diffraction.

2-Aminomethyl-7-methoxycarbonyl-1-azathioxanthone (48)[94]

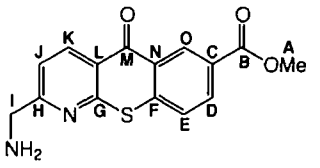

A solution of 2-phthalimidomethyl-7-methoxycarbonyl-1-azathioxanthone (0.055 g, 0.128 mmol) and $NH_2NH_2.H_2O$ (0.5 ml, 10.3 mmol) in DCM:MeOH (3:7, 10 ml) was heated at 50°C for 2 h at which point TLC analysis showed all starting 2-phthalimidomethyl-7-methoxycarbonyl-1-azathioxanthone to have been consumed. The clear yellow solution was allowed to cool followed by the addition of conc. $HCl_{(aq)}$ until a pH of 2 was reached. The resultant solution containing a white precipitate was heated at 60°C for 2 h then allowed to cool to room temperature, the solution was filtered followed by the drying of the yellow filtrate under reduced pressure to yield a yellow powder. The yellow solid was dissolved in H_2O containing 1 eq. NaOMe then extracted with DCM (5 ml), the organic phase was dried under reduced pressure to leave the desired product as a white powder (0.037 g, 0.123 mmol, 96 %); ^{1}H-NMR ($CDCl_3$, 500 MHz) δ 9.21 (d, 1H, J=2.0 Hz, H_O), 8.78 (d, 1H, J=8.0 Hz, H_K), 8.27 (dd, 1H, J=8.0, 1.5 Hz, H_D), 7.71 (d, 1H, J=8.0 Hz, H_E), 7.47 (d, 1H, J=8.0 Hz, H_J), 4.12 (s, 2H, H_I), 3.99 (s, 3H, H_A), 1.78 (s br, 2H, NH_2); ^{13}C-NMR ($CDCl_3$, 125 MHz, ^{1}H decoupled 500 MHz) δ 180.3 (1C, C_M), 167.4 (1C, C_H),. 166.3 (1C, C_B), 158.1 (1C, C_G), 142.7 (1C, C_F), 138.7 (1C, C_K), 133.1 (1C, C_D), 131.8 (1C, C_O), 129.2 (1C, C_N), 129.0 (1C, C_C), 127.1 (1C, C_E), 125.3 (1C, C_L), 120.4 (1C, C_J), 52.8 (1C, C_A), 48.0 (1C, C_I); MS (ES^+) m/z 301.0 $[M + H]^+$ 100 %; HRMS (ES^+) m/z found 301.0642 $[M + H]^+$ $C_{15}H_{13}O_3N_2{}^{32}S$ requires 301.0641.

2-[(2-(7-*tert*-Butoxycarbonyl-4,10-bis-[((S)-1-phenyl-ethylcarbamoyl)-methyl]-1-yl)-acetylamino)-methyl]-5-oxo-5*H*-[1]benzothiopyrano[2,3-*b*]pyridine-7-carboxylic acid methyl ester[94]

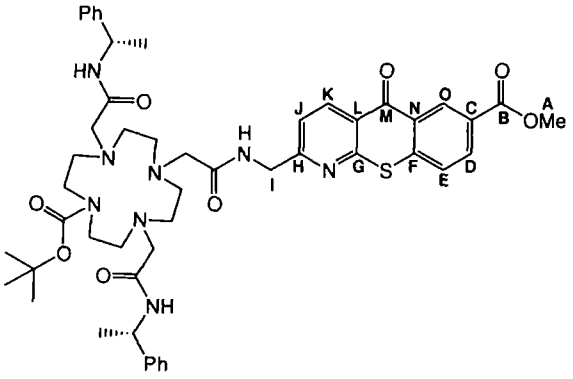

7-Carboxymethyl-4,10-bis-[((S)-1-phenyl-ethylcarbamoyl)-methyl]-1,4,7,10-tetra aza-cyclododecane-1-carboxylic acid *tert*-butyl ester (0.109 g, 0.167 mmol), EDC.HCl (0.031 g, 0.162 mmol), HOBt.H_2O (5 mg) and NEt_3 (0.093 ml, 0.668 mmol) in $CHCl_3$ (5 ml) were stirred for 45 min at room temperature to form a yellow tinged solution. 2-Aminomethyl-7-methoxycarbonyl-1-azathioxanthone (0.033 g, 0.110 mmol) in $CHCl_3$ (5 ml) was then added to form a dark yellow solution that was left to stir for 12 h at room temperature. The resulting yellow solution was extracted with $HCl_{(aq)}$ (0.025 M, 10 ml) then H_2O (5 ml), the combined aqueous fractions were backwashed with $CHCl_3$ (5 ml) then the combined organic layers were dried under reduced pressure to leave the crude product as a yellow-brown foam. The desired product was isolated via alumina column chromatography (using a graduated solvent system starting from 100% DCM with 0.1% MeOH increments every 50 ml) as a pale yellow glassy solid (0.060 g, 0.064 mmol, 58 %); R_F (alumina, DCM-MeOH, 98.5:1.5) : 0.25; ^{1}H-NMR ($CDCl_3$, 500 MHz) δ 9.14 (s, 1H, H_O), 8.68 (d, 1H, J=8.5 Hz, H_K), 8.22 (dd, 1H, J=8.5, 1.5 Hz, H_D), 7.65 (d, 1H, J=8.5 Hz, H_E), 7.15-7.30 (m, 13H, amide arms Ar, amide arms NH and H_J), 5.93 (s br, 1H, linker amide NH), 5.07 (m, 2H, arm CH), 4.49 (m, 2H, H_I), 3.94 (s, 3H, H_A), 2.40-3.30 (m br, 22H, cyclen CH_2 and amide arms CH_2CO), 1.43 (d, 6H, J=7.0 Hz, amide arms CH_3), 1.37 (s, 9H, ^{t}Bu CH_3); ^{13}C-NMR ($CDCl_3$, 125 MHz, ^{1}H decoupled 500 MHz) δ 179.9 (1C, C_M), 170.1 (3C, amide arms and linker C=O), 166.1 (1C, C_B), 162.6 (1C, C_H),

157.8 (1C, C_G), 156.1 (1C, ^{t}Boc C=O), 143.5 (2C br, amide arms $Ar_{(q)}$), 142.1 (1C, C_F), 138.8 (1C, C_K), 133.1 (1C, C_D), 131.7 (1C, C_O), 129.2 (1C, C_N), 129.1 (1C, C_C), 128.9, 127.6, 126.5 (10C, amide arms Ar), 127.1 (1C, C_E), 125.4 (1C, C_L), 120.9 (1C, C_J), 80.2 (1C, ^{t}Boc$_{(q)}$), 60.0, 58.0, 54.7, 53.6 (8C, cyclen CH_2), 52.8 (1C, C_A), 49.0 (2C, amide arms CH), 48.7, 48.2 (3C, amide arms and linker CH_2CO), 44.6 (1C, C_I), 28.8 (3C, ^{t}Boc CH_3), 22.0 (2C, amide arms CH_3); MS (ES^+) *m/z* 935.2 [M + H]$^+$ 100 %; HRMS (ES^+) *m/z* found 935.4495 [M + H]$^+$ $C_{50}H_{63}O_8N_8{}^{32}S$ requires 935.4484.

2-[(2-(4,10-Bis-[((S)-1-phenyl-ethylcarbamoyl)methyl]-1-yl)acetylamino)-methyl]-5-oxo-5*H*-[1]benzothiopyrano[2,3-*b*]pyridine-7-carboxylic acid methyl ester (L^{44b})[94]

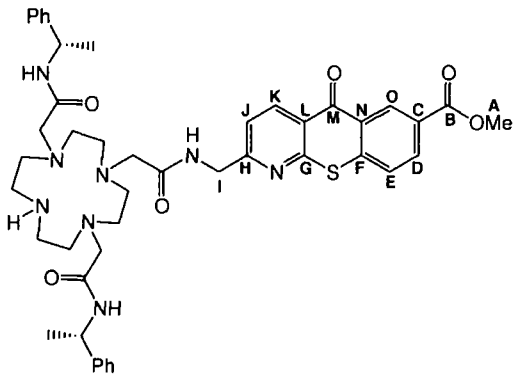

2-[(2-(7-*tert*-Butoxycarbonyl-4,10-bis-[((S)-1-phenyl-ethylcarbamoyl)-methyl]-1-yl)-acetylamino)-methyl]-5-oxo-5*H*-[1]benzothiopyrano[2,3-*b*]pyridine-7-carboxylic acid methyl ester (36 mg, 0.038 mmol) in DCM:TFA (1:1, 2 ml) was stirred in a sealed flask overnight at room temperature yielding a dark yellow solution. Solvent was removed under reduced pressure to yield the TFA salt of the desired product as a glassy orange solid in quantitative yield; ^{1}H-NMR (CD_3CN, 500 MHz) δ 8.99 (s, 1H, H_O), 8.67 (d, 1H, J=8.0 Hz, H_K), 8.24 (dd, 1H, J=8.5 Hz 1.5 Hz, H_D), 7.81 (d, 1H, J=8.5 Hz, H_E), 7.47 (d, 1H, J=8.0 Hz, H_J), 7.24-7.34 (m br, 10H, arm Ar), 4.88-4.96 (m br, 2H, arm CH), 4.57 (m br, 2H, H_I), 3.95 (s, 3H, H_A), 2.91-3.57 (m br, 22H, cyclen, arm and linker CH_2), 1.40 (d, 6H, J=7.0 Hz, amide arms CH_3); ^{13}C-NMR (CD_3CN, 125 MHz, ^{1}H decoupled 500 MHz) δ 180.5 (1C, C_M), 171.3 (1C, linker arm C=O), 170.9, 170.4 (2C, amide arm C=O), 166.6 (1C, C_B), 162.9 (1C,

C_H), 160.3 (q, 1C, TFA C=O), 158.3 (1C, C_G), 144.8, 144.5 (2C, arm $Ar_{(q)}$), 142.9 (1C, C_F) 139.1 (1C, C_K), 133.6 (1C, C_D), 131.3 (1C, C_O), 129.8, 129.7 (2C, C_C and C_N) 129.4, 127.9, 126.9 (10C, arm Ar), 128.2 (1C, C_E), 126.1 (1C, C_L), 121.3 (1C, C_J), 116.9 (q, 1C, TFA CF_3), 55.5, 51.0, 50.0 (br, 8C, cyclen CH_2), 53.2 (1C, C_A), 49.8 (br, 2C, arm CH), 45.6 (1C, C_I), 43.7 (br, 3C, arm and linker CH_2), 22.7, 22.6 (br, 2C, amide arm CH_3); MS (ES^+) *m/z* 835.4 $[M + H]^+$ 25 %; HRMS (ES^+) *m/z* found 835.3959 $[M + H]^+$ $C_{45}H_{55}O_6N_8{}^{32}S$ requires 835.3960.

Eu(III) complex of 2-[(2-(4,10-bis-[((S)-1-phenyl-ethylcarbamoyl)methyl]-1-yl)acetylamino)-methyl]-5-oxo-5*H*-[1]benzothiopyrano[2,3-*b*]pyridine-7-carboxylic acid methyl ester ($[EuL^{44b}]^{3+}$)[94]

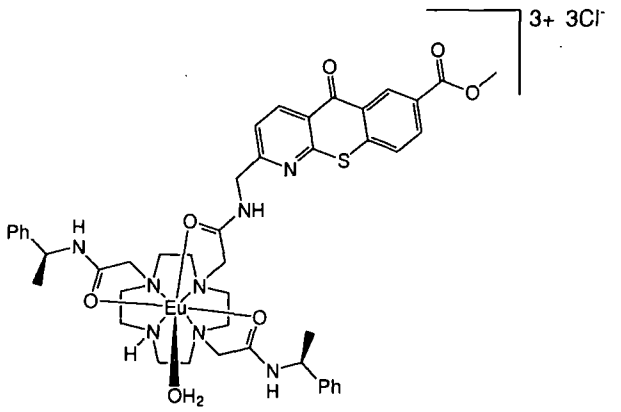

A solution of 2-[(2-(4,10-bis-[((S)-1-phenyl-ethylcarbamoyl)methyl]1-yl)acetylamino)-methyl]-5-oxo-5*H*-[1]benzothiopyrano[2,3-*b*]pyridine-7-carboxylic acid methyl ester (43 mg, 0.051 mmol) and $Eu(OTf)_3.6H_2O$ (21 mg, 0.030 mmol) in MeCN (1.5 ml) was heated at reflux under argon, in a Schlenk tube, for 48 h. Solvent was removed under reduced pressure to leave a yellow glassy solid. Dichloromethane (5 ml) was added to the solid which was sonicated for 5 min, solvent was then decanted to leave a orange residue. The sonication process was repeated followed by drying of the remaining residue, under reduced pressure, to yield the triflate salt of the desired product as a fine yellow coloured powder (36 mg, 0.025 mmol, 83 %). The solid was made water soluble by the exchange of triflate anions for chloride anions using DOWEX 1x8 200-400 mesh Cl ion exchange resin, as described earlier, to yield the dull yellow coloured complex in quantitative yield; ^{1}H-NMR (as tri-

chloride salt, D_2O, 500 MHz, partial data and assignment) δ 24.7 (1H, NH), 16.6 (1H, H_{ax}), 16.2 (1H, H_{ax}), 13.7 (1H, H_{ax}), 11.5 (1H, H_{ax}); MS (ES^+) *m/z* 515.3 $[M + HCO_2]^{2+}$ 50 %; HRMS (ES^+) *m/z* found 1043.3146 $[M + CH_3CO_2 - H]^+$ $C_{47}H_{56}O_8N_8{}^{32}S^{151}Eu$ requires 1043.3135; $\lambda_{abs}(H_2O)$: 372 nm; $\tau_{(H_2O)}$: 0.33 ms, $\tau_{(D_2O)}$: 0.65 ms; HPLC (solvent system A, 4.6 x 150 mm 4 μm Phenomenex Synergi Fusion RP 80Å analytical column): t_R = 9.7 min.

Gd(III) complex of 2-[(2-(4,10-bis-[((S)-1-phenyl-ethylcarbamoyl)methyl]-1-yl)acetylamino)-methyl]-5-oxo-5*H*-[1]benzothiopyrano[2,3-*b*]pyridine-7-carboxylic acid methyl ester ($[GdL^{44b}]^{3+}$)[92]

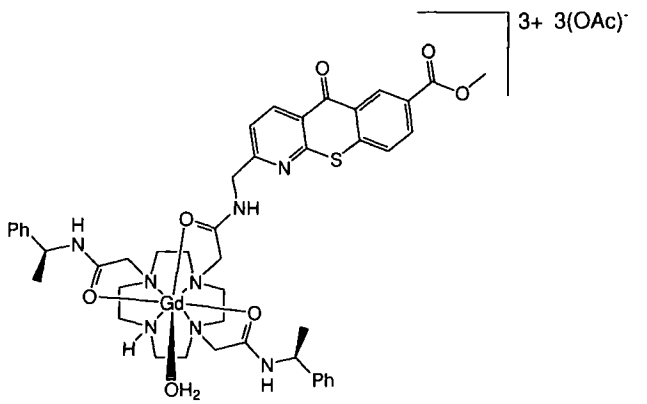

A solution of 2-[(2-(4,10-bis-[((S)-1-phenyl-ethylcarbamoyl)methyl]1-yl)acetylamino)-methyl]-5-oxo-5*H*-[1]benzothiopyrano[2,3-*b*]pyridine-7-carboxylic acid methyl ester (13 mg, 0.016 mmol) and $Gd(OAc)_3.4H_2O$ (4 mg, 0.012 mmol) in MeOH:H_2O (1:1, 1 ml) was heated at reflux under argon for 48 h. The solution was allowed to cool then solvent removed under reduced pressure. The residue was redissolved in water (2 ml), filtered then dried under reduced pressure leaving the desired complex as a pale yellow solid (11 mg, 0.009 mmol, 56 %); MS (ES^+) *m/z* 525.5 $[M + CH_3CO_2]^{2+}$ 100 %; HRMS (ES^+) *m/z* found 1050.3180 $[M + CH_3CO_2 - H]^+$ $C_{47}H_{56}O_8N_8{}^{32}SGd$ requires 1050.3198; $\lambda_{abs}(H_2O)$: 375 nm; HPLC (solvent system A, 4.6 x 150 mm 4 μm Phenomenex Synergi Polar-RP 80Å analytical column): t_R = 18.8 min.

2-(7-*tert*-Butoxycarbonyl-4,10-bis-[((S)-1-phenyl-ethylcarbamoyl)-methyl]-1-ylmethyl)-5-oxo-5*H*-[1]benzothiopyrano[2,3-*b*]pyridine-7-carboxylic acid methyl ester[92]

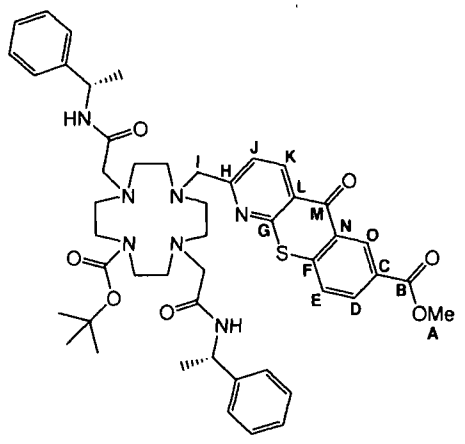

4,10-Bis-[((S)-1-phenyl-ethylcarbamoyl)-methyl]-1,4,7,10-tetraaza-cyclododecane-1-carboxylic acid *tert*-butyl ester (77 mg, 0.130 mmol), 2-bromomethyl-7-methoxycarbonyl-1-azathioxanthone (47 mg, 0.129 mmol) and K_2CO_3 (18 mg, 0.130 mmol) in dry MeCN (5 ml) were heated at reflux, under argon, for 12 h. The resultant yellow mixture was dried under reduced pressure, the residue taken up in DCM (5 ml) then extracted with $HCl_{(aq)}$ (0.05 M, 10 ml) then H_2O (2 x 10 ml). The organic phase was dried under reduced pressure followed by isolation of the desired product from the yellow residue by column chromatography (alumina using a DCM/MeOH solvent system starting from 100 % DCM then increasing the volume of MeOH by 0.1 % every 100 ml thereafter) to yield the desired product as a clear yellow glassy solid (100 mg, 0.114 mmol, 88 %); m.p. 56-58°C; R_F (Alumina, DCM-MeOH, 98.5:1.5) : 0.33; ^{1}H-NMR ($CDCl_3$, 500 MHz) δ 9.24 (d, 1H, J=1.5 Hz, H_O), 8.66 (d, 1H, J=8.5 Hz, H_K), 8.32 (dd, 1H, J=8.0, 1.5 Hz, H_D), 7.73 (d, 1H, J=8.5 Hz, H_E), 7.64 (br, 1H, amide arm NH), 7.36 (br, 1H, amide arm NH), 7.31 (d, 1H, J=8.5 Hz, H_J), 7.19-7.28 (m, 10H, amide arms Ar), 5.17 (m, 2H, amide arms CH), 4.02 (s, 3H, H_A), 3.58 (m, 2H, H_I), 2.41-3.48 (br m, 20H, cyclen and amide arms CH_2), 1.48 (m, 15H, amide arms and ^{t}Bu CH_3); ^{13}C-NMR ($CDCl_3$, 125 MHz, ^{1}H decoupled 500 MHz) δ 179.8 (1C, C_M), 170.4, 169.9 (2C, amide arms C=O), 165.9 (1C, C_B), 163.8 (1C, C_H), 157.7 (1C, C_G), 155.9 (1C, ^{t}Bu C=O), 143.5, 142.6 (2C, amide arms $Ar_{(q)}$),

142.1 (1C, C_F), 138.1 (1C, C_K), 132.9 (1C, C_D), 131.5 (1C, C_O), 128.9, 128.8 (2C, $C_{N,C}$), 126.8 (1C, C_E), 128.5, 127.2, 126.5, 126.3 (10C, amide arms Ar), 125.0 (1C, C_L), 121.7 (1C, C_J), 80.0 (1C, $^tBu_{(q)}$), 60.2 (2C, amide arms CH_2), 59.2 (1C, C_I), 54.1-52.9 (8C, cyclen CH_2), 52.6 (1C, C_A), 48.1, 47.9, 47.6 (2C, amide arms CH), 28.6 (3C, ^tBu CH_3), 21.6, 20.9 (2C, amide arms CH_3); MS (ES^+) *m/z* 877.9 $[M + H]^+$ 100 %, 899.9 $[M + Na]^+$ 40 %. HRMS (ES^+) *m/z* found 878.4266 $[M + H]^+$ $C_{48}H_{60}O_7N_7{}^{32}S$ requires 878.4270.

2-(4,10-Bis-[((S)-1-phenyl-ethylcarbamoyl)-methyl]-1-ylmethyl)-5-oxo-5*H*-[1]benzothiopyrano[2,3-*b*]pyridine-7-carboxylic acid methyl ester (L^{51b})[92]

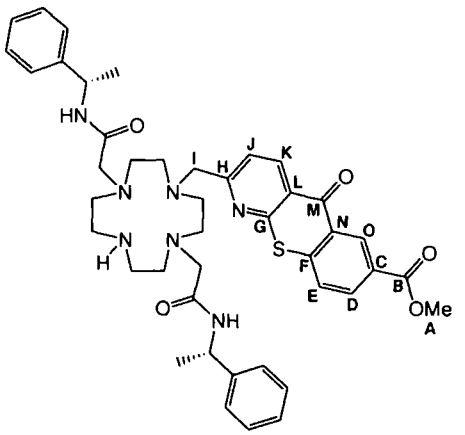

2-(7-*tert*-Butoxycarbonyl-4,10-bis-[((S)-1-phenyl-ethylcarbamoyl)-methyl]-1-yl-methyl)-5-oxo-5*H*-[1]benzothiopyrano[2,3-*b*]pyridine-7-carboxylic acid methyl ester (0.100 g, 0.114 mmol) was dissolved in DCM:TFA (1:1, 2 ml) then stirred overnight in a stoppered flask to yield a bright yellow solution. The solution was dried under reduced pressure to yield the desired product, as a glassy yellow solid, in quantitative yield; ^{1}H-NMR (CD_3CN, 500 MHz) δ 8.81 (d, 1H, J=2.0 Hz, H_O), 8.50 (d, 1H, J=8.5 Hz, H_K), 8.06 (dd, 1H, J=8.5, 2.0 Hz, H_D), 7.51 (d, 1H, J=8.5 Hz, H_E), 7.24 (d, 1H, J=8.0 Hz, H_J), 6.92-7.08 (m, 10H, amide arms Ar), 4.71 (m, 1H, amide arm CH), 4.63 (m, 1H, amide arm CH), 4.24 (m, 2H, H_I), 3.80 (s, 3H, H_A), 2.77-3.60 (br m, 20H, cyclen and amide arms CH_2), 1.16 (m, 6H, amide arms CH_3); ^{13}C-NMR (CD_3CN, 125 MHz, ^{1}H decoupled 500 MHz) δ 180.2 (1C, C_M), 171.5, 170.4 (2C, amide arms C=O), 166.6 (1C, C_B), 160.4 (q, 1C, TFA C=O), 158.3 (1C, C_H), 156.3

(1C, C_G), 144.5, 144.4 (2C, amide arms $Ar_{(q)}$), 142.5 (1C, C_F), 139.7 (1C, C_K), 133.9 (1C, C_D), 131.4 (1C, C_O), 130.1 (2C, $C_{N,C}$), 128.2 (1C, C_E), 129.4, 128.0, 126.7 (10C, amide arms Ar), 127.0 (1C, C_L), 123.7 (1C, C_J), 116.9 (q, 1C, TFA CF_3), 57.8 (2C, amide arms CH_2), 55.6 (1C, C_I), 43.9, 50.7, 51.1, 52.8, 53.6 (8C, cyclen CH_2), 53.2 (1C, C_A), 50.2, 49.7 (2C, amide arms CH), 22.5, 22.4 (2C, amide arms CH_3); MS (ES^+) *m/z* 778.7 $[M + H]^+$ 100 %, 800.7 $[M + Na]^+$ 15 %. HRMS (ES^+) *m/z* found 778.3740 $[M + H]^+$ $C_{43}H_{52}O_5N_7{}^{32}S$ requires 778.3745.

Eu(III) complex of 2-(4,10-bis-[((S)-1-phenyl-ethylcarbamoyl)-methyl]-1-ylmethyl)-5-oxo-5*H*-[1]benzothiopyrano[2,3-*b*]pyridine-7-carboxylic acid methyl ester ($[EuL^{51b}]^{3+}$)[92]

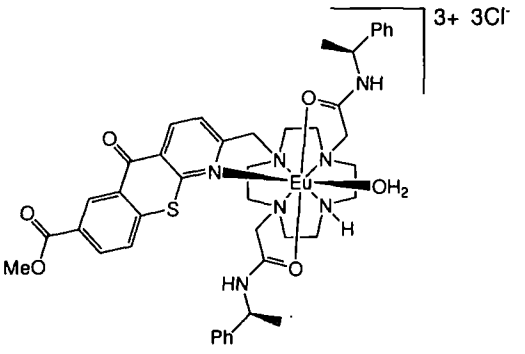

A solution of 2-(4,10-bis-[((S)-1-phenyl-ethylcarbamoyl)-methyl]-1-ylmethyl)-5-oxo-5*H*-[1]benzothiopyrano[2,3-*b*]pyridine-7-carboxylic acid methyl ester (15.4 mg, 0.020 mmol) and $Eu(OTf)_3.6H_2O$ (13.4 mg, 0.019 mmol) in MeCN (1 ml) was heated at 70°C for 72 h. The resultant orange solution was dried under reduced pressure to yield a glassy orange solid that was sonicated in DCM (5 ml) followed by decanting of the solvent. The remaining solid was further sonicated in DCM (5 ml) followed by decanting of the solvent to yield a orange solid that was dried under reduced pressure. The solid was made water soluble by the exchange of triflate anions for chloride anions using DOWEX 1x8 200-400 mesh Cl ion exchange resin, as described earlier, to yield the complex as a orange solid (15.5 mg, 0.015 mmol, 79 %); ^{1}H-NMR (as tri-chloride salt, D_2O, 700 MHz) δ Broadened resonances between +43 and -21 ppm; MS (ES^+) *m/z* 1048.3 $[M + 2CH_3CO_2]^+$ 100 %; HRMS (ES^+) *m/z* found 1048.3126 $[M + 2CH_3CO_2]^+$ $C_{47}H_{57}O_9N_7{}^{153}Eu^{32}S$ requires 1048.3145; $\lambda_{abs}(H_2O)$:

375 nm; $\tau_{(H_2O)}$: 0.32 ms, $\tau_{(D_2O)}$: 0.62 ms; HPLC (solvent system A, 4.6 x 150 mm 4 μm Phenomenex Synergi Fusion RP 80Å analytical column): t_R = 9.9 min.

2-(7-*tert*-Butoxycarbonyl-4,10-bis-[((S)-1-phenyl-ethylcarbamoyl)-methyl]-1,4,7,10-tetraaza-cyclododec-1-ylmethyl)-10-oxo-10*H*-9-oxa-1-aza-anthracene-6-carboxylic acid methyl ester[92]

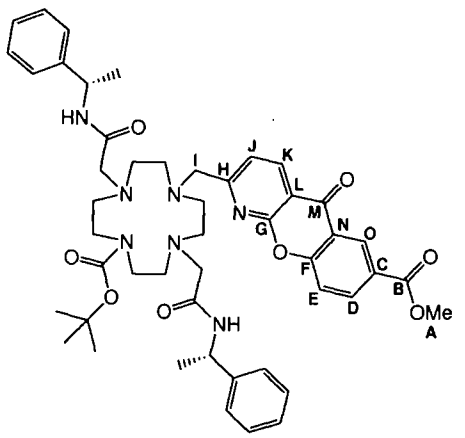

4,10-Bis-[((S)-1-phenyl-ethylcarbamoyl)-methyl]-1,4,7,10-tetraaza-cyclododecane-1-carboxylic acid *tert*-butyl ester (56 mg, 0.094 mmol), 7-methoxycarbonyl-2-bromomethyl-1-azaxanthone (33 mg, 0.095 mmol) and K_2CO_3 (13 mg, 0.094 mmol) in dry MeCN (2 ml) were heated at reflux, under argon, for 12 h. The resultant orange mixture was dried under reduced pressure, the residue taken up in DCM (10 ml) then extracted with H_2O (2 x 10 ml). The organic phase was dried under reduced pressure followed by isolation of the desired product from the yellow residue by column chromatography (alumina using a DCM/MeOH solvent system starting from 100 % DCM then increasing the volume of MeOH by 0.1 % every 100 ml thereafter) to yield the desired product as a clear yellow glassy solid (62 mg, 0.072 mmol, 77 %); m.p. 84-86°C; R_F (Alumina, DCM-MeOH, 97.5:2.5) : 0.51; ^{1}H-NMR ($CDCl_3$, 700 MHz) δ 8.99 (d, 1H, J=2.0 Hz, H_O), 8.48 (d, 1H, J=7.5 Hz, H_K), 8.42 (dd, 1H, J=8.5, 2.0 Hz, H_D), 7.64 (d, 1H, J=8.5 Hz, H_E), 7.64 (br, 1H, amide arm NH), 7.31 (br, 1H, amide arm NH), 7.14-7.27 (m, 11H, amide arms Ar and H_J), 5.16 (m, 2H, amide arms CH), 3.98 (s, 3H, H_A), 3.57 (m, 2H, H_I), 3.41 (br, 4H, amide arms CH_2), 2.40-3.13 (br m, 16H, cyclen CH_2), 1.43-1.48 (m, 15H, amide arms and ^{t}Bu CH_3); ^{13}C-NMR ($CDCl_3$, 175 MHz, ^{1}H decoupled 700 MHz) δ 176.9 (1C, C_M),

170.4, 170.1 (2C, amide arms C=O), 165.9 (1C, C_B), 165.4 (1C, C_H), 160.0 (1C, C_G), 158.5 (1C, C_F), 156.3 (1C, ^{t}Bu C=O), 142.8, 143.9 (2C, amide arms $Ar_{(q)}$), 137.9 (1C, C_K), 136.5 (1C, C_D), 129.5 (1C, C_O), 127.3 (1C, C_C), 129.0, 128.8, 126.8, 126.5 (10C, amide arms Ar), 121.7 (1C, C_N), 121.1 (1C, C_J), 119.2 (1C, C_E), 115.6 (1C, C_L), 80.3 (1C, ^{t}Bu$_{(q)}$), 60.6 (2C, amide arms CH_2), 59.7 (1C, C_I), 54.6-53.4 (8C, cyclen CH_2), 52.9 (1C, C_A), 48.5 (2C, amide arms CH), 28.9 (3C, ^{t}Bu CH_3), 22.0, 21.3 (2C, amide arms CH_3); MS (ES^+) *m/z* 862.4 $[M + H]^+$ 100 %. HRMS (ES^+) *m/z* found 862.4503 $[M + H]^+$ $C_{48}H_{60}O_8N_7$ requires 862.4498.

2-(4,10-Bis-[((S)-1-phenyl-ethylcarbamoyl)-methyl]-1,4,7,10-tetraaza-cyclododec-1-ylmethyl)-10-oxo-10*H*-9-oxa-1-azaanthracene-6-carboxylic acid methyl ester (L^{51a})[92]

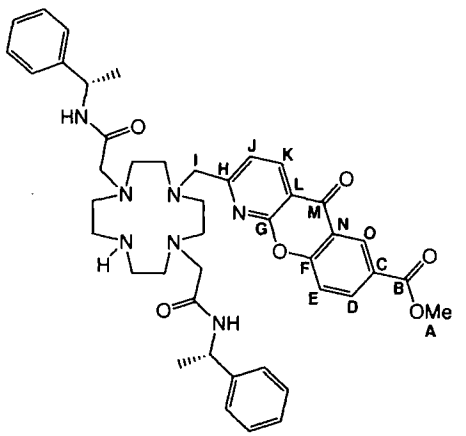

2-(7-*tert*-Butoxycarbonyl-4,10-bis-[((S)-1-phenyl-ethylcarbamoyl)-methyl]-1,4,7,10-tetraaza-cyclododec-1-ylmethyl)-10-oxo-10*H*-9-oxa-1-aza-anthracene-6-carboxylic acid methyl ester (25 mg, 0.029 mmol) was dissolved in DCM:TFA (1:1, 2 ml) then stirred for 12 h in a stoppered flask to yield a bright yellow solution. The solution was dried under reduced pressure to yield the desired product, as a glassy yellow solid, in quantitative yield; ^{1}H-NMR (CD_3CN, 700 MHz) δ 8.74 (d, 1H, J=2.0 Hz, H_O), 8.58 (d, 1H, J=8.5 Hz, H_K), 8.28 (dd, 1H, J=8.5, 2.0 Hz, H_D), 7.52 (d, 1H, J=9.0 Hz, H_E), 7.31 (d, 1H, J=7.5 Hz, H_J), 7.03-7.27 (m, 12H, amide arms Ar and NH), 4.81 (m, 1H, amide arm CH), 4.75 (m, 1H, amide arm CH), 4.35 (m, 2H, H_I), 3.94 (s, 3H, H_A), 2.94-3.80 (br m, 20H, cyclen and amide arms CH_2), 1.26 (d, 6H, J=6.5 Hz, amide arms CH_3); ^{13}C-NMR (CD_3CN, 175 MHz, ^{1}H decoupled

700 MHz) δ 177.2 (1C, C_M), 171.5, 170.5 (2C, amide arms C=O), 166.2 (1C, C_B), 160.3 (q, 1C, TFA C=O), 158.8 (1C, C_G), 156.8 (2C, $C_{H,F}$), 144.6, 144.3 (2C, amide arms $Ar_{(q)}$), 139.4 (1C, C_K), 136.9 (1C, C_D), 128.9 (1C, C_O), 128.1 (1C, C_C), 129.4, 129.2, 127.8, 126.9, 126.7 (10C, amide arms Ar), 122.8 (1C, C_J), 122.2 (1C, C_N), 120.1 (1C, C_E), 117.3 (1C, C_L), 116.9 (q, 1C, TFA CF_3), 57.4 (1C, C_I), 56.5, 55.6 (2C, amide arms CH_2), 43.9, 50.5, 51.2, 53.5 (8C, cyclen CH_2), 53.1 (1C, C_A), 50.1, (2C, amide arms CH), 22.5, 22.3 (2C, amide arms CH_3); MS (ES^+) *m/z* 762.3 [M + H]$^+$ 100 %. HRMS (ES^+) *m/z* found 762.3972 [M + H]$^+$ $C_{43}H_{52}O_6N_7$ requires 762.3974.

Eu(III) complex of 2-(4,10-bis-[((S)-1-phenyl-ethylcarbamoyl)-methyl]-1,4,7,10-tetraaza-cyclododec-1-ylmethyl)-10-oxo-10*H*-9-oxa-1-aza-anthracene-6-carboxylic acid methyl ester ([EuL^{51a}]$^{3+}$)[92]

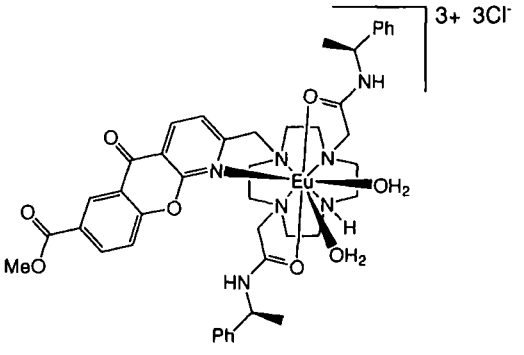

A solution of 2-(4,10-bis-[((S)-1-phenyl-ethylcarbamoyl)-methyl]-1,4,7,10-tetraaza-cyclododec-1-ylmethyl)-10-oxo-10*H*-9-oxa-1-aza-anthracene-6-carboxylic acid methyl ester (16 mg, 0.021 mmol) and $Eu(OTf)_3.6H_2O$ (11 mg, 0.018 mmol) in MeCN (1 ml) was heated at 90°C for 48 h. The resultant yellow solution was dried under reduced pressure to yield a glassy orange solid that was sonicated in $CHCl_3$ (5 ml) followed by decanting of the solvent. The remaining solid was further sonicated in $CHCl_3$ (5 ml) followed by decanting of the solvent to yield a orange solid that was dried under reduced pressure. The solid was made water soluble by the exchange of triflate anions for chloride anions using DOWEX 1x8 200-400 mesh Cl ion exchange resin, as described earlier, to yield the complex as a pale yellow powder (15 mg, 0.014 mmol, 78 %); ^{1}H-NMR (as tri-chloride salt, D_2O, 700 MHz) δ Broadened

resonances between +51 and -21 ppm; MS (ES^+) *m/z* 479.9 $[M + HCO_2]^{2+}$ 100 %, 958.3 $[M + HCO_2 - H]^+$ 70 %; HRMS (ES^+) *m/z* found 956.3007 $[M + HCO_2 - H]^+$ $C_{44}H_{51}O_8N_7{}^{151}Eu$ requires 956.2992; $\lambda_{abs}(H_2O)$: 333 nm; $\tau_{(H_2O)}$: 0.26 ms, $\tau_{(D_2O)}$: 0.60 ms; HPLC (solvent system A, 4.6 x 150 mm 4 μm Phenomenex Synergi Fusion RP 80Å analytical column): t_R = 10.7 min.

4,7,10-Tris-[((S)-1-phenyl-ethylcarbamoyl)-methyl]-1,4,7,10-tetraaza-cyclododecane-1-carboxylic acid *tert*-butyl ester

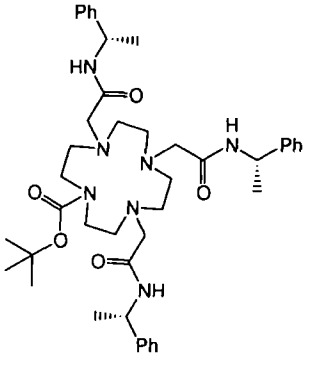

4,10-Bis-[((S)-1-phenyl-ethylcarbamoyl)-methyl]-1,4,7,10-tetraaza-cyclododecane-1-carboxylic acid *tert*-butyl ester (0.169 g, 0.284 mmol), 2-chloro-*N*-[(S)-1-phenyleth- yl]ethanamide (0.067 g, 0.339 mmol) and K_2CO_3 (0.047 g, 0.340 mmol) in MeCN (15 ml) were heated at reflux, under argon, for 12 h. Solvent was removed under reduced pressure to leave a crude orange coloured residue that was dissolved in DCM (10 ml) then washed with H_2O (2 x 10 ml). The organic phase was dried under reduced pressure, the desired product was then isolated by column chromatography on alumina (utilising an incremental solvent system of DCM/MeOH starting from 100 % DCM with 0.1 % MeOH increments) to yield, after drying, the desired product as a glassy colourless solid (0.193 g, 0.255 mmol, 90 %); R_F (Alumina, DCM-MeOH, 49:1) : 0.55; m.p. 59-62°C; ^{1}H-NMR ($CDCl_3$, 500 MHz) δ 7.26-7.39 (m br, 16H, Ar and amide NH), 7.03 (br, 1H, amide NH), 7.02 (br, 1H, amide NH), 5.17 (m, 3H, CH), 2.40-3.30 (m br, 22H, cyclen and arm CH_2), 1.45-1.56 (m, 18H, arm and ^{t}Bu CH_3); ^{13}C-NMR ($CDCl_3$, 125 MHz, ^{1}H decoupled 500 MHz) δ 170.4, 169.9 (3C, amide C=O), 156.0 (1C, ^{t}BOC C=O), 143.9, 143.3 (3C, $Ar_{(q)}$), 129.0, 128.8, 127.8, 127.4, 126.7, 126.5 (15C, Ar), 80.1 (1C,

$^{t}BOC_{(q)}$), 53.9 (3C, CH_2CO), 47.9-59.7 (m br, 8C, cyclen CH_2), 48.6 (3C, CH), 28.7 (3C, ^{t}BOC CH_3), 22.1, 21.5 (3C, amide arm CH_3); MS (ES^+) *m/z* 756.3 $[M + H]^+$ 100 %; HRMS (ES^+) *m/z* found 756.4794 $[M + H]^+$ $C_{43}H_{62}O_5N_7$ requires 756.4807.

2-(4,7-Bis-[((S)-1-phenyl-ethylcarbamoyl)-methyl]-1,4,7,10-tetraaza-cyclododec-1-yl)-*N*-((S)-1-phenyl-ethyl)acetamide

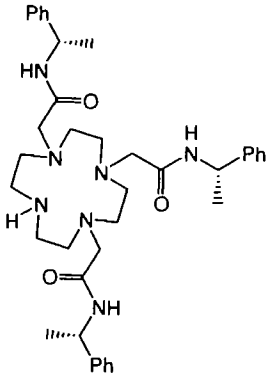

4,7,10-Tris-[((S)-1-phenyl-ethylcarbamoyl)-methyl]-1,4,7,10-tetraaza-cyclododecane-1-carboxylic acid *tert*-butyl ester (0.109 g, 0.144 mmol) was dissolved in DCM:TFA (3 ml, 2:1) then stirred for 2 h in a stoppered flask to yield a yellow tinged solution. The solution was dried under reduced pressure to yield the desired product as its TFA salt, as a glassy yellow solid, in quantitative yield. Immediately prior to further modification the solid was dissolved in DCM (10 ml) and washed with sat. $NaHCO_3$ solution (10 ml) followed by the drying of the organic phase under reduced pressure to yield the desired product as its free base; ^{1}H-NMR (CD_3CN, 500 MHz) δ 7.47 (s br, 1H, NH), 7.23-7.35 (m br, 17H, Ar and amide NH), 4.97 (m, 3H, CH), 3.78 (m, 2H, arm CH_2), 2.87-3.41 (m br, 20H, cyclen and arm CH_2), 1.41 (br, 9H, arm CH_3); ^{13}C-NMR (CD_3CN, 125 MHz, ^{1}H decoupled 500 MHz) δ 171.0, 170.6 (2C, amide C=O), 163.9 (1C, amide C=O), 160.3 (q, 1C, TFA C=O), 144.7, 144.5, 144.2 (3C, $Ar_{(q)}$), 129.6, 129.5, 128.3, 128.1, 127.1, 127.0 (15C, Ar), 116.8 (q, 1C, TFA CF_3), 56.3, 55.8, 53.1, 43.8, 43.6 (m br, 11C, cyclen and arm CH_2), 50.7, 49.9 (3C, CH), 22.6, 22.3 (3C, amide arm CH_3); MS (ES^+) *m/z* 359.7 $[M + Cu]^{2+}$ 60 %, 656.3 $[M + H]^+$ 100 %; HRMS (ES^+) *m/z* found 656.4276 $[M + H]^+$ $C_{38}H_{54}O_3N_7$ requires 656.4283.

4,7,10-Tris-[((S)-1-phenyl-ethylcarbamoyl)-methyl]-1,4,7,10-tetraaza-cyclododecane-1-carboxylic acid *tert*-butyl ester

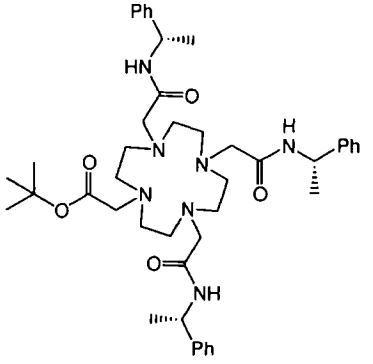

A solution of 2-(4,7-bis-[((S)-1-phenyl-ethylcarbamoyl)-methyl]-1,4,7,10-tetraaza-cyclododec-1-yl)-*N*-((S)-1-phenyl-ethyl)acetamide (338 mg, 0.52 mmol), *tert*-butyl bromoacetate (0.076 ml, 0.51 mmol) and NEt_3 (0.29 ml, 2.08 mmol) in MeCN (10 ml) was heated at reflux for 12 h under argon. After 12 h a further addition of *tert*-butyl bromoacetate (0.3 eq, 0.023 ml) was added to the reaction solution and the reaction was allowed to reflux for a further 6 h. The reaction was allowed to cool to room temperature, solvent was removed under reduced pressure and the residue was taken up in DCM (20 ml) followed by washing of the organic solution with H_2O (20 ml). The organic phase was collected and dried under reduced pressure to leave a crude yellow residue. The desired product was isolated by column chromatography on alumina (utilising an incremental solvent system of DCM/MeOH starting from 100 % DCM with 0.1 % MeOH increments) to yield, after drying, the desired product as a glassy colourless solid (0.110 g, 0.143 mmol, 28 %); R_F (Alumina, DCM-MeOH, 95:5) : 0.53; m.p. 53-56°C; ^{1}H-NMR ($CDCl_3$, 700 MHz) δ 7.51 (s br, 1H, NH), 7.18-7.35 (m br, 17H, Ar and amide NH), 5.06-5.13 (m br, 3H, CH), 2.50-3.02 (m br, 24H, cyclen and arm CH_2), 1.44-1.50 (m, 18H, arm and ^{t}Bu CH_3); ^{13}C-NMR ($CDCl_3$, 175 MHz, ^{1}H decoupled 700 MHz) δ 170.4, 170.0 (3C, amide C=O), 155.6 (1C, ^{t}Bu C=O), 143.5 (3C, $Ar_{(q)}$), 129.1, 129.0, 127.8, 126.8, 126.7 (15C, Ar), 81.9 (1C, $^tBu_{(q)}$), 59.9, 58.8, 56.2, 54.4, 54.0, 53.1, 48.6 (m br, 15C, cyclen and arm CH_2 and CH), 28.5 (3C, ^{t}Bu CH_3), 21.8,

21.6 (3C, amide arm CH_3); MS (ES^+) *m/z* 792.2 $[M + Na]^+$ 100 %; HRMS (ES^+) *m/z* found 770.4967 $[M + H]^+$ $C_{44}H_{64}O_5N_7$ requires 770.4964.

(4,7,10-Tris-[((S)-1-phenyl-ethylcarbamoyl)-methyl]-1,4,7,10-tetraaza-cyclododec-1-yl)-acetic acid

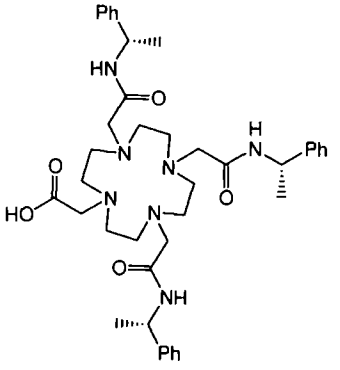

A solution of 4,7,10-tris-[((S)-1-phenyl-ethylcarbamoyl)-methyl]-1,4,7,10-tetra-aza-cyclododecane-1-carboxylic acid *tert*-butyl ester (0.11 g, 0.142 mmol) in DCM:TFA (3 ml, 2:1) was stirred at room temperature for 3 h. The solution was then dried under reduced pressure to leave a glassy yellow solid. The solid was redissolved in DCM (10 ml), the solution washed with sat. $NaHCO_3$ solution (10 ml) followed by the separation and drying of the organic phase under reduced pressure to leave the desired product as a glassy colourless solid (0.092 g, 0.129 mmol, 91 %); ^{1}H-NMR ($CDCl_3$, 500 MHz) δ 8.07 (s br, 2H, NH), 7.75 (s br, 1H, NH), 7.17-7.36 (m, 15H, Ar), 5.04 (m, 3H, CH), 2.63-3.35 (m br, 24H, cyclen and arm CH_2), 1.45-1.51 (m, 9H, arm CH_3); ^{13}C-NMR ($CDCl_3$, 125 MHz, ^{1}H decoupled 500 MHz) δ 169.5, 169.2 (3C, amide C=O), 144.1, 144.0 (3C, $Ar_{(q)}$), 128.9, 127.7, 127.5, 126.9, 126.7 (15C, Ar), 58.7 (1C, acid arm CH_2), 57.4, 57.2, 54.1, 52.8, 51.9, 50.0 (m, 11C, cyclen and amide arm CH_2), 49.1, 49.0 (3C, CH), 22.2, 22.0 (3C, CH_3); MS (ES^+) *m/z* 388.9 $[M + Cu]^+$ 100 %, 714.5 $[M + H]^+$ 25 %; HRMS (ES^+) *m/z* found 714.4333 $[M + H]^+$ $C_{40}H_{56}O_5N_7$ requires 714.4337.

10-Oxo-2-[(2-(4,7,10-tris-[((S)-1-phenyl-ethylcarbamoyl)-methyl]-1,4,7,10-tetraaza-cyclododec-1-yl)-acetylamino)-methyl]-10*H*-9-oxa-1-aza-anthracene-6-carboxylic acid methyl ester (L^{50})

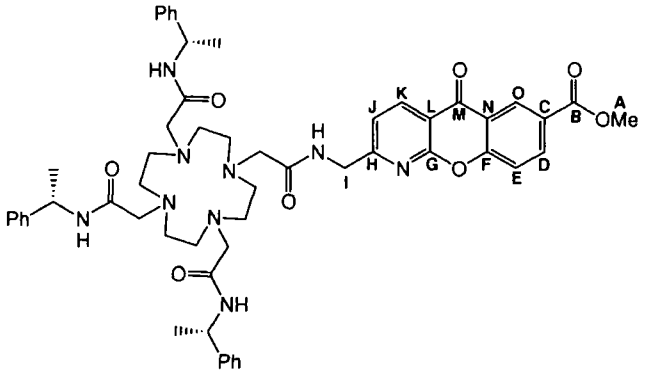

TBTU (34 mg, 0.106 mmol) and HOBt.xH_2O (2 mg, 0.015 mmol) were added to a stirring solution of (4,7,10-tris-[((S)-1-phenyl-ethylcarbamoyl)-methyl]-1,4,7,10-tetraaza-cyclododec-1-yl)-acetic acid (76 mg, 0.106 mmol) and NEt_3 (0.03 ml, 0.215 mmol) in anhydrous MeCN (1 ml) and allowed to stir for 15 min. A solution of 7-methoxycarbonyl-2-aminomethyl-1-azaxanthone (24 mg, 0.084 mmol) in MeCN:$CHCl_3$ (1.5 ml, 1:0.5) was added to the solution and the reaction was allowed to stir, under argon, for 16 h. The dark orange solution was then dried under reduced pressure, taken up in DCM (10 ml) and washed with sat. $NaHCO_3$ (10 ml), $HCl_{(aq)}$ (0.1 M, 10 ml) then H_2O (10 ml). The organic phase was separated then dried under reduced pressure. The desired product was isolated by column chromatography on alumina (utilising an incremental solvent system of DCM/MeOH starting from 100 % DCM with 0.1 % MeOH increments) to yield, after drying, the product as a orange colourless solid. A remaining contaminant was removed by sonication of the solid with benzene followed by the decanting of the solvent and drying of the remaining solid to yield a glassy orange material (40 mg, 0.041 mmol, 49 %); R_F (Alumina, DCM-MeOH, 24:1) : 0.43; m.p. 75-77°C; ^{1}H-NMR ($CDCl_3$, 700 MHz) δ 8.96 (d, 1H, J=1.5 Hz, H_O), 8.57 (d, 1H, J=8.5 Hz, H_K), 8.37 (d, 1H, J=8.5 Hz, H_D), 8.23 (s br, 1H, arm NH), 7.56 (d, 1H, J=8.5 Hz, H_E), 6.98-7.36 (m br, 19H, arm Ar, H_J and amide NH), 5.05-5.09 (m br, 3H, arm CH), 4.50 (m, 2H, H_I), 3.98 (s, 3H, H_A), 2.60-3.05 (m br, 24H, cyclen, arm and linker CH_2), 1.42-1.47 (m, 9H,

arm CH_3); ^{13}C-NMR ($CDCl_3$, 175 MHz, ^{1}H decoupled 700 MHz) δ 176.9 (1C, C_M), 171.9, 170.0 (4C, amide arm C=O and linker arm C=O), 165.9 (1C, C_B), 164.8 (1C, C_H), 160.2 (1C, C_G), 158.4 (1C, C_F), 143.6, 143.3 (3C, arm $Ar_{(q)}$), 138.2 (1C, C_K), 136.4 (1C, C_D), 129.5 (1C, C_O), 129.0, 128.9, 128.8, 128.7, 127.8, 126.7, 126.6, 126.5 (15C, arm Ar), 127.2 (1C, C_N), 121.7 (1C, C_C), 120.1 (1C, C_J), 119.1 (1C, C_E), 115.6 (1C, C_L), 59.8, 59.7, 59.2, 53.8, 53.6 (br, 12C, cyclen, arm and linker CH_2), 52.9 (1C, C_A), 48.7 (br, 3C, arm CH), 44.9 (1C, C_I), 21.9 (br, 3C, amide arm CH_3); MS (ES^+) *m/z* 980.9 $[M + H]^+$ 100 %; HRMS (ES^+) *m/z* found 980.5037 $[M + H]^+$ $C_{55}H_{66}O_8N_9$ requires 980.5029.

Eu(III) complex of 10-Oxo-2-[(2-(4,7,10-tris-[((S)-1-phenyl-ethyl-carbamoyl)-methyl]-1,4,7,10-tetraaza-cyclododec-1-yl)-acetylamino)-methyl]-10*H*-9-oxa-1-aza-anthracene-6-carboxylic acid methyl ester ($[EuL^{50}]^{3+}$)

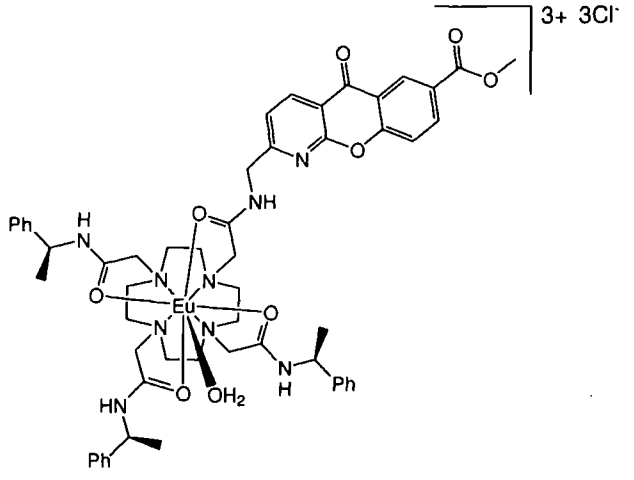

10-Oxo-2-[(2-(4,7,10-tris-[((S)-1-phenyl-ethylcarbamoyl)-methyl]-1,4,7,10-tetraaza-cyclododec-1-yl)-acetylamino)-methyl]-10*H*-9-oxa-1-aza-anthracene-6-carboxylic acid methyl ester (14 mg, 0.014 mmol) and $Eu(OTf)_3$ (8 mg, 0.013 mmol) in MeCN (1 ml) were heated at reflux for 24 h. The solution was then dried under reduced pressure and the residue sonicated in DCM (10 ml) followed by centrifugation to isolate the solid, this washing procedure was repeated twice. The dried isolated solid was made water soluble by the exchange of the triflate anions for chloride anions using 'DOWEX 1x8 200-400 mesh Cl' ion exchange resin, as described previously,

to yield the desired complex as its trichloride salt as a white powder (11 mg, 0.009 mmol, 69 %); ^{1}H-NMR (D_2O, 500 MHz, partial data and assignment) δ 28.1 (1H, H_{ax}), 26.6 (1H, H_{ax}), 26.3 (1H, H_{ax}), 25.4 (1H, H_{ax}), 8.5 (2H), 8.4 (1H), 7.9 (1H), 7.6 (1H), further resonances between 5.5 and -14.8 ppm; MS (ES^+) *m/z* 588.7 [M + HCO_2]$^{2+}$ 55 %, 1130.4 [M - 2H]$^+$ 5 %, 1175.8 [M - H + HCO_2]$^+$ 5 %; HRMS (ES^+) *m/z* found 376.8047 [M]$^{3+}$ $C_{55}H_{65}O_8N_9{}^{151}Eu$ requires 376.8046. $\lambda_{abs}(H_2O)$: 332 nm; $\tau_{(H_2O)}$: 0.58 ms, $\tau_{(D_2O)}$: 2.27 ms; HPLC (solvent system A, 4.6 x 150 mm 4 μm Phenomenex Synergi Polar-RP 80Å analytical column): t_R = 12.0 min.

5.2.2 Dimeric complexes and precursors

Bis-7-[(1S,2S)-1,2-diphenyl-ethylcarbamoyl]-methyl-4,10-bis-[((S)-1-phenyl-ethylcarbamoyl)-methyl]-1,4,7,10-tetraaza-cyclododecane-1-carboxylic acid *tert*-butyl ester

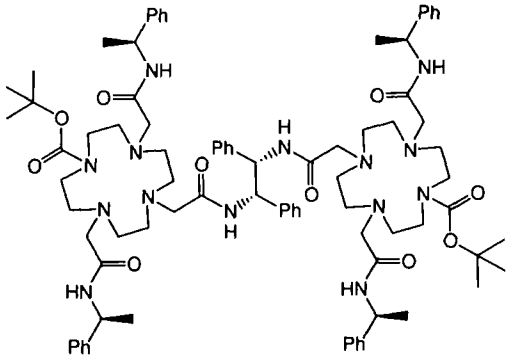

7-Carboxymethyl-4,10-bis-[((S)-1-phenyl-ethylcarbamoyl)-methyl]-1,4,7,10-tetra aza-cyclododecane-1-carboxylic acid *tert*-butyl ester (0.166 g, 0.254 mmol), EDC.HCl (0.054 g, 0.282 mmol), HOBt.xH_2O (10 mg) and NEt_3 (0.1 ml, 0.717 mmol) in $CHCl_3$ (5 ml) were stirred at room temperature. After 25 min (1*S*,2*S*)-(-)-1,2-diphenylethylen- ediamine (0.024 g, 0.113 mmol) was added to the solution which was stirred for a further 10 h then extracted with sat. $NaHCO_{3(aq)}$ (10 ml) followed by H_2O (10 ml). The clear organic solution was dried under reduced pressure then purified by column chromatography (alumina using a DCM/MeOH solvent system starting from 100 % DCM then increasing the volume of MeOH by 0.5 % every 50 ml thereafter) to yield the desired product as a clear glassy solid (0.126 g, 0.085 mmol, 75 %); R_F (Alumina, DCM-MeOH, 99:1) : 0.80; m.p. 89-91°C; ^{1}H-NMR

($CDCl_3$, 400 MHz) δ 9.82 (s br, 1H, NH), 9.08 (s br, 1H, NH), 7.88 (s br, 4H, arm NH), 7.18-7.28 (m br, 30H, arm and linker Ar protons), 5.39 and 5.53 (s br, 2H, linker CH), 5.01 (s br, 4H, arm CH), 2.03-3.30 (m br, 44H, cyclen CH_2, amide arm CH_2CO and linker CH_2CO), 1.39 (m br, 30H, amide arm CH_3 and ^{t}Bu CH_3); ^{13}C-NMR ($CDCl_3$, 100 MHz, ^{1}H decoupled 400 MHz) δ 170.8 (m br, 6C, amide arms C=O and linker C=O), 156.1 (2C, ^{t}Boc C=O), 143.6 (6C, amide arms and linker $Ph_{(q)}$), 128.9, 127.6, 126.6 (br, 30C, amide arm and linker Ph), 80.0 (2C, ^{t}Boc$_{(q)}$), 46.9-62.6 (br, 24C, cyclen CH_2, amide arm CH_2, linker CH_2 and linker stereocentre C), 28.7 (6C, ^{t}Boc CH_3), 22.3 (4C, amide arm CH_3). MS (ES^-) *m/z* 1480.4 $[M - H]^-$ 35 %, 1517.5 $[M + Cl]^-$ 50 %; HRMS (ES^+) *m/z* found 1481.9108 $[M + H]^+$ $C_{84}H_{117}O_{10}N_{14}$ requires 1481.9072.

Bis-7-[(1S,2S)-1,2-diphenyl-ethylcarbamoyl]-methyl-4,10-bis-[((S)-1-phenyl-ethylcarbamoyl)-methyl]-1,4,7,10-tetraaza-cyclododecane (L^{57})

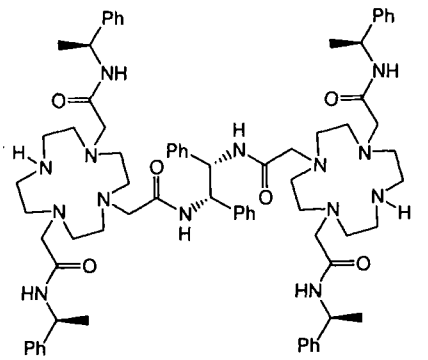

A colourless solution of bis-7-[(1S,2S)-1,2-diphenyl-ethylcarbamoyl]-methyl-4,10-bis-[((S)-1-phenyl-ethylcarbamoyl)-methyl]-1,4,7,10-tetraaza-cyclododecane-1-carboxylic acid *tert*-butyl ester (0.093 g, 0.063 mmol) in DCM:TFA (50:50, 5 ml) was stirred for 12 h in a sealed flask. The resultant yellow tinged solution was dried under reduced pressure to yield the TFA salt of the desired product, as a glassy yellow solid, in quantitative yield; ^{1}H-NMR (CD_3CN, 500 MHz) δ 9.77 (d, 2H, J=9.5 Hz, cyclen NH), 7.77 (s br, 4H, arm NH), 7.04-7.48 (m, 30H, arm and linker Ar), 5.67 (d, 2H, J=9.0 Hz, linker CH), 5.05 (m, 2H, arm CH), 4.69 (m, 2H, arm CH), 3.92 (d, 2H, J=15.5 Hz, linker CH_2), 3.71 (d, 2H, J=15.5 Hz, linker CH_2), 2.62-3.29 (m, 40H. cyclen CH_2 and arm CH_2), 1.46 (d, 6H, J=7.0 Hz, arm CH_3), 1.24 (d, 6H,

J=7.0 Hz, arm CH_3); ^{13}C-NMR (CD_3CN, 125 MHz, ^{1}H decoupled 500 MHz) δ 170.7 (4C, arms C=O), 164.4 (2C, linker C=O), 160.4 (q, 2C, TFA C=O), 144.7, 144.4 (4C, arm $Ar_{(q)}$), 139.8 (2C, linker $Ar_{(q)}$), 129.7, 129.5, 129.3, 128.8, 2 x 128.0, 127.1, 127.0 (30C, arm and linker Ar), 115.7 (q, 2C, TFA CF_3), 58.7 (2C, linker CH), 56.7, 55.9, 53.0, 52.3, 51.8, 50.8, 49.1, 48.4 (16C, cyclen CH_2), 55.4 (2C, linker CH_2), 49.8, 49.7 (4C, arm CH), 43.8, 43.7 (4C, arm CH_2), 22.6, 22.1 (4C, arm CH_3). MS (ES^+) m/z 641.4 $[M + 2H]^{2+}$ 100 %; HRMS (ES^+) m/z found 641.4055 $[M + 2H]^{2+}$ $C_{74}H_{102}O_6N_{14}$ requires 641.4048.

Eu(III) complex of bis-7-[(1S,2S)-1,2-diphenyl-ethylcarbamoyl]-methyl-4,10-bis-[((S)-1-phenyl-ethylcarbamoyl)-methyl]-1,4,7,10-tetraaza-cyclododecane ($[Eu_2L^{57}]^{6+}$)

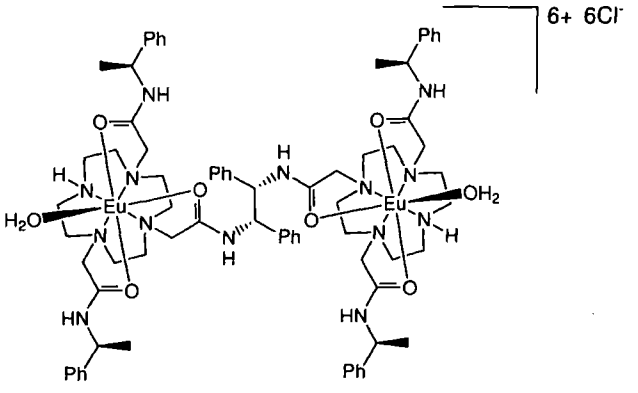

Bis-7-[(1S,2S)-1,2-diphenyl-ethylcarbamoyl]-methyl-4,10-bis-[((S)-1-phenyl-ethylcarbamoyl)-methyl]-1,4,7,10-tetraaza-cyclododecane as its TFA salt (0.082 g, 0.064 mmol, molar mass of ligand as its free base used) and $Eu(OTf)_3$ (0.230 g, 0.384 mmol) in dry MeCN (1.75 ml) were heated at reflux for 36 h, in Schlenk apparatus, under an atmosphere of argon. The solution was then cooled to room temperature followed by removal of the solvent under reduced pressure. The solid was sonicated in DCM (2 x 5 ml) followed by solid collection by centrifugation and decanting of the DCM phase, the solid was dried under reduced pressure. The grey solid left was sonicated in water (5 ml), the water was then decanted followed by the drying of the remaining solid under reduced pressure. The solid was made water soluble by the exchange of the triflate anions for chloride anions using 'DOWEX 1x8 200-400 mesh Cl' ion exchange resin (0.2 g) as described earlier. The crude complex was isolated

from excess $EuCl_3$ using benzoylated dialysis tubing, as described earlier, to yield the desired product as a white powder (0.089 g, 0.047 mmol, 74 %); MS (ES^+ in the presence of excess ammonium acetate) *m/z* 567.1 $[M + 2CH_3CO_2 - H]^{3+}$ 95 %, 850.2 $[M + 2CH_3CO_2 - 2H]^{2+}$ 100%; HRMS (ES^+) *m/z* found 849.3217 $[M + 2CH_3CO_2 - 2H]^{2+}$ $C_{78}H_{104}O_{10}N_{14}{}^{151}Eu_2$ requires 849.3223; HPLC (solvent system B, 4.6 x 150 mm 4 μm Phenomenex Synergi Fusion RP 80Å analytical column): t_R = 8.5 min.

Tb(III) complex of bis-7-[(1S,2S)-1,2-diphenyl-ethylcarbamoyl]-methyl-4,10-bis-[((S)-1-phenyl-ethylcarbamoyl)-methyl]-1,4,7,10-tetraaza-cyclododecane ($[Tb_2L^{57}]^{6+}$)

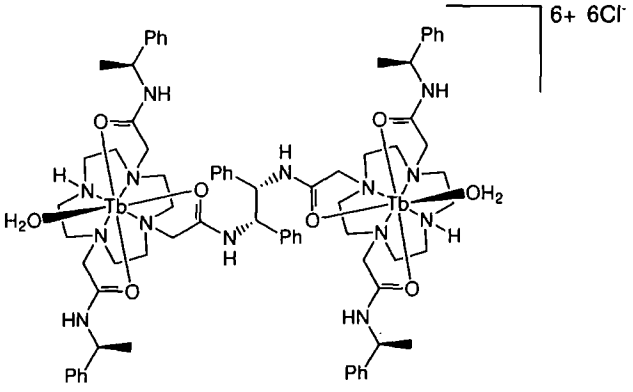

Bis-7-[(1S,2S)-1,2-diphenyl-ethylcarbamoyl]-methyl-4,10-bis-[((S)-1-phenyl-ethylcarbamoyl)-methyl]-1,4,7,10-tetraaza-cyclododecane as its TFA salt (0.017 g, 0.013 mmol, molar mass of ligand as its free base used) and $TbCl_3.6H_2O$ (0.031 g, 0.083 mmol) in dry MeOH (1.5 ml) were heated at reflux for 36 h, in Schlenk apparatus, under an atmosphere of argon. The solution was then cooled to room temperature followed by removal of the solvent under reduced pressure. The solid was sonicated in DCM (2 x 5 ml) followed by solid collection by centrifugation and decanting of the DCM phase, the solid was dried under reduced pressure. The grey solid left was sonicated in water (5 ml), the water was then decanted followed by the drying of the remaining solid under reduced pressure. The complex was isolated from excess $TbCl_3$ using benzoylated dialysis tubing (9 mm flat width), as described earlier, to yield the desired product as a white powder (0.020 g, 0.010 mmol, 80 %); MS (ES^+ in the presence of excess ammonium acetate) *m/z* 571.7 $[M + 2CH_3CO_2 - H]^{3+}$ 90 %, 857.2 $[M + 2CH_3CO_2 - 2H]^{2+}$ 100 %; HRMS (ES^+) *m/z* found 857.3270

$[M + 2CH_3CO_2 - 2H]^{2+}$ $C_{78}H_{104}O_{10}N_{14}{}^{159}Tb_2$ requires 857.3278; HPLC (solvent system B, 4.6 x 150 mm 4 μm Phenomenex Synergi Fusion RP 80Å analytical column): t_R = 8.7 min.

Yb(III) complex of bis-7-[(1S,2S)-1,2-diphenyl-ethylcarbamoyl]-methyl-4,10-bis-[((S)-1-phenyl-ethylcarbamoyl)-methyl]-1,4,7,10-tetraaza-cyclododecane ($[Yb_2L^{57}]^{6+}$)

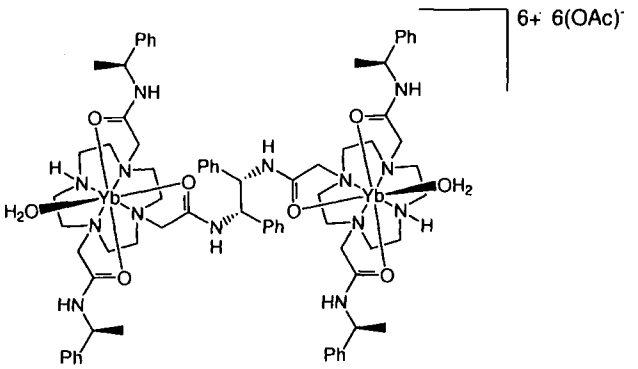

Bis-7-[(1S,2S)-1,2-diphenyl-ethylcarbamoyl]-methyl-4,10-bis-[((S)-1-phenyl-ethylcarbamoyl)-methyl]-1,4,7,10-tetraaza-cyclododecane as its TFA salt (0.044 g, 0.034 mmol, molar mass of ligand as free base used) and $Yb(OAc)_3.4H_2O$ (0.086 g, 0.20 mmol) in MeOH:H_2O (2 ml, 50:50) were heated at reflux for 48 h, in Schlenk apparatus, under an atmosphere of argon. The solution was then cooled to room temperature followed by removal of the solvent under reduced pressure. The complex was isolated from excess $Yb(OAc)_3$ using benzoylated dialysis tubing, as described earlier, to yield the desired product as a white solid (0.055 g, 0.028 mmol, 82 %); m.p. 191-192°C (decomposition point); MS (ES^+ in the presence of excess ammonium acetate) *m/z* 581.6 $[M + 2CH_3CO_2 - H]^{3+}$ 100 %, 872.2 $[M + 2CH_3CO_2 - 2H]^{2+}$ 5%; HRMS (ES^+) *m/z* found 869.3400 $[M + 2CH_3CO_2 - 2H]^{2+}$ $C_{78}H_{104}O_{10}N_{14}Yb_2$ requires 869.3391; HPLC (solvent system B, 4.6 x 150 mm 4 μm Phenomenex Synergi Fusion RP 80Å analytical column): t_R = 8.4 min.

Bis-7-[(1S,2R)-1,2-diphenyl-ethylcarbamoyl]-methyl-4,10-bis-[((S)-1-phenyl-ethylcarbamoyl)-methyl]-1,4,7,10-tetraaza-cyclododecane-1-carboxylic acid *tert*-butyl ester

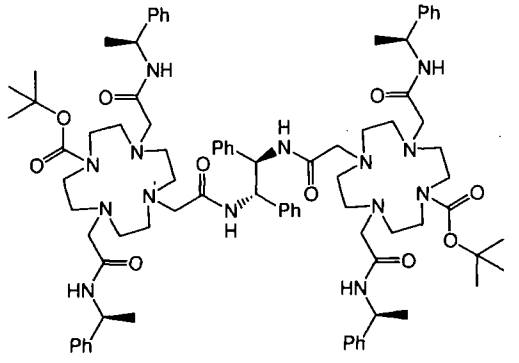

7-Carboxymethyl-4,10-bis-[((S)-1-phenyl-ethylcarbamoyl)-methyl]-1,4,7,10-tetra-aza-cyclododecane-1-carboxylic acid *tert*-butyl ester (0.070 g, 0.107 mmol), TBTU (0.034 g, 0.106 mmol), HOBt.xH_2O (0.014 g, 0.104 mmol) and NEt_3 (0.03 ml, 0.215 mmol) in MeCN (1.5 ml) were stirred, under argon, at room temperature for 15 min followed by the addition of *meso*-1,2-diphenylethylenediamine (0.011 g, 0.052 mmol). The pale yellow solution was stirred at room temperature for 24 h followed by the removal of solvent under reduced pressure. The remaining yellow residue was taken up in DCM (10 ml) to give a solution that was extracted with $HCl_{(aq)}$ (0.1 M, 20 ml), sat. $NaHCO_3$ (10 ml) then H_2O (10 ml). The organic solution was concentrated to a volume of 1 ml under reduced pressure then dripped into cold diethyl ether (15 ml). The pale yellow precipitate was collected by centrifugation then dried under reduced pressure to yield the desired product as a cream coloured powder (0.042 g, 0.028 mmol, 54 %); m.p. 92-94°C; ^{1}H-NMR ($CDCl_3$, 500 MHz) δ 7.73 (s br, 1H, amide NH), 7.14-7.29 (m br, 35H, arm and linker Ar protons and amide NH), 5.40 (m, 2H, linker CH), 5.12 (m br, 4H, arms CH), 2.25-3.23 (m br, 44H, cyclen CH_2, arms CH_2CO and linker CH_2CO), 1.46 (m br, 12H, arms CH_3), 1.41 (m br, 18H, ^{t}Bu CH_3); ^{13}C-NMR ($CDCl_3$, 125 MHz, ^{1}H decoupled 500 MHz) δ 170.6 and 170.5 (br, 6C, arms and linker C=O), 156.3 (2C, ^{t}Boc C=O), 143.5 and 138.8 (br, 6C, arms and linker $Ph_{(q)}$), 128.9, 128.5, 127.9, 126.8, 126.6 (30C, arms and linker Ph), 80.1 (2C, ^{t}Boc$_{(q)}$), 60.3, 58.0, 57.2, 54.3, 53.2, 48.7 (br, 28C, cyclen CH_2, arms CH_2, linker CH_2 and arms and linker

CH), 28.8 (6C, ^{t}Boc CH_3), 22.3, 21.7 (4C, amide arm CH_3); MS (ES^+) m/z 742.0 $[M + 2H]^{2+}$ 100 %, 1481.8 $[M + H]^+$ 5 %, 1503.8 $[M + Na]^+$ 3 %; HRMS (ES^+) m/z found 1481.9060 $[M + H]^+$ $C_{84}H_{117}O_{10}N_{14}$ requires 1481.9072.

Bis-7-[(1S,2R)-1,2-diphenyl-ethylcarbamoyl]-methyl-4,10-bis-[((S)-1-phenyl-ethylcarbamoyl)-methyl]-1,4,7,10-tetraaza-cyclododecane (L^{58})

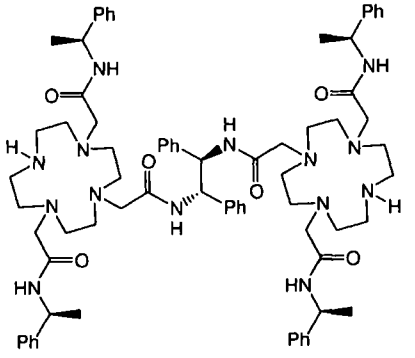

A colourless solution of bis-7-[(1S,2R)-1,2-diphenyl-ethylcarbamoyl]-methyl-4,10-bis-[((S)-1-phenyl-ethylcarbamoyl)-methyl]-1,4,7,10-tetraaza-cyclododecane-1-carboxylic acid *tert*-butyl ester (0.038 g, 0.026 mmol) in DCM/TFA (2:1, 3 ml) was stirred for 12 h in a sealed flask. The resultant yellow tinged solution was dried under reduced pressure to yield the TFA salt of the desired product, as a glassy yellow solid, in quantitative yield; ^{1}H-NMR (CD_3CN, 500 MHz) δ 7.93 (d, 1H, J=9.0 Hz, linker amide NH), 7.86 (d, 1H, J=9.0 Hz, linker amide NH), 7.00-7.59 (m, 34H, arm and linker Ar and arm NH), 5.32 (m, 2H, linker CH), 5.08 (m, 1H, amide arm CH), 4.90 (m, 1H, amide arm CH), 4.77 (m, 1H, amide arm CH), 4.66 (m, 1H, amide arm CH), 2.45-3.62 (m, 44H, cyclen CH_2, arm CH_2 and linker CH_2), 1.49, 1.44, 1.22 (m, 12H, arm CH_3); ^{13}C-NMR (CD_3CN, 125 MHz, ^{1}H decoupled 500 MHz) δ 171.2, 170.8 (4C, arms C=O), 163.6, 163.5 (2C, linker C=O), 159.7 (q, 4C, TFA C=O), 144.8, 144.3 (4C, arm $Ar_{(q)}$), 139.5, 139.2 (2C, linker $Ar_{(q)}$), 129.8, 129.5, 129.4, 129.2, 129.1, 128.1, 128.0, 127.1 (30C, arm and linker Ar), 116.4 (q, 4C, TFA CF_3), 58.8 (2C, linker CH), 47.0-56.6 (m br, 22C, cyclen CH_2, linker CH_2, arm CH), 44.0 (4C, arm CH_2), 22.9, 22.6, 22.1, 22.0 (4C, arm CH_3). MS (ES^+) m/z 641.6 $[M + 2H]^{2+}$ 100 %; HRMS (ES^+) m/z found 641.4038 $[M + 2H]^{2+}$ $C_{74}H_{102}O_6N_{14}$ requires 641.4048.

Eu(III) complex of bis-7-[(1S,2R)-1,2-diphenyl-ethylcarbamoyl]-methyl-4,10-bis-[((S)-1-phenyl-ethylcarbamoyl)-methyl]-1,4,7,10-tetraaza-cyclododecane ($[Eu_2L^{58}]^{6+}$)

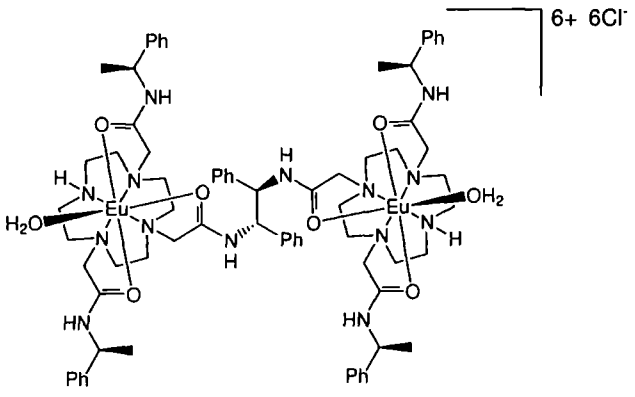

Bis-7-[(1S,2R)-1,2-diphenyl-ethylcarbamoyl]-methyl-4,10-bis-[((S)-1-phenyl-ethylcarbamoyl)-methyl]-1,4,7,10-tetraaza-cyclododecane as its TFA salt (0.019 g, 0.015 mmol, molar mass of ligand as its free base used) and $Eu(OTf)_3$ (0.053 g, 0.088 mmol) in dry MeCN (1.75 ml) were heated at reflux for 72 h, in Schlenk apparatus, under an atmosphere of argon. The solution was then cooled to room temperature followed by removal of the solvent under reduced pressure. The solid was sonicated in DCM (2 x 5 ml) followed by solid collection by centrifugation and decanting of the DCM phase, the solid was dried under reduced pressure. The resultant cream coloured solid was sonicated in ether (5 ml), the ether was then decanted followed by the drying of the remaining solid. The solid was made water soluble by the exchange of the triflate anions for chloride anions using 'DOWEX 1x8 200-400 mesh Cl' ion exchange resin as described earlier. The complex was isolated from excess $EuCl_3$ using benzoylated dialysis tubing, as described previously, to yield the desired product as a white solid (10 mg, 0.005 mmol, 33 %); MS (ES^+ in the presence of excess ammonium acetate) *m/z* 567.3 $[M + 2CH_3CO_2 - H]^{3+}$ 100 %, 850.5 $[M + 2CH_3CO_2 - 2H]^{2+}$ 50%; HRMS (ES^+) *m/z* found 849.3222 $[M + 2CH_3CO_2 - 2H]^{2+}$ $C_{78}H_{104}O_{10}N_{14}{}^{151}Eu_2$ requires 849.3223; HPLC (solvent system B, 4.6 x 150 mm 4 μm Phenomenex Synergi Fusion RP 80Å analytical column): t_R = 8.8 min.

Tb(III) complex of bis-7-[(1S,2R)-1,2-diphenyl-ethylcarbamoyl]-methyl-4,10-bis-[((S)-1-phenyl-ethylcarbamoyl)-methyl]-1,4,7,10-tetraaza-cyclododecane ($[Tb_2L^{58}]^{6+}$)

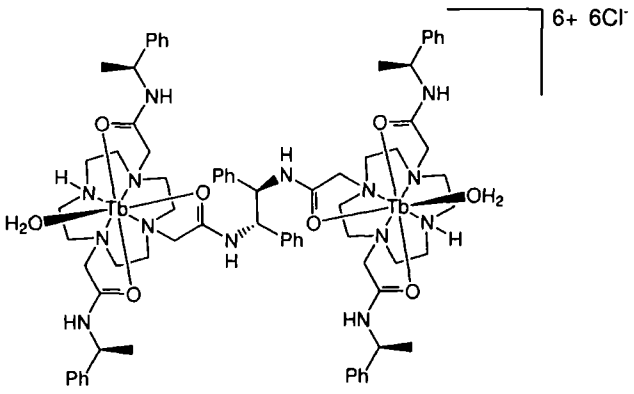

Bis-7-[(1S,2R)-1,2-diphenyl-ethylcarbamoyl]-methyl-4,10-bis-[((S)-1-phenyl-ethylcarbamoyl)-methyl]-1,4,7,10-tetraaza-cyclododecane as its TFA salt (0.008 g, 0.006 mmol, molar mass of ligand its free base used) and $TbCl_3.6H_2O$ (0.014 g, 0.037 mmol) in dry MeOH (1 ml) were heated at reflux for 48 h, in Schlenk apparatus, under an atmosphere of argon. The solution was then cooled to room temperature followed by removal of the solvent under reduced pressure. The solid was sonicated in DCM (2 x 1 ml), the DCM was each time decanted followed by the further sonication then drying of the solid under reduced pressure. The complex was isolated from excess $TbCl_3$ using benzoylated dialysis tubing, as described earlier, to yield the desired product as a white powder (0.007 g, 0.0036 mmol, 60 %); MS (ES^+ in the presence of excess ammonium acetate) *m/z* 572.3 $[M + 2CH_3CO_2 - H]^{3+}$ 83 %, 857.6 $[M + 2CH_3CO_2 - 2H]^{2+}$ 100 %; HRMS (ES^+) *m/z* found 857.3284 $[M + 2CH_3CO_2 - 2H]^{2+}$ $C_{78}H_{104}O_{10}N_{14}{}^{159}Tb_2$ requires 857.3278; HPLC (solvent system B, 4.6 x 150 mm 4 μm Phenomenex Synergi Fusion RP 80Å analytical column): t_R = 8.9 min.

Yb(III) complex of bis-7-[(1S,2R)-1,2-diphenyl-ethylcarbamoyl]-methyl-4,10-bis-[((S)-1-phenyl-ethylcarbamoyl)-methyl]-1,4,7,10-tetraaza-cyclododecane ($[Yb_2L^{58}]^{6+}$)

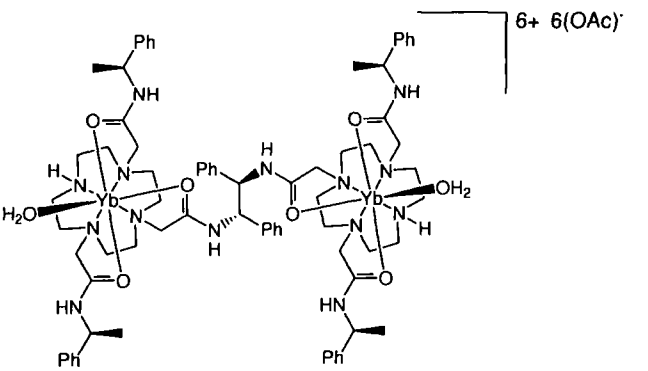

Bis-7-[(1S,2R)-1,2-diphenyl-ethylcarbamoyl]-methyl-4,10-bis-[((S)-1-phenyl-ethylcarbamoyl)-methyl]-1,4,7,10-tetraaza-cyclododecane as its TFA salt (0.063 g, 0.049 mmol, molar mass of ligand its free base used) and $Yb(OAc)_3.4H_2O$ (0.123 g, 0.29 mmol) in MeOH:H_2O (2 ml, 50:50) were heated at reflux for 48 h, in Schlenk apparatus, under an atmosphere of argon. The solution was allowed to cool to room temperature followed by removal of the solvent under reduced pressure. The complex was isolated from excess $Yb(OAc)_3$ using benzoylated dialysis tubing, as described earlier, to yield the desired product as a white solid (0.065 g, 0.031 mmol, 64 %); m.p. 196-197°C (decomposition point); MS (ES^+ in the presence of excess ammonium acetate) *m/z* 581.6 $[M + 2CH_3CO_2 - H]^{3+}$ 100 %, 872.0 $[M + 2CH_3CO_2 - 2H]^{2+}$ 15%; HRMS (ES^+) *m/z* found 869.3392 $[M + 2CH_3CO_2 - 2H]^{2+}$ $C_{78}H_{104}O_{10}N_{14}Yb_2$ requires 869.3391; HPLC (solvent system B, 4.6 x 150 mm 4 μm Phenomenex Synergi Fusion RP 80Å analytical column): t_R = 8.7 min.

5.2.3 Solid phase supported complex

N-[(S)-1-(4-Bromo-phenyl)-ethyl]-2,2,2-trifluoro-acetamide[134]

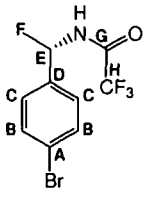

(S)-(-)-α-methylbenzylamine (13.4 ml, 105.3 mmol) in CH_2Cl_2 (25 ml) was added dropwise to a stirring solution of trifluoroacetic anhydride (14.8 ml, 106.5 mmol) in CH_2Cl_2 (70 ml), under argon, at 0°C. After the addition was complete the solution was allowed to warm to room temperature then stirred for a further 3 h. The solution was further cooled to 0°C followed by the addition of 70% methanesulfonic acid (22.9 ml, 314.3 mmol) then 1,3-dibromo-5,5-dimethylhydantoin (15 g, 52.5 mmol). The suspension was allowed to warm to room temperature then stir for 18 h to yield a bright orange solution that was washed with aq. $NaHSO_3$ solution (1 M, 700 ml) then H_2O (500 ml). The resultant colourless organic layer was evaporated to dryness under reduced pressure to yield a crude white product that was twice recrystallised from diethyl ether/hexane to yield the desired product as white needle-like crystals (7.2 g, 24.3 mmol, 23 %); m.p. 154-156°C (Lit.[146] 153-155°C); ^{1}H-NMR ($CDCl_3$, 700 MHz) δ 7.51 (d, 2H, J=7.5 Hz, H_B), 7.20 (d, 2H, J=8.5 Hz, H_C), 6.38 (s br, 1H, NH), 5.11 (m, 1H, H_E), 1.58 (d, 3H, J=7.0 Hz, H_F); ^{13}C-NMR ($CDCl_3$, 175 MHz, ^{1}H decoupled 700 MHz) δ 156.8 (1C, C_G), 140.3 (1C, C_D), 132.5 (2C, C_B), 128.3 (2C, C_C), 122.5 (1C, C_A), 49.6 (1C, C_E), 21.4 (1C, C_F); ^{19}F-NMR ($CDCl_3$, 658 MHz) δ -75.9 (3F, CF_3); MS (ES^+) m/z 318.1 $[M + Na]^+$ 100 %; HRMS (ES^+) m/z found 317.9713 $[M + Na]^+$ $C_{10}H_9ON^{79}BrF_3{}^{23}Na$ requires 317.9712; $C_{10}H_9BrF_3NO$ (%): calcd C 40.57, H 3.06, N 4.73; found C 40.47, H 3.03, N 4.67.

N-[(S)-1-(4-Cyano-phenyl)-ethyl]-2,2,2-trifluoro-acetamide

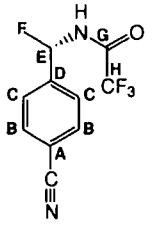

CuCN (1.46 g, 16.3 mmol) was added to a stirring solution of N-[(S)-1-(4-bromo-phenyl)-ethyl]-2,2,2-trifluoro-acetamide (3.72 g, 12.56 mmol) in anhydrous DMF (15 ml) followed by the reflux of the resultant mixture at 150°C for 96 h. The resultant dark green solution was left to cool to room temperature followed by removal of solvent under reduced pressure. The crude residue was taken up in DCM (100 ml) then washed with aq. HCl (1 M, 2 x 100 ml), sodium bisulfite solution (1 M, 100 ml) then H_2O (100 ml). The organic layer was dried under reduced pressure to leave the desired product as a crystalline brown solid (2.13 g, 8.79 mmol, 70 %); m.p. 98-99°C; ^{1}H-NMR ($CDCl_3$, 500 MHz) δ 7.68 (d, 2H, J=6.5 Hz, H_B), 7.43 (d, 2H, J=8.0 Hz, H_C), 6.56 (s br, 1H, NH), 5.16 (m, 1H, H_E), 1.60 (d, 3H, J=7.5 Hz, H_F); ^{13}C-NMR ($CDCl_3$, 125 MHz, ^{1}H decoupled 500 MHz) δ 156.7 (1C, C_G), 146.6 (1C, C_D), 133.2 (2C, C_B), 127.2 (2C, C_C), 118.7 (1C, -CN), 112.4 (1C, C_A), 49.9 (1C, C_E), 21.5 (1C, C_F); ^{19}F-NMR ($CDCl_3$, 470 MHz, ^{1}H decoupled 500 MHz) δ -76.1 (3F, CF_3); MS (ES^-) m/z 241.1 $[M - H]^-$ 100 %; HRMS (ES^-) m/z found 241.0594 $[M - H]^-$ $C_{11}H_8ON_2F_3$ requires 241.0594; $C_{11}H_9F_3N_2O$ (%): calcd C 54.55, H 3.75, N 11.57; found C 54.48, H 3.85, N 11.65.

(*S*)-*N*-Ethanoyl-1-(4-bromophenyl)ethylamine[68]

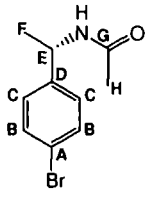

Acetyl chloride (0.231 ml, 3.25 mmol) was added dropwise to a vigorously stirring anhydrous solution of *S*-(-)-1-(4-bromophenyl)ethylamine (0.365 ml, 2.50 mmol) and NEt_3 (0.452 ml, 3.25 mmol) in diethyl ether (30 ml) at -10°C. The solution was allowed to warm to room temperature then stir for a further 2 h. The resultant cloudy white mixture was washed with H_2O (100 ml) then $HCl_{(aq)}$ (0.1 M, 30 ml), the ether layer was separated, dried with sodium sulfate then evaporated under reduced pressure to leave the desired product as a white solid (0.606 g, 2.50 mmol, 100 %). A small amount of product recrystallised from diethyl ether for characterisation purposes was isolated as white needle-like crystals; m.p. 127-129°C (Lit.[68] 127-130°C); ^{1}H-NMR ($CDCl_3$, 400 MHz) δ 7.45 (dd, 2H, J=6.5, 1.5 Hz, H_B), 7.19 (dd, 2H, J=6.5, 2.5 Hz, H_C), 5.64 (s br, 1H, NH), 5.08 (m, 1H, H_E), 1.96 (s, 3H, H_H), 1.46 (d, 3H, J=7.0 Hz, H_F); ^{13}C-NMR ($CDCl_3$, 100 MHz, ^{1}H decoupled 400 MHz) δ 169.3 (1C, C_G), 142.5 (1C, C_D), 132.0 (2C, C_B), 128.2 (2C, C_C), 121.4 (1C, C_A), 48.5 (1C, C_E), 23.7 (1C, C_H), 21.9 (1C, C_F); MS (ES^+) m/z 264.0 $[M + Na]^+$ 15 %, 296.0 $[M + Na + MeOH]^+$ 100 %; HRMS (ES^+) m/z found 263.9994 $[M + Na]^+$ $C_{10}H_{12}ON^{79}Br^{23}Na$ requires 263.9995; $C_{10}H_{12}BrNO$ (%): calcd C 49.61, H 5.00, N 5.79; found C 49.48, H 4.98, N 5.52.

(*S*)-*N*-Ethanoyl-1-(4-cyanophenyl)ethylamine[68]

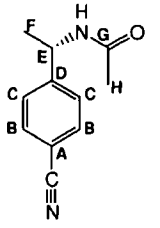

CuCN (0.29 g, 3.24 mmol) was added to a stirring solution of (*S*)-*N*-ethanoyl-1-(4-bromophenyl)ethylamine (0.606 g, 2.50 mmol) in anhydrous DMF (30 ml) followed by the reflux of the resultant mixture at 150°C for 96 h. The resultant dark green solution was left to cool to room temperature followed by the addition of $HCl_{(aq)}$ (6M, 40 ml) in a well ventilated fumehood. The resulting solution was extracted with DCM (2 x 20 ml) followed by washing of the obtained organic phase with H_2O (2 x 30 ml). The organic layer was dried under reduced pressure followed by recrystallisation of the crystalline brown solid obtained from ethyl acetate/hexane to give the desired product as rectangular white crystals (0.228 g, 1.21 mmol, 48 %); m.p. 188-190°C (Lit.[68] 187-189°C); ^{1}H-NMR ($CDCl_3$, 500 MHz) δ 7.64 (dd, 2H, J=6.5, 1.5 Hz, H_B), 7.42 (d, 2H, J=8.5 Hz, H_C), 5.71 (s br, 1H, NH), 5.14 (m, 1H, H_E), 2.03 (s, 3H, H_H), 1.48 (d, 3H, J=7.0 Hz, H_F); ^{13}C-NMR ($CDCl_3$, 125 MHz, ^{1}H decoupled 500 MHz) δ 169.6 (1C, C_G), 149.1 (1C, C_D), 132.9 (2C, C_B), 127.2 (2C, C_C), 119.1 (1C, -CN), 111.5 (1C, C_A), 49.0 (1C, C_E), 23.7 (1C, C_H), 21.9 (1C, C_F); MS (ES^+) m/z 189.1 $[M + H]^+$ 65 %; HRMS (ES^+) m/z found 189.1023 $[M + H]^+$ $C_{11}H_{13}ON_2$ requires 189.1022; $C_{11}H_{12}N_2O$ (%): calcd C 70.19, H 6.43, N 14.88; found C 70.05, H 6.49, N 15.00.

(*S*)-4-(1-Aminoethyl)benzoic acid[68]

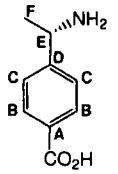

A solution of (*S*)-*N*-ethanoyl-1-(4-cyanophenyl)ethylamine (0.228 g, 1.21 mmol) in $HCl_{(aq)}$ (6M, 50 ml) was heated at reflux for 96 h. The solution was left to cool then solvent was removed under reduced pressure to leave the hydrochloride salt of the desired product, as an off-white crystalline solid, in quantitative yield. ^{1}H-NMR (D_2O, 500 MHz) δ 7.86 (dd, 2H, J=7.0, 2.0 Hz, H_B), 7.37 (dd, 2H, J=6.5, 1.5 Hz, H_C), 4.48 (q, 1H, J=7.0 Hz, H_E), 1.52 (d, 3H, J=7.0 Hz, H_F); ^{13}C-NMR (D_2O, 125 MHz, ^{1}H decoupled 500 MHz) δ 170.2 (1C, CO_2H), 143.1 (1C, C_D), 132.3 (1C, C_A), 130.6 (2C, C_B), 126.9 (2C, C_C), 50.8 (1C, C_E), 19.4 (1C, C_F); MS (ES^-) *m/z* 164.4 $[M - H]^-$ 100 %; HRMS (ES^-) *m/z* found 164.0715 $[M - H]^-$ $C_9H_{10}O_2N$ requires 164.0717.

(*S*)-4-(1-Aminoethyl)benzoic acid was also obtained via the reflux of *N*-[(S)-1-(4-cyano-phenyl)-ethyl]-2,2,2-trifluoro-acetamide (2.13 g, 8.79 mmol) in $HCl_{(aq)}$ (6M, 50 ml) for 72 h. The solution was allowed to cool, filtered then dried under reduced pressure to leave the hydrochloride salt of the desired product in quantitative yield. Spectral properties of the product were identical to those reported in the above method.

(*S*)-Methyl-4-(1-aminoethyl)benzoate (59)[68]

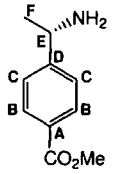

Concentrated $HCl_{(aq)}$ (12M, 2.5 ml) was added dropwise to a solution of the hydrochloride salt of (*S*)-4-(1-aminoethyl)benzoic acid (0.243 g, 1.21 mmol) in anhydrous methanol (15 ml) and heated at reflux, under argon, for 24 h. The solution was allowed to cool to room temperature then dried under reduced pressure to leave the desired product, as its hydrochloride salt, in quantitative yield. ^{1}H-NMR (CD_3OD, 400 MHz) δ 8.10 (d, 2H, J=8.5 Hz, H_B), 7.59 (dd, 2H, J=9.0, 0.5 Hz, H_C), 4.56 (q, 1H, J=7.0 Hz, H_E), 3.92 (s, 3H, OMe), 1.66 (d, 3H, J=7.0 Hz, H_F); ^{13}C-NMR (CD_3OD, 100 MHz, ^{1}H decoupled 400 MHz) δ 168.6 (1C, CO_2Me), 145.4 (1C, C_D), 132.8 (1C, C_A), 132.1 (2C, C_B), 128.8 (2C, C_C), 53.6 (1C, OMe), 52.7 (1C, C_E), 21.4 (1C, C_F); MS (ES^+) m/z 180.0 $[M + H]^+$ 100 %; HRMS (ES^+) m/z found 180.1019 $[M + H]^+$ $C_{10}H_{14}O_2N$ requires 180.1019.

7-([(S)-1-(4-Methoxycarbonyl-phenyl)-ethylcarbamoyl]-methyl)-4,10-bis-[((S)-1-phenyl-ethylcarbamoyl)-methyl]-1,4,7,10-tetraaza-cyclododecane-1-carboxylic acid *tert*-butyl ester (60)

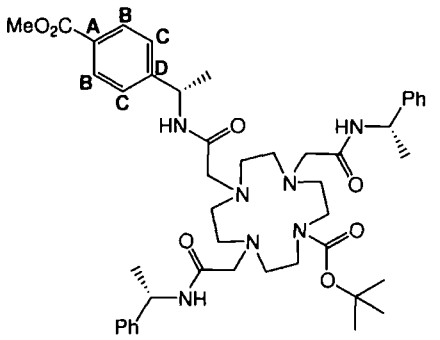

A solution of 7-carboxymethyl-4,10-bis-[((S)-1-phenyl-ethylcarbamoyl)-methyl]-1,4,7,10-tetraaza-cyclododecane-1-carboxylic acid *tert*-butyl ester (0.164 g, 0.267 mmol), EDC.HCl (0.056 g, 0.292 mmol), HOBt.H_2O (20 mg) and NEt_3 (0.11 ml, 0.789 mmol) in chloroform (10 ml) was stirred for 20 minutes at room temperature. (*S*)-Methyl-4-(1-aminoethyl)benzoate (0.057 g, 0.318 mmol) in chloroform (2 ml) was then added to form a yellow tinged solution that was stirred for a further 12 hours. The resultant solution was extracted with sat. $NaHCO_3$ solution (10 ml) then H_2O (30 ml) followed by drying of the organic phase under reduced pressure to leave a yellow tinged glassy residue. The desired product was isolated from the crude solid by column chromatography (alumina using a DCM/MeOH solvent system starting from 100 % DCM then increasing the volume of MeOH by 0.1 % every 100 ml thereafter) to yield the desired product as a clear glassy solid (167 mg, 0.205 mmol, 77 %); R_F (Alumina, DCM-MeOH, 98.5:1.5) : 0.51; m.p. 43-46°C; ^{1}H-NMR ($CDCl_3$, 500 MHz) δ 7.93 (d, 2H, J=8.5 Hz, H_B), 7.21-7.30 (m, 13H, H_C, arm Ar and linker amide NH), 6.99 (s br, 2H, arm amide NH), 5.10 (m, 3H, arm and linker CH), 3.87 (s, 3H, OMe), 2.36-3.26 (m br, 22H, cyclen, linker and arm CH_2), 1.46 (d, 6H, J=7.0 Hz, amide arm CH_3), 1.43 (d, 3H, J=7.0 Hz, linker CH_3), 1.39 (s, 9H, ^{t}Bu CH_3); ^{13}C-NMR ($CDCl_3$, 125 MHz, ^{1}H decoupled 500 MHz) δ 170.4, 170.2, 169.9 (3C, arm and linker amide C=O), 167.0 (1C, methyl ester C=O), 156.1 (1C, ^{t}Bu C=O), 148.7 (1C, C_D), 143.9, 143.3 (2C, arm $Ar_{(q)}$), 130.3 (2C, C_B), 129.5 (1C, C_A), 129.0, 128.9, 127.9, 127.5, 126.8 (10C, arm Ar), 126.6 (2C, C_C), 80.2 ($^tBu_{(q)}$),

59.7, 58.9 (2C, amide arm CH_2), 57.8 (1C, linker CH_2), 54.1, 53.9, 53.2 (br, 8C, cyclen CH_2), 52.5 (1C, OMe), 48.5, 48.1, 47.8 (3C, amide arm and linker CH), 28.8 (3C, ^{t}Bu CH_3), 22.2, 21.7 (3C, amide arm and linker CH_3); MS (ES^+) *m/z* 814.5 $[M + H]^+$ 100 %. HRMS (ES^+) *m/z* found 814.4870 $[M + H]^+$ $C_{45}H_{64}O_7N_7$ requires 814.4862.

4-[(S)-1-(2-(4,10-Bis-[((S)-1-phenyl-ethylcarbamoyl)-methyl]-1,4,7,10-tetraaza-cyclododec-1-yl)-acetylamino)-ethyl]-benzoic acid methyl ester (L^{61})

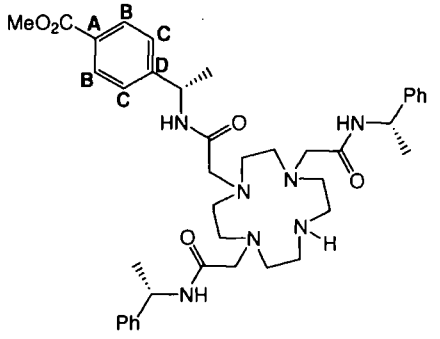

A solution of 7-([(S)-1-(4-methoxycarbonyl-phenyl)-ethylcarbamoyl]-methyl)-4,10-bis-[((S)-1-phenyl-ethylcarbamoyl)-methyl]-1,4,7,10-tetraaza-cyclododecane-1-carboxylic acid *tert*-butyl ester (114 mg, 0.160 mmol) in DCM:TFA (3 ml, 50:50) was left to stir, in a sealed flask at room temperature, for 12 hours. The resultant solution was dried under reduced pressure to leave the TFA salt of the desired product, as a colourless glassy solid, in quantitative yield; ^{1}H-NMR (CD_3CN, 500 MHz) δ 7.95 (d, 2H, J=8.5 Hz, H_B), 7.81 (d, 1H, J=7.5 Hz, linker amide NH), 7.41 (d, 2H, J=8.0 Hz, H_C), 7.23-7.30 (m, 12H, amide arms Ar and NH), 4.97 (m, 3H, arm and linker CH), 3.84 (s, 3H, OMe), 2.84-3.38 (m br, 22H, cyclen, linker and arm CH_2), 1.38-1.41 (m, 9H, arm and linker CH_3); ^{13}C-NMR (CD_3CN, 125 MHz, ^{1}H decoupled 500 MHz) δ 171.0, 170.5 (2C, arm amide C=O), 167.4 (1C, methyl ester C=O), 164.1 (1C, linker amide C=O), 160.7 (q, 1C, TFA C=O), 149.7 (1C, C_D), 144.8, 144.6 (2C, amide arm $Ar_{(q)}$), 130.6 (2C, C_B), 130.2 (1C, C_A), 129.5, 129.4, 128.1, 128.0, 127.0 (10C, amide arm Ar), 127.2 (2C, C_C), 115.9 (q, 1C, TFA CF_3), 56.4, 55.8 (2C, amide arm CH_2), 55.4 (1C, linker CH_2), 53.0, 50.9, 50.4, 49.9,

49.7, 49.3 (11C br, cyclen CH_2 and arm and linker CH), 52.7 (1C, OMe), 22.6, 22.3 (3C, arm and linker CH_3); MS (ES^+) *m/z* 714.5 $[M + H]^+$ 100 %; HRMS (ES^+) *m/z* found 714.4346 $[M + H]^+$ $C_{40}H_{56}O_5N_7$ requires 714.4337.

Eu(III) complex of 4-[(S)-1-(2-(4,10-bis-[((S)-1-phenyl-ethylcarbamoyl)-methyl]-1,4,7,10-tetraaza-cyclododec-1-yl)-acetylamino)-ethyl]-benzoic acid methyl ester ($[EuL^{61}]^{3+}$)

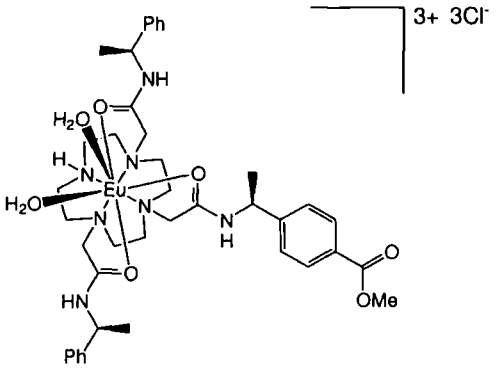

A solution of 4-[(S)-1-(2-(4,10-bis-[((S)-1-phenyl-ethylcarbamoyl)-methyl]-1,4,7,10-tetraaza-cyclododec-1-yl)-acetylamino)-ethyl]-benzoic acid methyl ester as its TFA salt (115 mg, 0.139 mmol) and $Eu(OTf)_3$ (74 mg, 0.124 mmol) in MeCN (1 ml) was heated at reflux, under argon, for 48 hours. The resultant yellow solution was dried under reduced pressure to leave a yellow glassy solid. DCM (2 ml) was added to the solid and the mixture sonicated for 5 minutes followed by the decanting of solvent, this procedure was repeated followed by the drying of the resultant solid to yield the triflate salt of the desired product as a pale brown powder (109 mg, 0.081 mmol, 65 %). The complex was further obtained as its chloride salt by the stirring of the triflate salt in a H_2O:MeOH solution (5 ml, 50:50) containing Dowex 1x8 200-400 mesh Cl ion exchange resin, as described earlier, to yield the desired chloride salt as a white powder (74 mg, 0.073 mmol, 90 %); m.p. (chloride salt) >250°C; ^{1}H-NMR (as tri-chloride salt, D_2O, 500 MHz, partial data and assignment) δ 26.8 (1H, NH), 17.7 (1H, H_{ax}), 15.2 (1H, H_{ax}), 11.3 (1H, H_{ax}), 10.7 (1H, H_{ax}), -3.3 (1H), -3.9 (1H), -4.4 (1H), -4.8 (1H), -5.2 (1H), -5.3 (1H), -7.4 (1H), -9.0 (1H), -9.8 (1H), -10.2 (1H), -11.3 (1H), -13.9 (1H), -14.1 (1H), -15.5 (1H), -15.8 (1H), -18.8 (1H); MS (ES^+) (as triflate salt) *m/z* 1014.4 $[M - H + CF_3SO_3]^+$ 100 %, 1164.4 $[M + 2CF_3SO_3]^+$ 10 %

(cone-voltage of 90V), 488.7 $[M + CF_3CO_2]^{2+}$ 75 %, 507.7 $[M + CF_3SO_3]^{2+}$ 100 %, 1014.5 $[M - H + CF_3SO_3]^+$ 15 %, 1128.5 $[M + CF_3SO_3 + CF_3CO_2]^+$ 85 %, 1164.5 $[M + 2CF_3SO_3]^+$ 90 % (cone-voltage of 30V); HRMS (ES^+) *m/z* found 1164.2542 $[M + 2CF_3SO_3]^+$ $C_{42}H_{55}O_{11}EuN_7F_6S_2$ requires 1164.2512; $\tau_{(H_2O)}$: 0.28 ms, $\tau_{(D_2O)}$: 0.61 ms; HPLC (solvent system B, 4.6 x 150 mm 4 μm Phenomenex Synergi Fusion RP 80Å analytical column): t_R = 10.5 min.

7-([(S)-1-(4-Carboxy-phenyl)-ethylcarbamoyl]-methyl)-4,10-bis-[((S)-1-phenyl-ethylcarbamoyl)-methyl]-1,4,7,10-tetraaza-cyclododecane-1-carboxylic acid *tert*-butyl ester

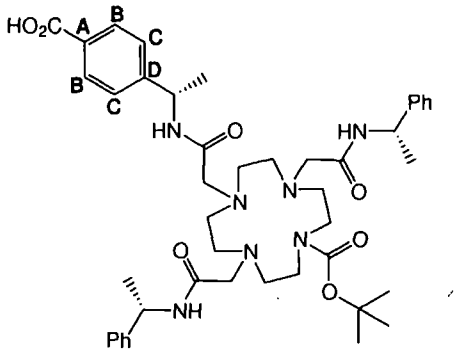

7-([(S)-1-(4-Methoxycarbonyl-phenyl)-ethylcarbamoyl]-methyl)-4,10-bis-[((S)-1-phenyl-ethylcarbamoyl)-methyl]-1,4,7,10-tetraaza-cyclododecane-1-carboxylic acid *tert*-butyl ester (40 mg, 0.049 mmol) and $LiOH.H_2O$ (6 mg, 0.143 mmol) were dissolved in H_2O:MeOH (50:50, 4 ml) and heated at reflux for 12 h with vigorous stirring. The solution was allowed to cool then MeOH was removed under reduced pressure, the pH of the remaining aqueous phase was adjusted to 7 with dilute $HCl_{(aq)}$ followed by extraction with $CHCl_3$ (3 x 10 ml). The combined organic extracts were dried under reduced pressure to leave the desired product as a white glassy solid (39 mg, 0.049 mmol, 100 %); ^{1}H-NMR ($CDCl_3$, 500 MHz) δ 7.86 (d, 2H, J=6.0 Hz, H_B), 7.43 (d, 2H, J=7.0 Hz, H_C), 7.23-7.35 (m, 12H, amide arms Ar and NH), 5.77 (s br, 1H, acid arm NH), 5.14 (m, 1H, acid arm CH), 4.98 (m, 2H, amide arms CH), 2.91-3.70 (m br, 22H, cyclen and arms CH_2), 1.50 (d, 9H, J=7.0 Hz, acid arm and amide arms CH_3), 1.40 (s, 9H, ^{t}Bu CH_3); ^{13}C-NMR ($CDCl_3$, 125 MHz, ^{1}H decoupled 500 MHz) δ 168.9, 167.5 (3C, acid and amide arm amide C=O),

156.0 (1C, ^{t}Bu C=O), 143.9 (2C, amide arm $Ar_{(q)}$), 143.4 (1C, C_D), 130.6 (2C, C_B), 129.0 (1C, C_A), 128.9, 127.8, 126.5 (10C, arm Ar), 126.7 (2C, C_C), 81.5 ($^tBu_{(q)}$), 56.7, 53.8 (br, 8C, cyclen CH_2), 49.8 (2C, amide arms CH), 49.2 (1C, acid arm CH), 46.7 (3C, acid and amide arm CH_2), 28.7 (3C, ^{t}Bu CH_3), 22.6 (2C, amide arm CH_3), 22.0 (1C, acid arm CH_3); MS (ES^-) *m/z* 797.6 $[M - H]^-$ 100 %, 833.5 $[M + Cl]^-$ 60 %. HRMS (ES^+) *m/z* found 800.4690 $[M + H]^+$ $C_{44}H_{62}O_7N_7$ requires 800.4705.

4-[(S)-1-(2-(4,10-Bis-[((S)-1-phenyl-ethylcarbamoyl)-methyl]-1,4,7,10-tetraaza-cyclododec-1-yl)-acetylamino)-ethyl]-benzoic acid (L^{62})

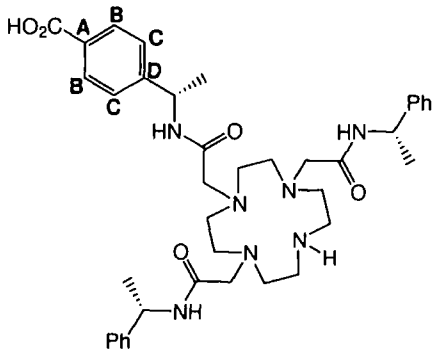

A solution of 7-([(S)-1-(4-carboxy-phenyl)-ethylcarbamoyl]-methyl)-4,10-bis-[((S)-1-phenyl-ethylcarbamoyl)-methyl]-1,4,7,10-tetraaza-cyclododecane-1-carboxylic acid *tert*-butyl ester (41 mg, 0.051 mmol) in DCM:$CHCl_3$:TFA (1:1:1, 3ml) was stirred in a sealed flask overnight at room temperature. The resulting yellow tinged solution was dried under reduced pressure to yield the TFA salt of the desired product, as a colourless glassy solid, in quantitative yield. ^{1}H-NMR (CD_3CN, 500 MHz) δ 8.31 (s br, 1H, acid arm NH), 8.00 (d, 2H, J=8.5 Hz, H_B), 7.60, 7.55 (s br, 2H, amide arms NH), 7.45 (d, 2H, J=8.0 Hz, H_C), 7.27-7.39 (m, 10H, amide arms Ar), 5.02 (m, 3H, acid and amide arm CH), 3.82 (m, 2H, acid arm CH_2), 2.92-3.40 (m br, 20H, cyclen and amide arm CH_2), 1.47 (d, 3H, J=7.0 Hz, acid arm CH_3), 1.43 (d, 6H, J=7.0 Hz, amide arm CH_3); ^{13}C-NMR (CD_3CN, 125 MHz, ^{1}H decoupled 500 MHz) δ 171.3, 170.8, 170.5 (3C, acid and amide arm amide C=O), 168.1 (1C, COOH), 161.0 (q, 1C, TFA C=O), 149.7 (1C, C_D), 144.6 (2C, amide arm $Ar_{(q)}$), 130.9 (2C, C_B), 130.3 (1C, C_A), 129.5, 128.1, 127.1 (10C, amide arm Ar), 127.8 (2C, C_C), 115.9 (q, 1C, TFA CF_3), 56.7, 56.3 (2C, amide arm CH_2), 55.3 (1C, acid arm

CH_2), 53.0, 51.2 (8C br, cyclen CH_2), 50.5, 50.0, 49.8 (3C, acid and amide arm CH), 22.9, 22.7, 22.3 (3C, arm and linker CH_3); MS (ES^+) *m/z* 381.9 $[M + Cu]^{2+}$ 100 %, 700.4 $[M + H]^+$ 40 %; HRMS (ES^+) *m/z* found 700.4171 $[M + H]^+$ $C_{39}H_{54}O_5N_7$ requires 700.4181.

Eu(III) complex of 4-[(S)-1-(2-(4,10-bis-[((S)-1-phenyl-ethylcarbamoyl)-methyl]-1,4,7,10-tetraaza-cyclododec-1-yl)-acetyl-amino)-ethyl]-benzoic acid ($[EuL^{62}]^{2+}$)

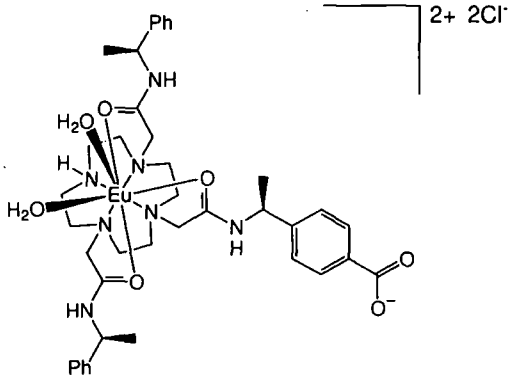

A solution of 4-[(S)-1-(2-(4,10-bis-[((S)-1-phenyl-ethylcarbamoyl)-methyl]-1,4,7,10-tetraaza-cyclododec-1-yl)-acetylamino)-ethyl]-benzoic acid as its TFA salt (115 mg, 0.141 mmol) and $Eu(OTf)_3$ (70 mg, 0.115 mmol) in MeCN (3 ml) was heated at reflux, under argon, for 48 h. The resultant yellow tinged solution was dried under reduced pressure to leave a yellow glassy solid. DCM (2 ml) was added to the solid and the mixture sonicated for 5 minutes followed by the decanting of solvent, this procedure was repeated with DCM then diethyl ether (3 ml) followed by the drying of the resultant solid to yield the triflate salt of the desired product as a pale brown powder. The solid was made water soluble by the exchange of triflate anions for chloride anions using DOWEX 1x8 200-400 mesh Cl ion exchange resin, as described earlier, to yield the complex as its chloride salt (100 mg, 0.101 mmol, 88 %); ^{1}H-NMR (as tri-chloride salt, D_2O, 500 MHz, partial data and assignment) δ 26.9 (1H, NH), 17.9 (1H, H_{ax}), 15.3 (1H, H_{ax}), 11.4 (1H, H_{ax}), 10.7 (1H, H_{ax}), 7.6 (1H), -3.2 (1H), -4.1 (1H), -4.6 (1H), -4.8 (1H), -5.2 (1H), -5.4 (1H), -7.4 (1H), -9.1 (1H), -9.9 (1H), -10.3 (1H), -11.3 (1H), -13.9 (1H), -14.3 (1H), -15.6 (1H), -16.0 (1H), -18.9 (1H); MS (ES^+) (in the presence of excess ammonium acetate) *m/z* 455.9 [M

+ $CH_3CO_2]^{2+}$ 100 %, 910.3 [M + CH_3CO_2 - H]$^+$ 5 %; HRMS (ES$^+$) *m/z* found 908.3371 [M + CH_3CO_2 - H]$^+$ $C_{41}H_{55}O_7N_7{}^{151}Eu$ requires 908.3356.

Eu(III) complex of 4-[(S)-1-(2-(4,10-Bis-[((S)-1-phenyl-ethylcarbamoyl)-methyl]-1,4,7,10-tetraaza-cyclododec-1-yl)-acetyl-amino)-ethyl]-benzoic acid 2,5-dioxo-pyrrolidin-1-yl ester

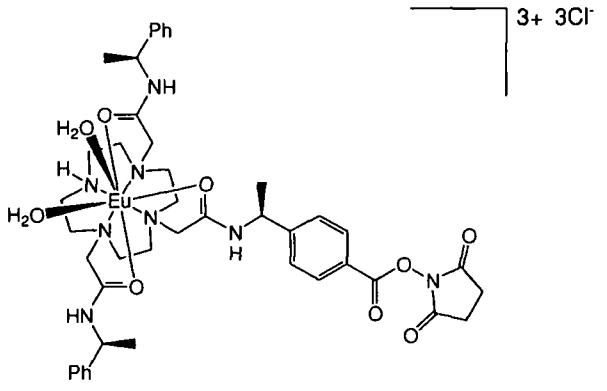

Eu(III) complex of 4-[(S)-1-(2-(4,10-Bis-[((S)-1-phenyl-ethylcarbamoyl)-methyl]-1,4,7,10-tetraaza-cyclododec-1-yl)-acetylamino)-ethyl]-benzoic acid (20 mg, 0.02 mmol), TBTU (8 mg, 0.025 mmol) and NEt_3 (0.006 ml, 0.043 mmol) in anhydrous DMF (0.5 ml) were stirred for 10 min followed by the addition of NHS (3 mg, 0.026 mmol). The solution was stirred for 12 h under argon followed by removal of solvent under reduced pressure. The residue was taken up in anhydrous MeCN (0.5 ml) followed by precipitation of the crude desired product by the addition of anhydrous diethyl ether (5 ml). The solid was isolated by centrifugation then dried under reduced pressure; MS (ES$^+$) *m/z* 497.4 [M + $CHCO_2]^{2+}$ 90 %, 993.3 [M + $CHCO_2$ - H]$^+$ 10 %; HRMS (ES$^+$) *m/z* found 496.1719 [M + $CHCO_2]^{2+}$ $C_{44}H_{57}O_9N_8{}^{151}Eu$ requires 496.1718.

Acetic acid 2,5-dioxo-pyrrolidin-1-yl ester

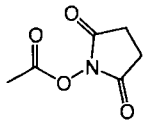

N-Hydroxysuccinimide (1.33 g, 11.56 mmol) was transferred to stirring dry DCM

(10 ml) followed by the addition of dry NEt_3 (3.23 ml, 23.17 mmol) to form a homogenous solution. Acetyl chloride (1.07 ml, 15.05 mmol) was then added dropwise over 5 min to form a yellow tinged solution. The mixture was stirred for 2 h followed by washing of the reaction solution with H_2O (2 x 5 ml). The organic phase was dried under reduced pressure to leave a yellow tinged solid. The solid was recrystallised from ethyl acetate/hexane to yield the desired product as a white solid (1.02 g, 6.49 mmol, 56 %); m.p. 132-134°C (Lit.[147] 131-134°C); ^{1}H-NMR (CD_3CN, 700 MHz) δ 2.76 (s, 4H, NHS CH_2), 2.30 (s, 3H, CH_3); ^{13}C-NMR (CD_3CN, 175 MHz, ^{1}H decoupled 700 MHz) δ 171.1 (2C, NHS C=O), 167.3 (1C, ester C=O), 26.4 (2C, NHS CH_2), 17.7 (1C, CH_3); MS (EI) *m/z* 42.9 $[CH_3CO]^+$ 100%, 156.9 $[M]^+$ 5 %.

Solid phase supported Eu(III) complex of 4-[(S)-1-(2-(4,10-Bis-[((S)-1-phenyl-ethylcarbamoyl)-methyl]-1,4,7,10-tetraaza-cyclododec-1-yl)-acetylamino)-ethyl]-benzoic acid

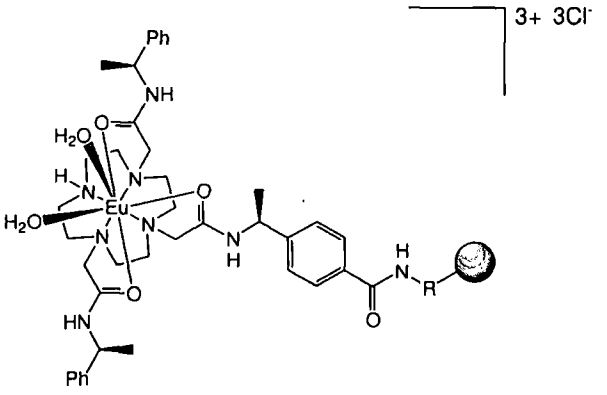

Affi-Gel® 102 bound complex

Affi-Gel® 102 (5 ml) was poured into an eppendorf followed by H_2O removal from the sample by centrifugation. The remaining gel was thrice washed with H_2O (5 ml) followed by centrifugation and solvent removal. H_2O (10 ml) was added to the remaining solid and the suspension was thoroughly vortex mixed, Eu(III) complex of 4-[(S)-1-(2-(4,10-bis-[((S)-1-phenyl-ethylcarbamoyl)-methyl]-1,4,7,10-tetraaza-cyclododec-1-yl)-acetylamino)-ethyl]-benzoic acid (56 mg, 0.056 mmol) was added to the resultant gel followed by immediate pH adjustment to 4.8 with dilute $KOH_{(aq)}$ solution. EDC.HCl (24 mg, 0.125 mmol) was added to the gel followed by vortex mixing,

the pH was immediately adjusted to 5 with dilute $HCl_{(aq)}$ solution. The gel was left mixing end over end for 12 h. The reaction solvent was removed by centrifugation and dried under reduced pressure, analysis showed unreacted complex was present. The dried solvent layer was redissolved in H_2O (10 ml) and added to the remaining solid followed by vortex mixing. EDC.HCl (50 mg, 0.261 mmol) was added to the gel followed by immediate pH adjustment to 4.8, the reaction was left stirring end over end. After 12 h the solvent was removed by centrifugation, the remaining solid was washed thrice with H_2O (10 ml) that was also removed by centrifugation. The remaining solid was dried under reduced pressure to leave the desired product as white granules. The resin was resuspended in DMF (1.5 ml) followed by the addition of acetic acid 2,5-dioxo-pyrrolidin-1-yl ester (24 mg, 0.153 mmol). The mixture was stirred end over end for 12 h. Solvent was removed and the resin was washed and dried as described above to leave the desired NH_2 capped resin as white granules. Elemental analysis determined Eu(III) content to be 0.22 %, 0.014 mmol g^{-1}.

TentaGel^{TM} S-NH_2 bound complex

TBTU (22 mg, 0.069 mmol) and HOBt.xH_2O (5 mg, 0.037 mmol) were added to a solution of Eu(III) complex of 4-[(S)-1-(2-(4,10-bis-[((S)-1-phenyl-ethylcarbamoyl)-methyl]-1,4,7,10-tetraaza-cyclododec-1-yl)-acetylamino)-ethyl]-benzoic acid (65 mg, 0.065 mmol) in DMF (1 ml) and stirred for 20 min. The yellow tinged solution was then added to TentaGel^{TM} S-NH_2 (530 mg) pre-soaked in DMF (2 ml), under argon. The mixture was stirred end over end for 24 h. Solvent was removed by centrifugation. The remaining resin was washed with DMF (2 x 5 ml) then H_2O (2 x 5 ml) with the resin being separated by centrifugation. The washed resin was dried under reduced pressure. The resin was resuspended in DMF (1.5 ml) followed by the addition of acetic acid 2,5-dioxo-pyrrolidin-1-yl ester (90 mg, 0.573 mmol). The mixture was stirred end over end for 12 h. Solvent was removed and the resin was washed and dried as described above to leave the desired NH_2 capped resin as yellow granules. Elemental analysis determined Eu(III) content to be 0.31 % or 0.020 mmol g^{-1}, this corresponds to 4.4 % derivatization as the resin NH_2 content is stated as $\sim$0.45 mmol g^{-1}.

A separate experiment followed the above procedure and used the following amounts of material; TentaGel^{TM} S-NH_2 (269 mg), TBTU (11 mg, 0.034 mmol), HOBt.xH_2O (1 mg, 0.007 mmol) and complex (33 mg, 0.033 mmol). The resin was capped with acetic acid 2,5-dioxo-pyrrolidin-1-yl ester (38 mg, 0.242 mmol). This yielded resin with a Eu(III) content of 1.01 % or 0.066 mmol g^{-1}, corresponding to 14.7 % derivatization. ^{1}H-NMR (CD_3OD, 500 MHz, MAS, partial data) Broadened peaks attributed to paramagnetically shifted resonances of the Eu(III) complex were observed at δ 34.5, 30.8, 20.8, 22.2, 18.4, 17.5, -7.5, -10.2, -11.2, -13.0, -16.5, -19.9, -28.6.

SiMAG-Amino bound complex

Solvent was removed from an aqueous suspension of SiMAG-Amino particles (50 mg in 1 ml) by centrifugation. The remaining particles were washed with an aqueous solution of MES (0.1 M, pH 6, 2 x 1 ml). EDC.HCl (10 mg, 0.005 mmol) was dissolved in fresh MES solution (0.25 ml) followed by addition of the Eu(III) complex of 4-[(S)-1-(2-(4,10-bis-[((S)-1-phenyl-ethylcarbamoyl)-methyl]-1,4,7,10-tetraaza-cyclododec-1-yl)-acetylamino)-ethyl]-benzoic acid (10 mg, 0.01 mM). The resulting solution was added to the SiMAG-Amino particles followed by addition of MES solution (0.5 ml). The suspension was stirred end over end for 24 h, followed by isolation of the solid by centrifugation. The isolated particles were further washed by H_2O (2 x 1 ml) and MeOH (1 ml), isolated by centrifugation each time followed by drying. The dried particles were suspended in anhydrous DMF (0.5 ml) followed by addition of acetic acid 2,5-dioxo-pyrrolidin-1-yl ester (5.5 mg, 0.035 mmol). The suspension was stirred end over end for 24 h followed by removal of solvent by centrifugation. The solid was washed as described previously to yield the desired capped orange-brown particles. Elemental analysis determined Eu(III) content to be 0.04 % or 0.0028 mmol g^{-1}, this corresponds to 0.8 % derivatization as the resin NH_2 content is stated as $\sim$0.35 mmol g^{-1}.

An alternative procedure was also followed. A solution of Eu(III) complex of 4-[(S)-1-

(2-(4,10-bis-[((S)-1-phenyl-ethylcarbamoyl)-methyl]-1,4,7,10-tetraaza-cyclododec-1-yl)-acetylamino)-ethyl]-benzoic acid (12 mg, 0.012 mmol) and EDC.HCl (3 mg, 0.016 mmol) in DMF (1 ml) was shaken for 10 min then added to dried SiMAG-Amino particles (66 mg). The resulting suspension was stirred end over end. After 24 h acetic acid 2,5-dioxo-pyrrolidin-1-yl ester (8 mg, 0.05 mmol) was added to the suspension and stirring continued for 3 h. The particles were then isolated by centrifugation, washed with H_2O (2 x 1 ml) and MeOH (2 x 1 ml), then dried under reduced pressure to leave the desired capped orange-brown particles. Elemental analysis determined Eu(III) content to be 0.02 % or 0.013 mmol g^{-1}, this corresponds to 3.8 % derivatization as the resin NH_2 content is stated as $\sim$0.35 mmol g^{-1}.

References

[1] J. W. Steed and J. L. Atwood, *Supramolecular chemistry*, John Wiley & Sons Ltd, Chichester, UK, 2000.

[2] R. S. Dickins and D. Parker, in *Macrocyclic Chemistry Current Trends and Future Perspectives-Signalling Reversible Anion Binding in Aqueous Media* (K. Gloe ed.), Springer, Dordrecht, The Netherlands, 2005; pp. 121–136.

[3] Y. Marcus, *J. Chem. Soc. Faraday Trans.*, 1991, **87(18)**, 2995.

[4] G. Zuber, C. Sirlin, and J.-P. Behr, *J. Am. Chem. Soc.*, 1993, **115(11)**, 4939.

[5] L. D'Agostino and A. Di Luccia, *Eur. J. Biochem.*, 2002, **269**, 4317.

[6] F. A. Cotton, E. E. Hazen Jr., and M. J. Legg, *Proc. Natl. Acad. Sci. USA*, 1979, **76(6)**, 2551.

[7] E. Graf and J.-M. Lehn, *J. Am. Chem. Soc*, 1976, **98(20)**, 6403.

[8] J.-M. Lehn, E. Sonveaux, and A. K. Willard, *J. Am. Chem. Soc*, 1978, **100(15)**, 4914.

[9] E. García-España, P. Díaz, J. M. Llinares, and A. Bianchi, *Coord. Chem. Rev.*, 2006, **250**, 2952.

[10] B. Dietrich, T. M. Fyles, J.-M. Lehn, L. G. Pease, and D. L. Fyles, *J. Chem. Soc. Chem. Commun.*, 1978, **21**, 934.

[11] S. Aoki and E. Kimura, *Rev. Mol. Biotech.*, 2002, **90(2)**, 129.

[12] P. A. Gale, S. E. García-Garrido, and J. Garric, *Chem. Soc. Rev.*, 2008, **37**, 151.

[13] P. Schießl and F. P. Schmidtchen, *Tett. Lett.*, 1993, **34(15)**, 2449.

[14] M. Kumbhakar, S. Nath, T. Mukherjee, J. P. Mittal, and H. Pal, *J. Photoch. Photobio. C*, 2004, **5**, 113.

[15] W. Tan, Z. Shi, S. Smith, D. Birnbaum, and R. Kopelman, *Science*, 1992, **258(5083)**, 778.

[16] W. Wróblewski, K. Wojciechowski, A. Dybko, Z. Brzózka, R. J. M. Egberink, B. H. M. Snellink-Ruël, and D. N. Reinhoudt, *Sens. Actuators B*, 2000, **68**, 313.

[17] J. Kim, D. M. Kang, S. C. Shin, M. Y. Choi, J. Kim, S. S. Lee, and J. S. Kim, *Anal. Chim. Acta*, 2008, **614**, 85.

[18] J. A. Adams, *Chem. Rev.*, 2001, **101**, 2271.

[19] G. Manning, D. Whyte, R. Martinez, T. Hunter, and S. Sudarsanam, *Science*, 2002, **298**, 1912.

[20] X.-L. Zhan, M. J. Wishart, and K.-L. Guan, *Chem. Rev.*, 2001, **101**, 2477.

[21] L. N. Johnson and R. J. Lewis, *Chem. Rev.*, 2001, **101**, 2209.

[22] T. Pawson and J. D. Scott, *Trends. Biochem. Sci.*, 2005, **30(6)**, 286.

[23] A. V. Gourine, E. Llaudet, N. Dale, and K. M. Spyer, *Nature*, 2005, **436(7047)**, 108.

[24] G. Burnstock, *Pharmacol. Rev.*, 2006, **58**, 58.

[25] C. Spangler, M. Schaeferling, and O. S. Wolfbeis, *Microchim. Acta.*, 2008, **161**, 1.

[26] A. Ojida, Y. Mito-oka, M. Inoue, and I. Hamachi, *J. Am. Chem. Soc.*, 2002, **124(22)**, 6256.

[27] A. Ojida, Y. Mito-oka, K. Sada, and I. Hamachi, *J. Am. Chem. Soc.*, 2004, **126(8)**, 2454.

[28] A. Ojida and I. Hamachi, *Bull. Chem. Soc. Jpn.*, 2006, **79(1)**, 35.

[29] A. Ojida, T. Kohira, and I. Hamachi, *Chem. Lett.*, 2004, **33(8)**, 1024.

[30] A. Ojida, M. Inoue, Y. Mito-oka, and I. Hamachi, *J. Am. Chem. Soc.*, 2003, **125(34)**, 10184.

[31] A. Ojida, M. Inoue, Y. Mito-oka, H. Tsutsumi, K. Sada, and I. Hamachi, *J. Am. Chem. Soc.*, 2006, **128(6)**, 2052.

[32] T. Anai, E. Nakata, Y. Koshi, A. Ojida, and I. Hamachi, *J. Am. Chem. Soc.*, 2007, **129(19)**, 6232.

[33] T. Hasegawa, K. Ohkubo, S. Yoshikawa, and T. Morii, *J. Surf. Sci. Nanotech.*, 2005, **3**, 33.

[34] T. Hasegawa, M. Hagihara, M. Fukuda, S. Nakano, N. Fujieda, and T. Morii, *J. Am. Chem. Soc.*, 2008, **130(27)**, 8804.

[35] A. Ojida, Y. Miyahara, J. Wongkongkatep, S. Tamaru, K. Sada, and I. Hamachi, *Chem. Asian. J.*, 2006, **1**, 555.

[36] A. Ojida, I. Takashimi, T. Kohiro, H. Nonaka, and I. Hamachi, *J. Am. Chem. Soc.*, 2008, **130(36)**, 12095.

[37] J. H. Zippin, L. R. Levin, and J. Buck, *Trends Endocrinol. Metab.*, 2001, **12(8)**, 366.

[38] J. R. Casey, *Biochem. Cell. Biol.*, 2006, **84**, 930.

[39] L. C. Costello, R. B. Franklin, and P. Feng, *Mitochondrion*, 2005, **5**, 143.

[40] I. Suzuki, M. Ui, and A. Yamauchi, *J. Am. Chem. Soc.*, 2006, **128(14)**, 4498.

[41] L. Fabbrizzi, A. Leone, and A. Taglietti, *Angew. Chem. Int. Ed.*, 2001, **40(16)**, 3066.

[42] B. Garcia-Acosta, F. Garcia, J. M. Garcia, R. Martinez-Mañez, F. Sancenón, N. San-José, and J. Soto, *Org. Lett.*, 2007, **9(13)**, 2429.

[43] E. Kimura, *Acc. Chem. Res.*, 2001, **34**, 171.

[44] E. Kimura, T. Shiota, T. Koike, M. Shiro, and M. Kodama, *J. Am. Chem. Soc.*, 1990, **112**, 5805.

[45] X. Zhang, R. Eldik, T. Koike, and E. Kimura, *Inorg. Chem.*, 1993, **32**, 5749.

[46] A. Metzger, V. M. Lynch, and E. V. Anslyn, *Angew. Chem. Int. Ed. Engl.*, 1997, **36(8)**, 862.

[47] A. Metzger and E. V. Anslyn, *Angew. Chem. Int. Ed.*, 1998, **37(5)**, 649.

[48] S. C. McCleskey, A. Metzger, C. S. Simmons, and E. V. Anslyn, *Tetrahedron*, 2002, **58**, 621.

[49] C. Schmuck and M. Schwegmann, *J. Am. Chem. Soc.*, 2005, **127(10)**, 3373.

[50] C. Schmuck and M. Schwegmann, *Org. Biomol. Chem.*, 2006, **4**, 836.

[51] L. Fabbrizzi, F. Foti, and A. Taglietti, *Org. Lett*, 2005, **7(13)**, 2603.

[52] T. Gunnlaugsson and J. P. Leonard, *Chem. Commun.*, 2005, **25**, 3114.

[53] D. Parker and J. A. G. Williams, in *Metal Ions in Biological Systems: The Lanthanides and their Interrelations with Biosystems (Volume 40)-Responsive Luminescent Lanthanide Complexes* (A. Sigel and H. Sigel eds.), Marcel-Dekker, New York, 2005; pp. 233–280.

[54] P. Atkinson, K. S. Findlay, F. Kielar, R. Pal, D. Parker, R. A. Poole, H. Puschmann, S. L. Richardson, P. A. Stenson, A. L. Thompson, and J. Yu, *Org. Biomol. Chem.*, 2006, **4**, 1707.

[55] J. L. Kropp and M. W. Windsor, *J. Chem. Phys.*, 1963, **39**, 2769.

[56] J. L. Kropp and M. W. Windsor, *J. Chem. Phys.*, 1965, **42(5)**, 1599.

[57] A. Beeby, I. M. Clarkson, R. S. Dickins, S. Faulkner, D. Parker, L. Royle, A. S. de Sousa, J. A. G. Williams, and M. Woods, *J. Chem. Soc. Perkin Trans. 2*, 1999, **3**, 493.

[58] J. I. Bruce, R. S. Dickins, L. J. Govenlock, T. Gunnlaugsson, S. Lopinski, M. P. Lowe, D. Parker, R. D. Peacock, J. J. B. Perry, S. Aime, and M. Botta, *J. Am. Chem. Soc.*, 2000, **122(40)**, 9674.

[59] D. R. Forster and F. S. Richardson, *Inorg. Chem.*, 1983, **22**, 3996.

[60] A. F. Kirby, D. Foster, and F. S. Richardson, *Chem. Phys. Lett.*, 1983, **95(6)**, 507.

[61] S. P. Babailov, *Prog. Nucl. Mag. Res. Sp.*, 2008, **52(1)**, 1.

[62] M. Allegrozzi, I. Bertini, M. B. L. Janik, Y. Lee, G. Liu, and C. Luchinat, *J. Am. Chem. Soc.*, 2000, **122(17)**, 4154.

[63] D. Parker, R. S. Dickins, H. Puschmann, C. Crossland, and J. A. K. Howard, *Chem. Rev.*, 2002, **102(6)**, 1977.

[64] R. S. Dickins, S. Aime, A. S. Batsanov, A. Beeby, M. Botta, J. I. Bruce, J. A. K. Howard, C. S. Love, D. Parker, R. D. Peacock, and H. Puschmann, *J. Am. Chem. Soc.*, 2002, **124(43)**, 12697.

[65] R. S. Dickins, D. Parker, J. I. Bruce, and D. J. Tozer, *Dalton Trans.*, 2003, **7**, 1264.

[66] P. Atkinson, Y. Bretonnière, D. Parker, and G. Muller, *Helv. Chim. Acta*, 2005, **88**, 391.

[67] R. S. Dickins, J. A. K. Howard, C. L. Maupin, J. M. Moloney, D. Parker, R. D. Peacock, J. P. Riehl, and G. Siligardi, *New J. Chem.*, 1998, **22(8)**, 891.

[68] R. S. Dickins, J. A. K. Howard, C. L. Maupin, J. M. Moloney, D. Parker, J. P. Riehl, G. Siligardi, and J. A. G. Williams, *Chem. Eur. J.*, 1999, **5(3)**, 1095.

[69] R. S. Dickins, J. A. K. Howard, C. W. Lehmann, J. Moloney, D. Parker, and R. D. Peacock, *Angew. Chem. Int. Ed. Engl.*, 1997, **36(5)**, 521.

[70] L. B. Bari, G. Pintacuda, P. Salvadori, R. S. Dickins, and D. Parker, *J. Am. Chem. Soc.*, 2000, **122(38)**, 9257.

[71] D. F. Henrie, R. L. Fellows, and G. R. Choppin, *Coord. Chem. Rev.*, 1976, **18**, 199.

[72] P. Atkinson, Y. Bretonnière, and D. Parker, *Chem. Commun.*, 2004, **4**, 438.

[73] P. Atkinson *Chemoselective Phospho-Anion Binding Studies,* PhD thesis, University of Durham, 2006.

[74] R. S. Dickins, A. S. Batsanov, J. A. K. Howard, D. Parker, H. Puschmann, and S. Salamano, *Dalton Trans.*, 2004, **1**, 70.

[75] S. Mameri, L. J. Charbonnière, and R. F. Ziessel, *Inorg. Chem.*, 2004, **43(6)**, 1819.

[76] L. J. Charbonnière, R. Schurhammer, S. Mameri, G. Wipff, and R. F. Ziessel, *Inorg. Chem.*, 2005, **44(20)**, 7151.

[77] L. J. Charbonnière, S. Mameri, P. Kadjane, C. Platas-Iglesias, and R. F. Ziessel, *Inorg. Chem.*, 2008, **47(9)**, 3748.

[78] N. Shao, J. Jin, G. Wang, Y. Zhang, R. Yang, and J. Yuan, *Chem. Commun.*, 2008, **9**, 1127.

[79] D. Parker and J. Yu, *Chem. Commun.*, 2005, **25**, 3141.

[80] Y. Bretonnière, M. J. Cann, D. Parker, and R. Slater, *Org. Biomol. Chem.*, 2004, **2**, 1624.

[81] J. P. Leonard, C. M. G. dos Santos, S. E. Plush, T. McCabe, and T. Gunnlaugsson, *Chem. Commun.*, 2007, **2**, 129.

[82] S. E. Plush, T. McCabe, and T. Gunnlaugsson, *Dalton Trans.*, 2008, **29**, 3801.

[83] M. Schäferling and O. S. Wolfbeis, *Chem. Eur. J.*, 2007, **13**, 4342.

[84] P. Atkinson, B. S. Murray, and D. Parker, *Org. Biomol. Chem.*, 2006, **4**, 3166.

[85] Z. Kovacs and A. D. Sherry, *J. Chem. Soc., Chem. Commun.*, 1995, **2**, 185.

[86] F. Kielar *Development of Lanthanide Probes for Cellular Imaging,* PhD thesis, University of Durham, 2008.

[87] F. Kielar, A. Congreve, G. Law, E. J. New, D. Parker, K. L. Wong, P. Castreño, and J. de Mendoza, *Chem. Commun.*, 2008, **21**, 2435.

[88] Hydrolysis of 7-methoxycarbonyl-2-methyl-1-azaxanthone using 12 M $HCl_{(aq)}$ at 100°C yielded the desired acid as its HCl salt. The acid could not be converted to the ^{t}Bu ester either through synthesis of the acyl chloride, carbodiimide mediated acid activation or by direct esterification. The acid could be activated and converted to a amide using EDC in anhydrous DMF. Amines used were mono-BOC protected ethylene diamine and mono-BOC protected hydrazine. Although these amide derivatives were successfully prepared, no further chromophore derivatization, e.g. benzylic bromination, was successfully achieved.

[89] J. I. Bruce, D. Parker, S. Lopinski, and R. D. Peacock, *Chirality*, 2002, **14**, 562.

[90] S. Aime, A. Barge, J. I. Bruce, M. Botta, J. A. K. Howard, J. M. Moloney, D. Parker, A. S. de Sousa, and M. Woods, *J. Am. Chem. Soc.*, 1999, **121(24)**, 5762.

[91] A. C. Samuels, J. O. Jensen, and H. F. Hameka, *J. Mol. Struc.*, 1998, **454**, 25.

[92] B. S. Murray, E. J. New, R. Pal, and D. Parker, *Org. Biomol. Chem.*, 2008, **6**, 2085.

[93] R. Pál *Ratiometric luminescent probes,* PhD thesis, University of Durham, 2007.

[94] L.-O. Pålsson, R. Pal, B. S. Murray, D. Parker, and A. Beeby, *Dalton Trans.*, 2007, **48**, 5726.

[95] J. Yu, D. Parker, R. Pal, R. A. Poole, and M. J. Cann, *J. Am. Chem. Soc.*, 2006, **128**, 2294.

[96] Although the excited state lifetimes for the $[EuL^{44b}]^{3+}$ estimates a change in q from 1.24 to 0.72 upon addition of HSA (0.35 mM), no significant change in the relaxivity of $[GdL^{44b}]^{3+}$ was observed, even in the presence of $\geq$0.35 mM HSA. This evidence suggests association of the complex with HSA, with most likely the loss of a coordinated water molecule, leaving one water coordinated to the metal ion. It is probable that HSA association occurs in such a fashion that water exchange at the metal centre is severly inhibited, resulting in the constant relaxivity values observed.

[97] J. Carmichael, W. G. DeGraff, A. F. Gazdar, J. D. Minna, and J. B. Mitchell, *Cancer Res.*, 1987, **47**, 936.

[98] R. Pal and D. Parker, *Chem. Commun.*, 2007, **5**, 474.

[99] R. Pal and D. Parker, *Org. Biomol. Chem.*, 2008, **6(6)**, 1020.

[100] A. J. Harte, P. Jensen, S. E. Plush, P. E. Kruger, and T. Gunnlaugsson, *Inorg. Chem.*, 2006, **45(23)**, 9465.

[101] T. Gunnlaugsson, A. J. Harte, J. P. Leonard, and M. Nieuwenhuyzen, *Chem. Comm.*, 2002, **18**, 2134.

[102] S. J. A. Pope, A. M. Kenwright, V. A. Boote, and S. Faulkner, *Dalton Trans.*, 2003, **19**, 3780.

[103] D. H. Powell, O. M. Ni Dhubhghaill, D. Pubanz, L. Helm, Y. S. Lebedev, W. Schlaepfer, and A. E. Merbach, *J. Am. Chem. Soc.*, 1996, **118(39)**, 9333.

[104] J. Rudovskỳ, M. Botta, P. Hermann, A. Koridze, and S. Aime, *Dalton Trans.*, 2006, **19**, 2323.

[105] Crystals of $[Yb_2L^{58}]^{6+}6(OAc)^-$ were grown using the hanging drop method, at 4°C. A PEG 6000 grid screen (Hampton research: HR2-213) was used to identify suitable crystallisation conditions. Crystals were isolated using 20 and 30 % w/v PEG 6000 (pH 9, 0.1 M bicine) and 5 % w/v PEG 6000 (pH 8, 0.1 M Tris) reservoir solutions (200 µl) from drops of an initial volume of 2µl (1:1, reservoir solution:complex solution (100 mg ml^{-1})). Unfortunately, due to internal twinning of the crystal the refinement of the structure could not be improved upon ~15 %, meaning the conformation of the complex about the central bond could not be determined. However, the data provides evidence for a regular square antiprismatic geometry about each Yb(III) ion.

[106] R. S. Dickins, T. Gunnlaugsson, D. Parker, and R. D. Peacock, *Chem. Commun.*, 1998, **16**, 1643.

[107] H. Donato Jr. and R. B. Martin, *Biochemistry*, 1974, **13(22)**, 4575.

[108] C. L.-. A. Wang, T. Tao, and J. Gergely, *J. Biol. Chem.*, 1982, **257(14)**, 8372.

[109] J. A. Mosely, B. S. Murray, and D. Parker, *Eur. J. Mass. Spectrom.*, 2008, **In press, doi (10.1255/ejms.941)**.

[110] Further work established methodology that facilitated the mono-introduction of the sulfate functionality at the *meta*-position of (1*S*,2*S*)-(-)-1,2-diphenylethylenediamine or *meso*-1,2-diphenylethylenediamine using fuming sulfuric acid. This modified linking group could be incorporated into a dimeric ligand structure using standard amide forming conditions, although the high water solubility of all reaction products inhibited the isolation of the required protected ligand. In addition, the synthesis of dimeric ligands bearing chiral amide arms with a methyl ester at the *para*-ring position was attempted through several synthetic routes. Whilst significant progress in many of these schemes was made, no pure ligand was able to be obtained.

[111] M. Zeller and S. König, *Anal. Bioanal. Chem.*, 2004, **378(4)**, 898.

[112] S. Krishnamoorthy, *PLoS ONE*, 2008, **3(8)**, e2877.

[113] E. G. Krebs, *Phil. Trans. R. Soc. Lond. B*, 1983, **302**, 3.

[114] T. Hunter, *Cell*, 1995, **80**, 225.

[115] T. Hunter, *Keio J. Med.*, 2002, **51(2)**, 61.

[116] P. Blume-Jensen and T. Hunter, *Nature*, 2001, **411(6835)**, 355.

[117] T. Hunter and B. M. Sefton, *Proc. Natl. Acad. Sci. USA*, 1980, **77(3)**, 1311.

[118] H. R. Matthews, *Pharmac. Ther.*, 1995, **67(3)**, 323.

[119] P. G. Besant, E. Tan, and P. V. Attwood, *Int. J. Biochem. Cell Biol.*, 2003, **35(3)**, 297.

[120] F. Tan, Y. Zhang, W. Mi, J. Wang, J. Wei, Y. Cai, and X. Qian, *J. Proteome Res.*, 2008, **7(3)**, 1078.

[121] K. Moser and F. M. White, *J. Proteome Res.*, 2006, **5(1)**, 98.

[122] L. Trojer, G. Stecher, I. Feuerstein, S. Lubbad, and G. K. Bonn, *J. Chromatogr. A*, 2005, **1079**, 197.

[123] W. Zhou, B. A. Merrick, M. G. Khaledi, and K. B. Tomer, *J. Am. Soc. Mass Spectrom.*, 2000, **11(4)**, 273.

[124] S. R. Hart, M. D. Waterfield, A. L. Burlingame, and R. Cramer, *J. Am. Soc. Mass Spectrom.*, 2002, **13(9)**, 1042.

[125] N. H. Aprilita, C. W. Huck, R. Bakry, I. Feuerstein, G. Stecher, S. Morandell, H.-L. Huang, T. Stasyk, L. A. Huber, and G. K. Bonn, *J. Proteome Res.*, 2005, **4(6)**, 2312.

[126] R. van der Veken, E. H. C. Dirksen, E. Ruijter, R. C. Elgersma, A. J. R. Heck, D. T. S. Rijkers, M. Slijper, and R. M. J. Liskamp, *CHEMBIOCHEM.*, 2005, **6(12)**, 2271.

[127] F. Thaler, B. Valsasina, R. Baldi, J. Xie, A. Stewart, A. Isacchi, H. M. Kalisz, and L. Rusconi, *Anal. Bioanal. Chem.*, 2003, **376(3)**, 366.

[128] A. J. Thompson, S. R. Hart, C. Franz, K.Barnouin, A. Ridley, and R. Cramer, *Anal. Chem.*, 2003, **75(13)**, 3232.

[129] H. Zheng, P. Hu, D. F. Quinn, and Y. K. Wang, *Mol. Cell. Proteomics*, 2005, **4(6)**, 721.

[130] J. Kim and F. M. White, *J. Immunol.*, 2006, **176(5)**, 2833.

[131] S. Kane, H. Sano, S. C. H. Liu, J. M. Asara, W. S. Lane, C. C. Garner, and G. E. Lienhard, *J. Biol. Chem.*, 2002, **277(25)**, 22115.

[132] M. Grønborg, T. Z. Kristiansen, A. Stensballe, J. S. Andersen, O. Ohara, M. Mann, O. N. Jensen, and A. Pandey, *Mol. Cell. Proteomics*, 2002, **1(7)**, 517.

[133] S. Li and D. Zeng, *Angew. Chem. Int. Ed.*, 2007, **46(25)**, 4751.

[134] B. B. Shankar, B. J. Lavey, G. Zhou, J. A. Spitler, L. Tong, R. Rizvi, D.-Y. Yang, R. Wolin, J. A. Kozlowski, N.-Y. Shih, J. Wu, R. W. Hipkin, W. Gonsiorek, and C. A. Lunn, *Bioorg. Med. Chem. Lett.*, 2005, **15**, 4417.

[135] The NHS ester of $[EuL^{62}]^{2+}$ was also synthesised following acid activation with TBTU in DMF. In this case, the crude complex was isolated and identified by HRMS (ES^+), providing direct evidence for the activation of $[EuL^{62}]^{2+}$.

[136] R. A. H. Binstead, B. Jung, and A. D. Zuberbühler, SPECFIT/32 Global Analysis System, version 3.0, Spectrum Software Associates, Marlborough, MA, USA, 2000-2005.

[137] H. Gampp, M. Maeder, C. J. Meyer, and A. D. Zuberbühler, *Talanta*, 1985, **32**, 95.

[138] M. Maeder and A. D. Zuberbühler, *Anal. Chem.*, 1990, **62**, 2220.

[139] SMART, Data Collection Software, version 5.625, Bruker Analytical X-ray Instruments Inc., Madison, Wisconsin, USA, 2001.

[140] SAINT, Data Reduction Software, version 6.45A, Bruker Analytical X-ray Instruments Inc., Madison, Wisconsin, USA, 2003.

[141] SHELXTL, version 6.14, Bruker Analytical X-ray Instruments Inc., Madison, Wisconsin, USA, 2003.

[142] T. Isshiki and Y. Kuwata, *Bull. Physiograph. Sci.*, 1951, **8**, 24.

[143] A. Mosandi, *Arch. Pharm.*, 1984, **317(4)**, 345.

[144] P. W. Erdhardt, W. G. Anderson, and R. J. Gorczynski, *J. Med. Chem.*, 1982, **25**, 1408.

[145] Y. Ikeya, K. Sugama, M. Okada, and H. Mitsuhashi, *Chem. Phar. Bull.*, 1991, **39(10)**, 2600.

[146] D. Lowe, W. Chang, J. Kozlowski, J. G. Berger, R. Mcquade, A. Barnett, M. Scherlock, W. Tom, S. Dugar, L.-Y. Chen, J. W. Clader, and S. Chackalamannil, WO/1996/026196.

[147] E. Malmström, R. D. Miller, and C. J. Hawker, *Tetrahedron*, 1997, **53(45)**, 15225.

Appendix A

HPLC conditions and representative traces

Solvent system A

Time	A	B	Gradient
0 - 5 min	100 %	0 %	N/A
5 - 20 min	100 % → 0 %	0 % → 100 %	Linear
20.1 - 25 min	0 % → 100 %	100 % → 0 %	Linear

Table A.1 – Flow rate: 1 ml min^{-1}; Solvent **A**: H_2O + 0.1 % HCOOH; Solvent **B**: MeCN + 0.1 % HCOOH.

Solvent system B

Time	A	B	Gradient
0 - 5 min	100 %	0 %	N/A
5 - 20 min	100 % → 0 %	0 % → 100 %	Linear
20.1 - 25 min	0 % → 100 %	100 % → 0 %	Linear

Table A.2 – Flow rate: 1 ml min^{-1}; Solvent **A**: H_2O + 0.1 % CF_3COOH; Solvent **B**: MeCN + 0.1 % CF_3COOH.

$[EuL^{44a}]^{3+}$

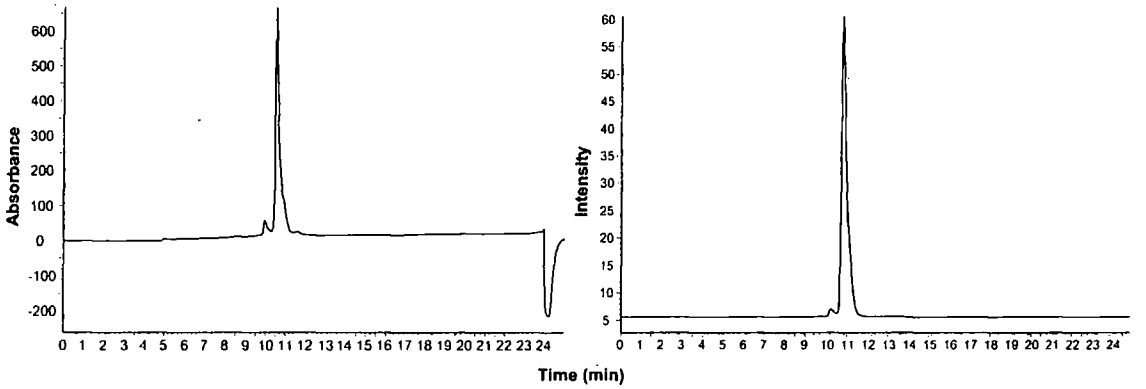

Figure A.1 – HPLC traces from analysis of $[EuL^{44a}]^{3+}$. Left: absorbance (335 nm); Right: emission (612 nm, λ_{exc} = 335 nm); Solvent system B; 4.6 x 150 mm 4 μm Phenomenex Synergi Fusion RP 80Å analytical column.

$[EuL^{49}]^{2+}$

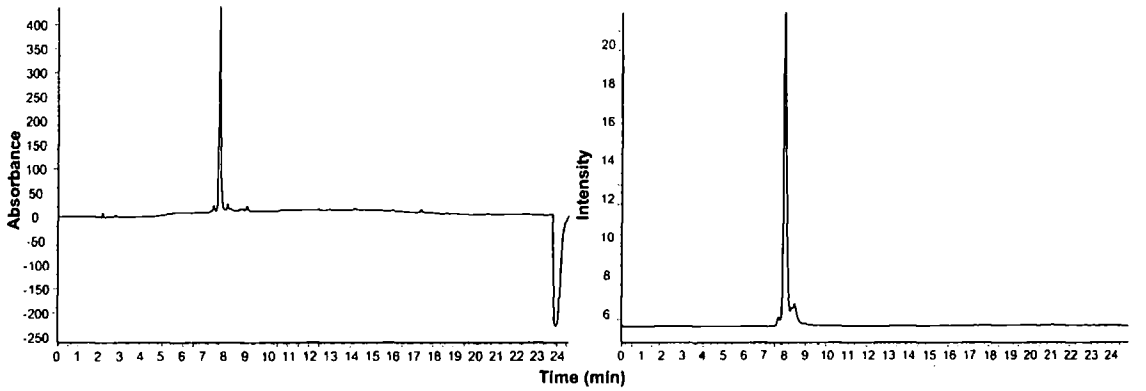

Figure A.2 – HPLC traces from analysis of $[EuL^{49}]^{2+}$. Left: absorbance (332 nm); Right: emission (612 nm, λ_{exc} = 332 nm); Solvent system A; 4.6 x 150 mm 4 μm Phenomenex Synergi Fusion RP 80Å analytical column.

$[\mathbf{EuL}^{50}]^{3+}$

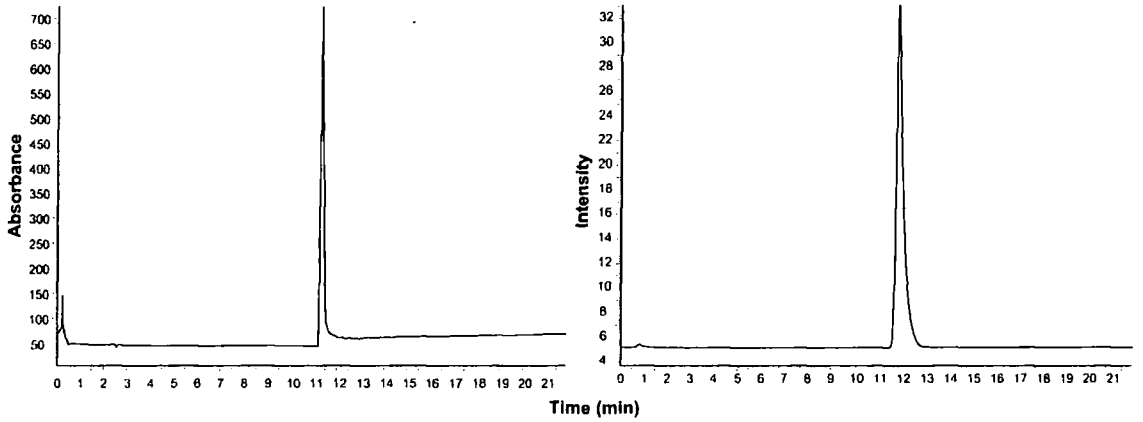

Figure A.3 – HPLC traces from analysis of $[\mathbf{EuL}^{50}]^{3+}$. Left: absorbance (335 nm); Right: emission (612 nm, λ_{exc} = 335 nm); Solvent system A; 4.6 x 150 mm 4 μm Phenomenex Synergi Polar-RP 80Å analytical column.

$[\mathbf{GdL}^{44b}]^{3+}$

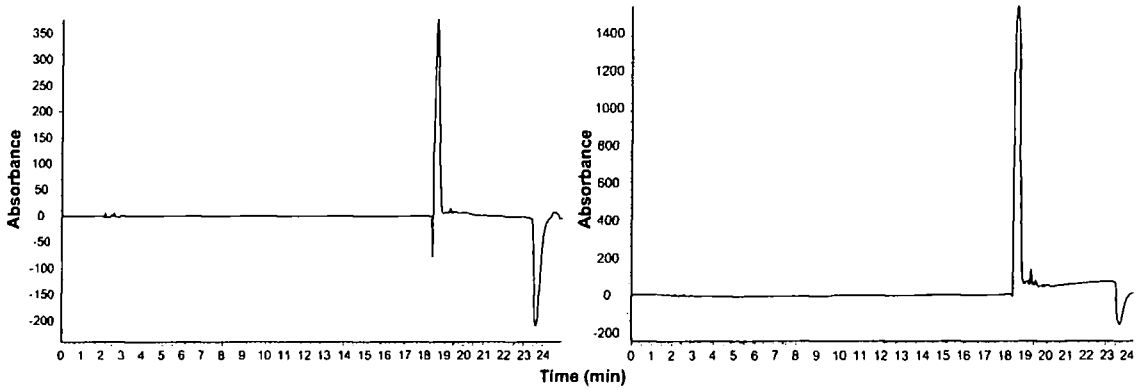

Figure A.4 – HPLC traces from analysis of $[\mathbf{GdL}^{44b}]^{3+}$. Left: absorbance (254 nm); Right: absorbance (380 nm); Solvent system A; 4.6 x 150 mm 4 μm Phenomenex Synergi Polar-RP 80Å analytical column.

$[EuL^{51b}]^{3+}$

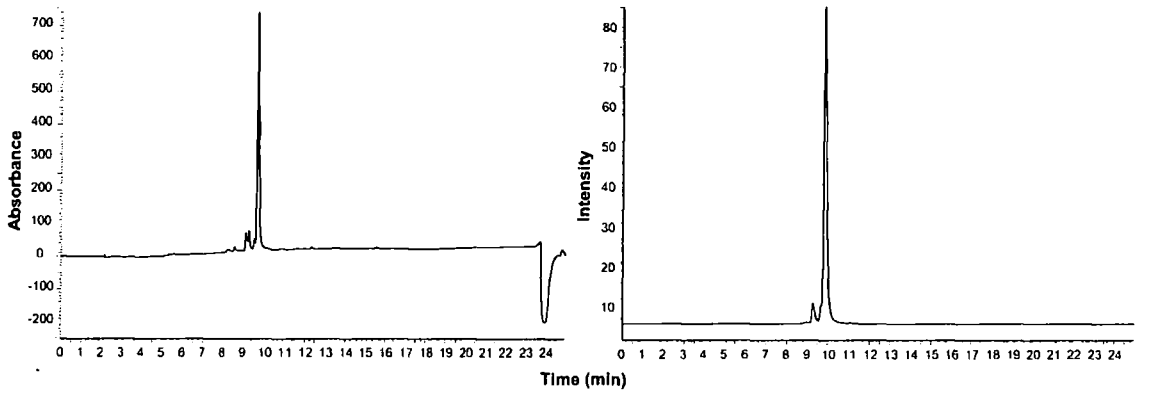

Figure A.5 – HPLC traces from analysis of $[EuL^{51b}]^{3+}$. Left: absorbance (370 nm); Right: emission (612 nm, λ_{exc} = 370 nm); Solvent system A; 4.6 x 150 mm 4 µm Phenomenex Synergi Fusion RP 80Å analytical column.

$[EuL^{61}]^{3+}$

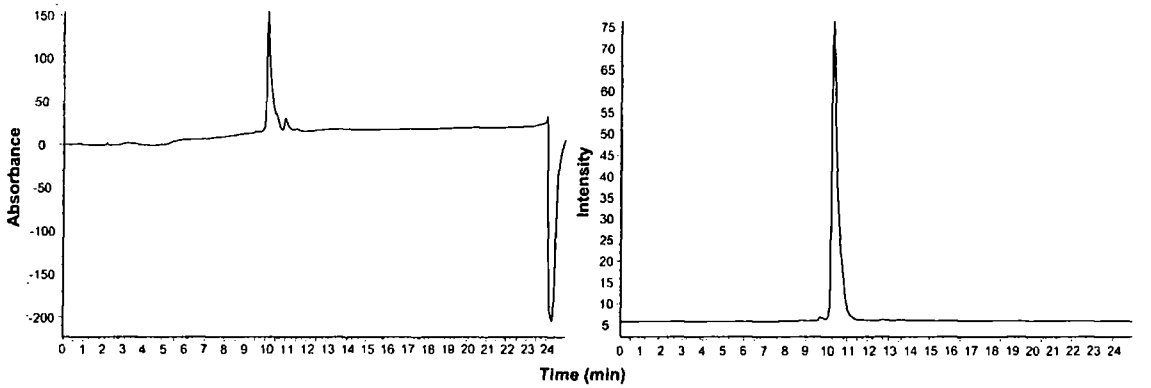

Figure A.6 – HPLC traces from analysis of $[EuL^{61}]^{3+}$. Left: absorbance (255 nm); Right: emission (612 nm, λ_{exc} = 255 nm); Solvent system B; 4.6 x 150 mm 4 µm Phenomenex Synergi Fusion RP 80Å analytical column.

Appendix B

Ligand ^{1}H-NMR spectra

Full ^{1}H-NMR spectra of all ligands are shown below.

$\mathbf{L}^{44a}$

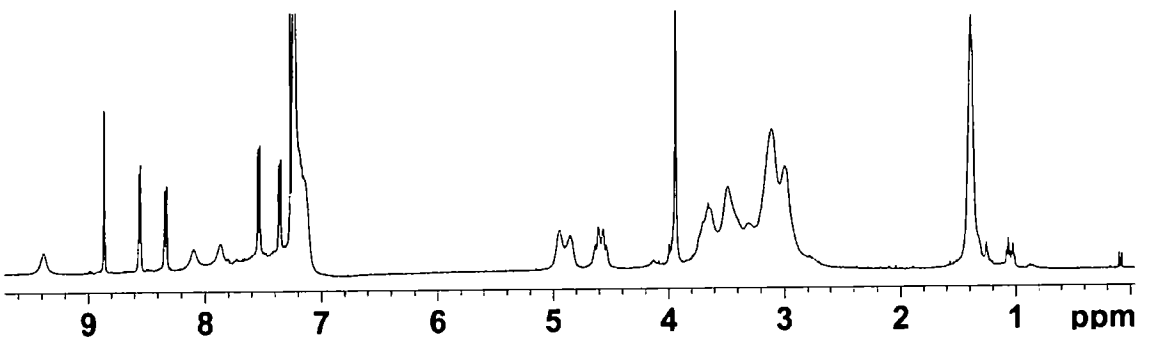

Figure B.1 – $CDCl_3$, 500 MHz, 295 K, 3 mM.

$\mathbf{L}^{44b}$

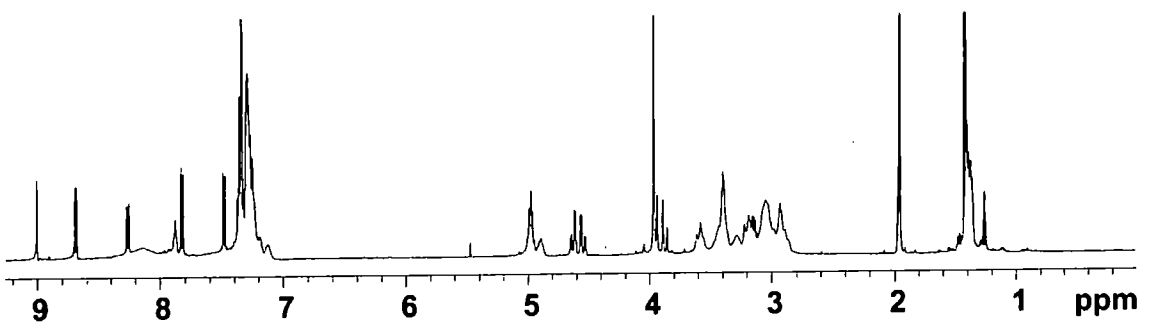

Figure B.2 – CD_3CN, 500 MHz, 295 K, 3 mM.

L^{49}

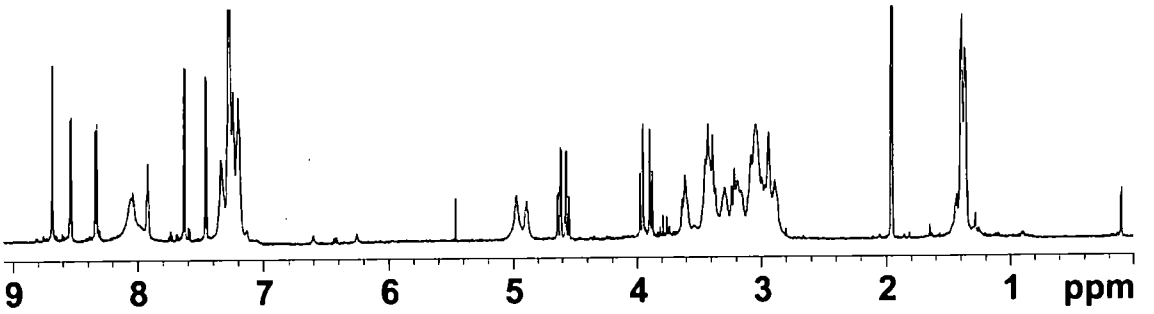

Figure B.3 – CD_3CN, 700 MHz, 295 K, 3 mM.

L^{50}

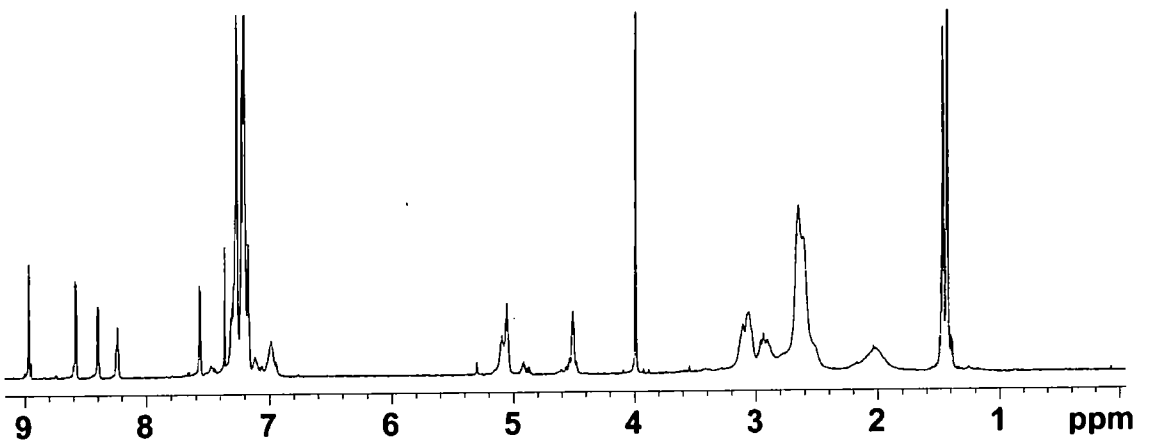

Figure B.4 – $CDCl_3$, 700 MHz, 295 K, 4 mM.

L^{51a}

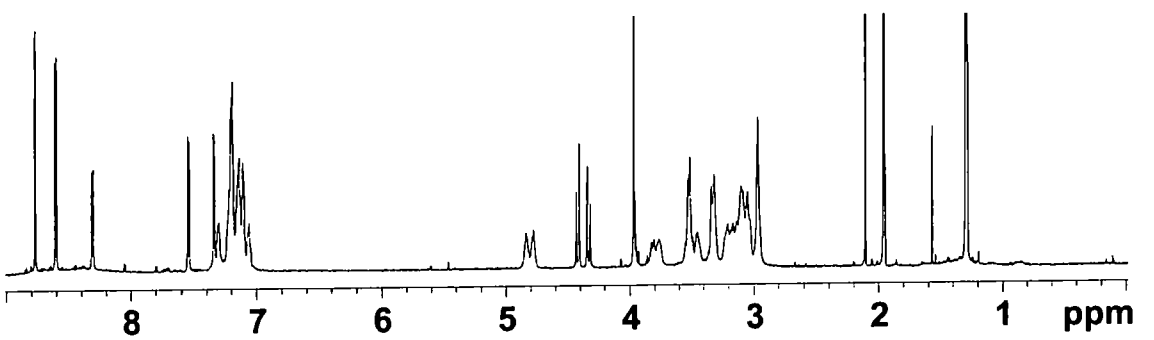

Figure B.5 – CD_3CN, 700 MHz, 295 K, 3 mM.

L^{51b}

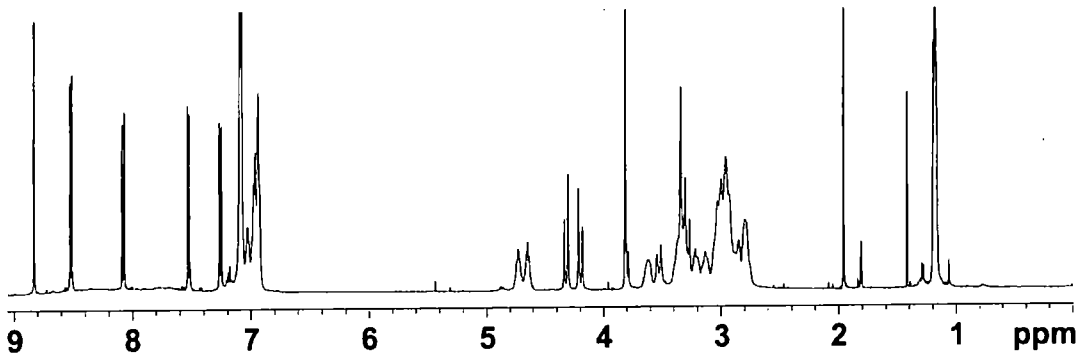

Figure B.6 – CD_3CN, 500 MHz, 295 K, 3 mM.

L^{57}

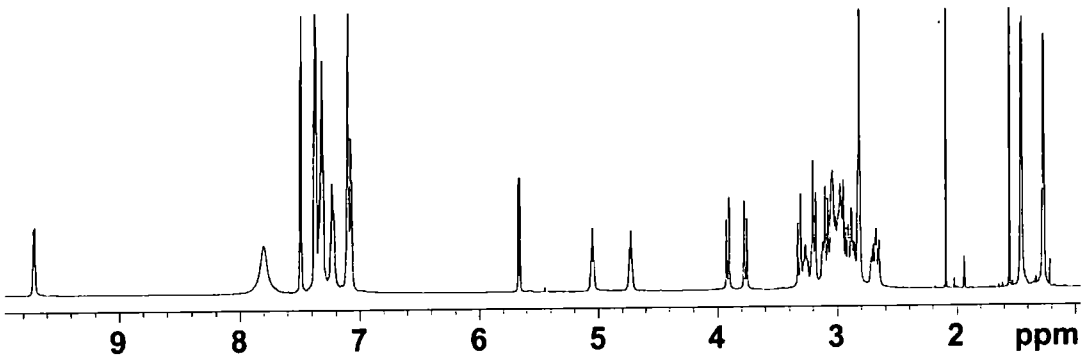

Figure B.7 – CD_3CN, 700 MHz, 295 K, 5 mM.

L^{58}

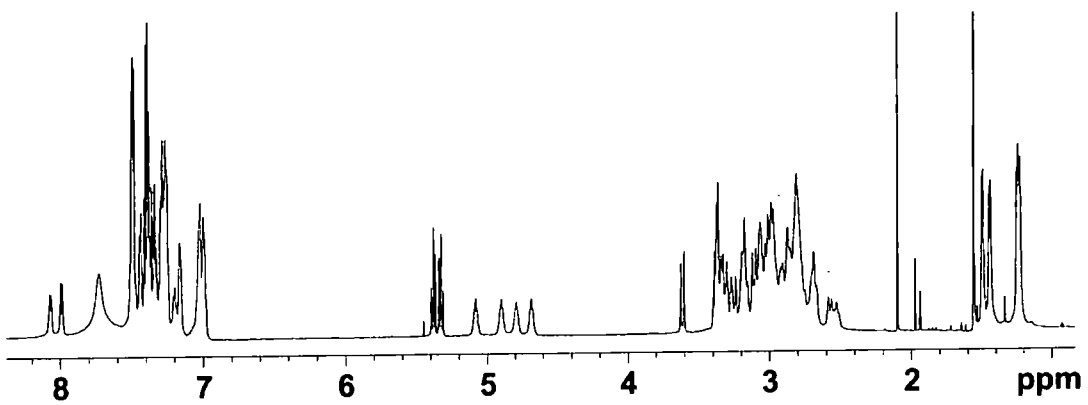

Figure B.8 – CD_3CN, 700 MHz, 295 K, 5 mM.

L^{61}

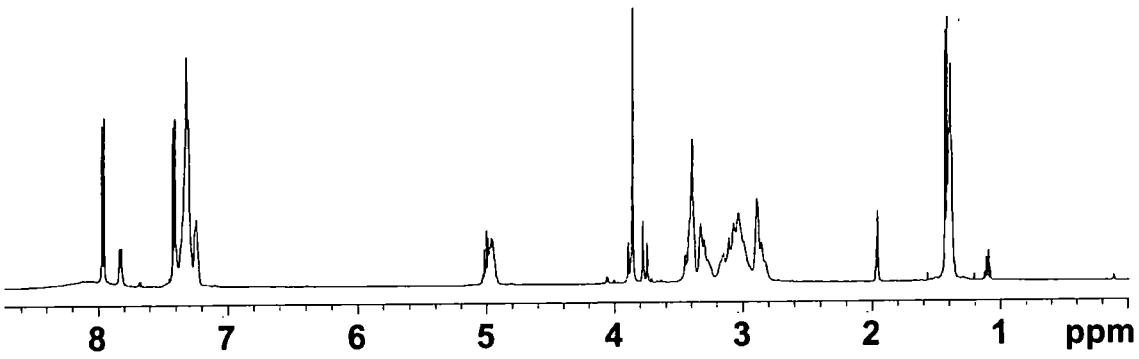

Figure B.9 – CD_3CN, 500 MHz, 295 K, 3 mM.

L^{62}

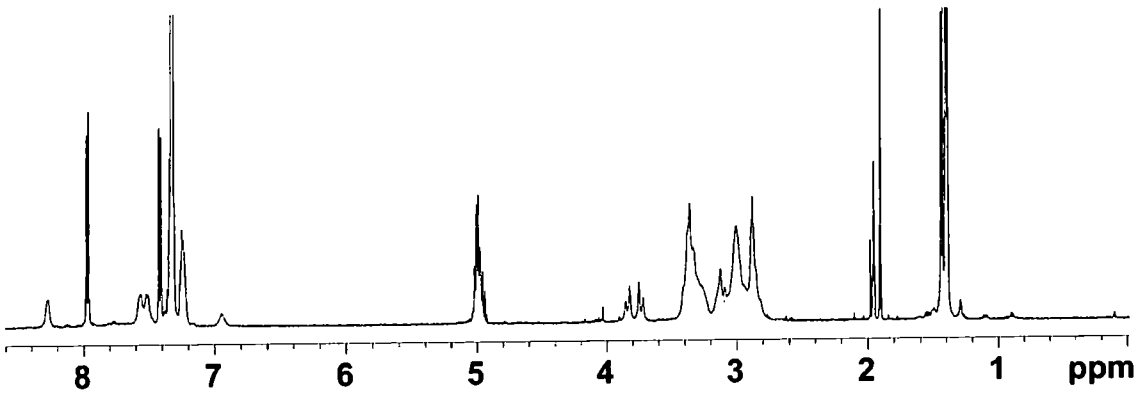

Figure B.10 – CD_3CN, 500 MHz, 295 K, 3 mM.

Appendix C

Crystal data

Data for 2-phthalimidomethyl-7-methoxycarbonyl-1-azathioxanthone

empirical formula	$C_{23}H_{14}N_2O_5S.0.5(C_6H_6)$
formula weight	469.48
T (K)	120 (2)
crystal system	triclinic
space group	P
a (Å)	13.2703 (17)
b (Å)	13.8540 (18)
c (Å)	13.9589 (18)
α (deg)	67.47 (1)
β (deg)	66.06 (1)
γ (deg)	73.64 (1)
V (Å^3)	2142.2 (5)
Z	4
μ (mm^{-1})	0.20
crystal dimensions (mm)	0.27 x 0.15 x 0.03

Appendix D

Notable structures

Notable structures discussed in this thesis, included for reference use.

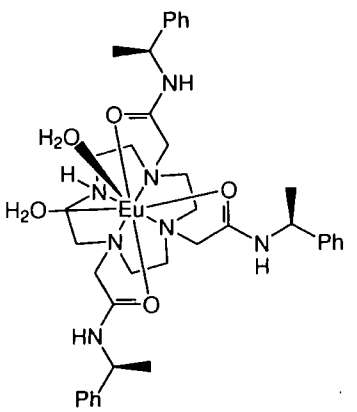

$[EuL^{24}]^{3+}$

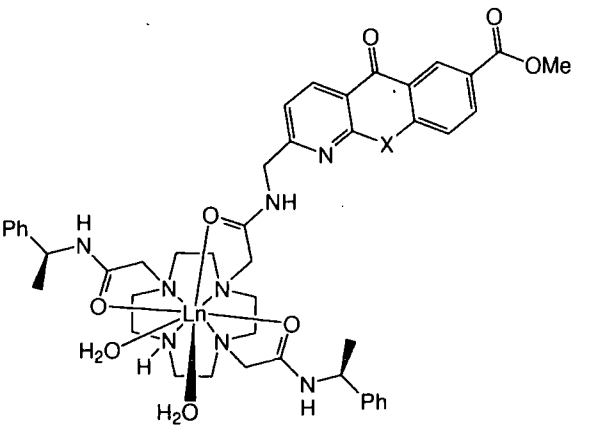

$[LnL^{44a}]^{3+}$ **(X = O)**
$[LnL^{44b}]^{3+}$ **(X = S)**

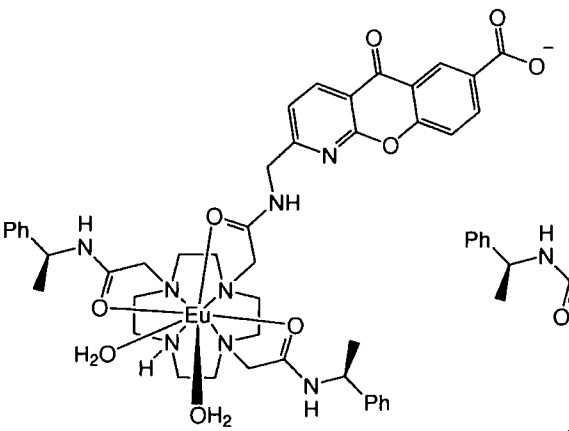

$[EuL^{49}]^{2+}$

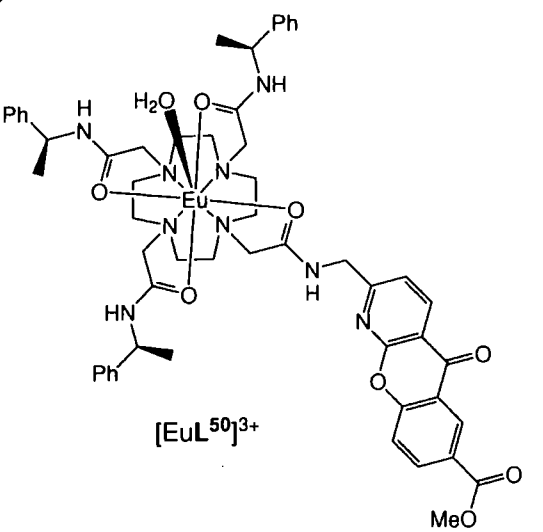

$[EuL^{50}]^{3+}$

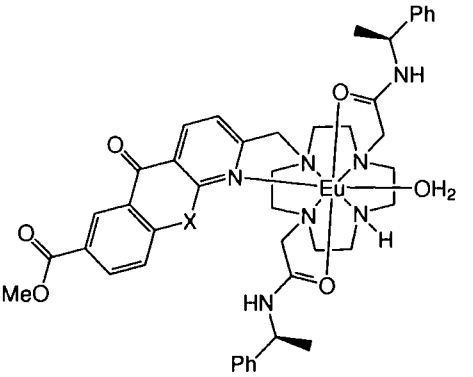

$[EuL^{51a}]^{3+}$ **(X = O)**
$[EuL^{51b}]^{3+}$ **(X = S)**

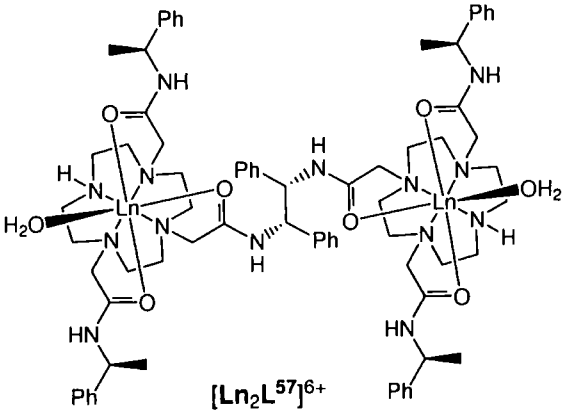

$[Ln_2L^{57}]^{6+}$

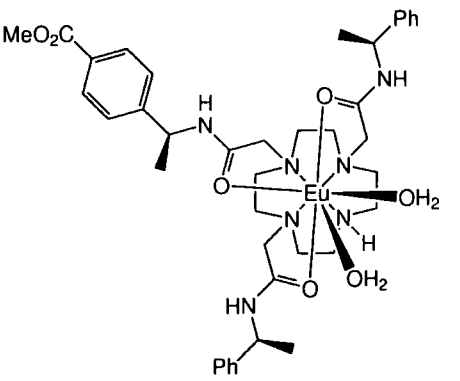

$[EuL^{61}]^{3+}$

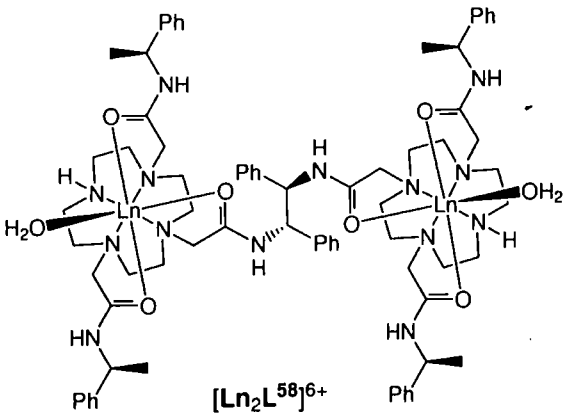

$[Ln_2L^{58}]^{6+}$

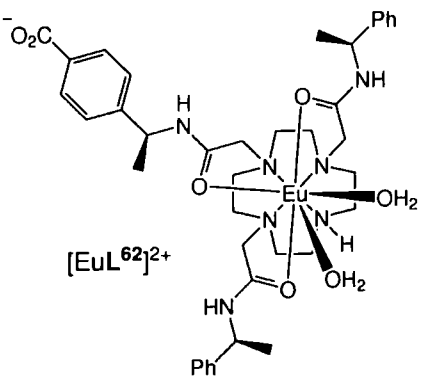

$[EuL^{62}]^{2+}$